Near–horizon physics of regular black holes

by

Ioannis Soranidis

A thesis submitted to Macquarie University
for the degree of Doctor of Philosophy

Faculty of Science and Engineering,
School of Mathematical and Physical Sciences

April, 2025

MACQUARIE
University
SYDNEY·AUSTRALIA

Except where acknowledged in the customary manner, the material presented in this thesis is, to the best of my knowledge, original and has not been submitted in whole or part for a degree at any university.

Ioannis Soranidis

Acknowledgements

I am deeply thankful to everyone who has helped and supported me throughout this journey. This thesis would not have been possible without the encouragement, guidance, and kindness of many people. I sincerely appreciate all those who stood by me, believed in me, and helped me overcome the difficulties along the way.

First and most importantly, I want to express my gratitude to my PhD advisor, Daniel Terno, for his unwavering support throughout my candidature. Not only did he give me the opportunity to pursue a PhD, but he also guided me through the complexities of physics, deepened my understanding of nature, and introduced me to the fascinating topic of regular black holes. He helped me navigate the challenges of academia and consistently demonstrated a sincere commitment to my personal and professional growth.

Many thanks to Sebastian Murk, who, in addition to being an excellent research collaborator and friend, acted as a supervisor during my PhD. He taught me, with his nitpicking attitude I should say, the art of paper writing, figure creating, and preparation of presentation slides. I would also like to extend my sincere thanks to those with whom I had the pleasure of collaborating during my candidature: Pravin Dahal and Swayamsiddha Maharana for working together on various projects and discussing physics; Fil Simovic for engaging me with the exciting field of black hole thermodynamics and for our stimulating conversations on both physics and non-physics related topics; and David Kubizňák for hosting me as a visitor at Charles University and showing me the best places in Prague.

Thank you to my Sydney friends: Riddhi Ghosh for moral support conversations near the Foosball table, sushi train, and enjoyable dinners; Zixin Huang for many research tips, exciting dinners, and catching-up sessions; Fotini Kouloukis for fun conversations, astronomy open night (plasma ball!), and introducing me to the best souvlaki place in Sydney (almost like Greece); Herman Li for teaching me how to not be weird while giving talks, exciting lunches, amazing trips to the centre, fun soccer games (and some less enjoyable ones), too much KFC and too much fun; Kayla Martin for many enjoyable conversations, dinners at heaps of restaurants serving only unhealthy food, long hikes that were not so long in the end, teaching me Aussie English along with many other things (as apparently I know nothing!), and Elisabeth Wagner for many interesting conversations and exciting hikes!

To my non-Sydney friends: Thodoris Goulas, Dimitris Lampriadis, Thanasis Mapakis, Odysseas Moulas, and Mpampis Vamvakas for being around since forever, supporting me in your own way, and making me as competitive as possible in every aspect of my life. (How many PhDs do you have?)

I would like to acknowledge funding from Macquarie University, the work in this thesis was supported by an International Macquarie University Research Excellence Scholarship (Allocation No. 20224281).

Finally, thank you to my sister Ralia and my parents, Anastasios and Anastasia, who have provided immeasurable support throughout my life, always encouraged me to pursue my dreams, and have provided me a home like no other. This thesis is dedicated to you!

Abstract

One of the most notable predictions of general relativity is the existence of black holes. Initially considered mere mathematical curiosities, advancements in astronomical observations have provided strong evidence for the existence of these compact objects, transforming our perception of black holes from abstract theoretical constructs to tangible physical entities. Their hallmark features are the existence of an event horizon and a singularity. The problems associated with these two characteristics are the teleological nature of the event horizon and breakdown of general relativity at the singularity.

The existence of singularities serves not only as motivation to seek a new theory but also provides insights into its potential structure. Various approaches have been proposed to address singularities, ranging from classical methods within general relativity by incorporating additional matter fields to higher-order curvature corrections and semiclassical effects. These approaches are valuable tools for identifying the properties of candidate quantum gravity theories, which are expected to resolve singularities and yield non-singular solutions. Based on the presence of a horizon, such solutions can be classified into two categories: regular black holes and horizonless configurations. Both share the common feature of a minimal length scale introduced to regularize spacetime.

This thesis investigates the properties of such ultracompact objects under the assumption of the validity of semiclassical gravity in their vicinity. We begin by examining static cases within the framework of general relativity, assuming negligible backreaction on the geometry due to quantum effects, using nonlinear electrodynamics as an effective way to source regular geometries. We analyze the thermodynamic properties of horizonful ultracompact objects through Hamiltonian formalism and Euclidean path integral methods, demonstrating consistency between these approaches in appropriate limits. Using the derived thermodynamic quantities, we examine the phase structure and show the absence of the Hawking–Page transition in the canonical ensemble due to the presence of the minimal length scale. Confirming or refuting the identity and properties of ultracompact objects, as well as the existence of such a minimal length scale, depends heavily on observational signatures. Our research examines the behavior of light rings around these objects, demonstrating that merely counting the number of light rings, without knowing the underlying theory, may be insufficient for definitive identification.

Considering backreaction effects on the geometry, we conduct a theory-agnostic study of dynamic regular black holes, assuming only the validity of semiclassical gravity near their apparent horizons and the finite formation time according to the clock of a distant observer. We analyze the null energy condition and find that it is violated near the outer apparent horizon but satisfied near the inner apparent horizon, effectively separating the trapped spacetime region into null energy condition-violating and null energy condition-non-violating domains. We show that within this framework, regular black holes end their life as cold remnants represented by extremal

black holes. Moreover, we demonstrate that massive observers and particles can cross both the inner and outer horizons on ingoing geodesics, allowing entry and exit from the supposedly trapped spacetime region without encountering infinite energy densities, commonly referred to as firewalls. Finally, we extend the study of thermodynamics in this dynamical context, showing the existence of a first law of black hole mechanics based solely on near-horizon quantities and demonstrating that the notion of internal energy is captured by the Misner–Sharp mass evaluated on the outer apparent horizon.

Contents

Acknowledgements iv

Abstract vi

Contents viii

List of Publications x

Foreword xiii

Introduction xv

1 Euclidean and Hamiltonian thermodynamics for regular black holes 1

2 Euclidean methods and phase transitions for the strongest deformations compatible with Schwarzschild asymptotics 23

3 Light rings and causality for nonsingular ultracompact objects sourced by nonlinear electrodynamics 50

4 Matter and forces near physical black holes 72

5 Kinematic and energy properties of dynamical regular black holes 86

6 Regular black holes and the first law of black hole mechanics 102

Conclusion 115

References 119

List of Publications

Publications included in this thesis (listed in the order of their appearance):

1. F. Simovic and I. Soranidis
   Euclidean and Hamiltonian thermodynamics for regular black holes
   E-print submitted to arXiv on 18 September 2023 [arXiv ID: 2309.09439]
   Published 20 February 2024 in Physical Review D (American Physical Society)
   Journal reference: Phys. Rev. D **109**, 044029 (2024) [DOI: 10.1103/PhysRevD.109.044029]

2. I. Soranidis
   Euclidean methods and phase transitions for the strongest deformations compatible with Schwarzschild asymptotics
   E-print submitted to arXiv on 11 October 2023 [arXiv ID: 2310.07228]
   Published 21 February 2024 in Physical Review D (American Physical Society)
   Journal reference: Phys. Rev. D **109**, 044041 (2024) [DOI: 10.1103/PhysRevD.109.044041]

3. S. Murk and I. Soranidis
   Light rings and causality for nonsingular ultracompact objects sourced by nonlinear electrodynamics
   E-print submitted to arXiv on 12 June 2024 [arXiv ID: 2406.07957]
   Published 29 August 2024 in Physical Review D (American Physical Society)
   Journal reference: Phys. Rev. D **110**, 044064 (2024) [DOI: 10.1103/PhysRevD.110.044064]

4. P. K. Dahal, I. Soranidis, and D. R. Terno
   Matter and forces near physical black holes
   E-print submitted to arXiv on 22 September 2022 [arXiv ID: 2209.10766]
   Published 30 December 2022 in Physical Review D (American Physical Society)
   Journal reference: Phys. Rev. D **106**, 124048 (2022) [DOI: 10.1103/PhysRevD.106.124048]

5. S. Murk and I. Soranidis
   Kinematic and energy properties of dynamical regular black holes
   E-print submitted to arXiv on 12 September 2023 [arXiv ID: 2309.06002]
   Published 4 December 2023 in Physical Review D (American Physical Society)
   Journal reference: Phys. Rev. D **108**, 124007 (2023) [DOI: 10.1103/PhysRevD.108.124007]

6. S. Murk and I. Soranidis
   Regular black holes and the first law of black hole mechanics
   E-print submitted to arXiv on 11 April 2023 [arXiv ID: 2304.05421]
   Published 1 August 2023 in Physical Review D (American Physical Society)
   Journal reference: Phys. Rev. D **108**, 044002 (2023) [DOI: 10.1103/PhysRevD.108.044002]

Publications not included in this thesis (sorted in chronological order):

1. P. K. Dahal, F. Simovic, I. Soranidis, and D. R. Terno
Black holes as spherically-symmetric horizon-bound objects
E-print submitted to arXiv on 28 March 2023 [arXiv ID: 2303.15793]
Published 8 November 2023 in Physical Review D (American Physical Society)
Journal reference: Phys. Rev. D **108**, 104014 (2023) [DOI: 10.1103/PhysRevD.108.104014]

2. P. K. Dahal, S. Maharana, F. Simovic, I. Soranidis, and D. R. Terno
Models of cosmological black holes
E-print submitted to arXiv on 28 December 2023 [arXiv ID: 2312.16804]
Published 14 August 2024 in Physical Review D (American Physical Society)
Journal reference: Phys. Rev. D **110**, 044032 (2024) [DOI: 10.1103/PhysRevD.110.044032]

3. I. Soranidis
Properties of dynamical regular black holes in semiclassical gravity
E-print submitted to arXiv on 14 August 2024 [arXiv ID: 2408.07290]
Contribution to the proceedings of the 17th Marcel Grossmann meeting (7-12 July 2024)
to be published by World Scientific [DOI: TBD]

4. S. Maharana, F. Simovic, I. Soranidis, and D. R. Terno
Padé metrics for black hole perturbations and light rings
E-print submitted to arXiv on 9 March 2025 [arXiv ID: 2503.06752]
Published 20 May 2025 in Physical Review D (American Physical Society)
Journal reference: Phys. Rev. D **111**, 104063 (2025) [DOI: 10.1103/PhysRevD.110.044032]

5. I. Soranidis and D. R. Terno
Exotic encounters: Buchdahl's conditions and physical black holes
E-print submitted to arXiv on 14 May 2025 [arXiv ID: 2505.09189]
Honorable Mention for the Gravity Research Foundation 2025 Awards for Essays on Gravitation to be published by International Journal of Modern Physics D [DOI:10.1142/S0218271825440134]

6. R. A. Hennigar, D. Kubizňák, S. Murk, and I. Soranidis
Thermodynamics of regular black holes in anti-de Sitter space
E-print submitted to arXiv on 16 May 2025 [arXiv ID: 2505.11623]
Submitted for publication in the Journal of High Energy Physics (JHEP) (under review)
[DOI: TBD]

Foreword

This thesis follows the "Thesis by publication" format as stipulated by Macquarie University. Rules and guidelines can be accessed here.

This thesis includes six publications [1–6]. It is important to note that the chronological order of these publications differs from their arrangement within the thesis (see "List of Publications" on pp. vii–viii). The references [7–9], though relevant, are not included here as they do not focus exclusively on the study of regular black holes. Additionally, while the conference paper [10] introduces new findings, some of its content overlaps with reference [5], and it has therefore been excluded to minimize redundancy. Lastly, although the relevant work on the publications [11, 12] began prior to the submission of this thesis, they were uploaded to the arXiv after its completion.

The thesis is organized as follows: The first chapter offers a critical introduction to the subject area and provides context for the problems explored in the published works. The main part of the thesis comprises six key publications [1–6], which lay the groundwork for the research presented. Each publication is preceded by a concise summary of its main results and additional commentary, including errata or differences in conventions, such as variations in notation or function definitions. U.S English is consistently used throughout the thesis. The published works, also adhere to U.S. English as required by the respective publishers. Journal abbreviations conform to the ISO4 standard.

The following abbreviations (including their plural forms) are commonly used throughout the thesis:

RBH	Regular black holes
PBH	Physical black holes
MBH	Mathematical black holes
NEC	Null energy condition
EMT	Energy-momentum tensor
NED	Nonlinear electrodynamics
ONF	Orthonormal frame
ADM	Arnowitt–Deser–Misner
GUT	Grand unified theories
KMS	Kubo-Martin-Schwinger
CFT	Conformal field theory
AdS	Anti-de Sitter
dS	de Sitter
GR	General relativity
MS	Misner-Sharp

Black holes ain't as black as they are painted. They are not the eternal prisons they were once thought. Things can get out of a black hole, both to the outside and possibly to another universe. So if you feel you are in a black hole, don't give up — there's a way out.

Stephen Hawking

Introduction

General relativity (GR) and quantum field theory are the two pillars of modern physics. While each of them provides an accurate description of nature within its domain of validity, they apply to vastly different regimes: GR pertains to the macroscopic scale of the universe, while quantum field theory governs the microscopic realm. Despite their individual successes, the quest of reconciling them has remained elusive so far. In 1965, Penrose demonstrated that under the assumptions of global hyperbolicity, the existence of a noncompact Cauchy hypersurface, the validity of classical Einstein equations, and the non-violation of the null energy condition (NEC), a spacetime containing trapped surfaces is inevitably geodesically incomplete, introducing the first "modern" singularity theorem [13]. The existence of inextensible geodesics is commonly equated with the presence of regions of unbounded curvature, known as gravitational singularities. While we adopt this assumption in this thesis, it is crucial to note that this equivalence does not always hold true [14–16]. Singularities pose a significant challenge as they signal the breakdown of the underlying theory, fundamentally limiting our ability to predict the future [17]. *"When a theory predicts singularities the theory is wrong*!" [18] or undoubtedly incomplete. It is anticipated that the merging of GR with quantum field theory into a unified theory of quantum gravity will resolve the singularity issues. Quantum effects are expected to play a pivotal and indispensable role in this resolution.

In the absence of a complete theory, research efforts are partially directed towards effective models capable of mimicking observable phenomena, such as light rings, while circumventing singularity issues. These models, known as black hole mimickers, are categorized into two distinct groups based on the absence or presence of a horizon [19]. The former corresponds to horizonless ultracompact objects (UCOs), which have the capacity to form two light rings around them, with one being stable and is linked to nonlinear spacetime instabilities [20, 21]. This property potentially renders them undesirable candidates for the objects we currently observe. The latter category comprises regular black holes (RBHs), which are trapped spacetime regions bounded by both an inner and an outer horizon and they are the primary focus of this thesis. In this scenario, the geometry near the singularity undergoes significant modification, resulting in the creation of a defocusing point at a finite distance, represented by the inner horizon in spherically symmetric scenarios [22]. It is important to highlight that the presence of an inner horizon poses significant challenges, primarily due to its inherent instability under small perturbations. These instabilities manifest as an exponential increase in gravitational energy near the inner horizon. This issue, known as mass inflation instability, is a key concern in the study of RBHs [23–28].

Current astrophysical observations, although in close agreement with the Kerr metric, are unable to distinguish between black hole mimickers and genuine black holes with singularities. Therefore, it is premature to conclusively identify the observed UCOs as black holes [29]. Furthermore, asserting that these objects are indeed black holes requires the observation of the event

horizon. However, such an entity is inherently teleological and fundamentally unobservable, even in principle [30]. It could be argued that the detection of a quasilocal apparent horizon should suffice to verify the presence of a trapped region but from the currently available data its existence cannot be inferred. Unfortunately, neither category of black hole mimickers constitutes a panacea to all of our problems, as substituting the singularity with an effectively regular spacetime results in peculiar features.

All singularity theorems rely on the assumption that collapsing matter behaves in accordance with certain energy conditions, which describe classical matter and aim to capture the property of the non-negativity of mass and the attractive nature of gravity [31, 32]. However, quantum fields systematically violate these classical energy conditions and consequently influence the theorems of GR in various ways [33]. For instance, during gravitational collapse, when matter is compressed to high densities, quantum effects are expected to become significant and violation of energy conditions may occur. But how does such a violation contribute to the resolution of singularities and the emergence of RBH spacetimes?

A star with appropriate mass will undergo gravitational collapse once sufficient thermal energy has been radiated away. The first mathematical model describing complete gravitational collapse was formulated by Oppenheimer and Snyder [34]. In this model, a spherically symmetric, homogeneous, collisionless matter collapses into a Schwarzschild black hole under the influence of gravity's attractive force. The formation of the singularity can only be prevented by introducing some repulsive effect to halt the collapse. This effect may arise from the breakdown of GR during the final stages of collapse and/or from violation of the NEC [22]. Various horizonful or horizonless geometries can emerge from this collapse, including RBHs, black-to-white hole bounces, and horizonless remnants [35, 36].

To quantify in a rigorous way how close a self-gravitating body is to a black hole, it is customary to introduce a so-called closeness parameter ϵ defined as $\epsilon = r_0/r_g - 1$, where r_g denotes the Schwarzschild radius of the object and r_0 the radius of its effective surface [19]. Black holes independent of if they are singular or not are characterized by $\epsilon = 0$ while horizonless configurations are described by $\epsilon > 0$. According to a distant observer, gravitational collapse beyond the density of a neutron star can have three possible outcomes [29, 37]:

(i) Formation of a transient object: the closeness parameter reaches a minimal value $\epsilon_{min} > 0$, either at some finite time t_{min} or asymptotically $t \to \infty$.

(ii) Perpetual ongoing collapse ($\epsilon \to 0$ as $t \to \infty$): the horizon exists only as an asymptotic ($t \to \infty$) concept. At times $t < \infty$, these objects remain horizonless by definition.

(iii) Formation of an apparent horizon in finite asymptotic time $t_f < \infty$, i.e., in finite time according to the clock of a distant observer.

These outcomes underscore the intricate nature of gravitational collapse, which is central to understanding the behavior of compact objects like black holes. To comprehend nature at its most fundamental level, a deep understanding of gravity is crucial. Fortunately, the thermodynamic properties of gravity offer a glimpse into its microscopic structure. For every system in the universe, the foundation of its thermodynamic behavior lies in the statistical mechanics of its fundamentally quantum constituents. In classical physics, black holes are considered nature's black boxes, swallowing all matter and emitting nothing. This view changed dramatically with the

advent of quantum field theory on curved backgrounds. It was discovered that black holes radiate with a black body spectrum at a temperature proportional to their surface gravity [38], thereby possessing finite entropy. Thus, black hole thermodynamics was born, with laws analogous to those of ordinary thermodynamics as formulated by Bardeen, Carter, and Hawking [39]. The field of black hole thermodynamics plays a significant role in advancing our understanding of quantum gravity, field theory in curved spacetime, and information theory [40, 41]. The thermodynamic parameters of black holes can be calculated using various methods, including the covariant phase space approach [42] and the Euclidean path integral formalism [43].

Black holes exhibit a fascinating trait: they can undergo phase transitions, much like ordinary thermodynamic systems. This idea was first introduced by Hawking and Page, who discovered that black holes embedded in anti-de Sitter (AdS) spacetime can transition between states [44]. Since then, this concept has been found to apply broadly across many types of black holes, including those in higher dimensions and in theories extending beyond GR [45, 46]. The exploration of the Hawking–Page transition has gained significant interest due to the anti-de Sitter/conformal field theory (AdS/CFT) correspondence. This correspondence posits an equivalence between a gravitational theory in a $\mathcal{D}$-dimensional AdS spacetime and a conformal field theory (CFT) in one less dimension on the boundary [47]. It is important to note that this duality holds in the limit of a large — or more precisely, infinite — number of degrees of freedom on the CFT side, to match those present in the AdS bulk. Within this duality, the transition between a black hole and thermal radiation in the AdS bulk is dual to a deconfinement transition in the boundary CFT [48].

The AdS/CFT dictionary has become a powerful tool in theoretical physics, offering insights into strongly coupled systems where standard perturbative techniques are ineffective, tackling the black hole information paradox, and calculating black hole entropy [40]. Moreover, any changes in the bulk gravity theory naturally influence the boundary CFT. Thus, the various extensions of the Hawking–Page transition, as well as the discovery of more unusual transitions, are expected to have important implications for the boundary theory, though this aspect has been explored less than the bulk phase structure. However, the corresponding interpretation of the first-order phase transition in the bulk theory is a transition between a low-entropy and a high-entropy CFT [49], and this is precisely the type of phase transition that will be examined in the phase structure of RBHs in this thesis.

Over the years, numerous studies have explored the thermodynamic properties of RBHs using various methods. In this thesis, we utilize NED theories to effectively model RBHs and address inconsistencies found in the existing literature. This type of theory was first employed by Born and Infeld to address the infinities associated with the self-energy of a point charge [50] and, interestingly, emerges from string theory as a low-energy effective field theory [51]. A few years later, Heisenberg and Euler developed a nonperturbative one-loop effective action that accounts for the nonlinear corrections to Maxwell electrodynamics arising from quantum electrodynamical vacuum polarization effects [52]. These include interactions of virtual electrons and positrons at the one-loop level without radiative corrections.

In classical electrodynamics, photons do not interact. However, quantum electrodynamics predicts that two photons can scatter off each other in vacuum through a higher-order process mediated by virtual charged particles in a one-loop diagram. This rare effect, known as light-by-light scattering, first appears at the fourth order in the fine-structure constant, $O(\alpha^4)$ and it can

be described by the Heisenberg-Euler NED Lagrangian mentioned above. This phenomenon was first observed quite recently by the ATLAS collaboration [53, 54]. This process becomes accessible at the Large Hadron Collider due to the intense electromagnetic fields produced during ultra-relativistic collisions of lead ions at a center-of-mass energy per nucleon-nucleon pair of 5.02 TeV.

While ultra-relativistic collisions provide one avenue for probing NED, several efforts have also been made to investigate its effects on larger, astrophysical scales. A prominent example is neutron stars, particularly those that possess exceptionally strong magnetic fields. One key prediction of quantum electrodynamics — as well as many NED models, with the notable exception of Born-Infeld theory [50] — is vacuum birefringence, where photons with different polarisations travel at different phase velocities in strong electromagnetic fields. As a result, when light passes through such a region, it effectively splits into two distinct polarised components. In thermally emitting isolated neutron stars, the observed radiation originates from a large portion of the stellar surface, where the magnetic field orientation varies significantly across different regions. Without accounting for vacuum polarization effects inherent to quantum electrodynamics, these variations would cause the polarisation signals from different surface elements to cancel out, leading to a strong depolarisation of the radiation detected by a distant observer [55, 56].

However, vacuum birefringence can greatly enhance the linear polarisation of the radiation emitted by neutron stars, potentially boosting it from just a few percent to nearly complete polarisation. The extent of this amplification depends strongly on factors such as the observer's line of sight and the nature of the star's surface emission process. Measuring the polarisation of thermal emission from the surface of an isolated neutron star would be highly significant. Regardless of the specific physical conditions in the emitting region, observing a high degree of linear polarisation would provide direct observational evidence for quantum electrodynamics vacuum polarisation effects in the strong-field regime [55, 56]. Observations of RX J1856.5-3754 — the closest known neutron star to date — reveal a polarisation degree of approximately 16.43%, a value sufficiently high to support the presence of vacuum birefringence as predicted by quantum electrodynamics and various NED models [57].

Additionally, it is worth noting that NED theories have been investigated in the context of cosmic birefringence, a phenomenon long regarded as a promising probe of new physics. A particularly intriguing scenario involves the Cosmic Microwave Background (CMB), where birefringence can be induced by the coupling between electromagnetism and an axion-like (pseudo)scalar field. This interaction causes a rotation of the CMB's linear polarisation plane as photons propagate over cosmological distances [58]. Interest in this mechanism has been renewed following claims of a detectable signal in the Planck 2018 data [59]. Furthermore, photon-photon forward scattering mediated by Heisenberg-Euler interactions may give rise to a degree of circular polarisation in the CMB — commonly referred to as V-modes — which also contributes to cosmic birefringence [60].

In a large number of cases NED theories coupled to GR are also sufficient to generate regular geometries and eliminate singularities only at the cost of using exclusively magnetic charge. The existence of this magnetic charge is closely linked to the minimal length scale introduced to regularize the spacetime. However, a significant challenge with these sources is that magnetic monopoles have yet to be detected in nature, despite extensive observational efforts [61–63].

Nevertheless, heavy magnetic monopoles, which are predicted to form in the early universe, remain a robust feature of grand unified theories (GUTs) [64–66]. These monopoles emerge from spontaneous symmetry breaking at the GUT scale of approximately 10^{16} GeV and have important ramifications for structure formation and early universe cosmology [67].

It is crucial to note that RBHs can be constructed using various NED theories, each characterized by a different weak-field limit. The deformations from the Schwarzschild geometry can be quantified based on the specific weak-field limit of the chosen NED theory. This implies that the resolution of singularities varies depending on the NED Lagrangian density employed. By selecting different NED frameworks, one can explore the distinct properties of RBHs and the mechanisms by which singularities are smoothed out. These differences manifest not only in the thermodynamic properties of the black holes but also in their observational signatures as it will be demonstrated in this thesis.

Until now, our study has neglected the backreaction of quantum effects on spacetime geometry. To move beyond these physically unrealistic stationary scenarios, we must account for these effects in a self-consistent manner, transitioning to a fully dynamic framework. The self-consistent approach [37] we will use to study dynamic RBHs is based on semiclassical gravity [68]. In this approach, spacetime is described by a metric $g_{\mu\nu}$, with concepts like particle trajectories and horizons assumed to be well-defined. This metric is a solution to the semiclassical Einstein equations, where the source term is the energy-momentum tensor (EMT) $\langle T_{\mu\nu}\rangle_\psi$, representing the renormalized expectation value of an EMT operator in a certain, though unspecified, quantum state of gravity and matter ψ. This method imposes no specific assumptions about the nature of the matter fields or their quantum states, nor does it differentiate between the background (such as cosmological or collapsing matter) and the resulting quantum excitations.

This self-consistent framework naturally leads to the concept of a physical black hole (PBH), defined as a trapped region in spacetime where both ingoing and outgoing future-directed null geodesics, emanating from a spacelike two-dimensional surface with spherical topology, exhibit negative expansion [69–71]. The apparent horizon serves as the boundary of this trapped region. Unlike the conventional black holes described in the literature, which are enclosed by event horizons, PBHs are bounded by dynamically evolving quasilocal horizons that form within a finite time according to a distant observer's clock. These horizons are, at least in principle, physically observable, meaning that their presence or absence can be determined through measurements conducted within a finite time interval and a finite region of spacetime [30]. This corresponds to the outcome of gravitational collapse described as scenario (iii).

The requirement of finite formation time, combined with the weakest form of the cosmic censorship conjecture [71–73] — which demands that all curvature scalars [69, 74] remain finite up to and on the apparent horizon — restricts the possible solutions to the Einstein equations. Based on near-horizon expansions of the metric functions, it has been demonstrated that only two classes of dynamic solutions to the semiclassical Einstein equations satisfy these conditions: either evaporating future apparent horizons or accreting anti-trapping apparent horizons. This model inherently leads to a violation of the NEC, the weakest of the energy conditions [69], consistent with studies showing NEC violation in the presence of Hawking radiation [72, 75–77]. Moreover, this aligns with the finding that the outer apparent horizon is not "visible" to a distant observer unless the NEC is violated [69, 72].

It should be noted that this thesis considers the standard formulation of the NEC; however,

refined or more modern versions have been proposed in the literature. One such example is the averaged null energy condition (ANEC), which, as the name suggests, involves averaging the NEC along a null geodesic trajectory. The primary aim of such improvements is to more accurately capture the behavior of matter content, typically described by quantum fields, within the framework of semiclassical gravity [78]. In certain field theories, "quantum energy inequalities" have been established, where integrals of the stress-energy tensor are not necessarily positive but are constrained by a lower bound [33]. In this spirit, a new bound known as the quantum null energy condition (QNEC) has been derived, involving the von Neumann entropy of quantum fields restricted to a finite or infinite spatial region [79]. Lastly, beyond the NEC and its refined versions, several other energy conditions are discussed in the literature. These include the weak energy condition (WEC), which ensures that the energy density measured by any observer is non-negative; the strong energy condition (SEC), which captures the idea that gravity should be attractive; and the dominant energy condition (DEC), which requires that the flow of energy remains causal and does not exceed the speed of light [80].

Since the self-consistent framework is not thoroughly developed in any of the papers included in this thesis, we provide a brief overview here to facilitate the reader's understanding. A general spherically symmetric metric in Schwarzschild coordinates [71] is given by

$$ds^2 = -e^{2h(t,r)} f(t,r) dt^2 + f(t,r)^{-1} dr^2 + r^2 d\Omega_2 \,, \tag{1}$$

while using the advanced null coordinate v results in the form

$$ds^2 = -e^{2h_+(v,r)} f_+(v,r) dv^2 + 2e^{h_+(v,r)} dv dr + r^2 d\Omega_2 \,. \tag{2}$$

The function f is coordinate-independent, i.e., $f(t,r) \equiv f_+\big(v(t,r),r\big)$ and in what follows we omit the subscript. In spherically symmetric spacetimes, the absence of gravitational radiation allows for a well-defined concept of energy—the Misner–Sharp (MS) mass, denoted as $C/2$ [92]. This function f can be conveniently expressed in terms of the MS mass as follows:

$$f = 1 - \frac{C(t,r)}{r} = 1 - \frac{C_+(v,r)}{r} = \partial_\mu r \partial^\mu r \,, \tag{3}$$

where the coordinate r is the areal radius [71] and $C(t,r) \equiv C_+(v(t,r),r)$. The functions h and h_+ play the role of integrating factors in the coordinate transformation

$$dt = e^{-h}(e^{h_+} dv - f^{-1} dr) \,. \tag{4}$$

In an asymptotically flat spacetime, $h \to 0$ and $f \to 1$ as $r \to \infty$, and t is the physical time of a stationary observer at spacelike infinity. For example, the Schwarzschild metric corresponds to $h \equiv 0$, $M_s \equiv C/2 = \text{const.}$, and $v = t + r_*$, where r_* is the tortoise coordinate [69]. A description in terms of the retarded null coordinate $u = t - r_*$ and its properties is provided in the appendix of Ref. [7]. However, since this is not relevant to our purpose, we will omit this discussion in the thesis.

In an asymptotically Minkowski spacetime the Schwarzschild radius r_g is the largest root of $f(t,r) = 0$. The invariance of the MS mass implies that

$$r_g(t) = C(t,r_g) = r_+\big(v(t,r_g(t))\big) = C_+(v,r_+), \tag{5}$$

where $r_+(v)$ is the largest root of $f_+(v,r) = 0$. It represents the location of the outer component of the apparent horizon. Unlike the globally defined event horizon, the apparent horizon is foliation-dependent, though it remains invariant in any foliation that respects spherical symmetry [70]. This surface serves as the boundary of the trapped region and is the defining characteristic of a PBH.

The spacetime is inherently dynamical, so analyzing various properties of a PBH requires generalizing the Killing vector field t^μ associated with time translation invariant. Generalizations of surface gravity to dynamical spacetimes [81, 82] are generally related to either the affine peeling surface gravity [83] or the so-called Kodama surface gravity [84–86]. However, since peeling surface gravity is ill-defined for a transient object that forms within the finite time of a distant observer [87–89], we will focus on the Kodama vector field k^μ. To give the reader an idea of this vector's form, for the metric in Eq. (2), the Kodama vector is given by:

$$\mathrm{k}^\mu = \left(e^{-h_+}, 0, 0, 0\right). \tag{6}$$

This vector is covariantly conserved

$$\nabla_\mu \mathrm{k}^\mu = 0, \tag{7}$$

and also generates a conserved current J^μ which is given, using the Einstein tensor $G_{\mu\nu}$, as

$$J^\mu = G^{\mu\nu}\mathrm{k}_\mu, \quad \nabla_\mu J^\mu = 0. \tag{8}$$

This provides a natural geometric interpretation of the Schwarzschild coordinate time and results in a Noether charge that corresponds to the MS mass.

In addition to requiring that a PBH forms in a finite time according to a distant observer, we also demand that all curvature scalars [69, 74] be finite both up to and on the apparent horizon. It is sufficient to ensure that only two of these scalars, R and $R_{\mu\nu}R^{\mu\nu}$, are finite [90]. Construction of finite invariants from the divergent quantities that describe a real-valued solution allows one to describe properties of the near-horizon geometry. Because the metric in Schwarzschild coordinates is singular at the apparent horizon, it will often be convenient to work in null coordinates instead.

Both the analysis of the Einstein equations and the evaluation of curvature invariants is conveniently performed using the effective EMT components τ_t, τ^r, and $\tau_t{}^r$ defined as [37]:

$$\tau_t := e^{-2h}T_{tt}\,, \qquad \tau^r := T^{rr}\,, \qquad \tau_t{}^r := e^{-h}T_t{}^r\,. \tag{9}$$

The Einstein equations, given by

$$G_{\mu\nu} = 8\pi T_{\mu\nu}, \tag{10}$$

where we define $T_{\mu\nu}$ as the renormalized expactation value of the EMT operator on a quantum state ψ, i.e., $\langle T_{\mu\nu}\rangle_\psi$. For the components G_{tt}, $G_t{}^r$, and G^{rr} we have then, respectively

$$\partial_r C = 8\pi r^2 \tau_t / f\,, \tag{11}$$

$$\partial_t C = 8\pi r^2 e^h \tau_t{}^r\,, \tag{12}$$

$$\partial_r h = 4\pi r\left(\tau_t + \tau^r\right)/f^2\,. \tag{13}$$

To ensure finite values of the curvature scalars, it is sufficient to work with only two invariant quantities

$$\bar{\mathrm{T}} := \mathrm{T} + 2T^{\theta}_{\theta}, \qquad \bar{\mathfrak{T}} := \mathfrak{T} + 2\left(T^{\theta}_{\theta}\right)^2, \tag{14}$$

where

$$\mathrm{T} := T^{\mu}{}_{\mu} = (\tau^r - \tau_t)/f \,, \tag{15}$$

$$\mathfrak{T} := T^{\mu\nu}T_{\mu\nu} = \left((\tau^r)^2 + (\tau_t)^2 - 2(\tau_t{}^r)^2\right)/f^2 \,, \tag{16}$$

where the contributions of $T^{\theta}_{\ \theta} = T^{\phi}_{\ \phi}$ are disregarded, as one can verify that they do not introduce further divergences [37, 90].

These considerations restrict the scaling of the effective EMT components near the apparent horizon, such that

$$\tau_t \propto f^k, \quad \tau^r \propto f^k, \quad \text{and} \quad \tau_t{}^r \propto f^k, \tag{17}$$

with $k = 0$ or $k = 1$. Solutions with $k = 0$ describe a PBH after its formation and before the possible disappearance of the trapped region. Dynamical RBH solutions, as discussed in this thesis [5], fall into this category. In contrast, the Reissner-Nordström solution and static RBH solutions correspond to $k = 1$. For the remainder of this work, we will primarily focus on $k = 0$ solutions.

The admissible real-valued solutions for this dynamic class satisfy

$$\lim_{r\to r_g} \tau_t = \lim_{r\to r_g} \tau^r = -\Upsilon^2(t) \,, \quad \lim_{r\to r_g} \tau_t{}^r = \pm\Upsilon^2(t) \,, \tag{18}$$

for some function $\Upsilon(t)$. The leading terms of the metric functions are given in terms of $x := r - r_g(t)$ as

$$C = r_g - 4\sqrt{\pi} r_g^{3/2} \Upsilon \sqrt{x} + O(x) \,, \tag{19}$$

$$h = -\frac{1}{2} \ln \frac{x}{\xi} + O(\sqrt{x}) \,. \tag{20}$$

The function $\Upsilon(t)$ determines the energy density, pressure, and flux at the apparent horizon, and $\xi(t)$ is determined by choice of the time variable. The higher-order terms are matched with higher-order terms in the EMT expansion [37, 91].

The semiclassical Einstein equation (12) serves as a consistency condition and establishes the relation between the rate of change of the MS mass and the leading terms of the metric functions,

$$r_g' = \pm 4\sqrt{\pi r_g}\sqrt{\xi}\,\Upsilon \,, \tag{21}$$

where primes indicate derivatives with respect to t and $\pm$ sign corresponds to the expansion and contraction of the Schwarzschild sphere, respectively. For a contracting Schwarzschild sphere the (v, r) coordinates are regular across it. Evaluation of the expansion of the geodesic

congruences identifies the solutions with $r_g' < 0$ as black holes with decreasing mass. Conversely, the case $r_g' > 0$ allows for a regular description in (u, r) coordinates. Then the region described by $f(u, r) < 0$ is anti-trapped, and the solution describes an expanding white hole. These observations summarize the key properties of the self-consistent framework, which also applies to the inner apparent horizon of a PBH, if one is present [37].

This thesis is effectively divided into two main parts. The first part includes the studies presented in Refs. [1–3], focusing on the thermodynamic [1, 2] and observational properties [3] of RBHs in a static regime, corresponding to the $k = 1$ class of solutions. The primary objective here is to establish the existence of a first law of black hole mechanics, which describes the quasi-static transition between two equilibrium states of a black hole using certain macroscopic quantities. This is achieved by treating the minimal length scale as a fundamental parameter, allowing for a theory-agnostic approach. The analysis is conducted for RBHs embedded in AdS, Minkowski, and de Sitter (dS) spacetimes. Notably, achieving thermodynamic equilibrium in dS spacetime is challenging due to the different temperatures of the black hole and cosmological horizons, which is addressed through the introduction of an isothermal cavity. The investigation begins with the study of the Hayward black hole [93], sourced by an NED theory that does not adhere to the Maxwell weak-field limit [1], and continues with an examination of the Bardeen black hole [94], which shares this characteristic. The focus then shifts to the model studied in Ref. [95], which conforms to the Maxwell weak-field limit [2] and is referred to as the Cadoni *et al.* model throughout this thesis.

It is important to note that the above analysis is conducted at the semiclassical level. However, additional corrections to the entropy can be obtained through the one-loop effective action. As we will demonstrate, the entropy calculation yields the expected Bekenstein-Hawking entropy, as we are working within the framework of general relativity. We can explicitly compute the "non-geometric" corrections to the Bekenstein-Hawking entropy, which arise from fluctuations of fields on the background geometry [96, 97]. These corrections also correspond to the entanglement entropy of the relevant fields. In Ref. [10], not included as a paper in this thesis, we show that these corrections are contingent upon the value of the minimal length scale and the manner in which the singularity is smoothed out.

We examine the phase structure of these models, revealing the presence of a first-order phase transition between small and large black hole phases. In AdS spacetime, this transition is marked by the typical swallowtail behavior, similar to that observed in the Reissner–Nordström black hole. The first-order phase transitions terminate at a single critical point, characterized by a second-order phase transition. However, in dS spacetime, we identify a unique swallowtube behavior due to the presence of two critical points, with a compact region between them where first-order phase transitions occur. While the analysis shares similarities across these scenarios, variations in the weak-field limit result in varying degrees of metric function deformation compared to the Schwarzschild geometry. These variations lead to deviations of different magnitudes from the typical Van der Waals behavior [98], as reflected in the mean-field theory ratio, while the critical exponents align with mean-field theory values [2]. The extent of these deviations is inherently tied to the deformation strength, which is linked to how the singularity is resolved.

Finally, using the derived thermodynamic quantities and by imposing conditions of thermodynamic stability and the existence of a trapped region, we establish constraints on the minimal length scale parameter. In Ref. [95], it was demonstrated that there are significant deviations

in the orbits of test particles when compared to the Schwarzschild solution. Specifically, the corrections to the perihelion precession angle were found to scale linearly with the minimal length scale. The constraints we establish in Ref. [2] are consistent with the observational limits derived from the current data on the S2 star's orbit around Sagittarius A*, as reported in Ref. [95].

After examining the thermodynamic properties and phase structure of these models, we turn our attention to the observational signatures of nonsingular UCOs regularized by NED. The inherent nonlinearity of the theory gives rise to birefringence, where photons with different polarizations propagate according to distinct metrics. This phenomenon leads to the formation of additional light rings surrounding the UCO. These structures provide concrete theoretical predictions that could become testable once the Event Horizon Telescope — which produced the first image of a black hole — achieves the necessary resolution. This would provide a complementary avenue for testing not only the nature of UCOs but also NED theories, alongside the probes from collisions, neutron star observations, and cosmological data discussed earlier in this chapter. Therefore, we can assess the viability of this effective description and compare it with alternative methods for generating these geometries. Furthermore, our investigation extends to the causality features of these spacetimes, revealing that no acausal regions exist when the NED theory adheres to the Maxwell weak-field limit. Collectively, these studies offer a comprehensive understanding of how the minimal length scale influences both the thermodynamic and observational properties of RBHs.

The second part of the thesis is based on Refs. [4–6]. It begins with a summary of the self-consistent approach [4] employed to study dynamic RBHs, which belong to the $k = 0$ class of solutions, enhancing the reader's understanding in conjunction with this thesis introduction. We should note that a more complete and detailed description of this framework is provided in Ref. [37]. We analyze the metric function expansions near the outer apparent horizon of a PBH, which encompasses dynamic RBHs as a subset. Our findings show that particles can escape the supposedly trapped region, experiencing only finite tidal forces and energy densities, but only along ingoing geodesic trajectories where the contracting outer apparent horizon overtakes them. We then examine a specific case of RBHs, demonstrating that similar escape is possible, and further show that a particle initially in the untrapped region near the center can also enter the trapped region along an ingoing geodesic trajectory [5].

Furthermore, we analyze the dynamic evolution of RBHs, highlighting that the disappearance of the trapped region results in an extremal RBH at the end of the evaporation process. During this evolution, the trapped region is divided into domains where the NEC is violated and domains where it is satisfied. This phenomenon is a direct consequence of the evaporating nature of the horizon, as dictated by the self-consistent analysis employed. We find that the maximal NEC violation occurs near the outer apparent horizon and just before the trapped region vanishes, indicating that quantum effects become more pronounced towards the final stages of evaporation.

The finite formation time of the apparent horizon is closely linked to the evaporating character of both the inner and outer horizons. That said, alternative models for the evolution of RBHs have been proposed in the literature. Some of these retain the null nature of the outer horizon while allowing the inner horizon to undergo a bounce — changing from timelike to spacelike — a feature often interpreted as a manifestation of quantum gravity effects [99]. These models, though, typically neglect semiclassical effects that alter the nature of the outer apparent horizon, which we have accounted for in our approach [5]. In addition, other scenarios have been studied

in which black holes transition into white holes, rather than ending their evolution as regular remnants. These are often motivated by loop quantum gravity [100]. While such transitions can, in suitable regimes, be captured by our self-consistent framework [8], we focus here on black holes and do not explore the white hole case further in this thesis.

In the last part of this thesis, we extend our study to the thermodynamic properties in the dynamic regime [6]. We address the challenge of the absence of a Killing vector, which is essential for studying thermodynamics in static scenarios by employing its dynamic counterpart, the Kodama vector. This allows us to establish a first law of black hole mechanics similar to that of Ref. [101], but based solely on near-horizon quantities. We also show that the minimal length scale introduces additional terms in this law, which can be interpreted as pressure terms. The dynamical first law was first established by Hayward in Ref. [102] and further studied in Ref. [101]. While that formulation relies on energy conditions such as the null and dominant energy conditions, the former is violated in our self-consistent dynamical evolution of RBHs [5]. Nevertheless, the first law we derive remains directly analogous to that of Refs. [101, 102], with the added advantage of incorporating the backreaction from Hawking radiation — one of the key factors responsible for both the NEC violation near the outer horizon and the evaporation of the black hole.

The second part of this thesis primarily focuses on asymptotically Minkowski spacetime, where the behavior of dynamic RBHs is analyzed in detail. However, it is crucial to emphasize that the concept of PBHs — of which RBHs are a particular instance — extends far beyond the specific case of Minkowski spacetime. This broader framework for PBHs is rigorously developed in several key references, notably Refs. [7, 8], which, although not included in this thesis, provide significant insights into the subject.

In Ref. [7], we focus on establishing the boundary conditions necessary for embedding the PBH model in a cosmological background. This involves a detailed study of how PBHs, including RBHs, interact with and evolve in a dynamic, expanding universe. Additionally, we investigate the linear evaporating process of a PBH. In this context, the first law of black hole thermodynamics, which we derived in Ref. [6], emerges in a general form applicable to a wide range of black holes, including dynamic RBHs. This complies with the inclusion of RBHs within the broader PBH category of horizonful UCOs.

Having successfully established this comprehensive framework, we are now well-equipped to explore the behavior of PBHs in various cosmological settings. This includes studying their potential roles in cosmological backgrounds representing different epochs. By understanding PBHs in this broader context, we can gain deeper insights into both classical and quantum aspects of black hole physics and their implications for cosmology as a whole. Recent research has increasingly concentrated on the concept of cosmological coupling, leading to a debate over whether the masses of local objects, such as black holes, are influenced by large-scale cosmological dynamics. By utilizing the extended framework of PBHs within a cosmological spacetime, we are able to examine this issue. In Ref. [8], we demonstrate that PBHs do not directly couple to the cosmological background in the current epoch. This conclusion also applies to RBHs, as they are simply non-singular PBHs.

Together, the analyses of Refs. [1–6], included in this thesis, provide a comprehensive understanding of RBHs, spanning their static properties, thermodynamics, phase transitions, dynamic evolution, and energetic characteristics. This introduction sets the stage for the detailed

investigations and insights into the nature of these intriguing objects that follow in the thesis.

JOURNAL ARTICLE

Euclidean and Hamiltonian thermodynamics for regular black holes

Brief summary

The thesis begins with an examination of the thermodynamic properties of the Hayward RBH using an NED Lagrangian density $\mathcal{L}(\mathcal{F})$, which depends solely on the magnetic charge Q_m. Here, the field strength $\mathcal{F}$ is defined as $\mathcal{F} = F_{\mu\nu}F^{\mu\nu}$, where $F_{\mu\nu}$ is the electromagnetic tensor. This Lagrangian admits a weak-field limit that is stronger than the Maxwell limit. We use this RBH model to demonstrate consistency between Euclidean and Hamiltonian thermodynamics across asymptotically AdS, Minkowski, and dS spacetimes. Our findings establish a first law of black hole thermodynamics, a linear Smarr relation despite the theory's nonlinearity, and highlight the absence of a Hawking–Page transition in the canonical ensemble, attributed to the presence of a minimal length scale l.

Authorship statement

Conceptualization of the research project and calculations for its development. Also contributed to the planning and writing of the article, interpretation of its results, proofreading, and revisions. Principal contributor to Sections II, III, and Appendix. Conducted part of the calculations for Section IV, specifically in subsection IV.A and was also involved in figure creating.

Euclidean and Hamiltonian thermodynamics for regular black holes

Fil Simovic[*] and Ioannis Soranidis[†]

School of Mathematical and Physical Sciences, Macquarie University, Sydney, New South Wales 2109, Australia

(Received 22 September 2023; accepted 10 January 2024; published 20 February 2024)

We investigate the thermodynamic properties of the Hayward regular black hole using both Euclidean path integral and Hamiltonian methods, in asymptotically anti–de Sitter, Minkowski, and de Sitter spacetimes. With the inclusion of matter fields which act as a source for the regular black hole geometry, an effective temperature emerges that differs from the conventional definition related to the Killing surface gravity. We posit that this temperature is the appropriate choice for studying thermodynamic phenomena, by demonstrating consistency between the Euclidean and Hamiltonian formulations in the appropriate limits. We examine the thermodynamic properties and phase structure of the Hayward black hole in the canonical ensemble and show that, counter to some earlier indications, standard mean-field theory critical behavior is observed when the cosmological constant is treated as a thermodynamic pressure. We note the absence of a Hawking-Page transition, and conjecture that quantum gravity corrections which are suitably strong to regulate the Schwarzschild singularity generically prevent the transition from occurring. We also show that the Smarr relation remains linear in all cases, despite the absence of a linearity proof for nonlinear electrodynamic theories with nonsymmetry inheriting fields.

DOI: 10.1103/PhysRevD.109.044029

I. INTRODUCTION

The singular nature of classical black hole solutions in general relativity remains one of the most important yet obtrusive features of prototypical black hole models. Signaling a breakdown of the effective field theory description of quantum gravity near the Planck scale, such singularities are believed to be largely provisional. Yet, how exactly a tentative quantum theory of gravity regulates the singularity, whether such a smoothing procedure propagates its effects beyond the Planck scale, and whether indeed the singularity can be tamed without invoking sub-Planckian or quantum degrees of freedom, remain important open questions.

The smoothing of the central singularity is inextricably tied to energy conditions. The original Hawking-Penrose singularity theorems achieve the required geodesic focusing via the strong energy condition (SEC), so naturally early regular black hole models such as the Bardeen black hole precisely drop this assumption on the classical collapsing matter. Since it is known that both classical and quantum field theory can violate the strong energy condition, the singularity theorems have since been revisited in a number of forms using the averaged null energy condition, weak energy condition, and various quantum energy inequalities in place of the SEC. A host of regular black hole models that generally involve violation of one or more of these energy conditions have come about since the introduction of the Bardeen black hole [1], including phantom black holes [2], noncommutative black holes [3] and the Hayward model [4].

Among the available singularity-free black hole models, certain candidates distinguish themselves by being generated by classical matter distributions coupled minimally to Einstein-Hilbert gravity. In particular, the Bardeen and Hayward metrics (as well as various extensions) can be sourced by electric and/or magnetic charges in general relativity coupled to nonlinear electrodynamics [5,6]. The nonlinear electrodynamic (NED) Lagrangians involved remain important sources in the context of string theory and the study of various condensed matter systems (see Ref. [7] for a recent review).

The nature of how regular black holes (RBHs) are sourced at the classical level has led to widespread disagreement on how to properly formulate the laws of thermodynamics for RBHs. Whenever new parameters enter into the Lagrangian, extra terms ostensibly appear in the mechanical first law which do not always lend themselves to an obvious thermodynamic interpretation. Additionally, some approaches maintain that the entropy is the Bekenstein-Hawking result of $S = A/4$, while others argue that corrections to the entropy arise [8]. The issue becomes even more subtle in the case of the Hayward model, since properly incorporating matter fields (which are required to generate the geometry) in the first law is

[*]fil.simovic@mq.edu.au
[†]ioannis.soranidis@hdr.mq.edu.au

highly nontrivial. Understanding the thermodynamic properties of regular black hole solutions is also important for studying how regularization of the central singularity propagates into the classical sector, since these solutions can be viewed as classical approximations to a regularized geometry arising from quantum gravity theory. Especially in the asymptotically anti–de Sitter case, we expect important modifications to the dual gauge theory description in the context of the anti–de Sitter/conformal field theory correspondence (AdS/CFT) [9].

There are a variety of methods available for studying black hole thermodynamics which have been developed since the pioneering work of Bekenstein, Hawking, and collaborators [10]. Simply computing the entropy of a black hole may be done using the covariant phase space approach of Iyer and Wald [11], the Euclidean path integral of Gibbons and Hawking [12], the conical deficit formula of Susskind [13], various entanglement entropy computations [14], CFT techniques [15], and more. While all of these seem to reproduce the famous $S = A/4$ result for black holes in Einstein-Hilbert gravity, not all of these techniques and their associated first law constructions are equivalent, and not all can be applied in the same contexts. For the Hayward regular black hole, which is sourced by a gauge field with nonlinear Lagrangian, it is especially unclear which method should be preferred. Over the years, a number of investigations have been carried out using different methods. The Hayward-AdS model was studied previously in [5,16] using variables defined through a Hamiltonian variation of the Komar mass, though in the former case we believe an unsuitable choice of thermodynamic variables has led to an unexpected departure from the expected behavior of AdS black holes in the extended phase space. The asymptotically flat case was considered in [17], taking $S = A/4$ as a given and assuming a Gibbsian thermodynamic interpretation from the onset, though no mechanism was given for establishing thermodynamic equilibrium, so it is not clear what ensemble is being defined there. The case of general Λ was considered in [18] using a Euclidean approach, but only the action was computed and no further thermodynamic analysis was done.

In this paper we aim to shed light on this state of affairs and resolve some of the disagreement between various implementations of the thermodynamical laws for regular black holes. We consider the Hayward black hole model in asymptotically flat, anti–de Sitter, and de Sitter spacetimes, and attempt to demonstrate consistency between the Hamiltonian and Euclidean path integral formulations where direct comparisons between the methods are possible. Properly accounting for the variation of Λ, the correct definition of mass for the Hayward black hole, and accounting for the mechanisms required to establish equilibrium for different asymptotic behavior, we examine the phase structure and thermodynamic stability of the various solutions. In the AdS case, our work differs from that of [5,16] in the choice of thermodynamic parameters, which in the former we believe have been incorrectly identified. As a result, we are able to show that the Hayward-AdS black hole does indeed possess the expected mean-field theory critical exponents.

This paper is organized as follows: in Sec. II we describe the general structure of NED theories, and demonstrate how the Hayward model arises, including its properties, source, and de Sitter embedding. In Sec. III, we discuss how the first law of black hole thermodynamics and Smarr relation apply to regular black holes and demonstrate consistency between Hamiltonian and Euclidean path integral frameworks. In Sec. IV we analyze the phase structure of the Hayward model. Specifically, in Sec. IV A we study the Hayward-AdS black hole, examining its thermodynamic stability, phase structure, and behavior near the critical point and in Secs. IV B and IV C we consider the asymptotically Minkowski and de Sitter cases, respectively. We conclude in Sec. V with a discussion of the main results and implications for future investigations. Throughout, we work in $d = 4$ and units where $\hbar = c = G = 1$ are used unless otherwise noted.

II. NON-LINEAR ELECTRODYNAMICS

Regular black hole geometries generically require additional matter fields to source their nonsingular metrics, with the first example of an exact solution being given by [19] using a nonlinear electrodynamic (NED) source. That NED can generate other well-known regular geometries was later demonstrated for the Bardeen black hole in [6] and further generalized to a variety of two-parameter families of spherically symmetric RBHs solutions in [20]. The geometry and dynamics are determined by the action of the given NED theory, which in the presence of a cosmological constant Λ has the general form

$$I = \frac{1}{16\pi}\int d^4x\sqrt{-g}[R - 2\Lambda + 4\mathcal{L}(\mathcal{F},\mathcal{G})], \tag{1}$$

where $g = \det g_{\mu\nu}$, R is the Ricci scalar, and $\mathcal{L}(\mathcal{F},\mathcal{G})$ is the Lagrangian density of the NED theory under consideration. $\mathcal{L}$ is a function of two electromagnetic invariants $\mathcal{F} \equiv F^{\mu\nu}F_{\mu\nu}$ and $\mathcal{G} \equiv F_{\mu\nu} \star F^{\mu\nu}$, which are functions of the field strength tensor $F_{\mu\nu} = \partial_\mu A_\nu - \partial_\nu A_\mu$. It may also be a function of a finite number of additional real parameters $\{\beta_i\}$. An auxiliary two-form can be defined as

$$Z_{\mu\nu} \equiv -4\left(\frac{\partial\mathcal{L}}{\partial\mathcal{F}}F_{\mu\nu} + \frac{\partial\mathcal{L}}{\partial\mathcal{G}} \star F_{\mu\nu}\right), \tag{2}$$

so that the equations of motion of the theory are the generalized source-free Einstein-Maxwell equations

$$G_{\mu\nu} = 8\pi T_{\mu\nu}, \qquad dF = 0, \qquad d \star Z = 0. \tag{3}$$

The Maxwell case corresponds to $\mathcal{L}(\mathcal{F},\mathcal{G})=\mathcal{L}(\mathcal{F})=-\mathcal{F}/4$. In general, the NED theory defined by (1) can possess both electric and magnetic charges, with the existence of an electromagnetic duality $F \to \star F$ being tied to the existence of a Maxwell limit. The electric and magnetic charges are defined, respectively, as Komar integrals over a smooth closed 2-surface $\mathcal{S}$ as

$$Q_e \equiv \frac{1}{4\pi}\int_{\mathcal{S}} \star Z, \qquad Q_m \equiv \frac{1}{4\pi}\int_{\mathcal{S}} F, \tag{4}$$

although many models can be generated by either electric or magnetic charge alone. For Lagrangians which have a Maxwellian weak-field limit, solutions *must* be sourced entirely by magnetic charge, with electrically sourced solutions generically requiring a different form of Lagrangian in the near and far regions [21]. A subclass of NED theories defined by (1) possess invariance under an electromagnetic duality transformation by

$$\begin{aligned} F &\to F\cos\alpha + \star Z \sin\alpha, \\ Z &\to Z\cos\alpha + \star F \sin\alpha, \end{aligned} \tag{5}$$

examples of which are Born-Infeld [22], ModMax [23], and power-Maxwell theories [24] along with standard Maxwell electrodynamics. The existence of such a duality is important for establishing linearity of the Smarr relation for such theories [25], while theories without the duality may exhibit nonlinear Smarr relations instead. These NED theories remain of broad theoretical interest for many reasons, having been introduced to regularize the classical divergences associated with point charges, and also arising as high-energy corrections to standard electrodynamics from more fundamental theories.

A. The Hayward model

One particularly important example of a geometry generated by NED theory is the Hayward regular black hole [4]. Regular black holes are of themselves of significant theoretical interest, representing classical black hole geometries with no central singularity. This is a highly nontrivial condition that entails finiteness of all algebraic curvature invariants at the center as well as flatness. A necessary requirement for regularity at the center is the existence of a de Sitter or anti–de Sitter core. The usual $r=0$ singularity common to textbook black hole solutions to general relativity signals a breakdown of the effective field theory description of general relativity and is expected to be resolved by an appropriate quantum theory of gravity. Classical regular black hole solutions therefore represent a first-order approximation to the geometry that results from whatever regularization procedure inevitably smooths the central singularity. It is therefore of significant theoretical interest to study the properties of regular black hole solutions. The Hayward model represents one such solution, and can be generated from the following Lagrangian density

$$\mathcal{L}(\mathcal{F}) = \frac{12}{\alpha}\frac{(\alpha\mathcal{F})^{3/2}}{(1+(\alpha\mathcal{F})^{3/4})^2}, \tag{6}$$

where α is one of the free parameters of the theory [20]. This theory is independent of $\mathcal{G}$ and possesses only magnetic charge. The vector potential is given explicitly by

$$A_\mu = (0,0,0,Q_m\cos\theta), \tag{7}$$

and the variation of the action (1) leads to

$$G_{\mu\nu} = 8\pi T_{\mu\nu} \quad \text{and} \quad \nabla_\mu\left(\frac{\partial\mathcal{L}}{\partial\mathcal{F}}F^{\mu\nu}\right) = 0, \tag{8}$$

where $G_{\mu\nu}$ is the Einstein tensor in the presence of a cosmological constant and the source term $T_{\mu\nu}$ is given by

$$T_{\mu\nu} = \frac{1}{4\pi}\left(\frac{\partial\mathcal{L}}{\partial\mathcal{F}}F_{\mu\lambda}F^{\lambda}_{\nu} - \frac{1}{4}g_{\mu\nu}\mathcal{L}\right). \tag{9}$$

The equations of motion admit a spherically symmetric geometry

$$ds^2 = -f(r)dt^2 + \frac{dr^2}{f(r)} + r^2 d\Omega_2, \tag{10}$$

where $d\Omega_2$ is the metric on $\mathcal{S}^2$ and the metric function $f(r)$ is given by

$$f(r) = 1 - \frac{2\alpha^{-1}q^3r^2}{r^3+q^3} - \frac{\Lambda}{3}r^2, \tag{11}$$

where Λ is the cosmological constant, and q is an integration constant related to the magnetic charge Q_m and coupling α of the theory through

$$Q_m = \frac{q^2}{\sqrt{2\alpha}}. \tag{12}$$

In the notation of [4], the metric function of the regular spherically symmetric geometry is given by

$$f(r) = 1 - \frac{2mr^2}{r^3+2ml^2} - \frac{\Lambda}{3}r^2, \tag{13}$$

where m is the mass parameter and l is a minimal length scale characterizing the size of the regular center. When $l \to 0$ this reduces to the Schwarzschild-anti-de Sitter (or -de Sitter) metric. Direct comparison to (11) allows one to identify q and α appearing in the NED metric as [26,27]

$$\alpha = 2l^2 \quad \text{and} \quad q^3 = 2ml^2. \tag{14}$$

Therefore the regularization of the central singularity, which is characterized by a minimal length scale l, can be given an effective description in terms of a nonlinear electromagnetic field sourced by magnetic charge.

A few comments are warranted concerning the Hayward model (13). First, the solution is sourced entirely by magnetic charge, which to date has not been observed in the Universe despite a number of significant observational efforts [28,29]. Nonetheless, heavy magnetic monopoles which form in the early Universe remain a generic prediction of grand unified theories [30–32], where they arise from spontaneous symmetry breaking at the GUT scale $\sim 10^{16}$ GeV, and have important implications for structure formation and early Universe cosmology (see Ref. [33] for a review). Second, one may readily observe that in the weak-field limit the Lagrangian (6) does not approach the Maxwell limit but rather $\mathcal{L} \sim \sqrt{\alpha}\mathcal{F}^{3/2}$ which is stronger than the Maxwell field. While this feature is somewhat unattractive, the Hayward model nonetheless represents one of the very few available classical regular black hole geometries that one can use to model quantum gravity effects on the central singularity, since there are strict no-go theorems which forbid regular geometries in ordinary Einstein-Maxwell theory. Furthermore, nonlinear theories with pure electric source that have a Maxwell weak-field limit are also known to not admit solutions with regular center [34]. The magnetically sourced Hayward model therefore serves as an extremely useful and minimal prototype model of a regular black hole.

In what follows we use the metric in the form of (13), considering the minimal length l as a more fundamental parameter than q and α, which arise in just one of a distinct number of ways to generate the same geometry. This is in contrast to earlier work on the Hayward-AdS black hole [5], whose results we regard with caution. Their work has treated Q_m and α (σ in their notation) as two independent parameters, when there is in fact only one (which we recast in terms of l) since Q_m depends only on α and the ADM mass m. The previous work does not identify m as the ADM mass, though it must be the case as pointed out initially by [35].

III. FIRST LAW AND SMARR FORMULA

A. Hamiltonian methods

The first law of black hole mechanics occupies a significant portion of the theoretical physics landscape. First derived in [10] as a relation between variations of the physical parameters describing a black hole in Einstein gravity, an analogous relation has since been shown to hold in any theory of gravity arising from a diffeomorphism-invariant Lagrangian [11,36]. The generalization of the first law to nonlinear electrodynamics was first studied in [37], although the Smarr formula [38] was not found to be satisfied. This was later addressed in [39] by appropriately accounting for the extra parameters appearing in the NED theory. The result is a relation resembling the ordinary first law with additional terms:

$$dM = TdS + \Phi dQ_e + \Psi_H dQ_m + \sum_i K_i d\beta_i. \quad (15)$$

In the above, M is the Komar mass [40] which coincides with the ADM mass [41] in asymptotically flat spacetimes, T is the Hawking temperature (as determined the surface gravity κ through $T = \kappa/2\pi$), $S = A/4$ is the entropy, and $\{\Phi, \Psi_H\}$ are the electric and magnetic potentials associated with the electric and magnetic charges $\{Q_e, Q_m\}$. The terms K_i represent the potentials conjugate to the parameters β_i of the theory. In [39], these quantities are explicitly computed for the Bardeen black hole and black hole solutions in Born-Infeld theory. The Smarr relation was also shown to hold for both cases.

Using the definitions of [39], we explicitly compute the thermodynamic quantities entering the first law for the Hayward black hole, both in the presence and absence of a cosmological constant Λ. The cosmological constant, when treated as an independently varying parameter, naturally enters into the first law as a work term VdP with the identification $P = -\Lambda/8\pi$. In this extended phase space, the thermodynamic volume V appears naturally conjugate to variations in P [42] and the mass M is identified as a thermodynamic enthalpy [43]. The variation of P, and therefore Λ, arises naturally in a consistent variational principle [44], and can acquire a dynamical status through a 3-form gauge potential as in the Brown-Teitelboim mechanism [45]. The minimal length l is also treated as a variable parameter, on the basis that it emerges in more fundamental theories from vacuum expectation values of the elementary fields [46,47], and when back-reaction of the evaporation process is accounted for [48–50]. The variation of these additional parameters is also required to establish the correct Smarr relation [42,51], which is widely believed to be universal and arises from quite general scaling arguments.

We proceed with the explicit calculation of the quantities of the first law in the case of Hayward black hole embedded in a spacetime with a cosmological constant. In our case there is only a single additional parameter $\{\beta_i\} = \alpha$ appearing in (15), along with its conjugate potential K_α. The first law therefore becomes

$$dM = TdS + \Psi_H dQ_m + K_\alpha d\alpha + VdP. \quad (16)$$

The mass parameter can be written in terms of the event horizon radius r_h as

$$m = \frac{3r_h^3 - \Lambda r_h^5}{6r_h^2 - 2l^2(3 - \Lambda r_h^2)}, \quad (17)$$

so that (13) can be expressed as

$$f(r) = 1 - \frac{r^2 r_h^3 (3 - \Lambda r_h^2)}{3r^3 r_h^2 - l^2(3 - \Lambda r_h^2)(r^3 - r_h^3)}, \tag{18}$$

where r_h is the outermost real root of $f(r) = 0$ (unless $\Lambda > 0$). The Hawking temperature T is determined by the Killing surface gravity κ as

$$T = \frac{\kappa}{2\pi} = \frac{f'(r)}{8\pi}\bigg|_{r=r_h} = \frac{3r_h^2(1 - r_h^2\Lambda) - l^2(3 - r_h^2\Lambda)^2}{12\pi r_h^3}, \tag{19}$$

and the entropy is simply $S = A/4 = \pi r_h^2$ [52–54]. Since the spacetime is static, it admits a Killing vector $\xi^\mu = \partial_t$ through which the magnetic field H_μ is defined

$$H_\mu = - \star B_{\mu\nu}\xi^\nu, \tag{20}$$

where

$$\star B_{\mu\nu} = \frac{1}{2}\epsilon_{\mu\nu\rho\sigma}B^{\rho\sigma} \quad \text{and} \quad B^{\mu\nu} = \mathcal{L}'(\mathcal{F})F^{\mu\nu}, \tag{21}$$

with $\epsilon_{\mu\nu\rho\sigma}$ being the volume form. The magnetic potential Φ is related to the magnetic field through

$$H_\mu = \nabla_\mu \Psi, \tag{22}$$

whose integration along with the boundary condition $\lim_{r\to\infty} \Psi_H = 0$ gives

$$\Psi(r) = \frac{3q^4(2r^3 + q^3)}{\sqrt{2\alpha}(r^3 + q^3)^2}. \tag{23}$$

The quantity Ψ_H appearing in the first law is then simply $\Psi(r)$ evaluated on the horizon $r = r_h$. Finally, the conjugate potential K_α associated with the parameter α is given by [37,39]

$$K_\alpha = \frac{1}{4}\int_{r_h}^{\infty} r^2 \frac{\partial \mathcal{L}}{\partial \alpha}, \tag{24}$$

which upon integration gives

$$K_\alpha = \frac{6q^6(-2q^3 + r_h^3)}{4\alpha^2(r_h^3 + q^3)^2}. \tag{25}$$

Finally, the geometric volume is $V = 4\pi r_h^3/3$. It can be shown [55] that these quantities satisfy a linear Smarr relation

$$M = 2TS + \Psi_H Q_m + 2K_\alpha \alpha - 2PV, \tag{26}$$

where M is again the Komar mass. We will now rewrite the first law and Smarr relation solely in terms of the physically relevant parameters i.e. the horizon area A, the minimal length l and the cosmological constant Λ, instead of the parameters (Q_m, α, P) that appear in (16). We have that

$$Q_m = \frac{Al^{1/3}}{8\pi}\left(\frac{12\pi + 8\pi AP}{3A - 12\pi l^2 - 8\pi A l^2 P}\right), \tag{27}$$

and

$$\alpha = 2l^2, \tag{28}$$

with their differentials being given by

$$dQ_m = \frac{\partial Q_m}{\partial A}dA + \frac{\partial Q_m}{\partial l}dl + \frac{\partial Q_m}{\partial P}dP, \tag{29}$$

$$d\alpha = \frac{\partial \alpha}{\partial A}dA + \frac{\partial \alpha}{\partial l}dl + \frac{\partial \alpha}{\partial P}dP. \tag{30}$$

This gives the following form of modified first law

$$dM = \tilde{T}dS + \tilde{\Phi}dl + \tilde{V}dP, \tag{31}$$

where an effective temperature $\tilde{T}$ given by

$$\tilde{T} = T + 4\Psi_H \frac{\partial Q_m}{\partial A}, \tag{32}$$

naturally emerges, along with an effective potential $\tilde{\Phi}$ associated with the minimal length

$$\tilde{\Phi} = \Psi_H \frac{\partial Q_m}{\partial l} + K_\alpha \frac{\partial \alpha}{\partial l}, \tag{33}$$

and an effective thermodynamic volume $\tilde{V}$

$$\tilde{V} = V + \Psi_H \frac{\partial Q_m}{\partial P}, \tag{34}$$

where $V = 4\pi r_h^3/3$. These effective quantities also define a proper Smarr relation

$$M = 2\tilde{T}S + \tilde{\Phi}l - 2\tilde{V}P, \tag{35}$$

with the appropriate scaling invariance [42] under

$$\begin{aligned} &M \to cM, \quad l \to cl, \quad r_h \to cr_h, \quad P \to c^{-2}P, \\ &S \to cS^2, \quad \tilde{T} \to c^{-1}\tilde{T}, \quad \tilde{\Phi} \to \tilde{\Phi}, \quad \tilde{V} \to c^3\tilde{V}. \end{aligned} \tag{36}$$

Linearity of the Smarr relation is intimately tied to the symmetry inheritance properties of the gauge fields present in the theory. It is often assumed that if the underlying metric g possesses a symmetry $\mathcal{L}_\xi g_{ab} = 0$ generated by a Killing field ξ, the electromagnetic field will inherit the same symmetry, i.e. $\mathcal{L}_\xi F_{ab} = 0$. In $d = 4$ Einstein-Maxwell theory there are known counterexamples to this

assumption, as seen in certain classes of Bianchi type-V metrics [56] and pp-wave metrics [57], a phenomenon which extends to other symmetries such as the conformal group in multifluid spacetimes [58]. The symmetry inheritance property of the field is important for establishing constancy of the electromagnetic potential on the Killing horizon, and is also required for establishing linearity of the Smarr relation, as was done in [59]. In our case the gauge field does *not* inherit the symmetry of the spacetime, with $\mathcal{L}_{\xi_\theta} g = 0$ but $\mathcal{L}_{\xi_\theta} A^\mu \neq 0$, yet the Smarr relation remains linear. This suggests the condition presented in [59] may be sufficient but not necessary for linearity of the Smarr relation.

The explicit form of the quantities appearing in (31) are given below. The effective temperature is

$$\tilde{T} = \frac{3r_h(3r_h^2 - 3r_h^4\Lambda - l^2(-3 + r_h^2\Lambda)^2)}{4\pi(3r_h^2 + l^2(-3 + r_h^2\Lambda))^2}, \tag{37}$$

which is evidently different from the temperature (19) defined through the surface gravity, though they are simply related through

$$\tilde{T} = \frac{T}{\left(1 - \frac{l^2}{r_h^2}\left(1 - \frac{\Lambda}{3} r_h^2\right)\right)^2}. \tag{38}$$

The difference between the two arises from how one treats the contribution to the total energy variation of the first law arising from the matter, which may or may not be thermalized with respect to the Killing time. When matter is present, the entropy variation conjugate to the surface gravity κ does not necessarily refer only to the geometric entropy of the black hole, and requiring it to do so is accompanied by a modification of the conjugate temperature. The root cause arises from an ambiguity in the splitting of the Lagrangian into a geometric and matter contribution, which is manifest in the covariant formalism [60]. A similar modification can occur, for example, when scalar fields are present which do not minimally couple to gravity, as recently observed in $d = 4$ Gauss-Bonnet gravity [61]. When the minimal length vanishes however, the effective temperature and the surface gravity temperature coincide, as expected since in this limit the matter contribution to the total Lagrangian vanishes. The two remaining potentials are given by

$$\tilde{\Phi} = \frac{l r_h^3(-3 + \Lambda r_h^2)^2}{(3r_h^2 + l^2(-3 + \Lambda r_h^2))^2}, \tag{39}$$

$$\tilde{V} = \frac{12 r_h^7}{(3r_h^2 + l^2(-3 + \Lambda r_h^2))^2}. \tag{40}$$

Note that the same version of the first law (31) is obtained if one uses the fact that $Q_m = Q_m(m, l)$ and $\alpha = \alpha(l)$ through (12) and (14), giving

$$\begin{aligned} dM &= TdS + VdP + \Psi_H dQ_m + K_\alpha d\alpha \\ &= TdS + VdP + \left(\Psi_H \frac{\partial Q_m}{\partial m}\right) dm \\ &\quad + \left(\frac{\partial Q_m}{\partial l} + K_\alpha \frac{\partial \alpha}{\partial l}\right) dl. \end{aligned} \tag{41}$$

Now observing that for the Hayward metric, m is in fact equal to the ADM/Komar mass M appearing on the left-hand side of (16), one has that the variation of the mass satisfies

$$\begin{aligned} dM &= \left(\frac{T}{1 - \Psi_H \frac{\partial Q_m}{\partial m}}\right) dS + \left(\frac{V}{1 - \Psi_H \frac{\partial Q_m}{\partial m}}\right) dP \\ &\quad + \left(\frac{\frac{\partial Q_m}{\partial l} + K_\alpha \frac{\partial \alpha}{\partial l}}{1 - \Psi_H \frac{\partial Q_m}{\partial m}}\right) dl. \end{aligned} \tag{42}$$

where the quantities in brackets will be the same as the effective quantities appearing in (31).

B. Euclidean path integral methods

We will now elaborate on the relationship between the thermodynamic variables obtained from the Hamiltonian version of the first law above and another commonly employed method for understanding black hole thermodynamic—the Euclidean path integral. Developed by Gibbons and Hawking [12] and extended by York [62,63], this method has a basis in the fundamental relationship between the partition function $\mathcal{Z}$ of general quantum systems and the Euclidean path integral. The partition function for a continuous quantum system defined by canonical variables $\{q_i\}$ with Hamiltonian H at finite temperature $T = \beta^{-1}$ is

$$\mathcal{Z} = \int dq_i \langle q_i | e^{-\beta H} | q_i \rangle,$$

from which thermodynamic quantities for the statistical ensemble can be readily determined as

$$F = -T \ln \mathcal{Z}, \quad E = -\frac{\partial \ln \mathcal{Z}}{\partial \beta}, \quad S = -\beta \frac{\partial \ln \mathcal{Z}}{\partial \beta} + \ln \mathcal{Z}. \tag{43}$$

In the context of gravity, $\mathcal{Z}$ is formally given by an intractable path integral over an ill-defined measure $\mathcal{D}[g]$ which includes contributions from both matter and gravitational degrees of freedom. The partition function can however be computed in a semiclassical saddle-point approximation where

$$\mathcal{Z} = \int_{g(0)}^{g(\tau)} \mathcal{D}[g] e^{-I_E[g]} \approx \sum_{g_{cl}} e^{-I_E[g_{cl}]},$$

where $I_E[g]$ is the Euclidean action of the metric g, and $I_E[g_{cl}]$ is the saddle-point contribution from the Euclidean

metrics g_{cl} which solve the classical equations of motion and obey the prescribed boundary conditions.[1] The periodicity in τ implements the trace from (43) and encodes the Kubo-Martin-Schwinger (KMS) condition for finite-temperature fields [65,66]. We work in an on-shell spherical reduction, where the periodicity is naturally fixed to remove a would-be conical singularity at the origin of the Euclidean section (the black hole event horizon):

$$\beta^{-1} = \frac{\kappa}{2\pi}. \tag{44}$$

This method of computing thermodynamic quantities is particularly advantageous for black holes in de Sitter space, because one can fix boundary-value data (in our case the temperature) on a surface at some finite radius r_c between the black hole and cosmological horizons, and compute $\mathcal{Z}$ by performing the direct (now finite) integration. This physically corresponds to placing the black hole in an isothermal cavity, where the temperature at the cavity is fixed to be

$$\beta_c^{-1} = \frac{\kappa}{2\pi\sqrt{f(r_c)}}, \tag{45}$$

which is just the locally observed KMS temperature at r_c. This method has been applied to a wide variety of black hole spacetimes where a thermodynamic landscape comparably rich to that of AdS has been revealed [67–70]. In the case of the Hayward black hole model considered in this work we require the total reduced Euclidean action I_r for the Einstein-Hilbert-NED theory, given by

$$I_r = I_{\rm EH} + I_{\rm GHY} + I_M + I_{\rm EMB} - I_0, \tag{46}$$

where $I_{\rm EH}$ is the Einstein-Hilbert action, $I_{\rm GHY}$ the Gibbons-Hawking-York boundary term, I_M is the Euclidean action for any matter fields present, $I_{\rm EMB}$ is an electromagnetic boundary term required to fix the charge, and I_0 is a subtraction term which serves to regularize the infinite volume integral for a spacetime without boundary. Explicit calculation of each term can be found in the Appendix B. The individual terms are defined as

$$I_{\rm EH} = -\frac{1}{16\pi}\int_{\mathcal{M}} d^4x\sqrt{g}(R-2\Lambda), \tag{47}$$

$$I_{\rm GHY} = \frac{1}{8\pi}\int_{\partial\mathcal{M}} d^3x\sqrt{k}K, \tag{48}$$

where K is the trace of the extrinsic curvature of the spherical boundary $\partial\mathcal{M}$ at r_c and k is the determinant of the boundary metric,

$$I_M = \frac{1}{16\pi}\int_{\mathcal{M}} d^4x\sqrt{g}\mathcal{L}(\mathcal{F}), \tag{49}$$

is the matter action,

$$I_{\rm EMB} = -\frac{1}{16\pi}\int_{\partial\mathcal{M}} d^3x\sqrt{k}\left(\frac{\partial\mathcal{L}}{\partial\mathcal{F}}\right)F^{\mu\nu}n_\nu A_\mu, \tag{50}$$

is an electromagnetic boundary term which fixes the charge in the canonical ensemble, and the subtraction term I_0 is simply the total reduced action evaluated for the empty spacetime (Minkowski, AdS, or dS space, depending on which asymptotics are assumed). In asymptotically flat or AdS space this term removes the divergent part of the volume integral. In the case where the integration is cut at a finite boundary no such divergence appears, and instead I_0 simply normalizes the action such that $I_r = 0$ for the empty spacetime. After combining the terms and performing the required integrations, we find that total reduced action is given by

$$I_r = -\pi r_h^2 + \frac{\beta r_c}{3}\left(3 - r_c^2\Lambda - \sqrt{3-\Lambda r_c^2}\mathcal{X}\right), \tag{51}$$

where

$$\mathcal{X} \equiv \sqrt{\frac{(3-\Lambda r_c^2)\mathcal{Y} - 9r_c^2r_h^2\left(r_c - r_h - \frac{\Lambda}{3}(r_c^3+r_h^3)\right)}{\mathcal{Y} - 3r_c^3r_h^2}}, \tag{52}$$

and

$$\mathcal{Y} \equiv l^2(r_c^3 - r_h^3)(r_h^2\Lambda - 3). \tag{53}$$

The β-independent term ensures that the correct entropy is obtained from Eq. (43) which reduces to,

$$S = \beta\frac{\partial I_r}{\partial\beta} - I_r = \pi r_h^2. \tag{54}$$

The equilibrium temperature can be obtained by extremizing the action with respect to r_h and solving for β,

$$\frac{\partial I_r}{\partial r_h} = 0, \tag{55}$$

which gives a temperature $\mathcal{T} = \beta^{-1}$ of

$$\mathcal{T} = \frac{3r_c^6\sqrt{3-r_c^2\Lambda}(3r_h^3(1-r_h^2\Lambda) - l^2r_h(r_h^2\Lambda-3)^2)}{4\pi(3r_c^3r_h^2+\mathcal{Y}))^2\mathcal{X}}. \tag{56}$$

If there is no cosmological horizon then one can take the limit $r_c \to \infty$ and the above relation for $\mathcal{T}$ reduces to the effective temperature $\tilde{T}$ defined in Eq. (37). The mean thermal energy is

$$E = \frac{\partial I_r}{\partial\beta} = \frac{r_c}{3}\left(3 - r_c^2\Lambda - \sqrt{3-\Lambda r_c^2}\mathcal{X}\right), \tag{57}$$

[1]As discussed in [64], there are subtleties involved in this approximation which should be treated carefully.

and the potentials conjugate to l and Λ can be obtained by the variations

$$\varphi = \frac{1}{\beta}\frac{\partial I_r}{\partial l}, \qquad \mathcal{V} = -\frac{8\pi}{\beta}\frac{\partial I_r}{\partial \Lambda}, \tag{58}$$

which give

$$\varphi = \frac{l r_c^3 r_h^3 (r_c^3 - r_h^3)\sqrt{3 - r_c^2\Lambda}(-3 + r_h^2\Lambda)^2}{(3 r_c^3 r_h^2 + l^2(r_c^3 - r_h^3)(-3 + r_h^2\Lambda))^2 \mathcal{X}}, \tag{59}$$

and

$$\mathcal{V} = \frac{8\pi r_c^3}{3}\left(1 + \frac{\sqrt{3 - \Lambda r_c^2}\mathcal{X}'}{r_c^2} - \frac{\mathcal{X}}{2\sqrt{3 - \Lambda r_c^2}}\right), \tag{60}$$

where a prime denotes a derivative with respect to Λ. For asymptotically flat ($\Lambda = 0$) or anti–de Sitter ($\Lambda < 0$) spacetimes, one can take the limit $r_c \to \infty$ and find that φ and $\mathcal{V}$ coincide with $\tilde{\Phi}$ and $\tilde{V}$, which are respectively given by Eqs. (39) and (40), demonstrating that the Euclidean formulation is consistent with the Hamiltonian one used in the AdS case, in the regime where the two methods are comparable. The Euclidean formulation is however more broadly applicable since it can be implemented for any standard choice of asymptotics, while the Hamiltonian formulation requires a Killing vector field which is timelike in the asymptotic region to associate the conserved energy with.

In the presence of a cavity, and additional work term λdA_c enters into the first law relating the cavity tension λ and variations of its area A_c [63]. The tension λ is determined through

$$\lambda = \frac{1}{\beta}\frac{\partial I_r}{\partial A_c}, \tag{61}$$

and is given in Appendix C. With the quantities above, the following form of the Smarr relation is satisfied

$$E = 2\mathcal{T}S + \varphi l + 2\lambda A_c - 2P\mathcal{V}. \tag{62}$$

Note that the thermal energy E and the mass M are not equal except in the limit when $r_c \to \infty$. We now argue that the correct choice of thermodynamic variables entering the first law for the Hayward solution are the ones given above, based on their agreement with the quantities computed from the Hamiltonian construction (when appropriate limits can be taken to sensibly relate the two). As there are a number of different frameworks available for computing thermodynamic quantities associated with black hole spacetimes, a natural question is whether one should expect the Euclidean path integral method of Gibbons and Hawking to agree with a Hamiltonian formulation in the first place. This has been discussed previously by Iyer and Wald [71], who showed that the covariant phase space construction of the first law (under which the Hamiltonian form originally given by [10] is subsumed) is equivalent to a Euclidean path integral formulation based on the semiclassical approximation to the partition function, provided that the Lagrangian is at most linear in the curvature.

IV. HAYWARD PHASE STRUCTURE

A. Anti–de Sitter $\Lambda < 0$

Asymptotically anti–de Sitter black holes readily admit a thermodynamic interpretation owing to the confining effective potential of anti–de Sitter space. Free particles (both massive and massless) follow periodic closed orbits in an AdS background, so Hawking radiation from a black hole is naturally confined provided reflecting boundary conditions are imposed at the timelike boundary. Therefore, subtleties in determining when/if thermodynamic equilibrium is achieved by a large black hole are avoided since one can simply assume that sufficient time has passed for the outgoing radiation to equilibrate with the black hole (provided it is sufficiently large compared to the AdS length scale). It has long been known that the unique boundary conditions of anti–de Sitter space allow for a gauge-gravity duality relating quantum gravity theory in the bulk of AdS to a conformal field theory on the boundary of AdS. This is the basis of the anti–de Sitter/conformal field theory correspondence, which has proven to be both extremely useful in practical computations and of great theoretical importance. The prototypical example is the exact correspondence between type IIB string theory in the bulk and $\mathcal{N} = 4$ super-Yang Mills theory on the boundary [9]. The study of bulk gravitational physics in asymptotically AdS spacetimes is therefore of direct relevance for the study of strongly coupled gauge theories [72].

It is in this asymptotically anti–de Sitter context that the well-known Hawking-Page [73] transition occurs: at low temperature a would-be small black hole will simply evaporate, and the AdS space is eventually filled with free radiation. A sufficiently large black hole however will persist long enough to come into equilibrium with its own Hawking radiation, which returns from the boundary in finite time. There is a critical temperature T_c separating these two regimes at which the Hawking-Page transition occurs. Note that unlike asymptotically flat black holes, the temperature of asymptotically AdS black holes does not monotonically decrease with the size of the black hole. This Hawking-Page transition corresponds to a deconfinement transition in the boundary CFT, and has long been studied to understand nonperturbative features of strongly coupled CFT systems and the black hole information problem [74,75].

We would like to examine whether this transition persists when the central singularity is absent in the classical metric, and whether new types of transitions appear. The phase

structure of the Hayward-AdS black hole can be determined through the Gibbs free energy $G = M - \tilde{T}S$, which is globally minimized by the equilibrium state of the system. Using (17) and (37), the free energy is

$$G = \frac{l^2 r_h^3(\Lambda r_h^2 - 3)^2 + 3r_h^5(\Lambda r_h^2 + 3)}{4(l^2(\Lambda r_h^2 - 3) + 3r_h^2)^2}, \tag{63}$$

which can be plotted parametrically as a function of the equilibrium temperature $\tilde{T}$ using r_h as a parameter. The result is shown in Fig. 1.

Two characteristically distinct behaviors are revealed in Fig. 1 depending on the value of the cosmological constant Λ and the regularization length scale l. For fixed $\Lambda = -0.04$, there is a critical length scale $l_c \approx 0.35$ below

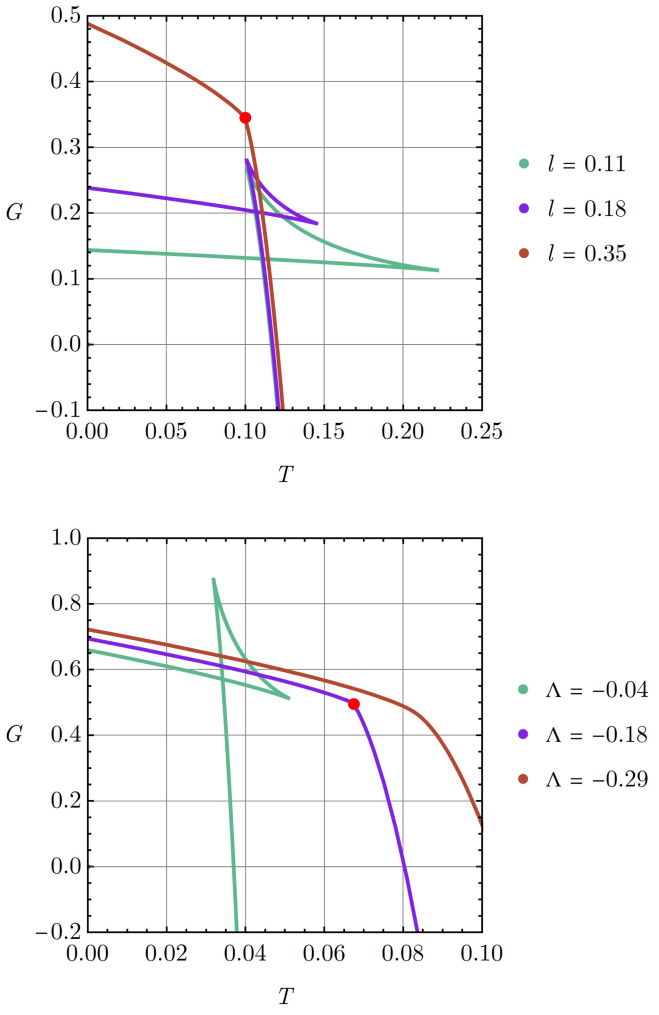

FIG. 1. Gibbs free energy G as a function of temperature T for the Hayward-AdS black hole. The horizon size r_h increases in the direction of the arrows. Top: fixed $\Lambda = -0.04$ for various l. The onset of a first-order phase transition from a small to large black hole is marked by a red dot at the critical temperature $T_c \sim 0.1$. Bottom: fixed $l = 0.5$ for various Λ. The critical temperature occurs at $T_c \sim 0.68$.

which a first-order phase transition from a small to large black hole occurs. Likewise when l is fixed, there is a critical Λ_c below which a similar transition is present. Above both critical values there is no phase transition, while at the critical point the transition becomes second-order (the precise location of the critical points for variable l and Λ is determined below). This is reminiscent of the small-large transition observed previously in Reissner-Nordstrom-AdS black holes [70]. Although the small black hole phase has greater free energy than the radiation phase at $G = 0$, the would-be Hawking-Page transition does not occur since the system is in a fixed-charge (canonical) ensemble. Unlike the Reissner-Nordstrom case however, the presence of charge here is tied directly to the existence of a minimal length scale. The radiation phase is inaccessible as long as $Q_m > 0$ which through (14) corresponds to $l > 0$. Therefore, the presence of a quantum gravity regulator of the Schwarzschild singularity appears to prevent the Hawking-Page transition from occurring.

This has important implications for AdS-CFT, because it is usually assumed that the bulk gravity theory is some suitable low-energy limit of a full quantum gravity theory. The standard Hawking-Page transition is between a classical Schwarzschild black hole and the empty AdS geometry, corresponding to a deconfinement transition in the dual CFT. What we demonstrate is that a first-order approximation to a regularized Schwarzschild geometry, where there is no backreaction and the action does not yet include higher curvature terms in an effective field theory description of the full gravitational sector, eliminates the Hawking-Page transition altogether, at least when the regulator can be understood through the effective action of a $U(1)$ gauge field. At the same time it is known that the Hawking-Page transition persists when higher curvature corrections like $R^2 - 4R_{ab}R^{ab} + R_{abcd}R^{abcd}$ are explicitly included in the bulk gravitational action, though such corrections do not regularize the Schwarzschild singularity. Since the Hayward metric is a rather generic approximation to a smoothed geometry which can in principle arise from any quantum theory of gravity, we propose that quantum gravity corrections to Einstein-Hilbert gravity which are in some sense "strong enough" to regularize the central singularity may generically prevent the Hawking-Page transition from occurring, and likewise will have important implications for the critical behavior of the dual CFT theory.

In the extended phase space, the Hayward-AdS black hole exhibits critical behavior analogous to the mean-field theory critical behavior of ordinary fluid systems (see Ref. [43] for a review). In Fig. 2 we demonstrate the standard "swallowtail" behavior that generically occurs for asymptotically AdS black holes in the extended phase space, with the corresponding coexistence line shown in Fig. 3. Above the critical pressure (critical Λ) is a "superfluid" phase where the system smoothly transitions from a

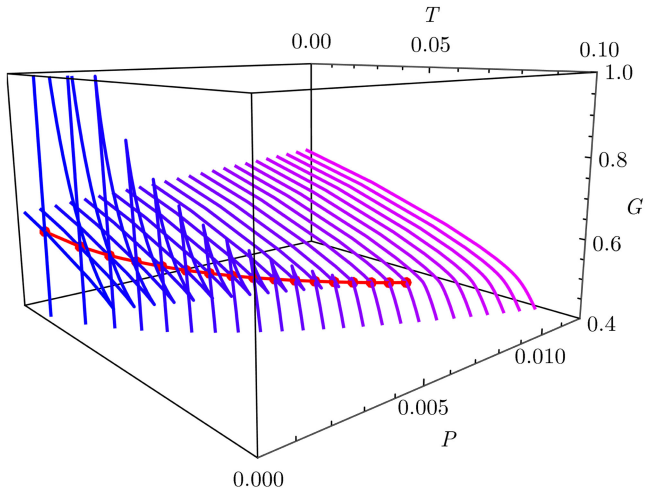

FIG. 2. Gibbs free energy G as a function of temperature T and pressure P for the Hayward-AdS black hole, demonstrating the formation of a swallowtail below the critical point. For $l = 0.5$ this occurs as $\{P_c, T_c\} = \{0.0083, 0.072\}$.

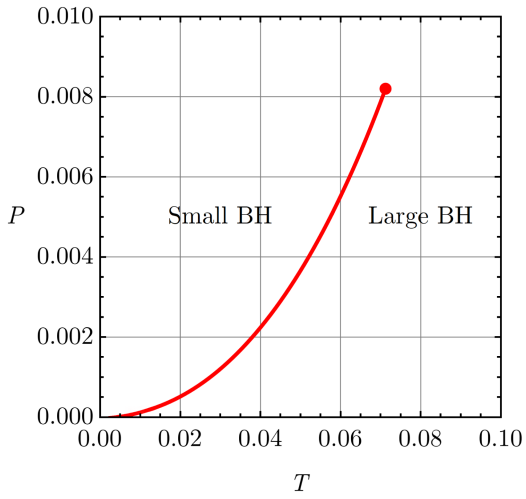

FIG. 3. Coexistence line for the Hayward-AdS black hole for $l = 0.5$. A series of first-order phase transitions occur along the red line, terminating at a critical point $\{P_c, T_c\} = \{0.0083, 0.072\}$ where the transition becomes second-order.

small to a large black hole as the temperature is increased. This transition is exactly analogous to the liquid-gas transition occurring in a traditional van der Waals fluid system. The transition can be examined further by constructing the equation of state $P(V, T)$ for the system. With $\Lambda = -8\pi P$ one obtains from (37) that

$$P = \frac{3(3r_h^5 - 2l^2 r_h^3(3 - 4\pi r_h T) - 8\pi l^4 r_h^2 T - \sqrt{r_h^7 X})}{16\pi l^2 r_h^4 (4\pi l^2 T + 3r_h)}, \quad (64)$$

where $X \equiv 9r_h^3 - 24l^2 r_h - 32\pi l^4 T$. Here and in what follows, we omit the tilde on thermodynamic variables with

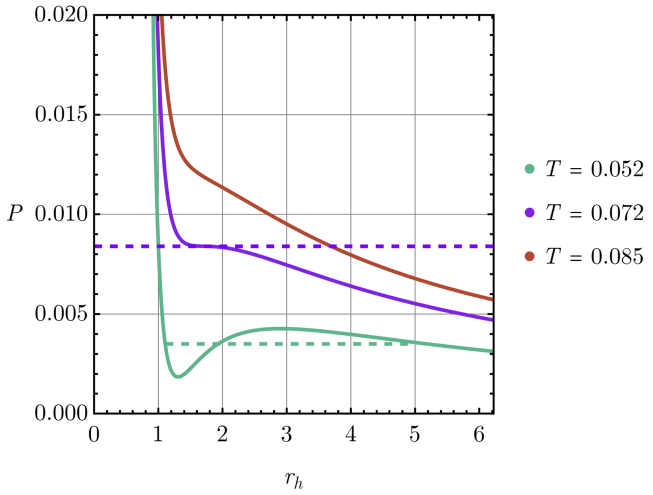

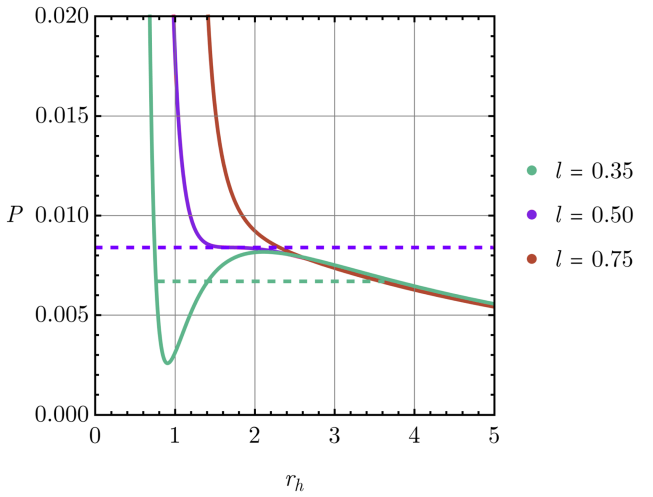

FIG. 4. Isotherms of the equation of state $P(r_h, T)$ for the Hayward-AdS black hole. Top: fixed $l = 0.5$ for various T. The onset of the Van der Waals transition is marked by an inflection point at the critical temperature $T_c \sim 0.072$. Bottom: fixed $T = 0.072$ with varying l. The critical pressure is marked by the red dashed line, while the coexistence line is marked by the blue dashed line.

the understanding that they refer to the quantities in (31). The thermodynamic volume is a 7th degree polynomial in r_h,

$$V = \frac{12\pi r_h^7}{(3r_h^2 + l^2(\Lambda r_h^2 - 3))^2}, \quad (65)$$

preventing one from writing the equation of state in analytic form as $P(V, T)$. However since the volume $V(r_h, l)$ is a monotonic function of the horizon size r_h for fixed length scale l, one can freely use r_h as a parameter. In Fig. 4 the equation of state is given as a function of horizon size r_h (it is qualitatively identical when given parametrically as a function of V). The red dashed line marks the onset of

the small-large transition at the critical point, which simultaneously satisfies

$$\frac{\partial P}{\partial V}=0, \qquad \frac{\partial^2 P}{\partial V^2}=0. \tag{66}$$

Below the critical temperature/length scale there is an unphysical region where $\partial P/\partial V>0$, and two more unstable regions. One may also observe that if the temperature T or critical length scale l are small enough, the system appears to enter a region where $P<0$ corresponding to a transition to asymptotically de Sitter space. Both pathologies are avoided because the system instead evolves along the dashed line of Fig. 4, which is determined by the condition that the small and large black hole phases have the same free energy. This coexistence line always lies above $P=0$. Figure 1 indicates a minimal horizon size at $T=0$, which corresponds to the extremal limit and implies the constraint that

$$r_h>\sqrt{\frac{3+6l^2\Lambda-3\sqrt{1-8l^2\Lambda}}{6\Lambda+2l^2\Lambda^2}}. \tag{67}$$

On the other hand, at fixed $T>0$ the equation of state instead implies a lower bound of

$$r_h>\frac{\sqrt[3]{16}[(l^3\sqrt{9\pi^2l^2T^2-2}+3\pi l^4T)^{2/3}+\sqrt[3]{2}l^2]}{3\sqrt[3]{l^3\sqrt{9\pi^2l^2T^2-2}+3\pi l^4T}}, \tag{68}$$

below which the pressure becomes imaginary. Surprisingly, the critical condition (66) can be solved analytically to find

$$P_c=\frac{5\sqrt{10}-13}{432\pi l^2}, \qquad V_c=\frac{8\pi\sqrt{\frac{2}{5}}(5\sqrt{10}+13)^{7/2}l^3}{375(\sqrt{10}+2)^2},$$
$$T_c=\frac{\sqrt{13\sqrt{\frac{5}{2}}-\frac{31}{2}}}{20\pi l}. \tag{69}$$

In terms of the reduced volume $v=2r_hl_p^2$ the "universal" ratio P_cv_c/T_c is

$$\frac{P_cv_c}{T_c}\approx 0.393\neq 3/8, \tag{70}$$

which represents a rare counterexample of the usual $3/8$ result for a four-dimensional black hole spacetime, signaling a potential departure from mean field theory critical behavior. This same ratio was computed in [5] using α and Q_m as the fundamental variable parameters of the theory. However we believe their analysis contained some inaccuracies which inevitably lead to different critical exponents, as detailed below.

In previous work [43], the reduced volume v was identified with the horizon radius by comparing the linear–T coefficient of the black hole equation of state to that of the van der Waals fluid. One can proceed the same way here by expanding Eq. (64) in powers of T to obtain

$$P=P_0+\frac{T}{\tilde{v}}+\mathcal{O}(T^2), \tag{71}$$

where

$$P_0=\frac{3r_h^2-6l^2-r_h\sqrt{9r_h^2-24l^2}}{16\pi l^2r_h^2}, \tag{72}$$

and the new reduced volume $\tilde{v}$ is identified to be

$$\tilde{v}=\frac{12r_h^2(3r_h^2-8l^2)}{(3r_h^2-4l^2)\sqrt{9r_h^2-24l^2}-24l^2r_h+9r_h^3}. \tag{73}$$

In the limit $l\to 0$ the reduced volume $\tilde{v}$ reduces to $\tilde{v}=2r_h+\mathcal{O}(l^2)$. Evaluating the critical ratio $P_c\tilde{v}_c/T_c$ in terms of this new reduced volume, we find that

$$\frac{P_c\tilde{v}_c}{T_c}\approx 0.391\neq\frac{3}{8}, \tag{74}$$

which is a small deviation from the value (70) obtained using the conventional reduced volume $v=2r_h$. In both cases the ratio differs from $3/8$.

Thermodynamic stability can further be assessed using the heat capacity, which is readily determined to be

$$C_V=T\left(\frac{\partial S}{\partial T}\right)\Big|_V$$
$$=\frac{2\pi r_h^2(l^2(\Lambda r_h^2-3)+3r_h^2)(l^2(\Lambda r_h^2-3)^2+3\Lambda r_h^4-3r_h^2)}{l^4(\Lambda r_h^2-3)^3+6l^2r_h^2(\Lambda r_h^2(\Lambda r_h^2-4)-9)+9(\Lambda r_h^6+r_h^4)}, \tag{75}$$

and is plotted in Fig. 5 for varying l. Positivity of the heat capacity indicates thermodynamic stability, while a divergence in the heat capacity generically indicates a phase transition. A sign change in C_V can occur either through a discontinuity or zero-crossing, with the divergences indicated by a vertical dashed line in the figure. Note that some of the unstable regions are excluded from the parameter space since they do not satisfy the constraint (68). The heat capacity diverges when

$$r_h^6(l^4\Lambda^3+6l^2\Lambda^2+9\Lambda)+r_h^4(-9l^4\Lambda^2-24l^2\Lambda+9)$$
$$+r_h^2(27l^4\Lambda-54l^2)-27l^4=0, \tag{76}$$

representing a cubic polynomial in r_h^2. The discriminant condition then determines that above a critical length scale

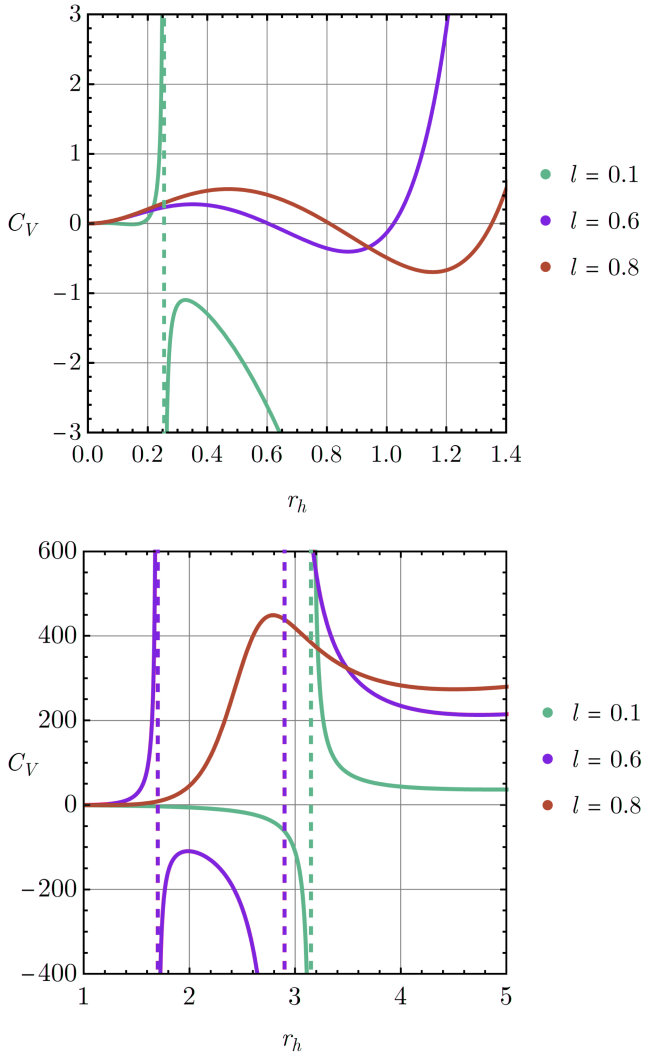

FIG. 5. Heat capacity C_V as a function of horizon size r_h for the Hayward-AdS black hole, for $\Lambda = -0.1$ and various l. Dashed lines correspond to a discontinuity in C_V. Top: small-r_h behavior. Bottom: large-r_h behavior.

l_c (for fixed Λ) or above a critical pressure P_c (for fixed l) given by

$$l_c = \frac{\sqrt{\frac{13}{\Lambda} - \frac{5\sqrt{10}}{\Lambda}}}{3\sqrt{6}}, \qquad P_c = \frac{5\sqrt{10} - 13}{432\pi l^2}, \tag{77}$$

there will be no divergence in the heat capacity, and furthermore all black hole phases become thermodynamically stable. The latter value of P_c can be seen to coincide with the critical pressure (69) determined from the equation of state. Note that, contrary to what is claimed in [5], the coexistence pressure $P = P_{\text{coex}}$ on the $P - V$ diagram constructed from the equal area law

$$\int_{v_s}^{v_l} (P(v) - P_{\text{coex}}) dv = 0, \tag{78}$$

is exactly in correspondence with the pressure at which the small and large black hole phases coexist on the $G - T$ diagram. Therefore, one obtains the same phase diagram from either the $P - V$ curve or the $G - T$ curve, and no redefinition of thermodynamic variables is required. That this is the case is not surprising since the equal area law condition is equivalent to the statement that the two phases have the same free energy, and no new information is contained in the $P - V$ diagram (it is just obtained by a rescaling $\Lambda \to -8\pi P$). We suspect that the earlier observation that the two coexistence lines differ is due to a numerical error, since in our case demonstrating that (78) holds requires computing the integration bounds (v_s, v_l) to a precision of at least 10^{-8}, otherwise the integral does not vanish at the same pressure as the $G - T$ diagram would suggest.

1. Critical exponents

Critical exponents govern the behavior of various thermodynamical parameters near a critical point, and separate physical systems into universality classes under which the scaling behavior of these parameters is identical, even if the underlying microscopic structure of the systems are vastly different. In terms of the reduced temperature $t \equiv T/T_c - 1$, they are defined through the scaling behavior of the following quantities:

$$C_V \propto |t|^{-\alpha}, \qquad \mathrm{g} = v_l - v_s \propto |t|^{\beta},$$
$$\kappa_T = -\frac{1}{V}\frac{\partial V}{\partial P}\bigg|_T \propto |t|^{-\gamma}, \qquad |P - P_c| \propto |V - V_c|^{\delta}. \tag{79}$$

C_V is the heat capacity at constant volume defined by (75), g is the order parameter (here the difference in volume of the large and small black hole phase), κ_T is the isothermal compressibility, and $|P - P_c|$ is the behavior of the pressure near the critical point. Since the entropy $S = \pi r_h^2$ is independent of temperature, one automatically finds that the critical exponent governing the behavior of the heat capacity near the critical point is $\alpha = 0$.

The exponent β is computed by examining the difference in size of the small and large black hole phases near the critical point. This cannot be done analytically since the horizon size r_h alone is given by a solution to a 5th degree polynomial, and the functions $G = G(r_h, \Lambda, l)$ and $T = T(r_h, \Lambda, l)$ cannot be solved analytically to find the location of the phase transition. Instead, we proceed numerically and compute the behavior of the order parameter $v_l - v_s$ near the critical point $t = 0$. This is done directly from the free energy G and temperature T, so that the result is independent of any particular identification of Λ and does not require using Maxwell's equal area law to find the coexistence line on the $P(V)$ diagram. The result is shown in Fig. 6 which clearly indicates that $\beta = 1/2$.

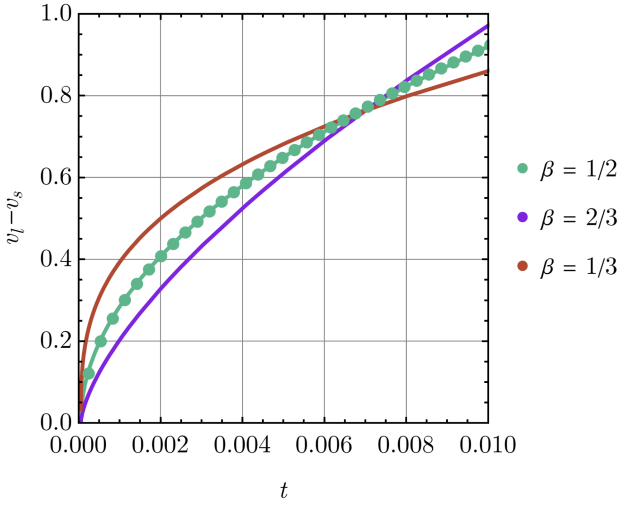

FIG. 6. Scaling behavior of the order parameter $v_l - v_s$ as a function of the reduced temperature t near the critical point. Dots represent numerical data while solid lines represent possible values of the critical exponent β.

The isothermal compressibility is determined by plotting κ_T vs t, which can also be done analytically since

$$\kappa_T \sim -\frac{1}{V}\left(\frac{\partial V}{\partial r_h}\right)\left(\frac{\partial P}{\partial r_h}\right)^{-1}\Bigg|_T. \tag{80}$$

It is straightforward to check that $\kappa_T \propto |t|^{-1}$ and therefore $\gamma = 1$.

Finally, the exponent δ can be determined by evaluating $|P - P_c|$ using (64) and (69) and plotting against $|V - V_c|$. We omit the resulting expression as it is lengthy and insightful. This can be done analytically by straightforward substitution, and a parametric plot of $|P - P_c|$ vs $|V - V_c|$ clearly shows that $\delta = 3$.

We have therefore determined that while the critical ratio $P_c v_c / T_c$ does indeed deviate slightly from the usual value of $3/8$ for the Hayward-AdS black hole (using either the thermodynamic volume V or reduced volume v), the critical exponents maintain their mean-field theory values of

$$\alpha = 0, \qquad \beta = \frac{1}{2}, \qquad \gamma = 1, \qquad \delta = 3. \tag{81}$$

As in other asymptotically AdS examples, this is quite surprising since in this case the equation of state clearly differs from that of the van der Waals fluid, yet the behavior near the critical point exhibits a universal behavior governed by (81).

B. Minkowski $\Lambda = 0$

Asymptotically flat ($\Lambda = 0$) black hole spacetimes admit a straightforward definition of both geometric and thermodynamic variables which enter into the first law, obtained through a Hamilton variation or equivalent covariant phase space formulation. However, the notion of thermodynamic equilibrium is more subtle compared to the asymptotically AdS case. There is no longer an effective potential which naturally confines radiation, and a black hole of any size is generically thermodynamically unstable with a negative specific heat capacity. Since physically reasonable sizes of black holes, which span masses from 10^1 to $10^{10} M_\odot$, have corresponding evaporation timescales on the order of 10^{74} to 10^{104} seconds, one way to approach the issue is to simply consider the system as being in a state of approximate thermal equilibrium over observationally relevant timescales. This assumption is certainly valid for physical-process interpretations of the first law as applied to physically realistic scenarios where the back-reaction from both Hawking radiation and infalling matter can reasonably be ignored. However, for holographic applications one can no longer make this approximation since the relevant state space is populated by distinct global configurations labelled by different values of the asymptotic mass, and the physically relevant timescale in the boundary theory may correspond to a bulk timescale for which evaporation cannot be ignored. Therefore, it is useful to introduce another mechanism to define the equilibrium ensemble in asymptotically flat spacetimes.

This is most straightforwardly accomplished by the introduction of a "cavity" representing fixed thermodynamic data on a compact codimension-2 surface outside of the black hole. As described in the previous section, this amounts to introducing a boundary in the Euclidean section where thermodynamic data is specified. Taking the $\Lambda \to 0$ limit of (56) we recover the equilibrium temperature for the Hayward-Minkowski black hole embedded in an isothermal cavity

$$\mathcal{T} = \frac{r_c^6(r_h^3 - 3l^2 r_h)}{4\pi(r_c^3 r_h^2 + l^2(r_c^3 - r_h^3)^2)\sqrt{\frac{r_c^2 r_h^2(r_c - r_h) - l^2(r_c^3 - r_h^3)}{r_c^3 r_h^2 - l^2(r_c^3 - r_h^3)}}}, \tag{82}$$

and the mean thermal energy of the ensemble, by taking the same limit of Eq. (57),

$$E = r_c - r_c\sqrt{\frac{l^2(r_h^3 - r_c^3) + r_c^2 r_h^2(r_c - r_h)}{l^2(r_h^3 - r_c^3) + r_c^3 r_h^2}}. \tag{83}$$

The free energy can then be computed as $F = \tilde{T} I_E = E - \tilde{T} S$. We find

$$F = -\frac{r_c^6 r_h^3 (r_h^2 - 3l^2)}{4\left(l^2(r_h^3 - r_c^3) + r_c^3 r_h^2\right)^2 \sqrt{\frac{r_c^2 r_h^3}{l^2(r_c^3 - r_h^3) - r_c^3 r_h^2} + 1}} + r_c - r_c \sqrt{\frac{r_c^2 r_h^3}{l^2(r_c^3 - r_h^3) - r_c^3 r_h^2} + 1}, \tag{84}$$

which can be plotted parametrically as a function of r_h as before, shown in Fig. 7. As expected, the behavior is qualitatively similar to the anti–de Sitter case, with a small-large black hole phase transition occurring below a critical value of l. Again the $F = 0$ phase corresponding to empty Minkowski space is inaccessible due to the finite fixed value of the magnetic charge Q_m required to have $l > 0$. Unlike the AdS case there is no notion of thermodynamic pressure for the system, so there is no analogy between the phase structure observed here and mean-field theory systems. The onset of the small-large transition is also controlled now by the cavity radius r_c, which when all other parameters are held fixed determines the relative scale between the black hole, cavity, and cosmological horizon.

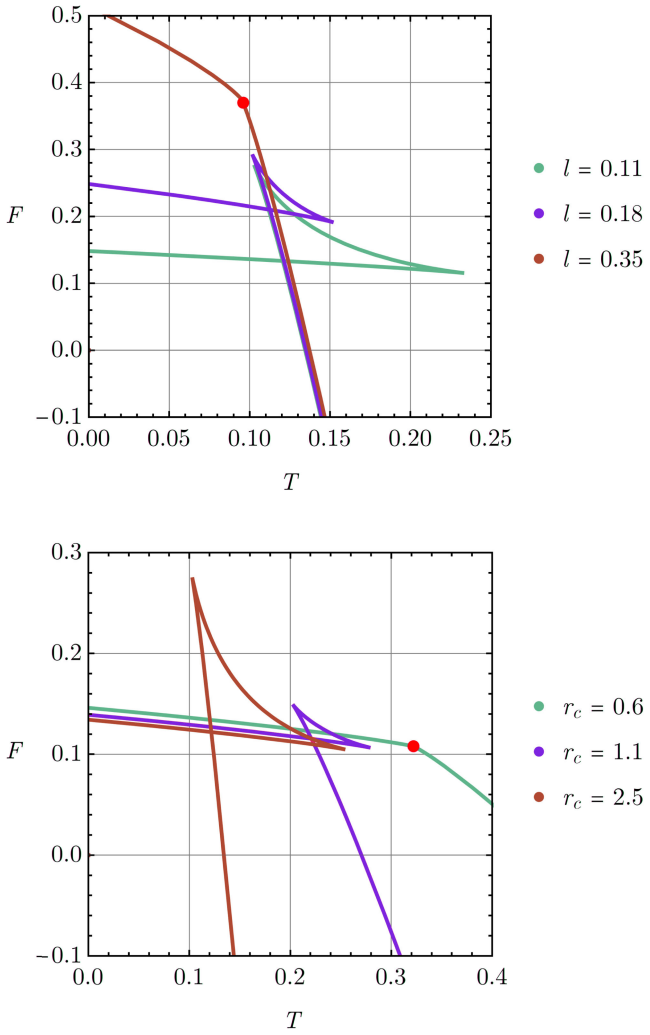

FIG. 7. Helmholtz free energy F as a function of temperature T for the asymptotically flat Hayward black hole. Top: fixed $r_c = 2$ for various l. The onset of a first-order phase transition from a small to large black hole is marked by a red dot at the critical temperature $T_c \sim 0.095$. Bottom: fixed $l = 0.1$ for various r_c. The critical temperature occurs at $T_c \sim 0.322$.

C. de Sitter $\Lambda > 0$

We finally turn to the asymptotically de Sitter ($\Lambda > 0$) case, which is at the same time the most technically challenging and astrophysically relevant, as there is incontrovertible evidence for both the existence of black hole-like objects [76] and for the accelerated expansion of the Universe [77–79]. The latter implies an asymptotically de Sitter geometry as being the relevant background for astrophysical black holes. Therefore, understanding black hole thermodynamics in asymptotically de Sitter spacetimes is important not only due to their observational relevance, but also for applications in the emerging field of de Sitter space holography [80–82].

Though the first law can be readily generalized to cases where $\Lambda \neq 0$, dS space presents a host of unique issues which are absent in AdS. The most salient is the presence of a cosmological horizon, which radiates at a much larger temperature than all but the smallest black holes, necessarily placing the system out of equilibrium due to the heat flux between the two horizons. Another issue with de Sitter spaces is a lack of globally timelike Killing vector field with which to associate the mass, making the construction of conserved charges difficult [83–85]. The masses which enter into the usual forms of the first law are defined for spacetimes which are asymptotically flat (ADM) or stationary (Komar). In de Sitter, one can recover stationarity by working in the static patch, but then the Killing vector ξ^a that would be used to define the mass becomes spacelike outside the cosmological horizon, rendering the mass conserved in space rather than time [86]. The variation of the would-be ADM mass is given by a boundary integral over an $\mathcal{S}^2$ at infinity

$$\delta M = -\frac{1}{16\pi}\int_\infty dS n_c B^c [\partial/\partial t] + \cdots,$$

but for the region outside the cosmological horizon the Killing vector $\partial/\partial t$ is spacelike, and M cannot support its usual Noether charge interpretation as being the conserved quantity associated with time-translation invariance. Therefore while a variation resembling the first law exists, one cannot straightforwardly interpret the variables entering it as the usual thermodynamical ones. The notion of a vacuum state is also problematic in de Sitter, since the global spacetime is nonstationary [87–89] and the vacuum state is not even known to be stable [90–92].

Various approaches aside from the Euclidean path integral adopted here have been developed to circumvent these

difficulties. One is the *effective temperature* approach, where a single temperature T_{eff} (which depends on both the cosmological and event horizon) is assigned to the entire spacetime [93]. This enables one to establish a "first law" which accounts for the presence of both horizons, but suffers from the fact that T_{eff} lacks a clear physical interpretation and the system still appears out of equilibrium to a local observer. Another approach is to consider only subsets of the parameter space where the two horizon temperatures are equal [94], in which case equilibrium is trivially established at the price of being limited to a measure-zero subset of possible configurations. One also requires sufficiently many "charges" to make the temperatures equal, which is not possible for ordinary Schwarzschild-de Sitter black holes.

As in the asymptotically flat case, the Euclidean path integral with finite boundary furnishes an equilibrium ensemble which can be used to study some features of static-patch thermodynamics in de Sitter space. The thermodynamic quantities obtained in Sec. III B remain valid when $\Lambda > 0$, provided that the boundary at r_c is placed between the event and cosmological horizons, such that $r_h < r_c < r_{\text{cosmo}}$ where r_{cosmo} is the largest real root of the metric function $f(r)$. Without the boundary, there is no choice of periodicity β which can eliminate the conical singularity at the event and cosmological horizons simultaneously, except in the degenerate Nariai limit where $r_h = r_{\text{cosmo}}$. Since $\Lambda > 0$ implies that $P < 0$, the quantity conjugate to Λ should be interpreted as a *tension* rather than a pressure. Despite the region of the static patch containing the cosmological horizon being effectively excised from the Euclidean section in this way, the effect of Λ still manifests in the required cavity temperature, which observes a significant blueshift when the cavity approaches the cosmological horizon.

The free energy is obtained from the on-shell Euclidean action as

$$F = \frac{l^2(\Lambda r_h^2 - 3)^2 + 3\Lambda r_h^4 - 3r_h^2}{12 r_h} - \frac{4r_c(\mathcal{Y}\sqrt{3 - \Lambda r_c^2} + \Lambda r_c^2 - 3)}{12}, \tag{85}$$

which is displayed in Fig. 8 as a function of the equilibrium temperature. The presence of a cosmological horizon significantly alters the observed phase structure of the Hayward black hole. As in the AdS case, one can observe a critical point at a maximal pressure ($\Lambda_c \sim 0.07$) below which a line of first-order small-large black hole transitions occurs. As before, above this pressure the system smoothly transitions in size as the temperature increases. However, in the dS case there emerges a second critical point at a lower critical value of $\Lambda \sim 0.02$, below which there is again no phase transition. This is a significant departure from the behavior observed in the asymptotically AdS case, where the small-large transition persists to arbitrarily small Λ.

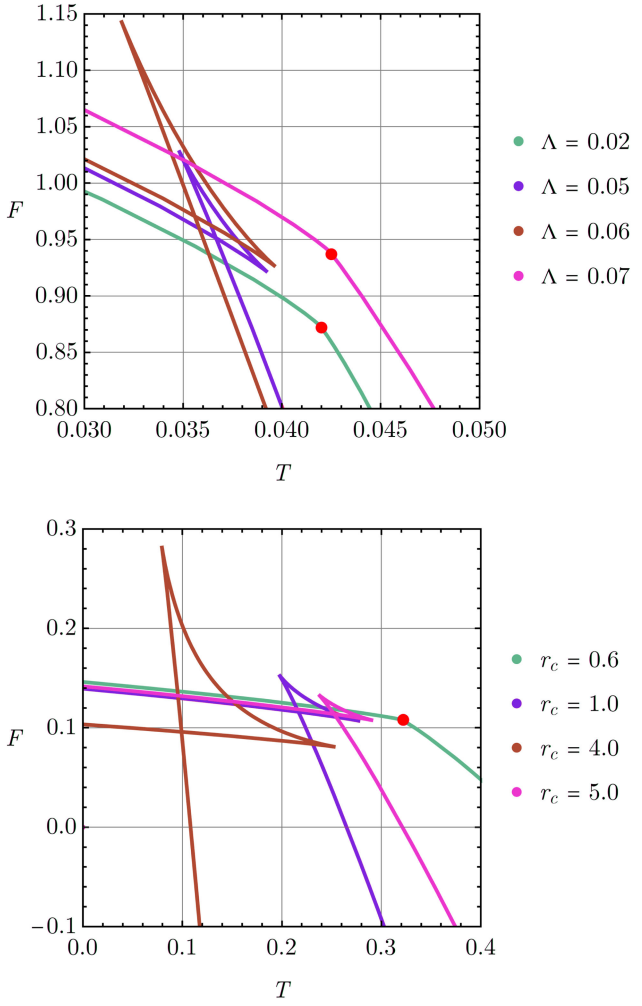

FIG. 8. Helmholtz free energy F as a function of temperature T for the Hayward-dS black hole. Top: fixed $l = 0.1$ and $r_c = 4$ for various Λ. Two critical points emerge, at $T_{c1} \sim 0.042$ and $T_{c2} \sim 0.043$. Bottom: fixed $\Lambda = l = 0.1$ for various r_c. The onset of a first-order phase transition from a small to large black hole is marked by a red dot at the critical temperature $T_c \sim 0.0315$.

Figure 9 illustrates this more clearly by showing a number of constant-pressure slices. The corresponding coexistence line is shown in Fig. 10.

Unlike AdS black holes in the extended phase space, whose phase structure typically resembles (and is sometimes exactly in correspondence with) the van der Waals fluid, the phase diagram in Fig. 10 more closely resembles that of something akin to the FCC transition of pure solid iron, or quantum critical points in e.g. the transverse field Ising model or a non-Fermi metal [95]. However, the phase diagram of Hayward-dS (and other asymptotically dS examples) cannot be in exact correspondence with such materials, because there is no critical point at the cusp of the $P - T$ curve, which is usually at $T = 0$ for quantum critical fluids or represents a triple point. Instead, the cusp marks a

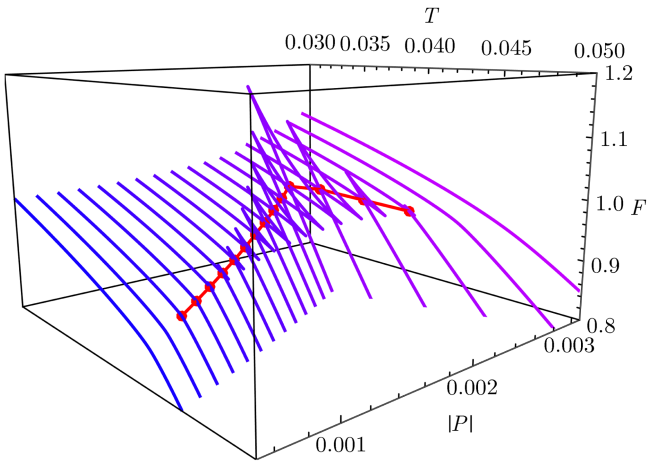

FIG. 9. Helmholtz free energy F as a function of temperature T and pressure P for the Hayward-dS black hole, demonstrating the formation of a swallowtube—a compact region in the parameter space where a small-large transition occurs.

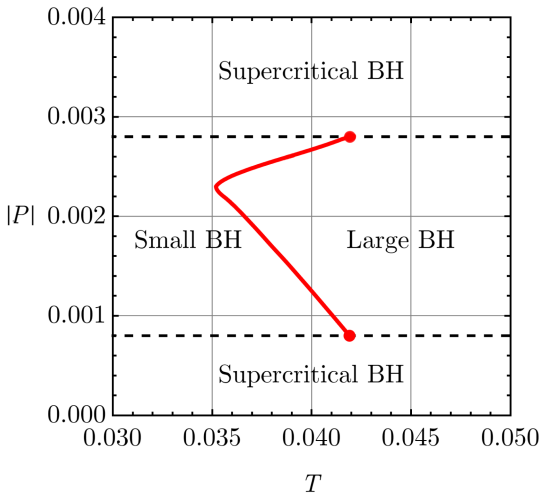

FIG. 10. Coexistence line for the Hayward-dS black hole, terminating at two second-order critical points. The system becomes supercritical outside of the region bounded by the dashed black lines.

smooth transition between a region where the cavity size is on the scale of the black hole horizon and where it is instead on the scale of the cosmological horizon. Furthermore, the coexistence line here terminates at two second-order critical points. It remains to be seen whether such a phase diagram can be understood in a holographic context or whether its novel features are the result of what is effectively a coupling of the black hole system to an external heat bath. We expect that such phase diagrams, like their AdS counterparts, will become increasingly important as a tool for understanding the phase structure of strongly coupled systems as holographic methods in de Sitter space become more refined.

V. CONCLUSIONS

The study of regular black hole solutions in general relativity is an important step toward understanding generic features of quantum gravity, both from a holographic and effective field theory point of view. Regular black hole solutions which can be sourced by matter coupled to Einstein-Hilbert gravity and manage to evade various no-go theorems are few and far between, with the Bardeen and Hayward model being prototypical examples sourced by nonlinear electrodynamics. While previous work which studied the thermodynamic properties of the Hayward solutions focussed on a specific choice of asymptotic metric and thermodynamic formulation/variables, we considered all three types of Hayward black hole (AdS, flat, and dS), discussed which thermodynamic formulation is most appropriate for each, and studied the resulting phase structure of the solutions.

In the first part of this work, we examined Hayward-AdS black holes with variable cosmological constant. We treated the minimal length scale l as a fundamental thermodynamic parameter, which may arise more generally from the regularization of the Schwarzschild singularity. We demonstrated a consistent version of the first law of black hole mechanics and Smarr relation based on this choice of variable, and studied the extended phase space thermodynamics that results. We found a second-order critical point which marks the formation of a swallowtail in $G-T-P$ space, and a series of first-order small-large black hole phase transitions below the critical temperature/pressure. The critical ratio $P_c v_c/T_c$ was found to deviate from the "universal" mean-field theory prediction of $3/8$ seen in most other four-dimensional AdS black holes, both when the ordinary reduced volume is used and the volume obtained from an expansion of the equation of state which allows a direct identification with the van der Waals fluid. Contrary to previous investigations into the extended phase structure of Hayward-AdS black holes, we computed the critical exponents and found that they agree with the predicted mean-field theory values.

We next studied asymptotically flat and de Sitter Hayward black holes. To define an equilibrium thermodynamic (canonical) ensemble, we fixed boundary-value data at a finite radius cavity outside of the black hole horizon (and inside the static-patch cosmological horizon, if it exists). The equilibrium temperature of the ensemble is determined by the choice that leaves the action stationary with respect to variations of the horizon size. Thermodynamic quantities were computed using a semiclassical Euclidean path integral with appropriate boundary terms, and shown to be consistent with the Hamiltonian formulation where the two methods were equally valid. The phase structure in the asymptotically flat case is similar to that of AdS, with a small-large transition occurring which is controlled by the regularization length scale. In asymptotically de Sitter space, two second-order critical points appear which bound a line of first-order

small-large transitions. The equation of state deviates significantly from standard van der Waals behavior, and the swallowtail closes at a finite nonzero value of the pressure (in contrast to AdS). The phase diagram contains two supercritical regions, and we conjecture that novel critical behavior may emerge where the two critical points meet.

A number of generalizations of our work naturally arise. First, it remains to be understood exactly which classes of black hole solutions (and theories) admit a consistent thermodynamic formulation from both the Hamiltonian and Euclidean framework when matter fields are present. While it is known that perfect fluids can be incorporated into the covariant formalism [60], this result has not been generalized past symmetry-inheriting matter fields. Furthermore, the linearity of the Smarr relation for nonlinear electrodynamic theories has only been proven for theories that admit a Maxwell weak-field limit, which nonetheless appears to also hold for the NED Lagrangian which generates the Hayward geometry. Another natural extension of our work would be to consider Kerr-Hayward-de Sitter black holes, representing the next logical step in studying thermodynamic features of models which hope to describe astrophysical black holes.

ACKNOWLEDGMENTS

F. S. is supported by the ARC Discovery Grant No. DP210101279. I. S. is supported by an International Macquarie University Research Excellence Scholarship.

APPENDIX A: ELECTROMAGNETIC POTENTIALS

In this appendix we collect various computations of thermodynamical quantities. We begin with the magnetic potential $\Psi(r)$. The only nonvanishing components of the electromagnetic field tensor are $F_{23} = -F_{32}$. In order to compute the magnetic potential one needs to first determine the magnetic field H_μ. From Eq. (21)

$$\star B_{\mu\nu} = \frac{1}{2}(\epsilon_{\mu\nu23} + \epsilon_{\mu\nu32})F^{23} = \epsilon_{\mu\nu23}B^{23}. \tag{A1}$$

Using the definition of the invariant 4-volume along with Eq. (21) we have that

$$\star B_{\mu\nu} = \sqrt{-g}[\mu\nu23]\mathcal{L}'(\mathcal{F})g^{22}g^{33}F_{23}. \tag{A2}$$

The only nonvanishing components are

$$\star B_{01} = -\star B_{10} = -\frac{\mathcal{L}'(\mathcal{F})Q_m}{r^2}, \tag{A3}$$

and using (20) then gives

$$H_1 = -\star B_{10}\xi^0 \Rightarrow \frac{\partial\Psi}{\partial r} = -\frac{\mathcal{L}'(\mathcal{F})Q_m}{r^2}. \tag{A4}$$

Next one computes (6) using

$$\mathcal{F} = F_{\mu\nu}F^{\mu\nu} = \frac{2Q_m^2}{r^4}, \tag{A5}$$

since

$$F_{\mu\nu} = -Q_m(\delta^\theta_\mu\delta^\phi_\nu - \delta^\theta_\nu\delta^\phi_\mu)\sin\theta. \tag{A6}$$

Therefore

$$\mathcal{L}'(\mathcal{F}) = \frac{18\sqrt{\alpha\mathcal{F}}}{(1+(\alpha\mathcal{F})^{3/4})^3}, \tag{A7}$$

and upon substituting Eq. (A5) we have

$$\mathcal{L}'(\mathcal{F}) = \frac{18q^2r^7}{(r^3+q^3)^3}. \tag{A8}$$

Using now Eq. (A4) along with the relation (12) for the magnetic charge and Eq. (A8) we have after integrating with respect to r that

$$\Psi(r) = \frac{3q^4(2r^3+q^3)}{\sqrt{2\alpha}(r^3+q^3)^3} + \Psi_0, \tag{A9}$$

where Ψ_0 is an integration constant which obeys $\Psi_0 = 0$ if the magnetic potential vanishes at large distances $r \to \infty$.

We now turn to the potential K_α conjugate to the parameter α. Starting from Eq. (24), the derivative of $\mathcal{L}(\mathcal{F})$ with respect to α is given by

$$\frac{\partial\mathcal{L}}{\partial\alpha} = \frac{6\mathcal{F}^2(-2\alpha\mathcal{F} + (\alpha\mathcal{F})^{1/4})}{(\alpha\mathcal{F} + (\alpha\mathcal{F})^{1/4})^3}, \tag{A10}$$

and then using Eq. (A5) we obtain

$$\frac{\partial\mathcal{L}}{\partial\alpha} = \frac{6q^6(-2q^3+r^3)}{a^2(r^3+q^3)^3}. \tag{A11}$$

The integration of Eq. (24) can then be performed using the above relation (A11) and the potential K_α given by Eq. (25) is obtained.

APPENDIX B: EUCLIDEAN ACTION

In this appendix, we compute the on-shell Euclidean action for the Einstein-Hilbert-NED theory in the semiclassical approximation. The total action will be

$$I_{\text{Total}} = I_{\text{EH}} + I_{\text{NED}} + I_B - I_0, \tag{B1}$$

where I_{EH} is the Einstein-Hilbert action with cosmological constant, I_{NED} is the action of the NED theory, I_B are appropriate boundary terms for a well-posed variational

principle, and I_0 is a background subtraction that serves to normalize the action such that $I_{\text{Total}} = 0$ for the empty (anti-)de Sitter spacetime.

The Einstein-Hilbert action with cosmological constant in four dimensions is

$$I_{\text{EH}} = -\frac{1}{16\pi}\int d^4x\sqrt{g}(R - 2\Lambda). \tag{B2}$$

We adopt a spherically symmetric ansatz for all dominant saddles contributing to the path integral, with Euclidean metrics of the form

$$ds^2 = f(r)d\tau^2 + f(r)^{-1}dr^2 + r^2 d\Omega_2, \tag{B3}$$

so that the Ricci scalar is given by

$$R = \frac{2 - f''(r)r^2 - 4rf(r) - 2f(r)}{r^2}. \tag{B4}$$

The reduced action is obtained by explicit integration of the action, which can be written as a sum of two terms:

$$\begin{aligned} I_{\text{EH}} &= I_R + I_\Lambda = -\frac{1}{16\pi}\int d^4x\sqrt{g}R, \\ I_\Lambda &= \frac{1}{8\pi}\int d^4x\sqrt{g}\Lambda. \end{aligned} \tag{B5}$$

The Ricci part of the Einstein-Hilbert action gives

$$I_R = -\frac{1}{16\pi}\int_0^{\beta_h} d\tau \int_0^{\pi} d\theta \int_0^{2\pi} d\phi \int_{r_h}^{r_c} r^2 \sin\theta R(r) dr, \tag{B6}$$

where the Euclidean section extends from the horizon at r_h to the cavity at r_c, and it is assumed in the de Sitter case that r_c is appropriately chosen to lie between the black hole and cosmological horizon, $r_h < r_c < r_{\text{cosmo}}$. The integration over Euclidean time τ is over one period β_h, which is chosen to eliminate the conical singularity in the τ-r plane at the horizon. After integrating over τ,θ and ϕ, one obtains

$$I_R = -\frac{\beta_h}{4}\int_{r_h}^{r_c} r^2 R(r) dr. \tag{B7}$$

Inserting (B4) into the above then gives

$$\int_{r_h}^{r_c} r^2 R(r) dr = \int_{r_h}^{r_c} [2 - f''(r)r^2 - 4rf'(r) - 2f(r)] dr, \tag{B8}$$

We define

$$\begin{aligned} G_0 &= \int_{r_h}^{r_c} f(r) dr, \qquad G_1 = \int_{r_h}^{r_c} rf'(r) dr, \\ G_2 &= \int_{r_h}^{r_c} r^2 f''(r) dr \end{aligned} \tag{B9}$$

Computing G_1 and G_2 using the fact that $f(r_h) = 0$ and integrating by parts reveals that

$$G_2 = r_c^2 f'(r_c) - r_h^2 f'(r_h) - 2G_1, \tag{B10}$$

$$G_1 = r_c f(r_c) - G_0. \tag{B11}$$

Inserting (B11) and (B10) into (B7) then gives

$$\begin{aligned} I_R = &-\frac{\beta_h}{4}(2(r_c - r_h) - 2r_c f(r_c) - r_c^2 f'(r_c)) \\ &-\frac{\beta_h}{4} r_h^2 f'(r_h), \end{aligned} \tag{B12}$$

and upon identifying the periodicity in τ with the Killing surface gravity

$$\beta_h^{-1} = \frac{\kappa}{2\pi} = \frac{f'(r_h)}{4\pi}, \tag{B13}$$

we finally obtain

$$I_R = -\frac{\beta_h}{4}[2(r_c - r_h) - 2r_c f(r_c) - r_c^2 f'(r_c)] - \pi r_h^2. \tag{B14}$$

Next, the cosmological term I_Λ is straightforwardly evaluated giving

$$\begin{aligned} I_\Lambda &= \frac{1}{8\pi}\int_0^{\beta_h} d\tau \int_0^{2\pi} d\phi \int_{r_h}^{r_c} \int_0^{\pi} r^2 \sin\theta \Lambda dr d\theta \\ &= \frac{\beta_h}{6}\Lambda(r_c^3 - r_h^3). \end{aligned} \tag{B15}$$

We next compute the Gibbons-Hawking-York boundary term (48), evaluated at $r = r_c$:

$$\begin{aligned} I_{\text{GHY}} &= \frac{1}{8\pi}\int_{\partial\mathcal{M}} \sqrt{k}K \\ &= \frac{1}{8\pi}\int_0^{\beta_h} d\tau \int_0^{2\pi} d\phi \int_0^{\pi} d\theta \sqrt{k}K|_{r_c}. \end{aligned} \tag{B16}$$

The induced metric k_{ab} on the boundary hypersurface is

$$ds^2 = f(r_c)d\tau + r_c^2 d\Omega, \tag{B17}$$

and the square root of the determinant of the induced metric is given by

$$\sqrt{k} = \sqrt{f(r_c)} r_c^2 \sin\theta. \tag{B18}$$

The trace K of the extrinsic curvature K_{ab} evaluated at the boundary is

$$K = -\frac{2\sqrt{f(r_c)}}{r_c} - \frac{f'(r_c)}{2\sqrt{f(r_c)}}. \tag{B19}$$

Combining (B16), (B18), and (B19) we find

$$I_{\mathrm{GHY}} = \frac{\beta_h}{2} r_c^2 K(r_c)\sqrt{f(r_c)}. \tag{B20}$$

Next, we compute the NED action given by (49) with Lagrangian density (6). Using (A5) we can write $\mathcal{L}(\mathcal{F})$ in terms of α and Q_M as

$$\mathcal{L}(\mathcal{F}) = \frac{24\sqrt{2\alpha}Q_m^3}{\left(1+\left(\frac{2\alpha Q_m^2}{r^4}\right)^{3/4}\right)^2 r^6}. \tag{B21}$$

Angular integration then reduces the action to

$$I_{\mathrm{NED}} = \frac{\beta_h}{4}\int_{r_h}^{r_c} r^2\mathcal{L}(\mathcal{F})dr, \tag{B22}$$

and the radial integration gives

$$I_{\mathrm{NED}} = 2\sqrt{2\alpha}Q_m^3\beta_h\left[\frac{1}{(2\alpha Q_m^2)^{3/4}+r_h^3} - \frac{1}{(2\alpha Q_m^2)^{3/4}+r_c^3}\right]. \tag{B23}$$

The final term we require is the electromagnetic boundary term, given by [96,97]

$$I_{\mathrm{EMB}} = -\frac{1}{16\pi}\int_{\partial M}\sqrt{k}\left(\frac{\partial\mathcal{L}}{\partial\mathcal{F}}\right)F^{\mu\nu}n_\nu A_\mu, \tag{B24}$$

where n_ν is the unit normal vector to the boundary ∂M. This term will vanish since we are integrating over a time slice of the spacetime and the only nonvanishing components of the $F_{\mu\nu}$ are $F_{23} = -F_{32}$. Finally, the term I_0 represents the action of the empty metric (in the absence of the black hole), which serves to normalize the action so that it vanishes when $r_h = 0$ i.e. when no black hole is present. Evaluating the total action for the empty metric (Minkowski, de Sitter, or anti–de Sitter), the subtraction term is given by

$$I_0 = \frac{\beta r_c}{3}(-3 + r_c^2\Lambda). \tag{B25}$$

APPENDIX C: CAVITY TENSION TERM

In this section we displayed the tension λ conjugate to the cavity area A_c, which appears in both the Smarr formula and the first law in the presence of a cavity. We first replace the areal radius r_c in the total reduced action (51) with the area of the cavity, given by $A_c = 4\pi r_c^2$. The conjugate potential is then given by

$$\lambda = \frac{1}{\beta}\frac{\partial I_r}{\partial A_c}. \tag{C1}$$

Explicit calculation yields the following, rather long, expression

$$\lambda = \frac{1}{48\pi r_c}\left(6(1-r_c^2\Lambda) + \frac{2r_c^2\Lambda}{\sqrt{3-r_c^2\Lambda}}\mathcal{X} - 2\sqrt{3-r_c^2\Lambda}\mathcal{X} + \frac{r_c^2\sqrt{3-r_c^2\Lambda}(2l^4(r_c^3-r_h^3)^2\Lambda(-3+r_h^2\Lambda)^2)}{(3r_c^2r_h^2+\mathcal{Y})^2\mathcal{X}}\right.$$
$$\left. + \frac{9r_c^3r_h^4(-3r_h+2r_c^3\Lambda+r_h^3\Lambda) + 3l^2r_h^2(4r_c^6\Lambda(-3+r_h^2\Lambda)+2r_h^4(-3+r_h^2\Lambda)^2) + r_c^3(9r_h+r_h^3\Lambda-3r_h^5\Lambda^2)}{(3r_c^2r_h^2+\mathcal{Y})^2\mathcal{X}}\right). \tag{C2}$$

[1] J. M. Bardeen in *Proceedings of the International Conference GR5* (Tbilisi University Press, Tbilisi, 1968).
[2] K. A. Bronnikov and J. C. Fabris, Phys. Rev. Lett. **96**, 251101 (2006).
[3] P. Nicolini, A. Smailagic, and E. Spallucci, Phys. Lett. B **632**, 547 (2006).
[4] S. A. Hayward, Phys. Rev. Lett. **96**, 031103 (2006).
[5] Z.-Y. Fan, Eur. Phys. J. C **77**, 266 (2017).
[6] E. Ayon-Beato and A. Garcia, Phys. Lett. B **493**, 149 (2000).
[7] D. P. Sorokin, Fortschr. Phys. **70**, 2200092 (2022).
[8] C. H. Nam, Eur. Phys. J. C **78**, 581 (2018).
[9] J. M. Maldacena, Int. J. Theor. Phys. **38**, 1113 (1999).
[10] J. M. Bardeen, B. Carter, and S. W. Hawking, Commun. Math. Phys. **31**, 161 (1973).
[11] V. Iyer and R. M. Wald, Phys. Rev. D **50**, 846 (1994).
[12] G. W. Gibbons and S. W. Hawking, Phys. Rev. D **15**, 2738 (1977).
[13] L. Susskind and J. Uglum, Phys. Rev. D **50**, 2700 (1994).
[14] S. N. Solodukhin, Living Rev. Relativity **14**, 8 (2011).
[15] S. Carlip, Phys. Rev. Lett. **82**, 2828 (1999).
[16] Z. Luo, H. Yu, S. Cao, and J. Li, Chin. Phys. C **47**, 065102 (2023).

[17] M. Molina and J. R. Villanueva, Classical Quantum Gravity **38**, 105002 (2021).
[18] C. Lan, H. Yang, Y. Guo, and Y-G Miao, Int. J. Theor. Phys. **62**, 202 (2023).
[19] E. Ayón-Beato and A. García, Phys. Rev. Lett. **80**, 5056 (1998).
[20] Z. Y. Fan and X. Wang, Phys. Rev. D **94**, 124027 (2016).
[21] K. A. Bronnikov, Phys. Rev. D **96**, 128501 (2017).
[22] M. Born and L. Infeld, Proc. R. Soc. A **144**, 425 (1934).
[23] I. Bandos, K. Lechner, D. Sorokin, and P. K. Townsend, Phys. Rev. D **102**, 121703 (2020).
[24] M. Hassaïne and C. Martínez, Phys. Rev. D **75**, 027502 (2007).
[25] A. Bokulić, I. Smolić, and T. Jurić, Phys. Rev. D **103**, 124059 (2021).
[26] V. Frolov, Phys. Rev. D **94**, 104056 (2016).
[27] L. Sebastiani and S. Zerbini, Astronomy **1**, 99 (2022).
[28] S. Balestra *et al.*, Eur. Phys. J. C **55**, 57 (2008).
[29] M. Ambrosio *et al.* (MACRO Collaboration), Eur. Phys. J. C **25**, 511 (2002).
[30] G. 't Hooft, Nucl. Phys. **B79**, 276 (1974).
[31] T. W. B. Kibble, Phys. Rep. **67**, 183 (1980).
[32] A. M. Polyakov, JETP Lett. **20**, 430 (1974), http://jetpletters.ru/ps/1789/article_27297.shtml.
[33] J. Preskill, Annu. Rev. Nucl. Part. Sci. **34**, 461 (1984).
[34] K. A. Bronnikov, Phys. Rev. D **63**, 044005 (2001).
[35] B. Toshmatov, Z. Stuchlík, and B. Ahmedov, Phys. Rev. D **98**, 028501 (2021).
[36] R. M. Wald, Phys. Rev. D **48**, R3427(R) (1993).
[37] D. A. Rasheed, arXiv:hep-th/9702087.
[38] L. Smarr, Phys. Rev. Lett. **30**, 71 (1973).
[39] Y. Zhang and S. Gao, Classical Quantum Gravity **35**, 145007 (2018).
[40] A. Komar, Phys. Rev. **129**, 1873 (1963).
[41] R. Arnowitt, S. Deser, and C. W. Misner, Phys. Rev. **116**, 1322 (1959).
[42] D. Kastor, S. Ray, and J. Traschen, Classical Quantum Gravity **26**, 195011 (2009).
[43] D. Kubizňák, R. B. Mann, and M. Teo, Classical Quantum Gravity **34**, 063001 (2017).
[44] M. Urano, A. Tomimatsu, and H. Saida, Classical Quantum Gravity **26**, 105010 (2009).
[45] J. D. Brown and C. Teitelboim, Phys. Lett. B **195**, 177 (1987).
[46] G. Gibbons, R. Kallosh, and B. Kol, Phys. Rev. Lett. **77**, 4992 (1996).
[47] J. D. E. Creighton and R. B. Mann, Phys. Rev. D **52**, 4569 (1995).
[48] C. Barceló, V. Boyanov, R. Carballo-Rubio, and L. J. Garay, Classical Quantum Gravity **38**, 125003 (2021).
[49] C. Barceló, V. Boyanov, R. Carballo-Rubio, and L. J. Garay, Phys. Rev. D **106**, 124006 (2022).
[50] R. Carballo-Rubio, F. Di Filippo, S. Liberati, and M. Visser, arXiv:2302.00028.
[51] N. Breton, Gen. Relativ. Gravit. **37**, 643 (2005).
[52] J. Bekenstein, Lett. Nuovo Cimento **4**, 737 (1972).
[53] J. Bekenstein, Phys. Rev. D **7**, 2333 (1973).
[54] J. Bekenstein, Phys. Rev. D **9**, 3292 (1974).
[55] Z. Y. Fan, Eur. Phys. J. C **77**, 266 (2017).
[56] C. Ftaclas and J. M. Cohen, Phys. Rev. D **18**, 4373 (1978).
[57] J. Wainwright and P. E. A. Yaremovicz, Gen. Relativ. Gravit. **7**, 345 (1976).
[58] A. Coley and K. Dunn, Astrophys. J. **348**, 26 (1990).
[59] L. Gulin and I. Smolić, Classical Quantum Gravity **35**, 025015 (2018).
[60] V. Iyer, Phys. Rev. D **55**, 3411 (1997).
[61] M. Liška, R. A. Hennigar, and D. Kubizňák, J. High Energy Phys. 11 (2023) 195.
[62] J. W. York, Jr., Phys. Rev. D **33**, 2092 (1986).
[63] H. W. Braden, J. D. Brown, B. F. Whiting, and J. W. York, Jr., Phys. Rev. D **42**, 3376 (1990).
[64] B. Banihashemi and T. Jacobson, J. High Energy Phys. 07 (2022) 042.
[65] R. J. Kubo, J. Phys. Soc. Jpn. **12**, 570 (1957).
[66] P. C. Martin and J. Schwinger, Phys. Rev. **115**, 1342 (1959).
[67] F. Simovic and R. B. Mann, J. High Energy Phys. 05 (2019) 136.
[68] S. Haroon, R. A. Hennigar, R. B. Mann, and F. Simovic, Phys. Rev. D **101**, 084051 (2020).
[69] F. Simovic, D. Fusco, and R. B. Mann, J. High Energy Phys. 02 (2021) 219.
[70] S. Carlip and S. Vaidya, Classical Quantum Gravity **20**, 3827 (2003).
[71] V. Iyer and R. M. Wald, Phys. Rev. D **52**, 4430 (1995).
[72] D. T. Son and A. O. Starinets, J. High Energy Phys. 09 (2002) 042.
[73] S. W. Hawking and D. N. Page, Commun. Math. Phys. **87**, 577 (1983).
[74] E. Witten, Adv. Theor. Math. Phys. **2**, 253 (1998).
[75] D. Harlow, Rev. Mod. Phys. **88**, 015002 (2016).
[76] R. Abbott *et al.*, Astrophys. J. Lett. **913**, L7 (2021).
[77] P. M. Garnavich *et al.*, Astrophys. J. **493**, L53 (1998).
[78] G. Goldhaber and D. B. Cline, AIP Conf. Proc. **1166**, 53 (2009).
[79] Planck Collaboration, Astron. Astrophys. **594**, A13 (2016).
[80] A. Strominger, J. High Energy Phys. 10 (2001) 034.
[81] F. Larsen, J. P. van der Schaar, and R. G. Leigh, J. High Energy Phys. 04 (2002) 047.
[82] V. Balasubramanian, J. de Boer, and D. Minic, Ann. Phys. (Amsterdam) **303**, 59 (2003).
[83] V. Balasubramanian, J. de Boer, and D. Minic, Phys. Rev. D **65**, 123508 (2002).
[84] R. Bousso, Rev. Mod. Phys. **74**, 825 (2002).
[85] D. Anninos, G. S. Ng, and A. Strominger, Classical Quantum Gravity **28**, 175019 (2011).
[86] A. M. Ghezelbash and R. B. Mann, J. High Energy Phys. 01 (2002) 005.
[87] E. Mottola, Phys. Rev. D **31**, 754 (1985).
[88] B. Allen, Phys. Rev. D **32**, 3136 (1985).
[89] N. Goheer, M. Kleban, and L. Susskind, J. High Energy Phys. 07 (2003) 056.
[90] J. D. Brown and C. Teitelboim, Nucl. Phys. **B297**, 787 (1988).
[91] P. R. Anderson and E. Mottola, Phys. Rev. D **89**, 104039 (2014).

[92] J. T. Firouzjaee and G. F. R. Ellis, Phys. Rev. D **91**, 103002 (2015).
[93] Z. Li-Chun, L. Huai-Fan, and Z. Ren, Acta Phys. Sin. **59**, 12 (2010).
[94] S. Mbarek and R. B. Mann, J. High Energy Phys. 02 (2019) 103.
[95] M. A. Metlitski, D. F. Mross, S. Sachdev, and T. Senthil, Phys. Rev. B **91**, 115111 (2015).
[96] H. E. Moumni and J. Khalloufi, Nucl. Phys. **B973**, 115593 (2021).
[97] H. E. Moumni and J. Khalloufi, Nucl. Phys. **B977**, 115731 (2022).

JOURNAL ARTICLE

Euclidean methods and phase transitions for the strongest deformations compatible with Schwarzschild asymptotics

Brief summary

In our previous paper, we examined the Hayward RBH model sourced by an NED Lagrangian $\mathcal{L}(\mathcal{F})$ that does not admit the Maxwell weak-field limit. In this study, we now focus on the Cadoni *et al.*, which notably does admit this limit. Using the same methodology, we once again demonstrate the presence of a first law of black hole thermodynamics and a linear Smarr relation. To compare how different deformation strengths from various NED Lagrangians affect thermodynamic properties, we also analyze the Bardeen RBH in Appendix D. We compare the mean-field theory ratios at the critical point in AdS spacetime, attributing deviations from the standard mean-field theory ratio of $3/8$ to the deformation strength and the manner in which the singularity is smeared. Finally, using the derived thermodynamic quantities, we provide constraints on the minimal length scale based on thermodynamic stability and the presence of a trapped region.

Errata and conventions

In this article, we use σ in the NED Lagrangian density $\tilde{\mathcal{L}}(\mathcal{F})$ of Eq. (21) instead of α, which was used in the previous article (Ref. [1]).

There are a few typos in this article that need correction. Firstly, the definition of the EMT in Eq. (11) is

$$T_{\mu\nu} = -4\mathcal{L}_{\mathcal{F}} F^{\alpha}{}_{\nu} F_{\mu\alpha} + \mathcal{L} g_{\mu\nu}, \tag{2.1}$$

while it should be corrected to:

$$T_{\mu\nu} = \frac{1}{4\pi}\left(\mathcal{L}_{\mathcal{F}} F^{\alpha}{}_{\nu} F_{\mu\alpha} - \frac{1}{4}\mathcal{L} g_{\mu\nu}\right). \tag{2.2}$$

This correction also impacts the Eqs. (15), (16), and (17). We provide the correct expressions bellow:

$$T_{00} = \frac{1}{16\pi} f(r)\mathcal{L}, \quad T_{11} = -\frac{1}{16\pi} f(r)^{-1}\mathcal{L}, \quad T_{22} = -\frac{1}{16\pi}\left(r^2\mathcal{L} + \frac{4Q_m^2}{r^2}\mathcal{L}_{\mathcal{F}}\right). \tag{2.3}$$

Despite these errors, Eq. (18), which provides the NED Lagrangian density as a function of the radial coordinate r, is correct. Finally, on page 4 of the article, at the end of the paragraph following Eq. (26), the phrase "whereas for the Hayward model is $O(\mathcal{F}^{5/2})$" should be corrected to "whereas for the Hayward model is $O(\mathcal{F}^{3/2})$".

Authorship statement

Conceptualization of the research project and calculations for its development. Sole author of this article.

Euclidean methods and phase transitions for the strongest deformations compatible with Schwarzschild asymptotics

Ioannis Soranidis*

School of Mathematical and Physical Sciences, Macquarie University, Sydney, New South Wales 2109, Australia

(Received 15 October 2023; accepted 28 January 2024; published 21 February 2024)

In this paper, we investigate the thermodynamic properties of a regular black hole model which exhibits the most significant subleading corrections to the Schwarzschild asymptotic behavior, in the context of general relativity, using the Euclidean path integral approach. We review the derivation of the Lagrangian for the matter fields which act as a source for this geometry, explicitly derive the proper thermodynamic quantities introduced in the first law of black hole mechanics, and show that they satisfy the Smarr formula. This analysis naturally leads to the emergence of an effective temperature that is distinct from the one associated with surface gravity. Furthermore, we study the phase structure in anti–de Sitter, Minkowski, and de Sitter spacetimes in the canonical ensemble, considering this effective temperature as the appropriate choice. We show that in this case the regularization of the singularity prevents the Hawking-Page transition and also leads to a deviation from the "universal" mean-field theory critical ratio. We conjecture that the way a singularity is rendered smooth plays a pivotal role to the degree of this deviation. Finally, we provide remarks on constraints imposed on the minimal length scale by observational data and the viability of regular black holes.

DOI: 10.1103/PhysRevD.109.044041

I. INTRODUCTION

Despite the incontrovertible evidence for the existence of dark massive ultracompact objects [1–7], their true identity remains elusive, with a plethora of scenarios under consideration [8–10]. The most commonly used type of black holes for comparison with available observational data are mathematical black holes, which are solutions of the Einstein equations in general relativity. Their hallmark features, which make them distinct from other categories like regular black holes (RBHs) [11–13], gravastars [14,15], wormholes [16–18], and fuzzballs [19,20] are the existence of an event horizon and a singularity. The problems associated with these two characteristics are the teleological nature of the event horizon and breakdown of general relativity at the singularity.

The former of these issues can be dealt with by replacing event horizons with quasilocally observable apparent horizons [21], while the latter one is resolved in two possible ways, which arise from the requirement of violation of Penrose's singularity theorem or more specifically at least one of its assumptions [22]. The singularity is inherently linked to the geodesic incompleteness of the geometry, so if we want to successfully eliminate it, we need to sufficiently modify the geometry surrounding the focusing point, i.e., the singularity. This can be achieved by two methods, namely either with the creation of a defocusing point at finite or infinite affine distance, or by displacing the focusing point at infinity [23]. The first case corresponds to regular black holes with the defocusing point coinciding with its inner horizon in spherically symmetric cases.

We assume the existence of a full quantum gravity theory that can lead to such a regularization, but its quantum nature is restricted to a finite domain, possibly of Planckian scale. The outcome of such a theory should be a globally hyperbolic and regular geometry, but since we do not possess such a theory yet, we turn our focus on how to source geometries of this nature in the context of general relativity. Historically, nonlinear electrodynamics (NED) was first used by Born and Infeld [24] to cure the infinities/singularities associated with the self-energy of a point charge, but in a large number of cases these types of theories coupled to general relativity are sufficient to generate regular geometries and eliminate singularities only at the cost of using exclusively magnetic charge [25]. The first source for such a geometry was found in Ref. [26] for the Bardeen black hole and further generalized to a variety of two-parameter families of spherically symmetric RBHs solutions in Ref. [27]. One notable issue with this type of sources is that magnetic monopoles have not been observed in nature despite significant observational efforts [28–30]. Additionally, some of these theories fail to provide a Maxwell weak-field limit [25], but exceptions do exist,

*ioannis.soranidis@hdr.mq.edu.au

and the model under consideration in this paper falls into this category.

In the case of classical singularities associated with the point charge, quantum electrodynamics was sufficient to remove them but at the same time make new predictions, which is a key feature of a successful theory, and therefore replaced the NED theories. Similar behavior is anticipated in the gravitational theory with general relativity to be replaced by a more fundamental theory, namely a full quantum gravity theory. In the absence of such a theory, NED coupled to general relativity may prove a valuable model/tool to extract features of quantum gravity. Based on this assumption, the magnetic charge will not be considered a fundamental parameter in our analysis, but rather the minimal length scale will be treated as one. By taking this approach, we can gain valuable insights into the quantum gravity theory within the framework of general relativity.

The four laws of black hole mechanics were first derived in Ref. [31] and close analogies with the four laws of thermodynamics were established. This important link connecting the two fields has since proven to be an important tool in advancing our understanding of black holes. In particular, the physical insights revealed in the rigorous mathematical derivation of the first law in the integral and differential formalism of Ref. [31] have provided strong motivation for further investigating their thermodynamic properties. If we believe in a quantum gravity theory which smooths out the singularity, the study of thermodynamic properties of RBHs cannot be an exception. To have a complete understanding of RBHs' thermodynamic properties necessitates the study of a plethora of these models which differ in the way they achieve singularity regularization and extract as much information as possible in order to establish some kind of universal behavior of the singularity smoothing and how it propagates into the classical sector.

In this paper, we will study a certain geometry proposed in Ref. [32]. The significance of investigating its properties lies in two distinct attributes that set it apart from RBH models proposed by Bardeen and Hayward: Firstly, the NED theory employed to generate this geometry admits the Maxwell weak-field limit, which is a highly desirable property in this type of theories. Potential corrections to the well-established Maxwell theory may manifest in higher energy regimes, while remaining absent in lower energies, giving rise to the conventional Maxwell theory. It is worth pointing out this is not the case for Bardeen or Hayward model which admit a weak-field limit stronger than Maxwell's theory. Therefore, this model is a better candidate for the description of actual astrophysical black holes, since it admits a weak-field limit compatible with a well-established theory. Secondly, this model has the strongest subleading corrections to the Schwarzschild asymptotic behavior, and therefore surpass the ones exhibited by Bardeen or Hayward RBHs. This is a noteworthy feature because effects of singularity smoothing will be more pronounced, making comparison with real astronomical data feasible. Based on these two features we try to establish to what extent there is a deviation of this model from the Bardeen model, studied in Appendix D, and the Hayward model studied extensively in Ref. [33]. Since in a number of black hole cases in anti–de Sitter (AdS) we have seen remarkable equivalence with the liquid-gas critical behavior, we mainly focus on the study of the mean-field theory critical ratio and exponents.

The paper is organized as follows. In Sec. II we describe how to generate the geometry using NED coupled to general relativity embedded in a spacetime with a cosmological constant by explicitly calculating the Lagrangian density.[1] In Sec. III we perform a detailed analysis of the Euclidean action and how to derive the proper thermodynamic quantities. In the beginning of Sec. IV, we provide some arguments on the reason we allow the cosmological constant and minimal length to vary, and then move on to the study of phase transitions. In Sec. IV A, we study the phase structure and thermodynamic stability of this model embedded in anti–de Sitter spacetime along with its behavior near the critical point. In Sec. IV B, we analyze the phase structure in asymptotically Minkowski spacetime with the implementation of an isothermal cavity to establish thermodynamic equilibrium. We also comment on the bounds imposed on the minimal length and its comparison with astronomical data, leading us to conclusions about the viability of RBHs. We perform a similar thermodynamic analysis in Sec. IV C for embedding in de Sitter spacetime with the isothermal cavity restricted between the outer black hole horizon radius and the cosmological horizon. In all of the above cases we demonstrate the existence of a proper Smarr formula [34] and first law of black hole thermodynamics. We conclude in Sec. V with a discussion of our main results and their ramifications, along with potential future research directions. Throughout this article, we restrict ourselves to four spacetime dimensions and we work in dimensionless units such that $\hbar = c = G = k_B = 1$.

II. REGULAR BLACK HOLE MODEL

In this paper, we focus on the spherically symmetric RBH model proposed in Ref. [32], which is described by a line element given by

$$ds^2 = -f(r)dt^2 + \frac{dr^2}{f(r)} + r^2 d\Omega_2, \tag{1}$$

where $d\Omega_2 = d\theta^2 + \sin^2\theta d\phi^2$ and

[1]To avoid confusion, we explicitly mention that we use the terms "Lagrangian" and "Lagrangian density" interchangeably throughout this article, but we always mean the Lagrangian density.

$$f(r) = 1 - \frac{2mr^2}{(r+l)^3} - \frac{\Lambda}{3}r^2, \tag{2}$$

with Λ being the cosmological constant and l the minimal length scale with the Schwarzschild limit attained for vanishing minimal length scale, i.e., when $l = 0$. We now explicitly derive the matter Lagrangian that serves as a source for this geometry. It is established that the majority of RBH models are generated by NED coupled to gravity [25,27,35] with the inclusion of magnetic charge. Nevertheless, it is worth noting that certain RBH metrics demand the presence of additional fields beyond the NED theory. An illustrative example of such a case is the Simpson-Visser metric [18], which interpolates between an RBH and a wormhole, where an additional phantom scalar field [36,37] is present in the matter content. For the case under consideration, we have the following action

$$I = \frac{1}{16\pi}\int d^4x\sqrt{-g}\big(R - \mathcal{L}(\mathcal{F},\Lambda)\big), \tag{3}$$

with R being the Ricci scalar and $\mathcal{L}(\mathcal{F},\Lambda)$ the Lagrangian density for the matter content which is comprised of the NED theory along with the cosmological constant component. For consistency, we require this Lagrangian to reduce to 2Λ, when the minimal length scale vanishes. Therefore, we have

$$\lim_{l\to 0}\mathcal{L} = 2\Lambda, \tag{4}$$

which is equivalent to the NED theory being absent. This Lagrangian is in general some NED Lagrangian, which is a function of the field strength $\mathcal{F} = F^{\mu\nu}F_{\mu\nu}$ combined with the cosmological constant term. The electoromagnetic field tensor is defined in the usual way from the relation

$$F_{\mu\nu} = \partial_\mu A_\nu - \partial_\nu A_\mu. \tag{5}$$

In our analysis, we examine a metric that exhibits spherical symmetry. The commonly adopted form of the vector potential A_μ in this case is given by

$$A_\mu = (-\phi(r), 0, 0, Q_m\cos\theta), \tag{6}$$

which corresponds to the presence of an electric and a magnetic charge [27]. To generate this geometry, we only need the presence of a magnetic charge Q_m, and thus the electric potential $\phi(r)$ will vanish. Therefore, we are led to the potential

$$A_\mu = (0, 0, 0, Q_m\cos\theta). \tag{7}$$

The only nonvanishing components of the electromagnetic strength tensor are

$$F_{23} = -F_{32} = -Q_m\sin\theta, \tag{8}$$

which leads to the field strength of the following form

$$\mathcal{F} = \frac{2Q_m^2}{r^4}. \tag{9}$$

To determine the appropriate Lagrangian $\mathcal{L}(\mathcal{F},\Lambda)$ for the matter fields, our initial step will be to use the Einstein equations and extract the Lagrangian by requiring that they yield as solution the metric described in Eq. (1) with the corresponding metric function of Eq. (2). In what follows the derived Lagrangian will be a function of the radial coordinate, but it may equivalently be expressed in terms of the field strength with Eq. (9) providing us with the connection between these two expressions/representations. Regardless of its specific form, the corresponding energy-momentum tensor (EMT) can be found after varying the action with respect to $g_{\mu\nu}$, which leads to the Einstein equations,

$$G_{\mu\nu} = 8\pi T_{\mu\nu}, \tag{10}$$

with an EMT of the form

$$T_{\mu\nu} = -4\frac{\partial\mathcal{L}}{\partial\mathcal{F}}F^\alpha_\nu F_{\mu\alpha} + \mathcal{L}g_{\mu\nu}. \tag{11}$$

For our case, the identification of the Lagrangian requires using the following components of the Einstein tensor $G_{\mu\nu}$,

$$G_{00} = \frac{f(r)}{r^2}\big(1 - f(r) - rf'(r)\big), \tag{12}$$

$$G_{11} = \frac{-1 + f(r) + rf'(r)}{r^2 f(r)}, \tag{13}$$

$$G_{22} = \frac{1}{2}r(2f'(r) + rf''(r)), \tag{14}$$

along with the corresponding EMT components on the right-hand side of Eq. (10), which are calculated by using the EMT of Eq. (11), and are given by

$$T_{00} = -f(r)\mathcal{L}, \tag{15}$$

$$T_{11} = f(r)^{-1}\mathcal{L}, \tag{16}$$

$$T_{22} = r^2\mathcal{L} - 4\frac{\partial\mathcal{L}}{\partial\mathcal{F}}\frac{Q_m^2}{r^2}. \tag{17}$$

In this derivation, we have assumed that the Lagrangian density shares the spherical symmetry of the geometry, and thus it is a function only of the radial coordinate r. Using the above equations, we find that the Lagrangian is given in terms of r by

$$\mathcal{L}(r) = \frac{2(1 - f(r) - rf'(r))}{r^2}. \tag{18}$$

Therefore, to generate the regular geometry we want to study in this paper, we need to substitute the metric function of Eq. (2) in Eq. (18), and arrive at the following Lagrangian:

$$\mathcal{L}(r) = \frac{12ml}{(r+l)^4} + 2\Lambda, \tag{19}$$

where it is evident that in the absence of the minimal length scale we are led to $\mathcal{L}(r) = 2\Lambda$ as is required for consistency. The mass m is the Komar mass [38] of the metric,[2] and we can write it as a function of the outer horizon radius r_h and the minimal length scale l by using the condition $f(r_h) = 0$, which leads to

$$m = \frac{(r_h + l)^3(3 - \Lambda r_h^2)}{6r_h^2}. \tag{20}$$

The root r_h corresponds to the largest root of the equation $f(r) = 0$, except in the case of a de Sitter spacetime which admits one more horizon, the cosmological one, at larger distance in comparison with the outer horizon of the black hole.

The source of this RBH is a particular case of the sources presented in Ref. [27] whose Lagrangian density, as a function of the field strength $\mathcal{F}$, is given by[3]

$$\tilde{\mathcal{L}}(\mathcal{F}) = \frac{4\mu}{\sigma} \frac{\sigma\mathcal{F}}{(1 + (\sigma\mathcal{F})^{1/4})^{\mu+1}}, \tag{21}$$

which leads to a geometry of the form

$$f(r) = 1 - \frac{2\sigma^{-1}q^3 r^{\mu-1}}{(r+q)^\mu}, \tag{22}$$

in an asymptotically flat spacetime ($\Lambda = 0$) with the magnetic charge given by

$$Q_m = \frac{q^2}{\sqrt{2\sigma}}. \tag{23}$$

The spacetime geometry analyzed in this article can be generated by the following choice of parameters

$$\mu = 3, \qquad q = l, \qquad \sigma = \frac{l^3}{m}, \tag{24}$$

which lead to a magnetic charge

$$Q_m = \sqrt{\frac{ml}{2}}, \tag{25}$$

and the Lagrangian density given by Eq. (19) once we use Eq. (9), which provides the link from one representation to another. Two brief comments are in order; firstly, the Lagrangian of Eq. (21) has a Maxwell weak-field limit, which can be seen by performing an expansion around $\mathcal{F}$, and leads to

$$\tilde{\mathcal{L}}(\mathcal{F}) = 4\mu\mathcal{F} + \mathcal{O}(\mathcal{F}^{5/4}). \tag{26}$$

This is a different feature of this subclass of NED Lagrangians in comparison with the ones used to generate other well-known models such as Bardeen or Hayward, which exhibit stronger weak-field limits than the Maxwell theory. To make this statement more precise, one finds using the sources described in Ref. [27] that for the Bardeen model the weak-field limit is $\mathcal{O}(\mathcal{F}^{5/4})$, whereas for the Hayward model is $\mathcal{O}(\mathcal{F}^{5/2})$.

Secondly, it is evident from relation (25) that the existence of the magnetic charge is tied to the presence of the minimal length scale. This means that in the case of vanishing charge, the minimal length vanishes as well and we retrieve the singular Schwarzschild geometry. Conversely, if we maintain a fixed nonzero magnetic charge, as we will in the study of phase transitions in the canonical ensemble, the minimal length persists as a fundamental feature.

Having established the matter Lagrangian that serves as a source for this theory, we can now proceed with the study of thermodynamics. We can approach this either using Hamiltonian methods [42] or Euclidean path integral methods. Both approaches lead to congruent thermodynamic quantities, in the regimes where they can be directly compared, which is a prerequisite for consistency. A detailed analysis on the consistency of these approaches has been conducted in Ref. [33] using as example the Hayward model. Without loss of generality, we restrict ourselves to the Euclidean path integral method described in the following section.

III. THERMODYNAMICS WITH EUCLIDEAN ACTION

In spite of its inherent technical issues, the path integral has been firmly established as an invaluable tool for our understanding of gravity beyond the classical realm. Aside from formally defining a quantum theory of gravity, it provides us with a powerful way to study gravitational thermodynamics, even in spacetimes that do not admit a

[2]When it comes to de Sitter spacetime, caution must be taken with this interpretation. This spacetime does not admit a globally timelike Killing vector field, so the construction of conserved charges is problematic [39–41]. This is due to the presence of a cosmological horizon leading to a spacelike character of the Killing vector ∂_t, assocciated with time translations at distances larger than the cosmological horizon.

[3]To avoid issues with the notation in this article we have replaced the parameter a used in Ref. [27] with the letter σ.

straightforward definition of temperature, as for example the de Sitter case, which we will analyze later on. In this application, we exploit the relation between the classical Euclidean action I_E and the quantum mechanical partition function $\mathcal{Z}$,

$$F = -T \log \mathcal{Z} \approx T I_E, \tag{27}$$

where F is the free energy of the system and T the temperature. The above relation holds in the semiclassical approximation. We are concerned with the interaction of quantum matter fields with the presumably quantum gravitational field. Thus the path integral measure should include both the metric associated with the gravitational field along with the matter fields. At leading order in m_p/M, with m_p representing the Planck mass, the matter fields do not contribute to the path integral. Consequently, the measure in use will solely originate from topologically distinct metrics. With all of these assumptions, the partition function can be approximated as

$$\mathcal{Z} = \int_{g(0)}^{g(\tilde{\tau})} \mathcal{D}[g] e^{-I_E[g]/\hbar}, \tag{28}$$

where $\tilde{\tau}$ is the periodicity. One further approximation can be made by considering only the leading contribution to the integral, which comes from metrics that are classical solutions to the equations of motion, namely those for which $\delta I_E[g_{cl}] = 0$. This is the saddle point approximation, in which

$$\int_{g(0)}^{g(\tilde{\tau})} \mathcal{D}[g] e^{-I_E[g]/\hbar} \approx e^{-I_E[g_{cl}]/\hbar}. \tag{29}$$

Therefore, we conclude that

$$\mathcal{Z} \approx e^{-I_E[g_{cl}]/\hbar} \Rightarrow F \approx T I_E. \tag{30}$$

This can be regarded as the zero loop approximation to the full partition function, which only includes the dominant contribution from the gravitational field. Using the partition function, we can define thermodynamic quantities using well-known formulas from statistical mechanics. Using the approximation (30), one can determine the internal energy and entropy of the system through the Euclidean action with the following formulas:

$$E = \frac{\partial I_E}{\partial \beta}, \qquad S = \beta \frac{\partial I_E}{\partial \beta} - I_E, \tag{31}$$

where β denotes the inverse temperature T^{-1}. This approach, in the case of black holes, was first developed by Gibbons and Hawking [43], and analyzed further by York in Ref. [44].

Having introduced the basic notation and methodology for the Euclidean path integral approach, we start our analysis with the calculation of the proper Euclidean action. For the model under consideration the total reduced action[4] I_r is given by

$$I_r = I_{\rm EH} + I_{\rm GHY} + I_M + I_{\rm EMB} - I_0. \tag{32}$$

We will proceed with the explanation and calculation (see Appendix A) of each term separately and then combine them to arrive at the final expression for the total reduced action. We start with the Einstein-Hilbert action $I_{\rm EH}$. We do not consider the cosmological constant in this action term since it is already implemented in the matter term I_M of the action. We have that

$$I_{\rm EH} = -\frac{1}{16\pi} \int d^4x \sqrt{g} R, \tag{33}$$

where R is the Ricci scalar for the Euclidean spacetime geometry. The next term of the action is the Gibbons-Hawking-York term [43,44] that is introduced when we perform an integration over a region of spacetime bounded by a hypersurface ∂M. This term of the action is computed at $r = r_c$ and is given by

$$I_{\rm GHY} = \frac{1}{8\pi} \int_{\partial M} \sqrt{k} K, \tag{34}$$

where K is the trace of the extrinsic curvature.

The matter part of the action which, as we saw in the derivation of the source of this geometry in Sec. II, contains the cosmological fluid part as well and is given by

$$I_M = \frac{1}{16\pi} \int d^4x \sqrt{g} \mathcal{L}(r), \tag{35}$$

where $\mathcal{L}$ is the Lagrangian density described by Eq. (19).

The next action term is the electromagnetic boundary term, which is introduced to keep the magnetic charge fixed since the thermodynamic analysis of this paper will be restricted to the canonical ensemble [45]. For an NED theory this term is given by

$$I_{\rm EMB} = -\frac{1}{16\pi} \int_{\partial M} \sqrt{k} \left(\frac{\partial \mathcal{L}}{\partial \mathcal{F}} \right) F^{\mu\nu} n_\nu A_\mu, \tag{36}$$

where n_ν is the unit normal vector to the boundary ∂M [46,47]. This term will vanish since we are integrating over a time slice of the spacetime and the only nonvanishing components of the electromagnetic tensor $F_{\mu\nu}$ are $F_{23} = -F_{32}$, as can be seen from Sec. II.

[4]We use the term "reduced" action to distinguish it from the original general form, i.e., before any integration has been carried out.

The final term of the action I_0 corresponds to a subtraction term introduced to regularize the action. It is chosen such that the total action vanishes when a black hole is not present, i.e., $m = 0$. Before we explicitly write the final expression for the reduced action, we point out that in order to properly compare a black hole spacetime to a spacetime without a black hole, we need to match the boundaries (cavity) in these two spacetimes leading to a new parameter β in the background action instead of β_h [45,48]. Once we combine all of the nonvanishing parts of the action, namely Eqs. (A7), (A12), (A14), and (A16), we are led to the final expression for the reduced action,

$$I_r = -\pi r_h^2 + \frac{\beta r_c}{3}\left(3 - r_c^2\Lambda - \sqrt{3 - r_c^2\Lambda}\sqrt{3 - r_c^2\Lambda + \frac{r_c^2(r_h + l)^3(-3 + r_h^2\Lambda)}{(r_c + l)^3 r_h^2}}\right). \tag{37}$$

Following the methodology in Ref. [45], we now proceed with the computation of the proper thermodynamic quantities. For the calculation of the temperature, we need to identify the stationary points of the action. This involves extremizing it with respect to the horizon radius r_h and leads to the equation,

$$\frac{\partial I_r}{\partial r_h} = 0, \tag{38}$$

which can be used to determine β. The solution β is a function of the cavity radius r_c, the horizon radius r_h, the minimal length scale l, and the cosmological constant Λ. Therefore, the temperature for this black hole will be $T = \beta^{-1}(r_h, r_c, l, \Lambda)$ and it is given by

$$T = \frac{r_c^3(r_h + l)^2\sqrt{3 - r_c^2\Lambda}(2l - r_h + r_h^3\Lambda)}{4\pi(r_c + l)^3 r_h^4 \mathcal{X}}, \tag{39}$$

where $\mathcal{X}$ is given by the following, rather long expression

$$\mathcal{X} = \sqrt{\frac{-(r_c - r_h)(9l^2 r_c r_h - 3r_c^2 r_h^2 + 3l^3(r_c + r_h) + r_c^2 r_h^2(3l^2 + r_c^2 + r_c r_h + r_h^2 + 3l(r_c + r_h))\Lambda)}{(r_c + l)^3 r_h^2}}. \tag{40}$$

We proceed with the calculation of the remaining thermodynamic quantities in the same manner as in Ref. [45]. For the minimal length scale l, the conjugate potential that appears in the first law of black hole thermodynamics and the Smarr formula is given by

$$\Phi = \frac{1}{\beta}\frac{\partial I_r}{\partial l}, \tag{41}$$

and an explicit calculation yields

$$\Phi = \frac{r_c^3(r_c - r_h)(l + r_h)^2\sqrt{3 - r_c^2\Lambda}(3 - r_h^2\Lambda)}{2(l + r_c)^4 r_h^2 \mathcal{X}}. \tag{42}$$

In the presence of a cosmological constant we have a relevant pressure/tension (depending on the sign) arising from it, which is defined via $P = -\Lambda/8\pi$. In a similar way, we find the conjugate variable to the pressure/tension P, which will correspond to the thermodynamic volume V. It is defined by

$$V = \frac{-8\pi}{\beta}\frac{\partial I_r}{\partial \Lambda}, \tag{43}$$

which leads to a rather long expression that does not provide any insight for the reader, so it is given in Appendix C. We emphasize here that we are working in the extended phase space, allowing for variations of Λ in the first law [49]. Motivation for permitting the variation of the cosmological constant and the minimal length scale is given in Sec. IV.

There is one more relevant potential, denoted as λ, that needs to be computed. It is conjugate to the area of the cavity $A_c = 4\pi r_c^2$. We will interpret this term as the surface pressure or tension, depending on the sign, resulting from the presence of the cavity. We have that

$$\lambda = \frac{1}{\beta}\frac{\partial I_r}{\partial A_c}. \tag{44}$$

In the above calculation, we first replace $r_c \to \sqrt{A_c/4\pi}$ and then take the derivative. After that, we substitute A_c with $4\pi r_c^2$ and we have the conjugate potential λ as a function of the cavity radius. The full expression is provided in Appendix C. In the absence of a cavity this term will not contribute to the first law or the Smarr formula, as we will see in the AdS and Minkowski cases later on.

Now that we have completed the computation of the conjugate potentials, we can proceed with the calculation of two highly significant quantities for thermodynamics,

namely the mean thermal energy E and the entropy S. These calculations are carried out using Eq. (31). The mean thermal energy plays the role of the internal energy in the first law and is given by

$$E = \frac{\partial I_r}{\partial \beta}, \tag{45}$$

which in the presence of an isothermal cavity yields

$$E = \frac{r_c}{3}\left(3 - r_c^2\Lambda - \sqrt{3 - r_c^2\Lambda} \times \sqrt{3 - r_c^2\Lambda + \frac{r_c^2(l + r_h)^3(-3 + r_h^2\Lambda)}{(l + r_c)^3 r_h^2}}\right). \tag{46}$$

The entropy is calculated from the Euclidean action from the relation

$$S = \beta\frac{\partial I_r}{\partial \beta} - I_r, \tag{47}$$

which leads to the well-known result due to Bekenstein and Hawking,

$$S = \frac{A}{4} = \pi r_h^2, \tag{48}$$

with A being the horizon area. The above quantities define a proper Smarr relation with the appropriate scaling arguments [50], which is written as

$$E = 2TS + \Phi l + 2\lambda A_c - 2PV. \tag{49}$$

The scaling arguments correspond to the following substitutions:

$$E \to cE, \quad l \to cl, \quad r_h \to c r_h, \quad \Lambda \to c^{-2}\Lambda, \quad S \to c^2 S, \quad T \to c^{-1}T, \quad \Phi \to \Phi, \quad \lambda \to c^{-1}\lambda, \quad V \to c^3 V. \tag{50}$$

The first law of black hole mechanics is given by

$$dE = TdS + \Phi dl + \lambda dA_c + VdP. \tag{51}$$

We note that in the above expression of the first law E is identified as the Komar mass in the absence of a cosmological constant, whereas if $\Lambda < 0$ is present E has to be interpreted as the enthalpy of the system [49]. Intuitively, this means that now E will correspond to the internal energy M of the system (Komar mass) in addition to the energy PV needed to displace the vacuum energy from its environment, or in other words, to embed the black hole in the spacetime with the negative cosmological constant. We note here that it is trickier to give, in an analogous way, thermodynamic/physical interpretations of quantities in de Sitter spacetime due to the presence of the cosmological horizon.

We will use the derived thermodynamic quantities with their appropriate limits, when possible, in the following section where we will analyze the phase structure of the model described by Eq. (2).

IV. FIRST LAW OF BLACK HOLE THERMODYNAMICS, SMARR FORMULA AND PHASE STRUCTURE

The first law of black hole mechanics derived in Ref. [31] has been proven to hold in any theory of gravity arising from a diffeomorphism-invariant Lagrangian [51,52]. Extension of the first law for the case of NED was first studied in Ref. [53], although the Smarr formula was not satisfied. This problematic behavior was fixed later on in Ref. [42], where the Bardeen black hole and the Born-Infeld theory [24] were studied, by appropriate accounting of the extra parameters of the theory. The mathematical formulation of the first law in an asymptotically flat spacetime in the case of NED theory is

$$dM = \mathcal{T}dS + \Phi_e dQ_e + \Psi_H dQ_m + \sum_i K_i d\beta_i, \tag{52}$$

where M is the Komar mass, $\mathcal{T}$ is the temperature given by the surface gravity κ as $\mathcal{T} = \kappa/2\pi$, S is the entropy, Φ_e and Ψ_H are the electric and magnetic potentials associated with the electric and magnetic charge Q_e and Q_m, respectively, and the terms K_i correspond to potentials linked to the extra parameters β_i of the theory. Using Hamiltonian methods it is possible to calculate these potentials and with appropriate change of variables we arrive at the thermodynamic quantities arising naturally from the Euclidean action [33].

In the following, the minimal length will be considered as a fundamental parameter and we will allow its variation in a region that will admit a regular black hole geometry (although not extremal). Before we proceed to the analysis of the first law, Smarr formula, and phase structure for each case of spacetime, it is useful to provide some motivation for allowing parameters such as the minimal length l and the cosmological constant Λ to vary and therefore appear in the first law. In general, we expect that there are more fundamental theories in which coupling constants or the cosmological constant are not predetermined but on the contrary emerge from vacuum expectation values allowing for possible variations thereof. Consequently, it is physically justified to include their variation in the first law [54,55]. In the presence of a cosmological constant or extra parameters of the theory, i.e., minimal length in the majority of RBHs, one can see that the Smarr relation is not satisfied, and therefore we have to include a variation of the extra parameters in the first law to ensure consistency [50,56].

We provide some additional motivation for the varying minimal length. Usually this length is associated with a fundamental scale set by a quantum gravity theory, i.e., the Planck scale [57,58]. However, studies that take into account backreaction in the black hole interior lead to an evolving minimal length l [23,59,60], therefore permitting its variation in the first law.

We now proceed with the study of the thermodynamics of the RBH in spacetimes with and without Λ. In the case of a negative cosmological constant, i.e., AdS spacetime, the thermal equilibrium is established naturally. The boundary of the AdS is timelike and this allows massless particles to reach it in finite proper time. The commonly accepted approach involves enforcing reflecting boundary conditions, effectively treating AdS spacetime as closed. As a result, massless particles will be reflected towards the center upon reaching $r = \infty$. The same behavior applies to massive particles, but this is because of the attractive nature of the potential when $\Lambda < 0$. This feature of the spacetime allows for sufficiently large black holes to reach a state where the rate of outgoing radiation matches the one of the reflected (ingoing) radiation, rendering the black hole stable. This leads to an equilibrium state with one temperature T which is the temperature of the black hole, or equivalently, of the radiation.

To enforce thermal equilibrium in spacetimes such as de Sitter and Minkowski, we need to introduce an isothermal cavity [61–65], otherwise this is not possible. In the de Sitter case, the presence of the cosmological horizon which, in general, radiates at a different temperature than the black hole horizon, leads to an observer situated inbetween them to observe a nonequilibrium state because of this temperature difference [66].

While studying phase transitions, we will consider the order parameter of the theory to be the horizon radius r_h, which represents the size of the black hole. It is worth pointing out that in this case the value $m = 0$ represent the empty spacetime, which is equivalent to $r_h = 0$ and $l = 0$ as we saw in Sec. II. We proceed with a separate study for each spacetime case now.

A. Embedding in anti–de Sitter

The AdS spacetime does not admit any other horizon apart from the black hole's inner and outer ones and therefore we are permitted to study the thermodynamic properties in the absence of a cavity, i.e., taking the cavity radius r_c to infinity. Based on this, we proceed with the computation of the appropriate thermodynamic quantities. We start with the temperature which is calculated, by taking the limit $r_c \to \infty$ of Eq. (39) to be

$$T_{\mathrm{AdS}} = \lim_{r_c\to\infty} T = \frac{(l+r_h)^2(r_h - 2l - r_h^3\Lambda)}{4\pi r_h^4}. \quad (53)$$

We should emphasize that this is an effective temperature that arises directly from the Euclidean path integral approach and differs from the ordinary/conventional definition of the temperature linked to the surface gravity κ.[5] To illustrate this point clearly, we provide the expression for this temperature as

$$\mathcal{T} = \frac{\kappa}{2\pi} = \frac{r_h - 2l - r_h^3\Lambda}{4\pi r_h(r_h + l)}. \quad (54)$$

An elegant relationship between these two temperatures becomes apparent, demonstrating that the effective temperature is slightly higher due to the regularization of the singularity through the introduction of the minimal length. This relation is

$$T_{\mathrm{AdS}} = \left(1 + \frac{l}{r_h}\right)^3 \mathcal{T}, \quad (55)$$

which leads to $T_{\mathrm{AdS}} > \mathcal{T}$, although by a small amount since we expect in general $l \ll r_h$.[6]

We will now comment on the possible reasons behind this distinction between surface gravity and effective temperature. One possible explanation lies in the definition of the temperature as the surface gravity which is derived solely from the kinematic aspects of the spacetime geometry. Gravitons also contribute to the Hawking radiation and therefore their kinematic properties will play a significant role in the computation of the temperature/surface gravity. It is usually assumed that they move at the speed of light, although, it has been shown in Ref. [68] that when we have scalar-tensor theories of gravity the propagation speed of gravitons is altered and they can move on timelike/spacelike trajectories. This could lead to a justified modification of the temperature. This reasoning was proposed as a

[5]We point out that in the form of the first law described by Eq. (52) the temperature $\mathcal{T}$ is given by the surface gravity. In our case, except for the magnetic charge Q_m, we have an additional parameter $\beta_i = \sigma$, which appears in the NED Lagrangian of Eq. (21). If we treat as fundamental thermodynamic variables the magnetic charge Q_m and the parameter σ, instead of the minimal length scale l, then the first law, in the AdS case, takes the form $dM = \mathcal{T}dS + \Psi_H dQ_m + K_\sigma d\sigma + VdP$. Under this assumption, using the Euclidean path integral formalism, the extremization of the action with respect to the horizon radius leads to the temperature being the surface gravity and the entropy remains the Bekenstein-Hawking entropy. For a detailed derivation of this result and a comparison between considering Q_m and σ as fundamental variables versus the minimal length scale l we refer the reader to Appendix B.

[6]We emphasize that this higher effective temperature is not unique to our scenario. It also manifests in singular geometries, as the one explored in Ref. [67]. This "modified" temperature should be attributed to the presence of matter. However, in the case we are considering, the matter fields are tied to the singularity regularization allowing us to make a direct connection between this increased temperature and the absence of singularity.

possible explanation in Ref. [67] for the case of 4D scalar-tensor Einstein-Gauss-Bonnet gravity. An analogous phenomenon might be present in RBHs, as some of them can also be generated in the same framework. Recently, the Hayward metric has been derived in this context in Ref. [69]. Another equally possible explanation relies in the interpretation of quantities introduced in the first law of black hole thermodynamics. When we consider variations of the energy in the first law, this energy represents the total energy of the spacetime, including the matter which may or may not be thermalized with respect to the Killing time. In this variation, maintaining the entropy of the total matter content as the geometric entropy necessitates a modification of the temperature, which is the one derived using the Euclidean path integral approach. However, when matter content is absent, for example by taking $l \to 0$ in Eq. (55), the two temperature definitions coincide.

We continue with the calculation of the conjugate potential for l, which is derived by taking the limit $r_c \to \infty$ of Eq. (42), and find

$$\Phi_{\mathrm{AdS}} = \frac{(l + r_h)^2(3 - r_h^2\Lambda)}{2r_h^2}. \tag{56}$$

Similarly, we derive the thermodynamic volume V_{AdS} by taking the limit $r_c \to \infty$ of Eq. (43), which leads to

$$V_{\mathrm{AdS}} = \frac{4\pi}{3}(r_h + l)^3. \tag{57}$$

We observe here the well-known result of the thermodynamic volume being different than the geometric one, while they happen to coincide when the minimal length scale vanishes, i.e., $l = 0$, which corresponds to the Schwarzschild-AdS case. The mean thermal energy is given by relation (46) taking the limit $r_c \to \infty$, and it is

$$E_{\mathrm{AdS}} = \frac{(l + r_h)^3(3 - r_h^2\Lambda)}{6r_h^2}. \tag{58}$$

We see that the thermal energy is the same as the Komar mass that someone will calculate by solving the equation $f(r_h) = 0$ given by Eq. (20). This is not the case in de Sitter spacetime as we can see from Eq. (46). Lastly, as the cavity is positioned at infinity, it does not contribute any pressure, so there is no term λ present in the first law or the Smarr formula.

Therefore, in the AdS spacetime for this RBH, we have that the first law of black hole thermodynamics is given by

$$dE = T_{\mathrm{AdS}}dS + \Phi_{\mathrm{AdS}}dl + V_{\mathrm{AdS}}dP. \tag{59}$$

We can also see that the Smarr formula is satisfied and it can be written in the form

$$E_{\mathrm{AdS}} = 2T_{\mathrm{AdS}}S + \Phi_{\mathrm{AdS}}l - 2PV_{\mathrm{AdS}}, \tag{60}$$

where the scaling arguments (50) hold. We note that the above Smarr relation is characterized by linearity even though the vector potential does not share the symmetry of the spacetime.[7] The symmetry inheritance of the spacetime from the fields is a sufficient condition for linearity [70], but in this case we see that this condition is not satisfied although linearity is preserved.

Since we have calculated the proper thermodynamic quantities for AdS, we can now proceed with the study of the phase structure of this geometry. We analyze it in the canonical ensemble, but before that, we need to calculate the crucial quantity for this study, which is the Gibbs free energy defined as

$$F_{\mathrm{AdS}} = E_{\mathrm{AdS}} - T_{\mathrm{AdS}}S. \tag{61}$$

After using Eqs. (58), (53), and (48), we have that

$$F_{\mathrm{AdS}} = \frac{(l + r_h)^2(12l + 3r_h + r_h^2\Lambda(r_h - 2l))}{12r_h^2}. \tag{62}$$

The equilibrium state of the thermodynamic system corresponds to the global minimization of the free energy. To properly study the phase structure, we need to study the free energy as a function of temperature by drawing parametric plots using the outer horizon radius as a parameter. Figure 1 reveals two distinct yet quite similar behaviors. The distinction comes from the fact that we vary different parameters in Figs. 1(a) and 1(b), i.e., the minimal length and the cosmological constant, respectively. We observe from Fig. 1 a characteristic swallowtail behavior. For a fixed value of the cosmological constant $\Lambda = -1$, there is a critical value for the minimal length $l_c \approx 0.156$ below which there is a first-order phase transition from a small to a large black hole, while above this critical value, no phase transition occurs. The same behavior is exhibited when we vary the cosmological constant, where the critical value is $\Lambda_c \approx -2.02$ below which no phase transition occurs, and above there is a small to large black hole first-order phase transition. The parameter that changes here is the horizon radius r_h; it increases from left to right along the near horizontal lines, which is the same direction as the increasing temperature. The direction of increasing radius is also indicated with arrows for the dashed light blue curve. Starting from low temperatures on this curve and increasing it gradually, we reach the crossing point. At this point, the system chooses the direction that minimizes the free energy which is downwards, indicating that from a small horizon radius, we go straight to a large horizon radius, i.e., a small to large phase transition. At the critical

[7]The fourth component of the vector potential A^μ depends on the angle θ as can be seen from Eq. (7).

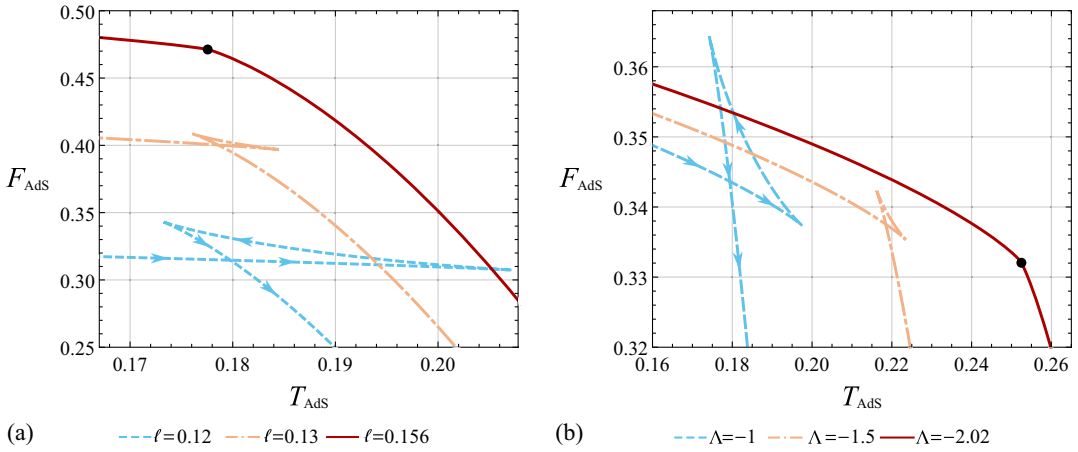

FIG. 1. (a) Free energy $F_{\rm AdS}$ as a function of the temperature $T_{\rm AdS}$ for a constant value of the cosmological constant $\Lambda = -1$ with varying minimal length l; (b) Free energy $F_{\rm AdS}$ as a function of the temperature $T_{\rm AdS}$ for a constant value of the minimal length $l = 0.11$ with varying cosmological constant Λ; In both cases, the arrows denote the direction in which the horizon radius r_h increases. For the sake of readability, we omit the arrows in the remaining curves, although the same pattern is implied.

point indicated by a black dot in Fig. 1, the transition becomes second order.

Therefore, in the extended phase space, this RBH model embedded in AdS exhibits the same critical behavior as ordinary fluid systems [49]. Combining all the crossing points, a swallowtail is created and it closes at the critical point. These crossing points represent states where the small and large phases coexist. Combining all of these points, we can illustrate the coexistence line in a $P-T$ diagram which terminates at the critical point, as can be seen from Fig. 2. At temperatures above $T^{(c)}_{\rm AdS}$ and/or pressures above $P^{(c)}$ there is no difference between the

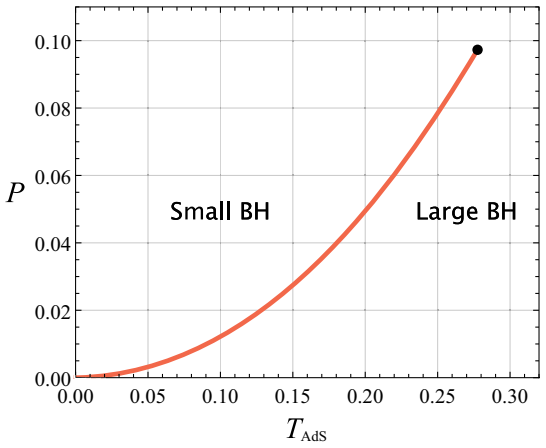

FIG. 2. Coexistence line for the RBH model in AdS for a fixed minimal length scale $l = 0.1$. The orange line represents points where first-order phase transitions occur, and the black dot represents the termination of the swallowtail with a second-order phase transition occurring at the critical point $(P^{(c)}, T^{(c)}_{\rm AdS}) = (0.2776, 0.0973)$. The origin $(0,0)$ of the diagram does not belong to the curve since the pressure must be positive in AdS.

two phases, so as the temperature increases we have a smooth transition from a small to a large black hole. This behavior is reminiscent of the liquid-gas transition.

The phase structure of this RBH is similar to the one encountered when studying the Reissner-Nordström metric in the canonical ensemble. There, the presence of a nonzero electric charge makes the line $F = 0$, i.e., pure radiation, inaccessible, thus preventing the Hawking-Page transition from occurring. This happens because in the presence of a nonzero charge the black hole cannot evaporate completely. This situation is similar to our case, where in the canonical ensemble the magnetic charge is fixed, leading to the same behavior. The main difference here is that the magnetic charge is inherently linked to the presence of the minimal length, as seen from Eq. (25), and therefore the singularity regularization. This suggests that there might be a strong connection between the presence of the singularity and the existence of a Hawking-Page transition. Similar behavior has been encountered before in the study of the Hayward black hole in Ref. [33].

We proceed now with the calculation of the critical point and examine if we have the usual mean-field theory behavior encountered in other black hole cases in AdS [49]. To do that, we write the pressure as a function of the temperature $T_{\rm AdS}$ and the thermodynamic volume $V_{\rm AdS}$. The volume expression, given in Eq. (57), is a monotonic function of the horizon size r_h, and we can freely use this parameter to calculate the critical points in its stead. Therefore, we write the pressure as a function $P(r_h, T_{\rm AdS})$ which is computed by solving Eq. (53) for Λ. The pressure is identified as $-\Lambda/8\pi$ and thus we conclude that

$$P(r_h, T_{\rm AdS}) = \frac{T_{\rm AdS}}{2r_h(1+\frac{l}{r_h})^2} - \frac{r_h - 2l}{8\pi r_h^3}. \tag{63}$$

From the above relation, we can extract information about the reduced volume, i.e., the volume over the number of particles, which is the inverse coefficient of the linear term of the temperature [71]. Therefore, we conclude that the reduced volume is given by

$$v = 2r_h\left(1+\frac{l}{r_h}\right)^2. \tag{64}$$

The definition of the reduced volume arises naturally from the Van der Waals-like form of Eq. (63), and here it is different than the usually assumed value $2r_h$ [49], although in the limit of vanishing minimal length we retrieve the usually defined quantity.

To calculate the critical point, we need to find solutions for the following system of equations:

$$\frac{\partial P}{\partial r_h}=0, \qquad \frac{\partial^2 P}{\partial r_h^2}=0. \tag{65}$$

Remarkably, analytic solutions for these equations are possible but because of their lengthy and complicated nature we omit them here and give instead approximate expressions. We find that

$$r_h^{(c)} \approx 4.66433l, \qquad T_{\mathrm{AdS}}^{(c)} \approx \frac{0.027758}{l}. \tag{66}$$

Substituting these expressions into Eqs. (63) and (64) we find the respective critical values,

$$P^{(c)} \approx \frac{0.0009728}{l^2}, \qquad v^{(c)} \approx 13.7574l. \tag{67}$$

For temperatures and pressures larger than the derived above critical values, phase transitions are not possible. This is also reflected later on in the study of the heat capacity.

When studying thermodynamic systems, stability requirements dictate the presence of a positive heat capacity, and pressure to be monotonically decreasing function of the volume. We can see from Fig. 3 (orange isotherm) that above the critical temperature the pressure is a monotonically decreasing function of the horizon radius r_h, and therefore the thermodynamic volume V_{AdS}, due to their monotonically increasing relation. At the critical temperature (dark red line) we have a certain horizon radius for which $\partial P/\partial r_h = 0$ and $\partial^2 P/\partial r_h^2 = 0$. Below the critical temperature, where phase transitions are possible, we have different monotonicity of the pressure with respect to the volume for different segments of the isotherm. The segments AB and CD correspond to the pressure being a decreasing function of the volume, and they represent metastable states (AB and CD correspond to superheated liquid and supercooled vapor in the liquid-gas case, respectively). The thermodynamic inequality $\partial P/\partial r_h < 0$ is satisfied in these segments, but this is not the case in the segment BC where pressure is an increasing function of the volume, which signifies the violation of the thermodynamic inequalities and consequently thermodynamic instability.

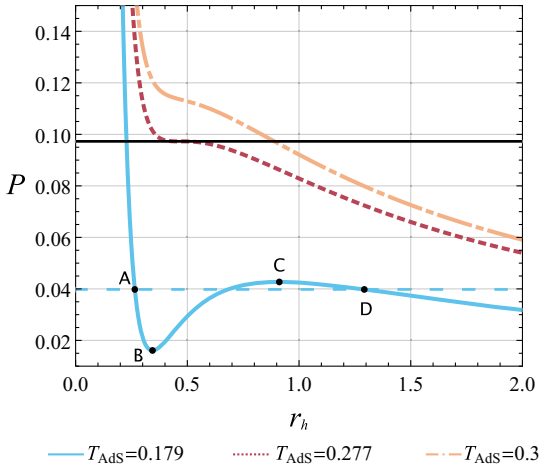

FIG. 3. Isotherms of the equation of state $P(r_h, T_{\mathrm{AdS}})$ for the RBH model in AdS for a fixed value of the minimal length $l = 0.1$ for various T_{AdS}. The solid horizontal black line represents the critical pressure $P^{(c)} \approx 0.973$, while the dashed horizontal light blue line depicts the coexistence line for the isotherm with temperature $T_{\mathrm{AdS}} = 0.179$.

The dashed horizontal light blue line in Fig. 3 corresponds to the coexistence pressure P_{coex} derived by Maxwell's construction. In a $P-V$ diagram, the area enclosed between the isotherm and the line representing the coexistence pressure vanishes. This is a condition derived directly from the assumption of thermodynamic equilibrium between two phases which can be written as

$$\int_{V_A}^{V_D}\left[P(r_h, T_{\mathrm{AdS}}) - P_{\mathrm{coex}}\right]dV = 0. \tag{68}$$

Here V_A corresponds to the small black hole phase and V_D to the large one. We can see by direct calculation that Eq. (68) holds and that the coexistence pressure is the same as the one extracted from the $F-T$ diagram. We point out that proper calculation requires using the volumes rather than the radii of the small and large black holes. If we attempt to use the radii to perform the integration of the pressure, we are led to an inconsistency, namely that the coexistence pressure defined from Maxwell's construction does not coincide with the one found from the $F-T$ diagram.

We proceed now with the calculation of the critical ratio, which can be calculated using the critical values of the pressure, temperature, and reduced volume and find that

$$\frac{P^{(c)}v^{(c)}}{T_{\mathrm{AdS}}^{(c)}} \approx 0.482197 \neq \frac{3}{8}. \tag{69}$$

TABLE I. In this table, the left column represents the RBH models we are considering, where the last model is the one analyzed in this paper. The middle column describes the asymptotic behavior where we have omitted the cosmological constant term. The right column describes the magnitude of the difference $|P^{(c)}v^{(v)}/T^{(c)}_{\rm AdS} - 3/8|$ between the critical ratios for these models with the usual mean-field theory (MFT) value 3/8. In the calculation of the MFT ratio deviation, we have used only the reduced volume that appears as an inverse coefficient of the temperature in the Van der Waals-like equation of state, which should be considered the appropriate choice.

RBH model	Asymptotic behavior	MFT ratio deviation
Hayward	$1-\frac{2m}{r}+\frac{4m^2l^2}{r^4}+\mathcal{O}(r^{-7})$	0.016
Bardeen	$1-\frac{2m}{r}+\frac{3ml^2}{r^3}+\mathcal{O}(r^{-5})$	0.025
Cadoni *et al.*	$1-\frac{2m}{r}+\frac{6ml}{r^2}+\mathcal{O}(r^{-3})$	0.107

This result indicates a deviation from the "universal" mean-field theory critical ratio. On the other hand, if we consider the ordinary definition of the reduced volume $\tilde{v}=2r_h$ used in the majority of studies of black hole phase transition, we are led to a different critical ratio,

$$\frac{P^{(c)}\tilde{v}^{(c)}}{T^{(c)}_{\rm AdS}}\approx 0.326968\neq\frac{3}{8}, \tag{70}$$

which also signifies the departure from the usual value for the Van der Waals fluids, although there is a significant difference between the critical values calculated for different definitions of the volume. This is in contrast with what we have seen in Ref. [33] and we attribute this deviation to the stronger deformation due to the minimal length in comparison with the Hayward model (See Table I).

It is interesting to compare the deviation from the value of the critical ratio of mean-field theory for a variety of RBH models that exhibit different corrections to the Schwarzschild asymptotic behavior. For this purpose, we consider the Hayward and Bardeen models[8] along with the one analyzed in this paper. We can see from Table I that the deviation from the mean-field theory ratio becomes larger as the deformations of the asymptotic behavior become larger. This indicates that there is a connection between the way the singularity is smoothed out and the thermodynamic properties of black holes in AdS. It appears that the stronger the deformation from the Schwarzschild behavior using a minimal length scale, the larger the deviation from the mean-field theory critical ratio.

We now turn to the study of the thermodynamic stability of this RBH, where the critical quantity for this analysis will be the heat capacity at constant volume defined as

[8]The thermodynamics of the Bardeen black hole is analyzed in the Appendix D.

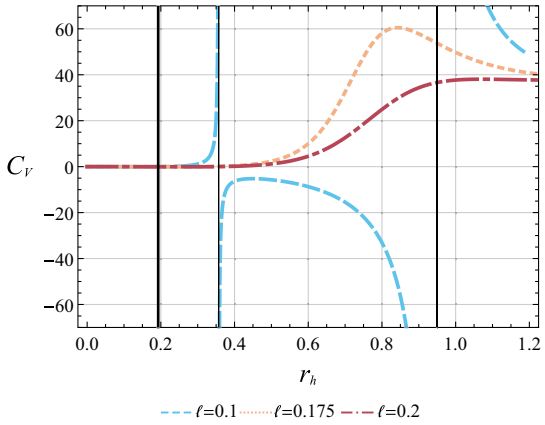

FIG. 4. Heat capacity C_V as a function of the horizon radius r_h for constant value $\Lambda=-1$ of the cosmological constant. Different colors/types represent different values of the minimal length parameter l. The thin vertical black lines correspond to infinities/discontinuities of the heat capacity while the thick vertical black line represents the minimal radius enforced by the extremal limit for the case $l=0.1$.

$$C_V=T\left(\frac{\partial S}{\partial T}\right)\Big|_V, \tag{71}$$

and it is calculated to be

$$C_V=\frac{2\pi r_h^2(r_h+l)(2l-r_h+r_h^3\Lambda)}{(r_h^2-8l^2+r_h^4\Lambda-lr_h(1+r_h^2\Lambda))}. \tag{72}$$

We can see from Fig. 4 that there are regions where the heat capacity is positive. They correspond to the thermodynamic stability of the RBH, whereas regions with the negative sign of C_V represent thermodynamically unstable regions. Caution must be taken in our analysis since there is one additional constraint when we are studying RBHs. The smaller possible radius will be the one of the extremal black hole. In this case, the RBH will have one horizon [72] which is characterized by zero surface gravity since it is degenerate leading to zero temperature. To identify this condition, we solve the following equation:

$$\kappa=\frac{f'(r_h)}{2}=0 \tag{73}$$

for r_h, which yields three solutions, only one of which is viable, and is given by

$$r_{\rm ext}=-\frac{3^{1/3}\Lambda+\left(9l\Lambda^2+\sqrt{3}\sqrt{\Lambda^3(-1+27l^2\Lambda)}\right)^{2/3}}{3^{2/3}\Lambda\left(9l\Lambda^2+\sqrt{3}\sqrt{\Lambda^3(-1+27l^2\Lambda)}\right)^{1/3}}. \tag{74}$$

We note that demanding the surface gravity to be zero is equivalent to demanding the effective temperature to be zero as seen from Eqs. (54) and (55). The extremal radius is a function of both the minimal length and the cosmological

constant which in this case is negative. An example of where this extremal radius is located can be seen in Fig. 4 depicted as a thick vertical black line for the values $l = 0.1$ and $\Lambda = -1$ with the approximate radius being $r_{\text{ext}} \approx 0.193$. This indicates that the heat capacity exhibits a divergent behavior at radii larger than the extremal limit, which makes the study of phase structure meaningful. We see that as we increase l past a certain value, we have no longer infinities/discontinuities, which is a restatement of the result we obtained in Fig. 1, i.e., the existence of a critical point. This behavior agrees, as required for consistency, with the critical values we derived in Eq. (67). For $\Lambda = -1$, it is easy to find that the corresponding critical minimal length is $l^{(c)} \approx 0.156$. We see in Fig. 4 that for critical lengths above this value, no phase transition occurs since there are no discontinuities of the heat capacity.

We now derive, once again, using this time the heat capacity, the critical values for the minimal length, and the cosmological constant. To do that we have to examine the discriminant of the denominator of the heat capacity. It is given by

$$\Delta = -4\left(33l^2\Lambda + 2170l^4\Lambda^2 + 33561l^6\Lambda^3 + 432l^8\Lambda^4\right). \tag{75}$$

Solving the equation $\Delta = 0$, treating Λ as a variable, yields four solutions. Two of the roots are $\Lambda = 0$ and $\Lambda = \Lambda^{(c)} = -8\pi P^{(c)}$, and the two remaining ones are

$$\Lambda_1 \approx -\frac{77.6228}{l^2}, \qquad \Lambda_2 \approx -\frac{0.0402495}{l^2}. \tag{76}$$

The discriminant in between these solutions has a positive sign, but yields only negative or imaginary solutions for the denominator, which means that in this region we do not have any discontinuities for the heat capacity. We conclude that for $\Lambda < \Lambda^{(c)}$ or, equivalently, for $P > P^{(c)}$, no discontinuities occur, and therefore no phase transitions in agreement with what we saw/derived previously using the critical point equations.

1. Critical exponents

The behavior of thermodynamic quantities near the critical point is described by the critical exponents. They do not depend on the details, i.e., microscopic structure of the physical system, but only on some general features. To calculate them in AdS for the RBH under consideration, we first define the quantity

$$t = \frac{T_{\text{AdS}}}{T^{(c)}_{\text{AdS}}} - 1, \tag{77}$$

which is called the reduced temperature. The main relations we are going to use are the following:

$$C_V \propto |t|^{-\alpha}, \quad g = v_l - v_s \propto |t|^{\beta},$$
$$\kappa_T = -\frac{1}{V}\frac{\partial V}{\partial P}\bigg|_T \propto |t|^{-\gamma}, \quad |P - P^{(c)}| \propto |V - V^{(c)}|^{\delta}, \tag{78}$$

where C_V is the heat capacity at constant volume, g is the order parameter, and κ_T is the isothermal compressibility.

We start with the calculation of the critical exponent α. We see from Eq. (72) that the heat capacity is independent of the temperature, and since this is also true for the entropy as seen from Eq. (48), we conclude that $\alpha = 0$.

To find the critical exponent β we need to find a way to relate the difference between the reduced volumes of the small and large black hole phases with the reduced temperature near the critical point. To proceed in an analytic way one can identify the points where the two phases coexist, i.e., $F|_{v_s} = F|_{v_l}$ and $T_{\text{AdS}}|_{v_s} = T_{\text{AdS}}|_{v_l}$, where v_s and v_l are the reduced volumes for small and large black holes, respectively. This requires finding solutions of fifth-degree polynomials to identify the point of the phase transition. Since this is not possible, we focus on finding the critical exponent β in a numerical way. We keep the minimal length fixed at $l = 0.1$ and start varying Λ near the critical value $\Lambda_c = -8\pi P^{(c)} \approx -2.445$ calculated from Eq. (67). Then, we find numerical solutions for the point of the phase transition, and by identifying the temperature T_{AdS} at this point, we also have the reduced temperature. For every value of the cosmological constant, we generate different points shown in Fig. 5. By appropriate fitting of curves of

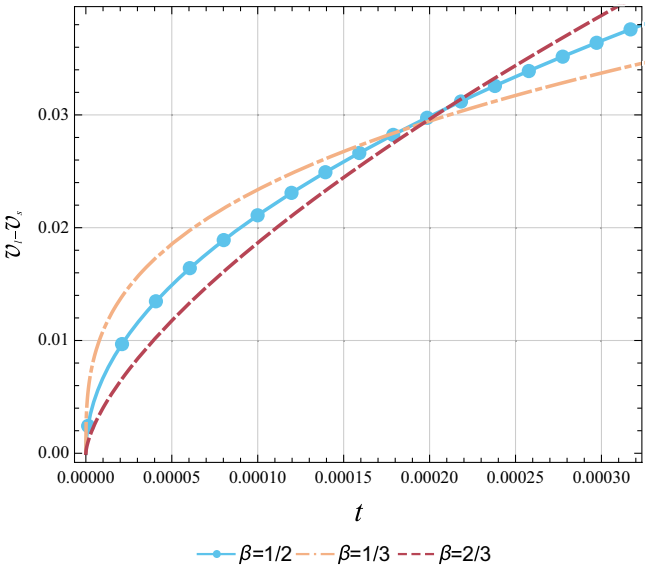

FIG. 5. Behavior of the order parameter g near the critical point as a function of the reduced temperature. Different colors/types represent different values of the coefficient β. The light blue dots represent numerical values of the points $(t, v_l - v_s)$ obtained by keeping fixed minimal length $l = 0.1$ and varying the cosmological constant Λ in the vicinity of the critical value $\Lambda^{(c)} \approx -2.445$.

the form $|t|^\beta$ we see that the exponent $\beta = 1/2$ is a perfect fit for the points obtained numerically.

For the critical exponent γ we need to plot the isothermal compressibility κ_T as a function of the reduced temperature, although in this case we can do the calculation analytically. Using the monotonicity of the volume with respect to the horizon radius, we have

$$\kappa_T = -\frac{1}{V}\left(\frac{\partial V}{\partial r_h}\right)\left(\frac{\partial P}{\partial r_H}\right)^{-1}\Big|_{T_{\mathrm{AdS}}}. \tag{79}$$

Calculation near the critical point yields a behavior

$$\kappa_T \propto |t|^{-1}, \tag{80}$$

and thus we conclude that the exponent $\gamma = 1$.

The last exponent we calculate is δ. This requires evaluating the absolute value of the difference between the pressure P given by Eq. (63) and the critical pressure $P^{(c)}$ given by Eq. (67). This can be done straightforwardly if we also use the critical radius $r_h^{(c)}$. Once we have the difference $|P - P^{(c)}|$, we can plot it and compare it with the difference $|V - V^{(c)}|$ near the critical point, and we see that the best-fit is for $\delta = 3$.

In summary, the four critical exponents are given by

$$\alpha = 0, \qquad \beta = \frac{1}{2}, \qquad \gamma = 1, \quad \delta = 3, \tag{81}$$

which are exactly the values expected from mean-field theory, even though we have a deviation from the critical ratio 3/8.

B. Embedding in Minkowski

In this section, we will study the thermodynamics in Minkowski spacetime starting with the definition of the proper thermodynamic quantities and continuing with the phase structure. As we saw at the beginning of Sec. III, here we no longer have an effective potential that confines the radiation as in the AdS case, so the implementation of an isothermal cavity is necessary to provide thermal equilibrium for the system. The temperature of the black hole is found by Eq. (39) taking the limit $\Lambda \to 0$ since a cosmological constant is not present in the spacetime. We find that

$$T_M = \frac{r_c^3(r_h - 2l)(l + r_h)^2}{4\pi(l + r_c)^3 r_h^4 \sqrt{\frac{-(r_c - r_h)(3l^2 r_c r_h - r_c^2 r_h^2 + l^3(r_c + r_h))}{(l+r_c)^3 r_h^2}}}. \tag{82}$$

Similarly, we calculate the conjugate potential for the minimal length l and cavity area A_c through Eq. (42) and (C2), respectively. They are given by

$$\Phi_M = \frac{3r_c^3(r_c - r_h)(l + r_h)^2}{2(l + r_c)^4 r_h^2 \sqrt{\frac{-(r_c - r_h)(3l^2 r_c r_h - r_c^2 r_h^2 + l^3(r_c + r_h))}{(l+r_c)^3 r_h^2}}}, \tag{83}$$

and

$$\lambda_M = \frac{1}{48\pi r_c}\left(6 + \frac{3r_c^2(2l - r_c)(l + r_h)^3}{(l + r_c)^{5/2}\sqrt{-(r_c - r_h)(3l^2 r_c r_h - r_c^2 r_h^2 + l^3(r_c + r_h))}} - 6\sqrt{\frac{-(r_c - r_h)(3l^2 r_c r_h - r_c^2 r_h^2 + l^3(r_c + r_h))}{(l + r_c)^3 r_h^2}}\right). \tag{84}$$

Two additional quantities need to be computed: First, the internal energy of the system, which is given by setting $\Lambda = 0$ in Eq. (46), and leads to

$$E_M = r_c\left(1 - \sqrt{1 - \frac{r_c^2(l + r_h)^3}{(l + r_c)^3 r_h^2}}\right), \tag{85}$$

and second, the entropy of the system which remains the Bekenstein-Hawking entropy as seen from the general result of Eq. (48). The above quantities give rise to a proper Smarr formula of the form

$$E_M = 2T_M S + \Phi_M l + 2\lambda_M A_c. \tag{86}$$

The above quantities are the ones that will be used for the study of the phase structure, although it is worth writing the explicit form of the thermodynamic quantities when we position the cavity at infinity. To indicate the absence of the cavity, we will use the superscript (0) in these expressions. The temperature is given by

$$T_M^{(0)} = \frac{(l + r_h)^2(r_h - 2l)}{4\pi r_h^4}, \tag{87}$$

and it is easy to check that it is connected to the surface gravity by the relation

$$T_M^{(0)} = \left(1 + \frac{l}{r_h}\right)^3 \mathcal{T}|_{\Lambda=0}, \tag{88}$$

as was the case for AdS. The conjugate potential Φ in the limit $r_c \to \infty$ takes the form

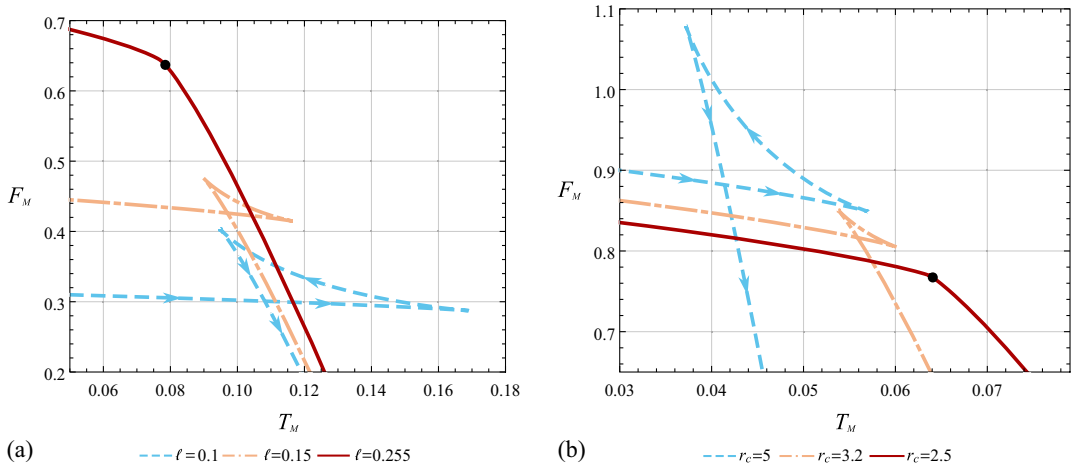

FIG. 6. (a) Free energy F_M as a function of the temperature T_M for a constant value of the cavity radius $r_c = 2$ with varying minimal length l; (b) Free energy F_M as a function of the temperature T_M for a constant value of the minimal length $l = 0.3$ with varying cavity radius r_c. In both cases, the arrows denote the direction in which the horizon radius r_h increases. For the sake of readability, we omit the arrows in the remaining curves, although the same pattern is implied.

$$\Phi_M^{(0)} = \frac{3(l+r_h)^2}{2r_h^2}, \tag{89}$$

while the energy becomes

$$E_M^{(0)} = \frac{(l+r_h)^3}{2r_h^2}, \tag{90}$$

which is the Arnowitt-Deser-Misner mass [73] of the spacetime. In terms of these quantities, it is obvious that the Smarr formula becomes

$$E_M^{(0)} = 2T_M^{(0)}S + \Phi_M^{(0)}l, \tag{91}$$

since we do not have a term due to the cavity. Having defined the proper thermodynamic quantities T_M, Φ_M, and E_M we proceed with the calculation of the free energy and move on to the study of the phase structure. The free energy is given by

$$F_M = E_M - T_M S, \tag{92}$$

which is calculated using Eqs. (82), (85), and (48), to be

$$F_M = \frac{r_c}{4(r_c+l)^3}\left(4l^3+12l^2r_c+12lr_c^2+4r_c^3 - \frac{4l^3+12l^2r_c+4r_c^3-\frac{3r_c^2}{r_h^2}(2l^3+5l^2r_h+r_h^3)}{\sqrt{1-\frac{r_c^2(l+r_h)^3}{(l+r_c)^3r_h^2}}}\right). \tag{93}$$

We see from Fig. 6 that we have the swallowtail structure once again, and the presence of the minimal length prevents the Hawking-Page transition from occurring. In Fig. 6(a) we keep the cavity radius constant at $r_c = 2$ and vary the minimal length. We see that with increasing temperature we are led to a first-order phase transition, which is from a small to a large black hole since the direction of increasing r_h is the same as that of the increasing temperature (the direction of increasing horizon radius is also indicated with arrows on the dashed light blue curve in Fig. 6). We have a critical value $l_c \approx 0.25$ of the minimal length above which no phase transition occurs. The same behavior is encountered in Fig. 6(b), where the minimal length scale remains constant at $l = 0.3$ and we vary the cavity radius r_c. Again, a first-order small to large phase transition occurs. There is a critical cavity radius $r_c^{(c)} \approx 2.5$ below which no phase transition occurs.

1. Constraints on the minimal length

In Ref. [32] corrections to the perihelion precession angle of test particles' orbits were found to scale linearly with the minimal length l. Using this result, it is possible to check if the bounds imposed on the minimal length from the requirement of thermodynamic stability and the extremal limit are compatible with available astrophysical data for the orbits of the S2 star around the Sagittarius A*. In this paper, we have an effective temperature, that differs from the one linked to surface gravity, and thus it will prove useful to once again check the minimal length's range of values. We start our analysis by taking the limit of $\Lambda \to 0^-$ of the heat capacity defined by Eq. (72). We find that

$$C_V = \frac{2\pi r_h^2(l+r_h)(2l-r_h)}{r_h^2 - lr_h - 8l^2}, \tag{94}$$

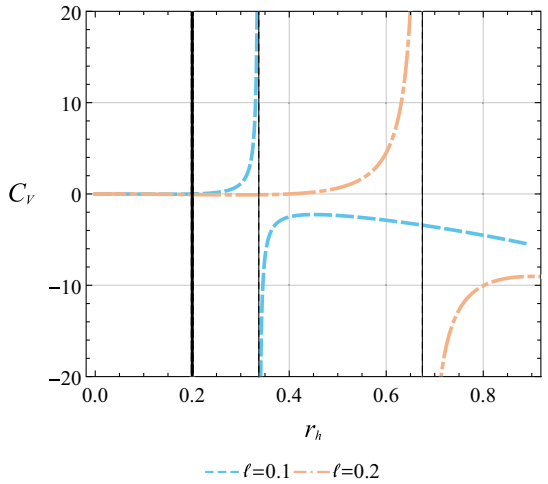

FIG. 7. Heat capacity C_V as a function of the horizon radius r_h for Minkowski spacetime. Different colors/types represent different values of the minimal length parameter l. The thin vertical black lines correspond to infinities/discontinuities of the heat capacity, while the thick vertical black line represents the minimal radius enforced by the extremal limit for the case $l = 0.1$.

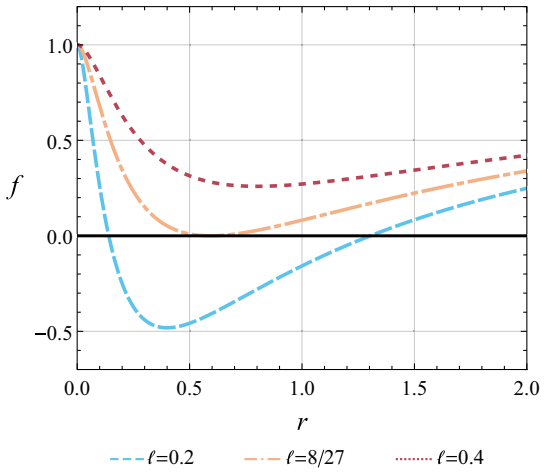

FIG. 8. Metric function f as a function of the radial coordinate r with vanishing cosmological constant $\Lambda = 0$ and mass $m = 1$. Different colors/types represent different values of the minimal length.

and it is shown in Fig. 7. We can see that there is only one infinity/discontinuity that separates thermodynamically stable and unstable regions. We have to point out that for this analysis, we have considered the cavity radius to be at infinity to retrieve the ordinary thermodynamic quantities. The point at which the discontinuity occurs is the positive root of the denominator of Eq. (94), which is

$$r_{\text{disc}} = \frac{1+\sqrt{33}}{2} l. \tag{95}$$

For values of the horizon radius smaller than r_{disc}, we have a thermodynamically stable RBH. It will be much more intuitive and useful for comparison with observational data to impose bounds on l with respect to the mass of the black hole. The extremal limit is the result of the outer horizon merging with the inner one forming a degenerate horizon [72]. In this case, we note that this occurs when l takes the value

$$\tilde{l} = \frac{8m}{27}, \tag{96}$$

although we will refrain from calling a "critical" length to avoid confusion with the one introduced while studying phase transitions.

We can see from Fig. 8 that the value $l = \tilde{l}$ corresponds to one double root of the function indicating the presence of an extremal black hole. For minimal lengths $l > \tilde{l}$ there is no black hole and this geometry represents a horizonless configuration whereas for $l < \tilde{l}$ we have an RBH. This condition places a constraint on the minimal length, which is a crucial factor to consider when assessing the feasibility of RBHs. Using Eq. (74) and taking the limit $\Lambda \to 0^-$, we find that the extremal radius is $r_{\text{ext}} = 2\tilde{l}$. This result can also be obtained directly from Eq. (82) by demanding the temperature to vanish. For the existence of a thermodynamically stable black hole, we must have then that $r_{\text{disc}} > r_{\text{ext}}$, which enforces the following lower bound on the minimal length:

$$r_{\text{disc}} > r_{\text{ext}} \Rightarrow l > \frac{4}{1+\sqrt{33}} \tilde{l}. \tag{97}$$

Combining the constraints mentioned above we have the following bounds for the minimal length:

$$\frac{4}{1+\sqrt{33}} \tilde{l} < l < \tilde{l}, \tag{98}$$

which can be rewritten, using Eq. (96), as

$$0.176 < \frac{l}{m} < 0.296. \tag{99}$$

This demonstrates that using the effective temperature derived from the Euclidean path integral approach leads to a lower bound than the one presented in Ref. [32], hence allowing for even smaller values of the parameter l, yet still affirming the potential of identifying the observed ultracompact objects as RBHs. We note that the bounds derived in this subsection are calculated within the framework of an asymptotically Minkowski spacetime. It is important to emphasize that the ultracompact objects under observation are situated within a spacetime characterized by a positive cosmological constant. Consequently, there will be corrections to these bounds due to its presence but we expect them

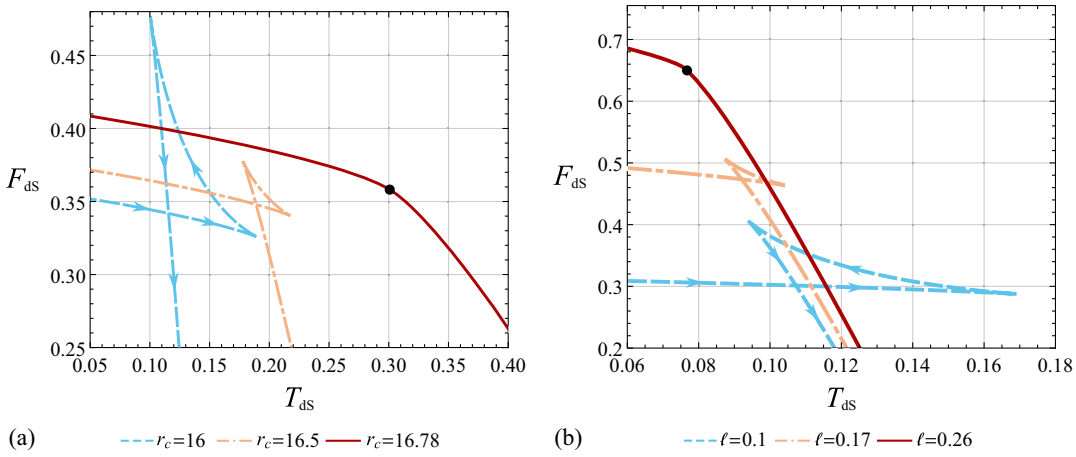

FIG. 9. (a) Free energy F_{dS} as a function of the temperature T_{dS} for constant value $l = 0.1$ for the minimal length and constant cosmological constant $\Lambda = 0.01$ with varying cavity radius r_c; (b) Free energy F_{dS} as a function of the temperature T_{dS} for constant value of cavity radius $r_c = 2$ and cosmological constant $\Lambda = 0.01$ with varying minimal length l. In both cases, the arrows denote the direction in which the horizon radius r_h increases. For the sake of readability, we omit the arrows in the remaining curves, although the same pattern is implied.

to be negligible since the cosmological constant is of the order $10^{-122} l_p^{-2}$ [74].

C. Embedding in de Sitter

Finally, in this section we are going to study the most physically relevant case, that of an asymptotically de Sitter spacetime. The cavity radius is now restricted to a domain between the black hole horizon and the cosmological horizon. The proper thermodynamic quantities in this case are defined by Eqs. (39), (42), (46), (C1), and (C2) but now with $\Lambda > 0$. The sign of Λ indicates that the quantity $P = -\Lambda/8\pi < 0$ should be interpreted as tension and not pressure. We explicitly add to these quantities a subscript dS to separate them from the general quantities derived from the Euclidean action in Sec. III, even though they are identical, and also to maintain consistency with the notation used in previous subsections. These thermodynamic quantities define the following Smarr relation written as

$$E_{dS} = 2T_{dS}S + \Phi_{dS} l + 2\lambda_{dS} A_c - 2PV_{dS}. \quad (100)$$

The free energy F_{dS} is calculated in the same manner as in previous subsections by using the mean thermal energy, the temperature, and the entropy,

$$F_{dS} = E_{dS} - T_{dS}S. \quad (101)$$

We omit the full expression for the free energy in the main text and provide it in Appendix C instead due to its extensive nature.

We once again create parametric plots of the free energy as a function of the temperature using the horizon radius r_h as a parameter. We see from Fig. 9 that we observe the same behavior as in the asymptotically flat spacetime with the variation of the cavity radius and the minimal length leading us to the swallowtail behavior. We can see that the first-order small to large phase transitions are in general present when the cavity radius is close to the black hole horizon r_h or the cosmological horizon $r_{\cos m}$. Fig. 9(a) represents the case where the cavity is close to the cosmological horizon $r_{\cos m} \approx \sqrt{(3/\Lambda)} \approx 17.32$. It is important to acknowledge that this approximation is because the cosmological horizon is influenced by the presence of the black hole, causing it to be situated closer to the black hole horizon than it would be if the black hole was absent. The same behavior is exhibited, as seen in Fig. 9(b), when the cavity is close to the black hole horizon and we vary the minimal length.

However, there is a main difference in comparison with the AdS spacetime. The variation of Λ leads to the swallowtail, but instead of terminating at one point, which represents a second-order phase transition, we now have two values of Λ that can lead to the closure of the swallowtail, and therefore it is transformed into a swallowtube. The one obvious value is $\Lambda \to 0^+$ since we are considering a de Sitter spacetime and the cosmological constant must remain positive, but independently of this restriction we see from Fig. 10 that for certain values of l and r_c the termination happens at a value of the parameter $\Lambda_1^{(c)} \approx 0.0216$ larger than zero. A second value of the cosmological constant $\Lambda_2^{(c)} \approx 0.225$ also leads to a termination of the first-order phase transitions. Therefore in de Sitter, we have two critical points with the coexistence line shown in Fig. 11.

To summarize, in a spacetime with a positive cosmological constant, under the choice of an appropriate parameter for the minimal length and the cavity radius, there is an interval $(P_{\min}, P_{\max})$ in which first-order small to

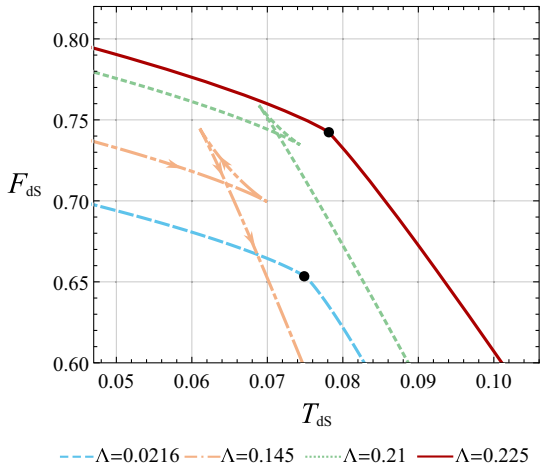

FIG. 10. Free energy F_{dS} as a function of the temperature T_{dS} for a constant value of the minimal length $l = 0.256$ and constant cavity radius $r_c = 2.01$ with varying cosmological constant Λ. The arrows denote the direction in which the horizon radius r_h increases. For the sake of readability, we omit the arrows in the remaining curves, although the same pattern is implied.

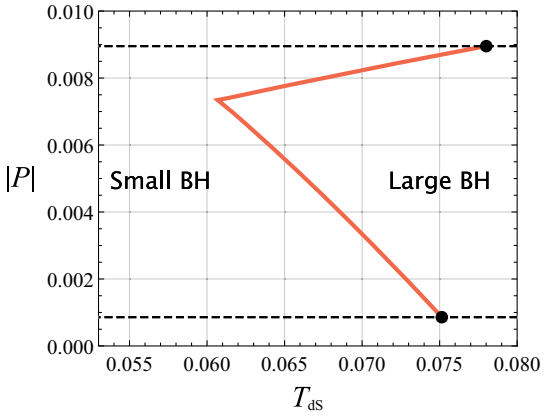

FIG. 11. Coexistence line for the RBH model in de Sitter spacetime. The black dots represent second-order phase transitions. The two horizontal dashed black lines illustrate the absolute value of the two critical pressures. The bottom line corresponds to $|P_1^{(c)}| = |\Lambda_1^{(c)}|/8\pi \approx 0.00085$ and the top one to $|P_2^{(c)}| = |\Lambda_2^{(c)}|/8\pi \approx 0.0089$.

large phase transitions are possible, but outside of which no phase transitions occur, i.e., the small to large phase transition is compact. This behavior is in stark contrast with AdS, where only one critical point exists, and for temperatures or pressures higher than this no phase transitions occur. Direct comparison of Fig. 11 with Fig. 2 makes evident the different and richer phase structure of the RBH in de Sitter spacetime in comparison with AdS. This novel feature can be solely attributed to the existence of a cosmological horizon, as the swallowtube behavior is absent in both AdS and Minkowski spacetime, rather than being influenced by the cavity's presence [62].

V. CONCLUSIONS

Studying various RBH models is crucial for gaining insights into how the smearing of the singularity, found in mathematical black holes, influences the classical sector. Assuming the existence of a quantum gravity theory that achieves such a regularization while preserving the hallmark feature of the horizon, RBHs emerge as the sole viable description for ultracompact objects. Numerous models have been proposed in the literature to describe such objects, with the common thread being the introduction of a minimal length scale, while allowing for distinct asymptotic behaviors. Most of these models can be described in the context of general relativity, having as a source an NED theory coupled to gravity with the incorporation of a magnetic charge, although alternative theories to describe such geometries are possible [69].

In this paper we analyzed the way to generate the model proposed in Ref. [32] in the framework of general relativity and derived the appropriate thermodynamic quantities using the Euclidean path integral approach. We conducted a comprehensive analysis of the thermodynamic properties and the phase structure of this model across anti–de Sitter, Minkowski and de Sitter spacetimes. Our findings imply/reveal a fundamental connection between the presence of a minimal length and the absence of the Hawking-Page transition in all three scenarios. Additionally, we observed that the method of singularity regularization influences the extent of the deviation from mean-field theory critical ratio in AdS. Both of these results arise from the fact that the singularity is not present. In AdS and Minkowski spacetime, the phase structure exhibits a typical swallowtail behavior, characterized by a unique critical point. However, in de Sitter spacetime, the swallowtail transforms into a swallowtube due to the emergence of a second critical point under specific values of the cavity radius and minimal length. In the asymptotically flat spacetime we established bounds on the minimal length, assuming the existence of a thermodynamically stable RBH. Our results indicate a lower bound smaller than the one previously predicted, implying the possibility of even smaller minimal length scales underpinning the possible existence of RBHs.

Our analysis has been restricted to a comparison of spherically symmetric RBHs, although realistic ultracompact objects are rotating and consequently characterized by axial symmetry. On this account, it will be intriguing to extend our investigation to include rotating RBHs. This extension should be based on the Euclidean path integral approach and will allow us to explore the thermodynamic properties and phase structure of these axially symmetric objects. Last but not least, the implications of singularity regularization in spherically symmetric setups have become evident in this paper, and thus analogous extensions should be considered in axially symmetric spacetimes.

Furthermore, this extension to physically realistic scenarios could potentially allow us to make contact with gravitational wave observations.

ACKNOWLEDGMENTS

I would like to thank Sebastian Murk, Fil Simovic, and Daniel Terno for useful discussions and helpful comments. I would also like to thank Zixin Huang for providing useful comments/advice regarding the figures created in this paper. I. S. is supported by an International Macquarie University Research Excellence Scholarship.

APPENDIX A: CALCULATION OF REDUCED EUCLIDEAN ACTION

In this section of the appendix we provide the explicit calculation of each term introduced in the reduced action, defined as

$$I_r = I_{\mathrm{EH}} + I_{\mathrm{GHY}} + I_M + I_{\mathrm{EMB}} - I_0. \tag{A1}$$

We start with the Einstein-Hilbert action I_{EH}, given by Eq. (33). We first perform the transformation $t \to -i\tau$ (Wick rotation) in the metric of Eq. (1), where τ is the Euclidean time, to obtain the Euclidean metric,

$$ds^2 = f(r)d\tau^2 + \frac{dr^2}{f(r)} + r^2 d\Omega_2, \tag{A2}$$

and we find that the Ricci scalar is

$$R = \frac{2 - f''(r)r^2 - 4rf'(r) - 2f(r)}{r^2}. \tag{A3}$$

Therefore,

$$I_{\mathrm{EH}} = -\frac{1}{16\pi}\int_0^{\beta_h} d\tau \int_0^{\pi} d\theta \int_0^{2\pi} d\phi \int_{r_h}^{r_c} r^2 \sin\theta R dr, \tag{A4}$$

where the integration of the radial part is up to the cavity radius r_c which is subject to restrictions in the presence of a cosmological horizon $r_{\cos m}$ with $r_h < r_c < r_{\cos m}$. If a cosmological horizon, is not present then the cavity radius is not bounded from above and we are allowed to take the cavity to be at infinity. The upper bound β_h of the integral over $d\tau$ is chosen as to eliminate the conical singularity at the origin of $\tau - r$ plane in the Euclidean section, which corresponds to the black hole horizon in the Lorentzian geometry. After integration of the angular part and integration by parts of the radial part, we have

$$I_{\mathrm{EH}} = \frac{\beta_h}{4}(2(r_c - r_h) - 2r_c f(r_c) - r_c^2 f'(r_c)) - \frac{\beta_h}{4} r_h^2 f'(r_h). \tag{A5}$$

Upon identifying the periodicity β_h with the Killing surface gravity κ [75,76] through the relation

$$\beta_h^{-1} = \frac{\kappa}{2\pi} = \frac{f'(r_h)}{4\pi}, \tag{A6}$$

we finally obtain

$$I_{\mathrm{EH}} = -\pi r_h^2 - \frac{\beta_h}{4}\big(2(r_c - r_h) - 2r_c f(r_c) - r_c^2 f'(r_c)\big), \tag{A7}$$

where the first term is shown to be the black hole entropy in Sec. III. We now proceed with the next term of the action which is the Gibbons-Hawking-York term

$$I_{\mathrm{GHY}} = \frac{1}{8\pi}\int_{\partial M} \sqrt{k}K = \frac{1}{8\pi}\int_0^{\beta_h} d\tau \int_0^{\pi} d\theta \int_0^{2\pi} d\phi \sqrt{k}K\Big|_{r_c}. \tag{A8}$$

The induced metric k_{ab} on the boundary hypersurface is given by the line element,

$$ds^2 = f(r_c)d\tau + r_c^2 d\Omega_2, \tag{A9}$$

and the square root of the determinant k of the induced metric is

$$\sqrt{k} = \sqrt{f(r_c)}r_c^2 \sin\theta. \tag{A10}$$

The trace of the extrinsic curvature K_{ab} evaluated at the boundary is

$$K(r_c) = -\frac{2\sqrt{f(r_c)}}{r_c} - \frac{f'(r_c)}{2\sqrt{f(r_c)}}. \tag{A11}$$

Combining now Eqs. (A8), (A10) and (A11), we have that

$$I_{\mathrm{GHY}} = \frac{\beta_h}{2} r_c^2 K(r_c)\sqrt{f(r_c)}. \tag{A12}$$

We now proceed with the calculation of the matter part of the action given by Eq. (35). The Lagrangian depends only on the radial coordinate so we proceed with the integration of the angular and Euclidean time parts to arrive at

$$I_M = \frac{\beta_h}{4}\int_{r_c}^{r_h} r^2 \mathcal{L}(r) dr. \tag{A13}$$

Instead of using Eq. (19), we can produce a more general result by using the original solution of the Einstein equations for $\mathcal{L}$ which is given by Eq. (18) and perform the integration, which gives the rather simple result,

$$I_M = \frac{\beta_h}{2}((r_c - r_h) - r_c f(r_c)). \tag{A14}$$

Since the next action term is the electromagnetic boundary term, which vanishes as explained in Sec. III, we proceed with the calculation of the final term I_0. We calculate this term by demanding the reduced action to vanish in the absence of a black hole. A comment is necessary here as to what condition we need to impose. Having a look at Eq. (20), we see that the condition $r_h \to 0$ does not correspond to vanishing mass $m = 0$. We point out that the proper condition in this case corresponds to first taking the limit $l \to 0$ and then taking the limit $r_h \to 0$. The limit cannot be taken in reverse order because there is no meaning in having a minimal length scale l without the presence of a horizon radius, i.e., a black hole.[9] Consequently, we have the following equivalence between these two conditions,

$$\lim_{m\to 0} I_r = 0 \Leftrightarrow \lim_{r_h\to 0}(\lim_{l\to 0} I_r) = 0. \tag{A15}$$

This condition leads to a vanishing action for the absence of a black hole, i.e., an empty spacetime which can either be Minkowski or AdS/dS, depending on the value of the cosmological constant. Implementing the above condition and taking into account the introduction of the new parameter β for appropriate comparison of the spacetimes with and without a black hole, leads to the expression,

$$I_0 = \frac{1}{3}\beta(-3 + r_c^2\Lambda), \tag{A16}$$

for the subtraction term.

Not surprisingly this action is precisely the one derived in Eq. (37) if we take the limit $r_c \to \infty$ and we also substitute Q_m, σ, and m in terms of r_h and l using Eqs. (24), (25), and subsequently Eq. (20). Importantly, both derivations of the action of Eq. (37) and Eq. (B4) are on shell, as indicated by Eq. (A6), where we have selected the inverse surface gravity as the periodicity and therefore we have eliminated the conical singularity [75,76].

However, there is a major difference between these two calculations arising from the choice of thermodynamic variables. Initially, we calculate the temperature by extremizing the action of Eq. (B4) with respect to the horizon radius, i.e.,

$$\frac{\partial I_r(r_h, Q_m, \sigma, \Lambda)}{\partial r_h} = 0, \tag{B5}$$

[9]The existence of a nonzero minimal length scale l is conceivable even in the absence of a horizon. However, under these circumstances, the object under consideration will no longer quantify as a black hole, i.e., a trapped region of spacetime. Instead, it would be classified as a horizonless object [23,35]. In such scenarios, the application of the Euclidean formalism, in this form, for the thermodynamic analysis becomes unsuitable, as it relies on the presence of a horizon.

APPENDIX B: CONSIDERING Q_m AND σ AS FUNDAMENTAL THERMODYNAMIC VARIABLES

In this section of the appendix, we derive the reduced Euclidean action when our RBH is embedded in AdS spacetime, treating Q_m and σ as fundamental thermodynamic variables. Choosing the AdS case, allows us to take the cavity radius r_c to infinity, simplifying considerably the expressions while still enabling a proper comparison. Using Eqs. (24), (25), and (20), we rewrite the metric function of Eq. (2) solely in terms of Q_m and σ. This results in

$$f(r) = 1 - \frac{2^{7/4}Q_m^{3/2}r^2}{(r + 2^{1/4}\sigma^{1/4}Q_m^{1/2})^3\sigma^{1/4}} - \frac{\Lambda}{3}r^2. \tag{B1}$$

We proceed with the calculation of the Euclidean action, using Eqs. (A7), (A12), (A14), (A16), and Eq. (B1) as the metric function. This leads to the reduced action

$$I_r = I_r(r_h, r_c, Q_m, \sigma, \Lambda), \tag{B2}$$

where we highlight once again that Q_m and σ are treated as independent thermodynamic variables. Upon taking the cavity to infinity we have that

$$I_r(r_h, Q_m, \sigma, \Lambda) = \lim_{r_c\to\infty} I_r(r_h, r_c, Q_m, \sigma, \Lambda), \tag{B3}$$

and we obtain

$$I_r(r_h, Q_m, \sigma, \Lambda) = -\pi r_h^2 + \beta\left(\left(\frac{r_h}{2} + \frac{2^{7/4}Q_m^{3/2}}{4\sigma^{1/4}}\right) - \frac{\Lambda}{6}\left(r_h^3 + \frac{3\cdot 2^{3/4}Q_m^{3/2}}{\Lambda\sigma^{1/4}}\right) + \frac{Q_m^2(6r_h^2 + 3\cdot 2^{5/4}Q_m^{1/2}r_h\sigma^{1/4} + 2^{3/2}Q_m\sigma^{1/2})}{(r_h + 2^{1/4}Q_m^{1/2}\sigma^{1/4})^3}\right). \tag{B4}$$

and solve for β which leads to the following relation for the temperature:

$$\mathcal{T} = \frac{1 - r_h^2\Lambda}{4\pi r_h} - \frac{12Q_m^2 r_h}{4\pi(r_h + 2^{1/4}Q_m^{1/2}\sigma^{1/4})^4}. \quad \text{(B6)}$$

After using Eqs. (24), (25), and (20) in the above expression we retrieve exactly the relation (54), i.e., the temperature being the surface gravity. Since now Q_m and σ are independent variables, they will have their own conjugate quantities in the first law and Smarr formula. We calculate them using a similar methodology as in Sec. III, but we only present here the expressions after we have substituted Q_m and σ in terms of r_h and l. These quantities, for the magnetic charge Q_m, the parameter σ, and the cosmological constant Λ, respectively, are given by the following relations:

$$\Psi_H = \frac{1}{\beta}\frac{\partial I_r(r_h, Q_m, \sigma, \Lambda)}{\partial Q_m}, \quad K_\sigma = \frac{1}{\beta}\frac{\partial I_r(r_h, Q_m, \sigma, \Lambda)}{\partial \sigma} \quad \text{(B7)}$$

and

$$\mathcal{V} = -\frac{8\pi}{\beta}\frac{\partial I_r(r_h, Q_m, \sigma, \Lambda)}{\partial \Lambda}, \quad \text{(B8)}$$

where now $\beta = \mathcal{T}^{-1}$. Explicit calculation yields

$$\Psi_H = \frac{\sqrt{3l(l + r_h)(3 - r_h^2\Lambda)}}{2r_h(l + r_h)^3}(4r_h^3 + 6r_h^2 l + 4r_h l^2 + l^3), \quad \text{(B9)}$$

$$K_\sigma = -\frac{(l + r_h)^2(l^2 + 4lr_h + 6r_h^2)(3 - r_h^2\Lambda)^2}{144 l r_h^4}, \quad \text{(B10)}$$

$$\mathcal{V} = \frac{4\pi r_h^3}{3}. \quad \text{(B11)}$$

Finally, we calculate the internal energy and entropy from Eq. (45) and Eq. (47), respectively, and we find

$$E = \frac{\partial I_r(r_h, Q_m, \sigma, \Lambda)}{\partial \beta} = \frac{(l + r_h)^3(3 - r_h^2\Lambda)}{6r_h^2} = m, \quad \text{(B12)}$$

$$S = \beta\frac{\partial I_r(r_h, Q_m, \sigma, \Lambda)}{\partial \beta} - I_r(r_h, Q_m, \sigma, \Lambda) = \pi r_h^2. \quad \text{(B13)}$$

The application of the Euclidean path integral formalism and its on shell consideration leads us to the Smarr formula,

$$E = 2\mathcal{T}S + \Psi_H Q_m + 2K_\sigma\sigma - 2\mathcal{V}P. \quad \text{(B14)}$$

We note that this is exactly the Smarr formula obtained from Hamiltonian methods as can be verified from the methodology of Ref. [42]. The choice of Q_m and σ as thermodynamic variables is based on the dependence of the NED Lagrangian of Eq. (21) on $\mathcal{F}$ and therefore Q_m while at the same time there is dependence on the parameter σ, which is one of the parameters β_i appearing in Eq. (52). (We refer the reader to Ref. [42] for a discussion and a general derivation of the above using Hamiltonian methods.)

The first law takes the form

$$dE = \mathcal{T}dS + \Psi_H dQ_m + K_\sigma d\sigma + \mathcal{V}dP, \quad \text{(B15)}$$

with $E = m$. In this derivation, the temperature coincides with the surface gravity. However, it is important to emphasize two key points: Firstly, considering Q_m and σ as independent variables is nonphysical, given that both depend on m and l. Any variations of Q_m and σ in the first law would result in variations of m and l on the right-hand side of Eq. (B15). This observation leads us to the second point, emphasizing that variation of the total energy of the spacetime should be present only on the left-hand side of Eq. (B15). Therefore, it is much more physically meaningful to consider the minimal length as a fundamental parameter and allow for its variation. With this in mind, we have that

$$dQ_m = \frac{\partial Q_m}{\partial m}dm + \frac{\partial Q_m}{\partial l}dl, \quad \text{(B16)}$$

and

$$d\sigma = \frac{\partial \sigma}{\partial m}dm + \frac{\partial \sigma}{\partial l}dl. \quad \text{(B17)}$$

So implementing the above in the first law of Eq. (B15) leads to

$$dE = \frac{\mathcal{T}}{(1 - \Psi_H\frac{\partial Q_m}{\partial m} - K_\sigma\frac{\partial \sigma}{\partial m})}dS + \frac{\Psi_H\frac{\partial Q_m}{\partial l} + K_\sigma\frac{\partial \sigma}{\partial l}}{(1 - \Psi_H\frac{\partial Q_m}{\partial m} - K_\sigma\frac{\partial \sigma}{\partial l})}dl + \frac{\mathcal{V}}{(1 - \Psi_H\frac{\partial Q_m}{\partial m} - K_\sigma\frac{\partial \sigma}{\partial l})}dP, \quad \text{(B18)}$$

and consequently to the effective thermodynamic quantities

$$T = \frac{\mathcal{T}}{(1 - \Psi_H\frac{\partial Q_m}{\partial m} - K_\sigma\frac{\partial \sigma}{\partial m})}, \quad \text{(B19)}$$

and

$$\Phi = \frac{\Psi_H \frac{\partial Q_m}{\partial l} + K_\sigma \frac{\partial \sigma}{\partial l}}{(1 - \Psi_H \frac{\partial Q_m}{\partial m} - K_\sigma \frac{\partial \sigma}{\partial l})}, \qquad V = \frac{\mathcal{V}}{(1 - \Psi_H \frac{\partial Q_m}{\partial m} - K_\sigma \frac{\partial \sigma}{\partial l})}. \tag{B20}$$

The above quantities are the conjugate potentials when we treat l as a fundamental variable. If we do their explicit calculation, using the relations (24), (25), and (20), we retrieve exactly the same conjugate potentials as the ones derived by the on shell Euclidean action method in Sec. IV A and specifically Eqs. (53), (56), and (57). This demonstrates consistency between the two derivations.

APPENDIX C: THERMODYNAMIC POTENTIALS

In this part of the appendix we give the rather long expressions for the thermodynamic volume V, the conjugate potential for the cavity area λ and the free energy F which will have the same expression as F_{dS} but with positive cosmological constant. They are calculated to be

$$V = \frac{-8\pi r_c^3}{6(l+r_c)^3 r_h^2 \sqrt{3 - r_c^2\Lambda}\,\mathcal{Y}} \Big(18 l^2 r_c r_h^2 - 3 r_h^2(-l^3 + 3 l^2 r_h + 3 l r_h^2 + r_h^3) - 6 l r_h^2 r_h^4 \Lambda - 2 r_c^5 r_h^2 \Lambda - 6 r_c^3 r_h^2 (-1 + l^2\Lambda) + r_c^2 \big[-3(l^3 + 3 l^2 r_h - 3 l r_h^2 + r_h^3) + 2 r_h^3 (3 l^2 + 3 l r_h + r_h^2)\Lambda \big] + (-2 l^3 r_h^2 - 6 l^2 r_c r_h^2 - 6 l r_c^2 r_h^2 - 2 r_c^3 r_h^2) \sqrt{3 - r_c^2\Lambda}\,\mathcal{Y} \Big), \tag{C1}$$

$$\lambda = \frac{1}{48\pi r_c} \Big(6(1 - r_c^2\Lambda) + \frac{2 r_c^2 \Lambda}{\sqrt{3 - r_c^2\Lambda}} \mathcal{X} - 2\sqrt{3 - r_c^2\Lambda}\,\mathcal{X} + \frac{r_c^2 \sqrt{3 - r_c^2\Lambda}\,(3(2l - r_c)(l + r_h)^3 + r_h^2(l^3(9 r_c - 6 r_h) + 3 l^2(4 r_c^2 + r_c r_h - 2 r_h^2) + l(8 r_c^3 + 3 r_c r_h^2 - 2 r_h^3) + r_c(2 r_c^3 + r_h^3))\Lambda)}{(l + r_c)^{5/2} r_h \sqrt{-(r_c - r_h)(3 l^3 (r_c + r_h) + 3 l r_c^2 r_h^2 (r_c + r_h)\Lambda + 3 l^2 r_c r_h (3 + r_c r_h \Lambda) + r_c^2 r_h^2 (-3 + (r_c^2 + r_c r_h + r_h^2)\Lambda))}} \Big), \tag{C2}$$

$$F_{dS} = \frac{-r_c}{12 r_h^2 (l + r_c)^3 \mathcal{Y}} \Big((12 l^3 r_h^2 - 18 l^3 r_c^2 - 45 l^2 r_c^2 r_h + 36 l^2 r_c r_h^2 + 12 r_c^3 r_h^2 - 9 r_c^2 r_h^3 - 12 l^2 r_c^3 r_h^2 \Lambda - 12 l r_c^4 r_h^2 \Lambda - 4 r_c^5 r_h^2 \Lambda + 9 l^2 r_c^2 r_h^3 \Lambda + 6 l r_c^2 r_h^4 \Lambda + r_c^2 r_h^5 \Lambda)\omega + (-12 l^3 r_h^2 - 36 l^2 r_c r_h^2 - 36 l r_c^2 r_h^2 - 12 r_c^3 r_h^2 + 4 l^3 r_c^2 r_h^2 \Lambda + 12 l^2 r_c^3 r_h^2 \Lambda + 12 l r_c^4 r_h^2 \Lambda + 4 r_c^5 r_h^2 \Lambda)\mathcal{Y} \Big), \tag{C3}$$

where we have defined for simplicity

$$\mathcal{Y} = \sqrt{3 - r_c^2\Lambda + \frac{r_c^2 (l + r_h)^3 (-3 + r_h^2\Lambda)}{(l + r_c)^3 r_h^2}}, \tag{C4}$$

$$\omega = \sqrt{3 - r_c^2\Lambda}. \tag{C5}$$

It is worth pointing out that these are the general expressions we derive from the Euclidean action and they coincide with the de Sitter case quantities.

APPENDIX D: THERMODYNAMICS OF THE BARDEEN RBH

In this part of the appendix we will derive the temperature for the Bardeen black hole model using exactly the same methodology as in Sec. III. This model is desrcibed by the metric function given by

$$f(r) = 1 - \frac{2 m r^2}{(r^2 + l^2)^{3/2}} - \frac{\Lambda}{3} r^2. \tag{D1}$$

We can easily derive the total reduced action by substituting this metric function to the general relations (A7), (A12), (A7), and (A16) derived in Appendix A. This metric is also derived exclusively by magnetic charge as shown in Ref. [27] and the only nonvanishing components of the electromagnetic tensor are $F_{23} = -F_{32}$. Since we want to study thermodynamics in the canonical ensemble, we need to introduce an electromagnetic boundary term in the action, which will vanish once again due to the integration on a constant time slice. Combining all of the above, we arrive at the following reduced action I_B for the Bardeen model:

$$I_B = -\pi r_h^2 + \beta r_c \left(1 - \frac{r_c^2\Lambda}{3} - \sqrt{3 - r_c^2\Lambda}\sqrt{3 - r_c^2\Lambda + \frac{r_c^2(l^2 + r_h^2)^{3/2}(-3 + r_h^2\Lambda)}{(l^2 + r_c^2)^{3/2} r_h^2}}\right). \tag{D2}$$

To find the temperature, we extremize it with respect to the horizon radius r_h and solve for β. We find that the temperature given by $T = \beta^{-1}$ is calculated to be

$$T = \frac{r_c^3\sqrt{l^2 + r_h^2}\sqrt{3 - r_c^2\Lambda}(2l^2 - r_h^2 + r_h^4\Lambda)}{4\pi(l^2 + r_h^2)^{3/2} r_h^4 \mathcal{X}_B}, \tag{D3}$$

where $\mathcal{X}_B$ has been introduced for convenience and is given by

$$\mathcal{X}_B = \sqrt{\frac{l^4 r_h^2(3 - r_c^2\Lambda) + r_c^2 r_h^2(3r_c^2 - r_c^4\Lambda + \mathcal{Y}_B(-3 + r_h^2\Lambda)) + l^2 r_c^2(r_h^2(6 - 2r_c^2\Lambda + \mathcal{Y}_B\Lambda) - 3\mathcal{Y}_B)}{(l^2 + r_c^2)^2 r_h^2}}, \tag{D4}$$

with $\mathcal{Y}_B = \sqrt{l^2 + r_h^2}\sqrt{l^2 + r_c^2}$. We introduced this section in the appendix because we are interested in the AdS case and the critical ratio. As we explained in the main part of this paper in the AdS case we are allowed to take the cavity radius at infinity and thus we have that the temperature is given by

$$T_B = \frac{\sqrt{l^2 + r_h^2}(-2l^2 + r_h^2 - r_h^4\Lambda)}{4\pi r_h^4}. \tag{D5}$$

Identifying the pressure as $P = -\Lambda/8\pi$ we can solve the above equation with respect to Λ and then find the pressure which will yield a Van der Walls-like equation of the form

$$P_B = \frac{T_B}{2\sqrt{r_h^2 + l^2}} - \frac{1}{8\pi r_h^2} + \frac{l^2}{4\pi r_h^4}. \tag{D6}$$

Using the above equation for the pressure, we can identify the critical radius and temperature by solving the system of equations

$$\frac{\partial P_B}{\partial r_h} = 0, \qquad \frac{\partial^2 P_B}{\partial r_h^2} = 0, \tag{D7}$$

which remarkably can be solved exactly and leads to the following solutions

$$r_h^{(c)} = \sqrt{2(2 + \sqrt{10})}\, l, \tag{D8}$$

and

$$T_B^{(c)} = \frac{25(31 + 13\sqrt{10})}{432\pi(5 + 2\sqrt{10})^{3/2} l}. \tag{D9}$$

The reduced volume is derived by observing the inverse coefficient of the temperature T_B in Eq. (D6) for the pressure and it is given by

$$v_B = 2\sqrt{r_h^2 + l^2}, \tag{D10}$$

with the critical value calculated, using Eq. (D8), to be

$$v_B^{(c)} = 2\sqrt{5 + 2\sqrt{10}}\, l. \tag{D11}$$

The last quantity we need for the calculation of the critical ratio is the critical pressure which is found by substituting Eqs. (D8) and (D9) in (D6), and leads to

$$P_B^{(c)} = \frac{5\left(53 + 17\sqrt{10}\right)}{24(30 + 9\sqrt{10})^2 \pi l^2}. \tag{D12}$$

Combining now Eqs. (D12), (D11), and (D9) we have that the critical ratio is given by

$$\frac{P_B^{(c)} v_B^{(c)}}{T_B^{(c)}} = \frac{2}{5} = 0.4. \tag{D13}$$

[1] A. M. Ghez, M. Morris, E. E. Becklin, A. Tanner, and T. Kremenek, Nature (London) **407**, 349 (2000).
[2] F. Nogueras-Lara, R. Schödel, A. T. Gallego-Calvente *et al.*, Nat. Astron. **4**, 377 (2020).
[3] LIGO Scientific and Virgo Collaborations, Astrophys. J. Lett. **913**, L7 (2021).
[4] C. Bambi, Rev. Mod. Phys. **89**, 025001 (2017).
[5] Event Horizon Telescope Collaboration, Astrophys. J. Lett. **875**, L4 (2019).
[6] A. R. Ingram and S. E. Motta, New Astron. Rev. **85**, 101524 (2019).
[7] C. S. Reynolds and M. A. Nowak, Phys. Rep. **377**, 389 (2003).
[8] V. Cardoso and P. Pani, Living Rev. Relativity **22**, 4 (2019).
[9] L. Barack, V. Cardoso, S. Nissanke, and T. P. Sotiriou, Classical Quantum Gravity **36**, 143001 (2019).
[10] S. Murk, Int. J. Mod. Phys. D **32**, 2342012 (2023).
[11] J. M. Bardeen in *Proceedings of the International Conference GR5* (Tbilisi University Press, Tbilisi, 1968).
[12] I. Dymnikova, Gen. Relativ. Gravit. **24**, 235 (1992).
[13] S. A. Hayward, Phys. Rev. Lett. **96**, 031103 (2006).
[14] P. O. Mazur and E. Mottola, Proc. Natl. Acad. Sci. U.S.A. **101**, 9545 (2004).
[15] P. O. Mazur and E. Mottola, Universe **9**, 88 (2023).
[16] H. G. Ellis, J. Math. Phys. (N.Y.) **14**, 104 (1973).
[17] M. S. Morris and K. S. Thorne, Am. J. Phys. **56**, 395 (1988).
[18] A. Simpson and M. Visser, J. Cosmol. Astropart. Phys. 02 (2019) 042.
[19] O. Lunin and S. D. Mathur, Nucl. Phys. **B623**, 342 (2002).
[20] S. D. Mathur, Fortschr. Phys. **53**, 793 (2005).
[21] M. Visser, Phys. Rev. D **90**, 127502 (2014).
[22] R. Penrose, Phys. Rev. Lett. **14**, 57 (1965).
[23] R. Carballo-Rubio, F. Di Filippo, S. Liberati, and M. Visser, arXiv:2302.00028.
[24] M. Born and L. Infeld, Proc. R. Soc. A **144**, 425 (1934).
[25] K. A. Bronnikov, Phys. Rev. D **63**, 044005 (2001).
[26] E. Ayon-Beato and A. Garcia, Phys. Lett. B **493**, 149 (2000).
[27] Z.-Y. Fan and X. Wang, Phys. Rev. D **94**, 124027 (2016).
[28] S. Balestra *et al.*, Eur. Phys. J. C **55**, 57 (2008).
[29] M. Ambrosio *et al.* (The MACRO Collaborations), Eur. Phys. J. C **25**, 511 (2002).
[30] B. Acharya, J. Alexandre, P. Benes *et al.*, Nature (London) **602**, 63 (2022).
[31] J. M. Bardeen, B. Carter, and S. W. Hawking, Commun. Math. Phys. **31**, 161 (1973).
[32] M. Cadoni, M. De Laurentis, I. De Martino, R. D. Monica, M. Oi, and A. P. Sanna, Phys. Rev. D **107**, 044038 (2023).
[33] F. Simovic and I. Soranidis, arXiv:2309.09439.
[34] L. Smarr, Phys. Rev. Lett. **30**, 71 (1973).
[35] *Regular Black Holes: Towards a New Paradigm of Gravitational Collapse*, edited by C. Bambi (Springer, Singapore, 2023).
[36] K. A. Bronnikov and R. K. Walia, Phys. Rev. D **105**, 044039 (2022).
[37] M. E. Rodrigues and M. V. de S. Silva, Phys. Rev. D **107**, 044064 (2023).
[38] A. Komar, Phys. Rev. **129**, 1873 (1963).
[39] V. Balasubramanian, J. de Boer, and D. Minic, Phys. Rev. D **65**, 123508 (2002).
[40] R. Bousso, Rev. Mod. Phys. **74**, 825 (2002).
[41] D. Anninos, G. S. Ng, and A. Strominger, Classical Quantum Gravity **28**, 175019 (2011).
[42] Y. Zhang and S. Gao, Classical Quantum Gravity **35**, 145007 (2018).
[43] G. W. Gibbons and S. W. Hawking, Phys. Rev. D **15**, 2752 (1977).
[44] J. W. York, Jr., Phys. Rev. D **33**, 2092 (1986).
[45] H. W. Braden, J. D. Brown, B. F. Whiting, and J. W. York, Jr., Phys. Rev. D **42**, 3376 (1990).
[46] H. E. Moumni and J. Khalloufi, Nucl. Phys. **B973**, 115593 (2021).
[47] H. E. Moumni and J. Khalloufi, Nucl. Phys. **B977**, 115731 (2022).
[48] S. Carlip and S. Vaidya, Classical Quantum Gravity **20**, 3827 (2003).
[49] D. Kubizňák, R. B. Mann, and M. Teo, Classical Quantum Gravity **34**, 063001 (2017).
[50] D. Kastor, S. Ray, and J. Traschen, Classical Quantum Gravity **26**, 195011 (2009).
[51] R. M. Wald, Phys. Rev. D **48**, R3427(R) (1993).
[52] V. Iyer and R. M. Wald, Phys. Rev. D **50**, 846 (1994).
[53] D. A. Rasheed, arXiv:hep-th/9702087.
[54] G. Gibbons, R. Kallosh, and B. Kol, Phys. Rev. Lett. **77**, 4992 (1996).
[55] J. D. E. Creighton and R. B. Mann, Phys. Rev. D **52**, 4569 (1995).
[56] N. Breton, Gen. Relativ. Gravit. **37**, 643 (2005).
[57] I. Booth, B. Creelman, J. Santiago, and M. Visser, J. Cosmol. Astropart. Phys. 09 (2019) 067.
[58] L. J. Garay, Int. J. Mod. Phys. A **10**, 145 (1995).
[59] C. Barceló, V. Boyanov, R. Carballo-Rubio, and L. J. Garay, Classical Quantum Gravity **38**, 125003 (2021).
[60] C. Barceló, V. Boyanov, R. Carballo-Rubio, and L. J. Garay, Phys. Rev. D **106**, 124006 (2022).
[61] D. Kubizňák and F. Simovic, Classical Quantum Gravity **33**, 245001 (2016).
[62] F. Simovic and R. B Mann, Classical Quantum Gravity **36**, 014002 (2018).
[63] F. Simovic and R. B Mann, J. High Energy Phys. 05 (2019) 136.
[64] S. Haroon, R. A. Hennigar, R. B. Mann, and F. Simovic, Phys. Rev. D **101**, 084051 (2020).
[65] F. Simovic, D. Fusco, and R. B. Mann, J. High Energy Phys. 02 (2021) 219.
[66] F. Simovic, Int. J. Mod. Phys. D **32**, 2342023 (2023).
[67] M. Liška, R. A. Hennigar, and D. Kubizňák, J. High Energy Phys. 11 (2023) 195.
[68] K. Hajian, S. Liberati, M. M. Sheikh-Jabbari, and M. H. Vahidinia, Phys. Lett. B **812**, 136002 (2021).
[69] S. Nojiri and G. G. L. Nashed, Phys. Rev. D **108**, 024014 (2023).
[70] L. Gulin and I. Smolić, Classical Quantum Gravity **35**, 025015 (2017).

[71] L. D. Landau and E. M. Lifshitz, *Statistical Physics* (Pergamon Press, Oxford, 1969).
[72] S. Murk and I. Soranidis, Phys. Rev. D **108**, 124007 (2023).
[73] R. Arnowitt, S. Deser, and C. W. Misner, Phys. Rev. **116**, 1322 (1959).
[74] Planck Collaboration, Astron. Astrophys. **641**, A6 (2020).
[75] V. Frolov and I. Novikov, *Black Hole Physics, Basic Concepts and New Developments* (Springer Verlag, Heidelberg, 1998).
[76] S. N. Solodukhin, Phys. Rev. D **51**, 609 (1995).

JOURNAL ARTICLE

Light rings and causality for nonsingular ultracompact objects sourced by nonlinear electrodynamics

Brief summary

After describing the thermodynamic properties of three specific RBH models and examining the impact of the minimal length scale, as well as how it is introduced into the metric function, we turn to the study of the observational effects that this scale can produce — specifically, light rings in such spacetimes. We demonstrate the phenomenon of birefringence, which arises due to the nonlinearity of the NED theory, and discuss potential causality issues. Our analysis focuses on the phase velocities of light and explores their connection to the weak-field limit of the theory.

Conventions

In contrast to Ref. [1], where the action I is expressed by the following equation:

$$I = \frac{1}{16\pi}\int d^4x\sqrt{-g}[R - 2\Lambda - 4\mathcal{L}(\mathcal{F},\mathcal{G})], \tag{3.1}$$

in this article, the symbol S is used for the action, which is given by:

$$S = \frac{1}{16\pi}\int d^4x\sqrt{-g}[R - 2\Lambda - \mathcal{L}(\mathcal{F},\mathcal{G})]. \tag{3.2}$$

The dependence on $\mathcal{G}$ is absent from any paper included in this thesis. Additionally, there is a factor of 4 difference between the NED Lagrangians used in the actions of Ref. [1] and Ref. [3]. In this article, the minimal length scale is denoted by ℓ, as opposed to l used in the other articles within this thesis. It is also worth noting that the Komar mass of the spacetime is represented by M, unlike Refs. [1] and [2], where m is used. Furthermore, while the outer horizon is denoted by r_h in Refs. [1] and [2], in this article, we use r_+ and r_- to denote the outer and inner horizons, respectively.

Authorship statement

Conceptualization of the research project and calculations for its development. Also contributed

to the planning and writing of the article, interpretation of its results, proofreading, and revisions. Principal contributor to Sections II, III, IV, and V and Appendix.

Light rings and causality for nonsingular ultracompact objects sourced by nonlinear electrodynamics

Sebastian Murk[1,*] and Ioannis Soranidis[2,†]

[1]*Quantum Gravity Unit, Okinawa Institute of Science and Technology, 1919-1 Tancha, Onna-son, Okinawa 904-0495, Japan*

[2]*School of Mathematical and Physical Sciences, Macquarie University, Sydney, New South Wales 2109, Australia*

(Received 18 June 2024; accepted 24 July 2024; published 29 August 2024)

We study observational signatures of nonsingular ultracompact objects regularized by nonlinear electrodynamics. The phenomenon of birefringence causes photons of different polarizations to propagate with respect to two distinct metrics, which manifests itself in the appearance of additional light rings surrounding the ultracompact object. We analyze the observational consequences of this result and illustrate our findings based on three regular black hole models commonly considered in the literature. We find that nonsingular horizonless ultracompact objects sourced by nonlinear electrodynamics possess an odd number of light rings and discuss the viability of this model as an effective description of their properties. In addition, we compare the phase velocities of polarized light rays propagating in nonsingular geometries sourced by nonlinear electrodynamics to the corresponding phase velocity in the Schwarzschild spacetime and demonstrate that regularizing the singularity by means of a theory that does not adhere to the Maxwell weak-field limit may lead to the emergence of acausal regions.

DOI: 10.1103/PhysRevD.110.044064

I. INTRODUCTION

Nonlinear theories of electrodynamics were initially conceived with the intent to cure the divergences associated with the electric field self-energy of charged particles present in the linear Maxwell theory [1–3]. Shortly after the 1933–1934 articles by Born and Infeld, Heisenberg and Euler devised a nonperturbative one-loop effective action that describes nonlinear corrections to Maxwell electrodynamics arising from quantum electrodynamical vacuum polarization effects (i.e., interactions of virtual electrons and positrons at the one-loop level without radiative corrections) [4]. In addition to quantum field effects such as vacuum polarization, the exploration of nonlinear electrodynamics (NED) is also interesting from a general relativistic perspective since the Einstein field equations predict nonlinearities due to the gravitational coupling of electromagnetic fields [5]. Elements of NED (most notably the nonlinear Born-Infeld action and its generalizations) also feature in different formulations of string theory/M-theory [6–11], where in some instances NED appears as a low-energy effective field theory, which is at least partially responsible for its revival after a prolonged period of dormancy. Since then, possible applications of NED have grown significantly, reaching far beyond string theory.[1] Interestingly, NED theories coupled to gravity have proven extremely fruitful in the construction of new black hole solutions without singularities, so-called regular black holes (RBHs) [13–26]. This particular application of NED theories is the focus of the present article.

While the existence of dark massive ultracompact objects (UCOs) has been established beyond reasonable doubt, the question of whether or not the observed astrophysical black hole candidates possess defining black hole features such as singularities and horizons is still open [27–30]. This motivates the study of observational signatures (such as those presented in Tables I and II and of this article) that can distinguish between

(1) singular vs. nonsingular ("regular")
(2) "horizonful" vs. horizonless

UCOs. In conjunction with gravitational wave detections and properties of accretion disks, optical signatures of the photon sphere such as light rings and shadows are among the principal observational tools expected to provide insights regarding the true physical nature of the observed astrophysical black hole candidates [28,31–33]. In this article, we analyze the physical properties of RBH solutions and closely related nonsingular horizonless UCO geometries arising from general relativity (GR) coupled to NED, focusing

*Contact author: sebastian.murk@oist.jp
†Contact author: ioannis.soranidis@hdr.mq.edu.au

[1]Reference [12] provides a short summary including recent developments.

specifically on features that may lead to potentially measurable differences in their observational signatures.

The remainder of this article is organized as follows: In Sec. II, we briefly review the relevant properties of NED theories. In Sec. III, we introduce the necessary ingredients needed to describe the purely magnetic NED solutions whose observational properties we investigate. In Sec. IV, we summarize the properties of three regular UCO models commonly considered in the literature and derive explicit expressions for their respective effective geometries when the singularity resolution is achieved by means of NED. In Sec. V, we determine the location of light rings in both the background and the effective geometries of these models, discuss their dynamical behavior and stability, and compare characteristic observational features. In Sec. VI, we derive the phase velocity of photons moving in the effective geometry for different propagation directions and compare them to the Schwarzschild case. Lastly, in Sec. VII, we summarize our results and outline their physical implications. For convenience, we review the phenomenon of birefringence in Appendix A. In Appendix B, we briefly comment on the singular behavior of the effective geometry. Throughout this article, we use the metric signature $(-,+,+,+)$ and work in dimensionless units such that $c = G = \hbar = k_B = 1$.

II. GENERAL RELATIVITY COUPLED TO NONLINEAR ELECTRODYNAMICS

The electromagnetic field tensor is defined in terms of the electromagnetic four-vector potential A_μ as

$$F_{\mu\nu} \coloneqq \partial_\mu A_\nu - \partial_\nu A_\mu. \tag{2.1}$$

Assuming a symmetric metric tensor $g_{\mu\nu}$, only two independent algebraic invariants can be formed from an antisymmetric tensor $F_{\mu\nu}$ [5], namely

$$\mathcal{F} = F_{\mu\nu}F^{\mu\nu}, \qquad \mathcal{G} = F_{\mu\nu}({}^\star F^{\mu\nu}), \tag{2.2}$$

where $\mathcal{F}$ denotes the electromagnetic field strength and $\star$ the Hodge star operator, i.e., ${}^\star F^{\mu\nu} \coloneqq \frac{1}{2}\varepsilon^{\mu\nu\rho\sigma}F_{\rho\sigma}$ with $\varepsilon^{\mu\nu\rho\sigma}$ the Levi-Civita symbol. We restrict our considerations to theories in which the effective action involves a one-parameter Lagrangian density that is a local function of $\mathcal{F}$, i.e., $\mathcal{L}(\mathcal{F},\mathcal{G}) \equiv \mathcal{L}(\mathcal{F})$. In this case, the most general Lorentz-invariant action for GR coupled to NED in four dimensions without cosmological constant term is given by

$$S = \frac{1}{16\pi}\int \sqrt{-g}[R - \mathcal{L}(\mathcal{F})]d^4x, \tag{2.3}$$

where $g \equiv \det(g_{\mu\nu})$ denotes the determinant of the metric tensor and $R = g_{\mu\nu}R^{\mu\nu}$ the Ricci curvature scalar.[2] The generalized NED field equations obtained from the principle of least action and the Bianchi identities are given by

$$\nabla_\mu(\mathcal{L}_\mathcal{F}F^{\mu\nu}) = 0, \qquad \nabla_\mu({}^\star F^{\mu\nu}) = 0, \tag{2.4}$$

respectively, where $\mathcal{L}_\mathcal{F} \coloneqq \partial\mathcal{L}/\partial\mathcal{F}$ denotes the first-order derivative of the Lagrangian density with respect to the electromagnetic field strength. The coupled Einstein equations corresponding to the action of Eq. (2.3) are given by

$$G_{\mu\nu} \coloneqq R_{\mu\nu} - \frac{1}{2}Rg_{\mu\nu} = 8\pi T_{\mu\nu}, \tag{2.5}$$

where the nonlinearities associated with the NED field enter via the energy-momentum tensor (EMT)

$$T_{\mu\nu} = \frac{1}{4\pi}\left(\mathcal{L}_\mathcal{F}F_{\mu\rho}F^\rho{}_\nu - \frac{1}{4}g_{\mu\nu}\mathcal{L}\right). \tag{2.6}$$

If the linear Maxwell theory is to be recovered in the weak-field limit (i.e., at small $\mathcal{F}$), then

$$\lim_{\mathcal{F}\to 0}\mathcal{L} \simeq \mathcal{F}, \qquad \lim_{\mathcal{F}\to 0}\mathcal{L}_\mathcal{F} \simeq 1, \tag{2.7}$$

must hold. It is worth mentioning that there exists an alternative but formally equivalent description of NED theories based on a dual representation that is obtained by means of a Legendre transformation [34]. However, for the purposes of our analysis in this article, it suffices to work in the Lagrangian formalism introduced above.

A static spherically symmetric metric is described by the line element

$$ds^2 = g_{\mu\nu}dx^\mu dx^\nu = -f(r)dt^2 + f(r)^{-1}dr^2 + r^2d\Omega^2, \tag{2.8}$$

where r denotes the areal radius and $d\Omega^2$ the normalized spherically symmetric Riemannian metric on the 2-sphere $\mathbb{S}^2$, which is given in terms of angular coordinates (θ,ϕ) by $d\Omega^2 \equiv d\theta^2 + \sin^2\theta d\phi^2$. In spherical symmetry, the only nonvanishing components of the electromagnetic field tensor are $F_{tr} = -F_{rt}$ (corresponding to a radial electric field) and $F_{\theta\phi} = -F_{\phi\theta}$ (corresponding to a radial magnetic field). From Eq. (2.4), the electric and magnetic charge are then identified as

$$Q_e = -r^2\mathcal{L}_\mathcal{F}F_{tr}, \qquad Q_m = -\frac{F_{\theta\phi}}{\sin\theta}, \tag{2.9}$$

respectively. One of the properties that make NED coupled to gravity an appealing candidate field theory for the construction of nonsingular spacetimes is that the EMT associated with the gauge-invariant Lagrangian density $\mathcal{L}(\mathcal{F})$ [cf. Eq. (2.6)] describes the spherically symmetric vacuum due to the symmetries $T_t{}^t = T_r{}^r$ (invariance under

[2]Derivatives of $F_{\mu\nu}$ are usually not considered in the action in order to avoid ghosts [12].

boosts in the radial direction) and $T_\theta{}^\theta = T_\phi{}^\phi$ (spherical symmetry) [35].

With the exception of Maxwell and Born-Infeld theories, a salient feature of NED theories is birefringence [36–38], i.e., the phenomenon that the two photon modes/polarizations associated with the two degrees of freedom encoded in the field effectively propagate with respect to two distinct metrics (see Appendix A for details). In the case $\mathcal{L} = \mathcal{L}(\mathcal{F})$ that we consider, one of them coincides with the background metric $g_{\mu\nu}$ of Eq. (2.8) which solves the field equations of GR coupled to NED [Eq. (2.5) with the EMT of Eq. (2.6)], and the other—referred to as effective metric in what follows—is given by

$$\bar{g}^{\mu\nu} = g^{\mu\nu} - 4\frac{\mathcal{L}_{\mathcal{FF}}}{\mathcal{L}_{\mathcal{F}}} F^{\mu}{}_{\rho} F^{\rho\nu}, \tag{2.10}$$

with the deviation from the background metric arising from the nonlinearity of the electromagnetic field, where $\mathcal{L}_{\mathcal{FF}} \coloneqq \partial\mathcal{L}_{\mathcal{F}}/\partial\mathcal{F}$ denotes the second-order derivative of $\mathcal{L}(\mathcal{F})$ with respect to the field strength $\mathcal{F}$, and the bar label is used to distinguish physical quantities associated with the effective geometry from those of the background geometry here and in what follows. In the linear Maxwell theory $\bar{g}^{\mu\nu} \equiv g^{\mu\nu}$ due to $\mathcal{L}_{\mathcal{F}} = \text{const}$ and $\mathcal{L}_{\mathcal{FF}} = 0$, and thus there is no birefringence.

Lastly, we note that solutions with an electric charge $Q_e \neq 0$ (including dyonic solutions where both $Q_e \neq 0$ and $Q_m \neq 0$) generally require a non-Maxwell behavior of the Lagrangian density $\mathcal{L}(\mathcal{F})$ at small $\mathcal{F}$ in order to maintain a regular center [14,19,24], i.e., in this case the Lagrangian density does not conform to the weak-field limit of Eq. (2.7). Although purely electric solutions ($Q_e \neq 0$ and $Q_m = 0$) with a regular center have been proposed in Refs. [15–17], any such solution inevitably requires a Lagrangian density that behaves nonlocally in the sense that different functions $\mathcal{L}(\mathcal{F})$ are required in different spacetime domains (specifically at small and large r with the former behaving non-Maxwellian in the limit $\mathcal{F} \to 0$) as pointed out in Refs. [18,19].[3] We therefore restrict our considerations to purely magnetic solutions ($Q_e = 0$ and $Q_m \neq 0$) in what follows. Prototypical examples of such solutions are the RBH models proposed by Bardeen [39] and Hayward [40].

III. MAGNETIC SOLUTIONS IN NONLINEAR ELECTRODYNAMICS

As motivated in the previous section, we restrict our considerations to purely magnetic solutions, i.e., $Q_e = 0$ and $Q_m \neq 0$ (cf. Sec. III in Ref. [23]). In this case, the generic form of the Lagrangian density that solves the Einstein equations of GR coupled to NED [Eqs. (2.5) and (2.6)] in spherical symmetry [Eq. (2.8)] is given by

$$\mathcal{L}(r) = -2\left(\frac{f'(r)}{r} + \frac{f(r)-1}{r^2}\right). \tag{3.1}$$

Using the identification $f(r) \equiv 1\text{–}2m(r)/r$, one further obtains

$$\mathcal{L}(r) = \frac{4m'(r)}{r^2}. \tag{3.2}$$

The four-potential, magnetic charge, and electromagnetic field strength are given by

$$A_\mu = (0,0,0,Q_m\cos\theta), \quad Q_m = \frac{q^2}{\sqrt{2\alpha}}, \quad \mathcal{F} = \frac{2Q_m^2}{r^4}, \tag{3.3}$$

respectively, where the parameter $\alpha > 0$ has dimensions of length squared and q denotes a free integration constant with dimensions of length. The precise form of the Lagrangian density depends on the choice of the mass function $m(r)$. We proceed with the generic form proposed by Fan and Wang [cf. Eq. (26) in Ref. [23]], namely

$$\mathcal{L}(\mathcal{F}) = \frac{4\mu(\alpha\mathcal{F})^{\frac{\nu+3}{4}}}{\alpha[1+(\alpha\mathcal{F})^{\frac{\nu}{4}}]^{1+\frac{\mu}{\nu}}}, \tag{3.4}$$

where $\mu \geq 3$, $\nu > 0$ are dimensionless constants and the choices $(\mu,\nu) = (3,2)$, $(\mu,\nu) = (3,3)$, and $(\mu,\nu) = (3,1)$ correspond to the Bardeen [39], Hayward [40], and the Maxwellian [23] RBH solutions, respectively. The geometry is specified in terms of μ, ν, α, and q by the metric function

$$f(r) = 1 - \frac{2Mr^{\mu-1}}{(r^\nu + q^\nu)^{\mu/\nu}}, \tag{3.5}$$

where $M \equiv q^3/\alpha$ corresponds to the gravitational mass (which in this case coincides with the electromagnetically induced mass, cf. Eqs. (8) and (9) of Ref. [25] and the discussion therein). In spherical symmetry, the effective metric according to which photons with one of the two possible polarizations move along null geodesics is given by [cf. Eq. (2.10)][4]

$$\bar{g}_{tt} = g_{tt}, \qquad \bar{g}_{rr} = g_{rr}, \tag{3.6}$$

[3]We also note the proposal of hybrid solutions which can circumvent the no-go theorem for solutions with an electric charge [14] by means of a phase transition to a dual magnetic phase near the core such that the electric field does not extend all the way to the center of the solution [20].

[4]The covariant effective metric tensor components $\bar{g}_{\mu\nu}$ are identified via the relation $\bar{g}^{\mu\rho}\bar{g}_{\rho\nu} = \delta^\mu{}_\nu$.

$$\bar{g}_{\theta\theta} = g_{\theta\theta}\left(1 + \frac{2\mathcal{F}\mathcal{L}_{\mathcal{F}\mathcal{F}}}{\mathcal{L}_{\mathcal{F}}}\right)^{-1}, \tag{3.7}$$

$$\bar{g}_{\phi\phi} = g_{\phi\phi}\left(1 + \frac{2\mathcal{F}\mathcal{L}_{\mathcal{F}\mathcal{F}}}{\mathcal{L}_{\mathcal{F}}}\right)^{-1}, \tag{3.8}$$

where the first line follows from $F_{tr} \propto Q_e = 0$ as we consider purely magnetic solutions with no electric charge. Since $F_{\theta\phi} \propto Q_m$ and $\mathcal{F} \propto Q_m^2$ [cf. Eq. (3.3)], one would naively expect that in the absence of magnetic charge ($Q_m = 0$) the angular effective metric tensor components of Eqs. (3.7) and (3.8) reduce to those of the background metric as well, that is $\bar{g}_{\theta\theta} = g_{\theta\theta}$ and $\bar{g}_{\phi\phi} = g_{\phi\phi}$. However, this is not always the case. This peculiar behavior is linked to the weak-field limit of the corresponding NED Lagrangian density $\mathcal{L}(\mathcal{F})$. As we shall see in what follows, the quantity $\mathcal{F}\mathcal{L}_{\mathcal{F}\mathcal{F}}/\mathcal{L}_{\mathcal{F}}$ does not vanish in the limit $Q_m \to 0$ in some RBH models.

IV. REGULAR BLACK HOLES AND NONSINGULAR HORIZONLESS ULTRACOMPACT OBJECTS

While keeping our analysis generic, we illustrate our results based on the RBH models proposed by Bardeen [39], Hayward [40], and Cadoni *et al.* [41] in what follows. These models are characterized by the strength of their respective deformations from the Schwarzschild geometry (with the model by Cadoni *et al.* corresponding to the strongest possible deformation) and exhibit different weak-field limits. Using the generic form of the Lagrangian density introduced in Eq. (3.4) of the previous section [or, equivalently, the generic form of the metric function $f(r)$ in Eq. (3.5)], each model is described by a distinct choice of the parameters $\alpha > 0$, $q > 0$, and $\nu > 0$.

We note here that in the original formulation of nonsingular RBH geometries the regularization of spacetime is achieved by means of a minimal length scale ℓ that appears in the metric function [cf. Eqs. (4.1), (4.11), and (4.21)] and acts as a Planckian cutoff beyond which GR is no longer valid. An alternative interpretation is to consider these metrics as a solution of the Einstein field equations with an EMT sourced by NED, cf. Eqs. (2.5) and (2.6) [19,23–25]. In the purely magnetic case that we consider due to the arguments laid out in the last paragraph of Sec. II, these types of solutions describe the gravitational field of a magnetic monopole. The difference in the interpretation of ℓ as a Planckian cutoff vs. ℓ arising from NED effects is that in the latter case macroscopic values are permissible [see Sec. V B, Table I]. Other ways of regularizing the black hole spacetime singularity have also been proposed in the literature, e.g., in 4D Einstein-Gauß-Bonnet theories [42], loop quantum gravity [43], and higher-dimensional approaches [44]. As we shall see in Sec. V, the precise quantification and comparison of light ring signatures may allow us to distinguish between nonsingular geometries obtained via different regularization methods and ultimately identify the underlying effective theory describing regular UCOs.

Depending on the minimal length scale ℓ and mass M, the geometry specified by the metric of Eq. (2.8) with $f(r)$ given by Eq. (3.5) can represent different types of UCOs. Setting $M \equiv 1$ and focusing on the case where the roots are real and positive [$r \in \mathbb{R}_{>0}$], solving the equation $f(r) = 0$ may result in either of the following distinct outcomes:

(I) Two roots [$\ell < \ell_c$], which corresponds to an RBH with an inner and an outer horizon.
(II) One root [$\ell = \ell_c$], which corresponds to an extremal RBH with one degenerate horizon.
(III) No roots [$\ell > \ell_c$], which corresponds to a nonsingular horizonless UCO.

Here, ℓ_c denotes the critical length at which the outer and inner horizon coalesce, $r_+(\ell_c) \equiv r_-(\ell_c)$.

A. Bardeen model

The Bardeen RBH [39] is described by the metric function

$$f_{\mathcal{B}}(r) = 1 - \frac{2Mr^2}{(r^2 + \ell^2)^{3/2}}, \tag{4.1}$$

where ℓ denotes the aforementioned minimal length scale introduced to regularize the black hole spacetime. Comparison with the generic metric function of Eq. (3.5) identifies the coefficients as $\mu_{\mathcal{B}} = 3$, $\nu_{\mathcal{B}} = 2$, and we can rewrite Eq. (4.1) as

$$f_{\mathcal{B}}(r) = 1 - \frac{2q^3r^2}{\alpha(r^2 + q^2)^{3/2}}. \tag{4.2}$$

This implies $q = \ell$ (note that $q \propto \ell$ is always expected based on our argumentation in the previous section) and [using Eq. (3.3)]

$$\alpha = \frac{\ell^3}{M}, \qquad Q_m = \sqrt{\frac{M\ell}{2}}. \tag{4.3}$$

The NED Lagrangian density is given by

$$\mathcal{L}_{\mathcal{B}}(\mathcal{F}) = \frac{12(\alpha\mathcal{F})^{5/4}}{\alpha[1 + (\alpha\mathcal{F})^{1/2}]^{5/2}}, \tag{4.4}$$

and expanding about the point $\mathcal{F} = 0$ reveals that the weak-field behavior of the NED Bardeen RBH is $\sim\mathcal{O}(\mathcal{F}^{5/4})$, i.e., stronger than that of the linear Maxwell theory.

Solving the equation $f_{\mathcal{B}}(r) = 0$ allows us to determine the roots representing the locations of the outer $r_+^{(\mathcal{B})}$ and inner $r_-^{(\mathcal{B})}$ horizon. Since the exact expressions are quite lengthy, we provide the leading-order terms in the series

expansion of small ℓ instead:

$$r_+^{(\mathcal{B})} = 2M - \frac{3\ell^2}{4M} + \mathcal{O}(\ell^4), \tag{4.5}$$

$$r_-^{(\mathcal{B})} = \frac{\ell^{3/2}}{\sqrt{2M}} + \frac{3\ell^{5/2}}{8\sqrt{2}M^{3/2}} + \mathcal{O}(\ell^{7/2}). \tag{4.6}$$

The critical length at which the two horizons coincide describes an extremal black hole. Solving $r_+^{(\mathcal{B})} = r_-^{(\mathcal{B})}$ leads to

$$\ell_c^{(\mathcal{B})} = \frac{4M}{3\sqrt{3}}. \tag{4.7}$$

For the Bardeen NED Lagrangian density Eq. (4.4), the effective metric tensor components are given explicitly by

$$\bar{g}_{tt} = -f_{\mathcal{B}}(r), \qquad \bar{g}_{rr} = f_{\mathcal{B}}(r)^{-1}, \tag{4.8}$$

$$\bar{g}_{\theta\theta} = g_{\theta\theta}\left(\frac{3}{2} - \frac{7\ell^2}{2(r^2+\ell^2)}\right)^{-1}, \tag{4.9}$$

$$\bar{g}_{\phi\phi} = g_{\phi\phi}\left(\frac{3}{2} - \frac{7\ell^2}{2(r^2+\ell^2)}\right)^{-1}, \tag{4.10}$$

where we observe that for vanishing magnetic charge $Q_m = 0$ [or, equivalently, vanishing minimal length $\ell = 0$ by virtue of Eq. (4.3)], the angular effective metric components do not coincide with those of the background metric tensor. The same behavior is exhibited in the asymptotic limit $r \to \infty$. The individual components of the term $\mathcal{F}\mathcal{L}_{\mathcal{F}\mathcal{F}}/\mathcal{L}_{\mathcal{F}}$ conspire in such a way so as to not yield the correct asymptotic behavior, which is an unavoidable by-product of the non-Maxwellian weak-field limit behavior.

B. Hayward model

The Hayward RBH [40] is described by the metric function

$$f_{\mathcal{H}}(r) = 1 - \frac{2Mr^2}{r^3 + 2M\ell^2}. \tag{4.11}$$

Comparison with the generic metric function of Eq. (3.5) identifies the coefficients as $\mu_{\mathcal{H}} = 3$, $\nu_{\mathcal{H}} = 3$, and we can rewrite Eq. (4.11) as

$$f_{\mathcal{H}}(r) = 1 - \frac{2q^3r^2}{\alpha(r^3+q^3)}. \tag{4.12}$$

This implies $q = (2M\ell^2)^{1/3}$ and [again using Eq. (3.3)]

$$\alpha = 2\ell^2, \qquad Q_m = \frac{M^{2/3}\ell^{1/3}}{2^{1/3}}. \tag{4.13}$$

The NED Lagrangian density is given by

$$\mathcal{L}_{\mathcal{H}}(\mathcal{F}) = \frac{12(\alpha\mathcal{F})^{3/2}}{\alpha[1+(\alpha\mathcal{F})^{3/4}]^2}, \tag{4.14}$$

and expanding about the point $\mathcal{F} = 0$ reveals that the weak-field behavior of the NED Hayward RBH is $\sim\mathcal{O}(\mathcal{F}^{3/2})$, which is stronger compared to both the linear Maxwell theory and the NED Bardeen RBH discussed in Sec. IV A.

Analogous to the previous subsection, we solve the equation $f_{\mathcal{H}}(r) = 0$ to determine the roots corresponding to the outer $r_+^{(\mathcal{H})}$ and inner $r_-^{(\mathcal{H})}$ horizon locations of the Hayward model. Once again, the exact expressions are rather lengthy, and thus we provide the leading terms in their series expansions for small ℓ instead:

$$r_+^{(\mathcal{H})} = 2M - \frac{\ell^2}{2M} + \mathcal{O}(\ell^4), \tag{4.15}$$

$$r_-^{(\mathcal{H})} = \ell + \frac{\ell^2}{4M} + \mathcal{O}(\ell^3). \tag{4.16}$$

The critical length at which the two horizons coincide and the Hayward RBH becomes extremal is given by

$$r_+^{(\mathcal{H})} = r_-^{(\mathcal{H})} \Rightarrow \ell_c^{(\mathcal{H})} = \frac{4M}{3\sqrt{3}}, \tag{4.17}$$

which coincides with the expression obtained for the Bardeen RBH [cf. Eq. (4.7)]. For the Hayward NED Lagrangian density Eq. (4.14), the effective metric tensor components are given explicitly by

$$\bar{g}_{tt} = -f_{\mathcal{H}}(r), \qquad \bar{g}_{rr} = f_{\mathcal{H}}(r)^{-1}, \tag{4.18}$$

$$\bar{g}_{\theta\theta} = g_{\theta\theta}\left(2 - \frac{9M\ell^2}{r^3+2M\ell^2}\right)^{-1}, \tag{4.19}$$

$$\bar{g}_{\phi\phi} = g_{\phi\phi}\left(2 - \frac{9M\ell^2}{r^3+2M\ell^2}\right)^{-1}. \tag{4.20}$$

As in the Bardeen model, the angular effective metric tensor components do not exhibit the correct limiting behaviors, neither for vanishing magnetic charge $Q_m = 0$ [$\ell = 0$] nor in the asymptotic regime $r \to \infty$. In contrast to the Bardeen case where the relation between Q_m and M [cf. Eq. (4.3)] leads to exact cancelations in the $\mathcal{F}\mathcal{L}_{\mathcal{F}\mathcal{F}}/\mathcal{L}_{\mathcal{F}}$ term, the effective metric tensor components arising from the Hayward NED Lagrangian density [Eq. (4.14)] depend explicitly on the gravitational mass M.

C. Cadoni *et al.* model

The model considered by Cadoni *et al.* in Ref. [41] belongs to the Maxwellian class of solutions first described in Sec. III C of Ref. [23]. Its metric function is given by

$$f_{\mathcal{C}}(r) = 1 - \frac{2Mr^2}{(r+\ell)^3}. \tag{4.21}$$

Comparison with the generic metric function of Eq. (3.5) identifies the coefficients as $\mu_{\mathcal{C}} = 3$, $\nu_{\mathcal{C}} = 1$, and Eq. (4.21) can be rewritten as

$$f_{\mathcal{C}}(r) = 1 - \frac{2q^3r^2}{\alpha(r+q)^3}. \tag{4.22}$$

This implies $q = \ell$ and

$$\alpha = \frac{\ell^3}{M}, \qquad Q_m = \sqrt{\frac{M\ell}{2}}, \tag{4.23}$$

analogous to the relations obtained for the Bardeen RBH described in Sec. IV A [cf. Eq. (4.3)]. The NED Lagrangian density is given by

$$\mathcal{L}_{\mathcal{C}}(\mathcal{F}) = \frac{12\mathcal{F}}{[1+(\alpha\mathcal{F})^{1/4}]^4}, \tag{4.24}$$

and expanding about the point $\mathcal{F} = 0$ reveals that the weak-field behavior of the NED Cadoni *et al.* RBH is $\sim\mathcal{O}(\mathcal{F})$, i.e., it reduces to the linear Maxwell theory.

Analogous to the previous two subsections, we solve the equation $f_{\mathcal{C}}(r) = 0$ to determine the roots corresponding to the outer $r_+^{(\mathcal{C})}$ and inner $r_-^{(\mathcal{C})}$ horizon locations of the Cadoni *et al.* model. Once again, the exact expressions are rather lengthy, and thus we provide the leading terms in their series expansions for small ℓ instead:

$$r_+^{(\mathcal{C})} = 2M - 3\ell - \frac{3\ell^2}{2M} + \mathcal{O}(\ell^3), \tag{4.25}$$

$$r_-^{(\mathcal{C})} = \frac{\ell^{3/2}}{\sqrt{2M}} + \frac{3\ell^2}{4M} + \mathcal{O}(\ell^{5/2}). \tag{4.26}$$

The critical length at which the two horizons coincide and the RBH considered by Cadoni *et al.* becomes extremal is given by

$$r_+^{(\mathcal{C})} = r_-^{(\mathcal{C})} \Rightarrow \ell_c^{(\mathcal{C})} = \frac{8M}{27}, \tag{4.27}$$

which is smaller compared to the critical lengths of the Bardeen and Hayward RBH $\ell_c^{(\mathcal{B})} = \ell_c^{(\mathcal{H})} = 4M/(3\sqrt{3})$ [cf. Eqs. (4.7) and (4.17)].

For the Cadoni *et al.* NED Lagrangian density Eq. (4.24), the effective metric tensor components are given explicitly by

$$\bar{g}_{tt} = -f_{\mathcal{C}}(r), \qquad \bar{g}_{rr} = f_{\mathcal{C}}(r)^{-1}, \tag{4.28}$$

$$\bar{g}_{\theta\theta} = g_{\theta\theta}\left(1 - \frac{5\ell}{2(r+\ell)}\right)^{-1}, \tag{4.29}$$

$$\bar{g}_{\phi\phi} = g_{\phi\phi}\left(1 - \frac{5\ell}{2(r+\ell)}\right)^{-1}. \tag{4.30}$$

It is evident from these relations that the effective metric tensor components of the NED Cadoni *et al.* RBH admit the correct limiting behaviors for vanishing minimal length and in the asymptotic regime, in contrast to those of the Bardeen [cf. Eqs. (4.8)–(4.10)] and Hayward [cf. Eqs. (4.18)–(4.20)] RBH models. This desirable property is inherently linked to the Maxwellian behavior $\sim\mathcal{O}(\mathcal{F})$ of the Cadoni *et al.* NED Lagrangian density [Eq. (4.24)] for small field strengths $\mathcal{F}$. Since the relation between Q_m and M in the model considered by Cadoni *et al.* is the same as that of the Bardeen RBH [cf. Eqs. (4.3) and (4.23)], the effective metric tensor components have once again no explicit dependence on the gravitational mass M, unlike those of the Hayward RBH.

V. LIGHT RINGS

A. Mathematical prerequisites

The Lagrangian for the motion of a free particle in a curved spacetime is given by

$$L_p = \frac{1}{2} g_{\mu\nu}\dot{x}^\mu\dot{x}^\nu, \tag{5.1}$$

where the dot denotes a derivative with respect to an appropriately chosen affine parameter (e.g., the proper time τ for timelike geodesics) characterizing the trajectory. Due to the spherical symmetry imposed by Eq. (2.8), we can limit our considerations to trajectories in the equatorial plane [$\theta = \pi/2$, $\dot{\theta} = 0$] without loss of generality in what follows. Denoting the four-velocity $u^\mu = (\dot{t}, \dot{r}, 0, \dot{\phi})$, we have

$$L_p = \frac{u^2}{2} = \frac{1}{2}(g_{tt}\dot{t}^2 + g_{rr}\dot{r}^2 + g_{\phi\phi}\dot{\phi}^2), \tag{5.2}$$

where $u^2 \coloneqq u_\mu u^\mu$. Using the corresponding Euler-Lagrange equations, it is straightforward to confirm that t and ϕ are cyclic variables,[5] resulting by virtue of Noether's theorem [45] in the conservation of their associated conjugate variables, namely the energy E and angular momentum L, i.e.,

[5]Recall that the metric of Eq. (2.8) is spherically symmetric and static, and thus $g_{\mu\nu}$ is independent of these coordinates.

$$\frac{\partial L_p}{\partial \dot{t}} = g_{tt}\dot{t} = -E, \qquad \frac{\partial L_p}{\partial \dot{\phi}} = g_{\phi\phi}\dot{\phi} = L. \tag{5.3}$$

As our interest lies in studying light rings formed by the null geodesics of photons, we substitute $\dot{t}$ and $\dot{\phi}$ from Eq. (5.3) into

$$g_{\mu\nu}\dot{x}^\mu\dot{x}^\nu = 0 \tag{5.4}$$

to obtain

$$\dot{r}^2 + V(r) = 0, \qquad V(r) \coloneqq \frac{E^2}{g_{tt}g_{rr}} + \frac{L^2}{g_{rr}g_{\phi\phi}}. \tag{5.5}$$

The location of the light rings is determined by the conditions $\dot{r} = 0$ and $\ddot{r} = 0$, which imply $V(r) = 0$ and $V'(r) = 0$, respectively [46,47]. Solving these equations for r yields the radius of the light ring and the impact parameter $b \coloneqq L/E$.

As alluded to previously (see Sec. II), UCOs sourced by NED will in general (i.e., with the exception of Maxwell and Born-Infeld theories) exhibit birefringence, and thus the two possible photon polarization propagate with respect to two different metrics and at different velocities.[6] Analogous to the derivation for the background metric above, photons propagating on null geodesics with respect to the effective metric [cf. Eqs. (2.10) and (3.6)–(3.8)] satisfy

$$\bar{g}_{\mu\nu}\dot{x}^\mu\dot{x}^\nu = 0, \tag{5.6}$$

and we obtain

$$\dot{r}^2 + \bar{V}(r) = 0, \qquad \bar{V}(r) \coloneqq \frac{\bar{E}^2}{\bar{g}_{tt}\bar{g}_{rr}} + \frac{\bar{L}^2}{\bar{g}_{rr}\bar{g}_{\phi\phi}}, \tag{5.7}$$

with the light ring locations equivalently specified by the conditions $\bar{V}(r) = 0$ and $\bar{V}'(r) = 0$. An alternative method to identify the light ring locations is to determine the critical points of the function (see Ref. [46] for a detailed derivation)

$$H = \frac{-g_{t\phi} \pm \sqrt{g_{t\phi} - g_{tt}g_{\phi\phi}}}{g_{\phi\phi}} \overset{(2.8)}{=} \frac{\sqrt{-g_{tt}g_{\phi\phi}}}{g_{\phi\phi}}, \tag{5.8}$$

which simplifies to the rightmost expression for static spherically symmetric metrics of the form of Eq. (2.8). The advantage of this approach is that it implicitly incorporates the condition $V(r) = 0$, thereby allowing one to disregard the conserved variables E and L. The same line of thought applies for the effective metric. We now proceed with the identification of light ring locations for the three RBH models described in Sec. IV.

B. Light ring locations

The methodology of our calculation can be applied analogously for the three RBH models described in Sec. IV [and any other RBH geometry whose metric can be cast into a form analogous to Eqs. (4.2), (4.12), and (4.22)]. For the three models considered in Sec. IV, the explicit form of the potentials in Eqs. (5.5) and (5.7) are given by

$$V_{\mathcal{B}}(r) = -E^2 + L^2\left(\frac{1}{r^2} - \frac{2M}{(r^2+\ell^2)^{3/2}}\right), \tag{5.9}$$

$$V_{\mathcal{H}}(r) = -E^2 + L^2\left(\frac{1}{r^2} - \frac{2M}{r^3+2M\ell^2}\right), \tag{5.10}$$

$$V_{\mathcal{C}}(r) = -E^2 + L^2\left(\frac{1}{r^2} - \frac{2M}{(r+\ell)^3}\right), \tag{5.11}$$

and

$$\bar{V}_{\mathcal{B}}(r) = -\bar{E}^2 + \frac{\bar{L}^2(3r^2-4\ell^2)\left((r^2+\ell^2)^{3/2}-2Mr^2\right)}{2r^2(r^2+\ell^2)^{5/2}}, \tag{5.12}$$

$$\bar{V}_{\mathcal{H}}(r) = -\bar{E}^2 + \frac{\bar{L}^2(2r^3-5M\ell^2)\left(r^3+2M(\ell^2-r^2)\right)}{(r^4+2M\ell^2)^2}, \tag{5.13}$$

$$\bar{V}_{\mathcal{C}}(r) = -\bar{E}^2 + \frac{\bar{L}^2(2r-3\ell)\left((r+\ell)^3-2Mr^2\right)}{2r^2(r+\ell)^4}, \tag{5.14}$$

respectively. The light ring locations in the background and in the effective geometry are determined by solving the equations $V'(r) = 0$ and $\bar{V}'(r) = 0$ for r. In what follows, we use a superscript "+" ("−") to label the outer (inner) light ring r_p^+ (r_p^-) and a subscript "p" for "photon sphere" to unambiguously distinguish the locations of the light rings from those of the outer and inner horizon r_+ and r_-, respectively. Once again, many of the exact expressions are quite lengthy and somewhat cumbersome to deal with by hand, and thus we do not provide them here. For the interested reader, all explicit expressions are provided in the Github repository linked as Ref. [49].[7] Since the procedure is analogous for the background and the effective geometry and follows the same steps for each RBH model, we do not repeat them explicitly here. The inner and outer horizons as well as the inner and outer light rings in the background [Eq. (2.8)] and effective [Eq. (2.10)] geometry for the three UCO models considered

[6] It is worth noting that Lagrangian densities based on the Born-Infeld nonlinearity cannot give rise to nonsingular black hole solutions in spherically symmetric settings [48].

[7] The code in this repository is written in *Mathematica* 12 [50].

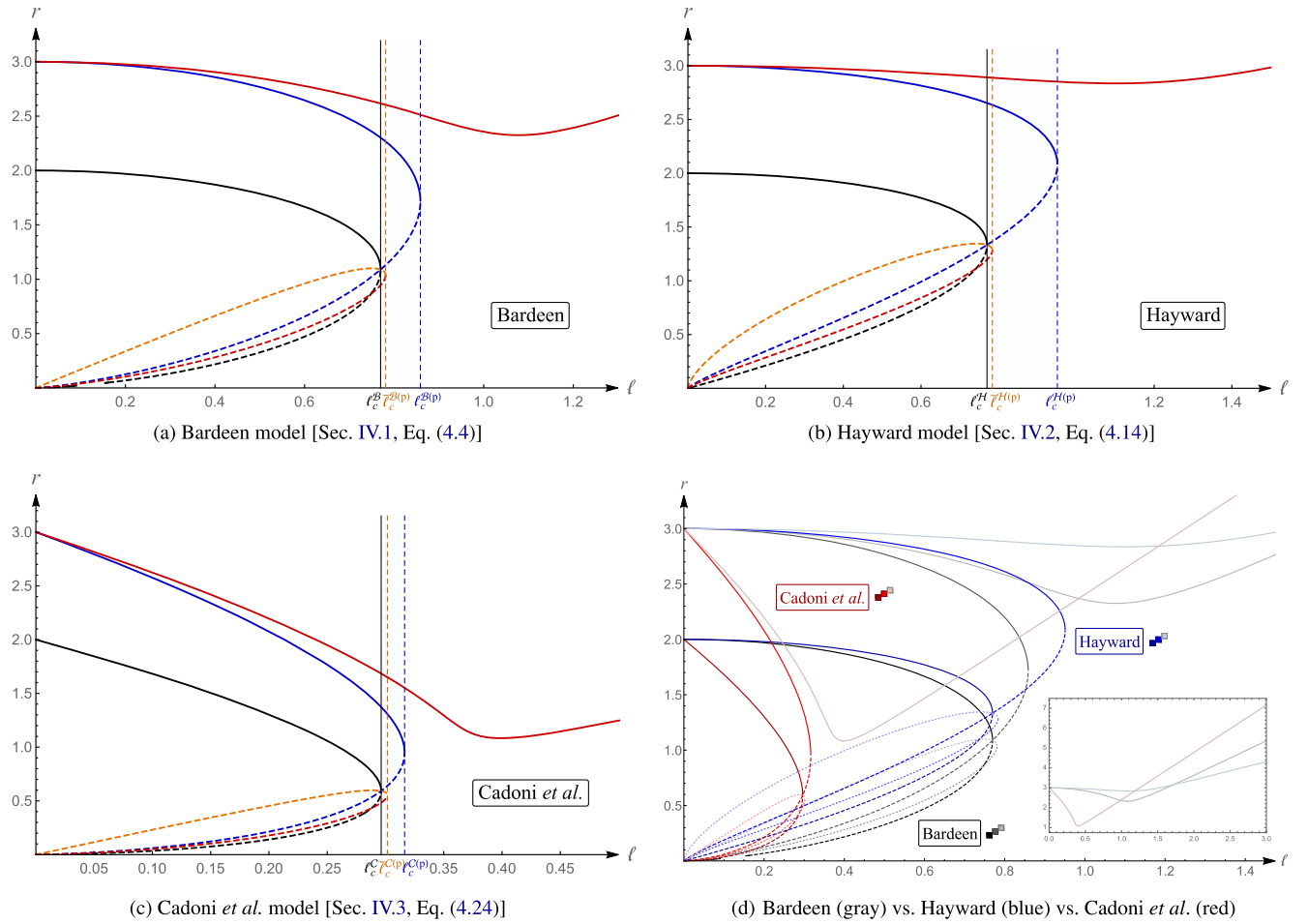

(a) Bardeen model [Sec. IV.1, Eq. (4.4)]

(b) Hayward model [Sec. IV.2, Eq. (4.14)]

(c) Cadoni *et al.* model [Sec. IV.3, Eq. (4.24)]

(d) Bardeen (gray) vs. Hayward (blue) vs. Cadoni *et al.* (red)

FIG. 1. Horizons, critical lengths, and light rings for the three nonsingular UCO models discussed in Sec. IV. In (a)–(c), the solid (dashed) black line represents the outer (inner) horizon r_+ (r_-), the solid (dashed) blue line represents the outer (inner) light ring r_p^+ (r_p^-) in the background geometry [Eq. (2.8)], and the solid (dashed) red line represents the outer (inner) light ring $\bar{r}_p^+$ ($\bar{r}_p^-$) in the effective geometry [Eq. (2.10)], which harbors a third light ring $\bar{r}_p^0$ situated between the two whose location is indicated by the dashed orange line. The critical lengths ℓ_c, $\bar{\ell}_c^{(p)}$, and $\ell_c^{(p)}$ at which the horizons [Eqs. (4.7), (4.17), and (4.27)], the two innermost light rings in the effective geometry, and the inner and outer light ring in the background geometry merge are indicated by the thin vertical black, thin vertical dashed orange, and thin vertical dashed blue line, respectively. The regularization parameter domain $0 < \ell \leqslant \ell_c$ ($\ell > \ell_c$) describes an RBH (a nonsingular horizonless UCO). The minimal length interval $\ell_c < \ell < \bar{\ell}_c^{(p)}$ ($\bar{\ell}_c^{(p)} < \ell < \ell_c^{(p)}$) is indicated by the region shaded in light orange (light blue) and corresponds to the second (third) column in Table II. The outer light ring in the effective geometry of the Bardeen (Hayward) [Cadoni *et al.*] model has a global minimum at $(r, \bar{\ell}_{\rm min}^{+(\mathcal{B})}) = (2.3251, 1.0766)$ ($(r, \bar{\ell}_{\rm min}^{+(\mathcal{H})}) = (2.8355, 1.1004)$) [$(r, \bar{\ell}_{\rm min}^{+(\mathcal{C})}) = (1.0834, 0.3991)$]. In (d), the Bardeen (Hayward) [Cadoni *et al.*] model is represented by the gray (blue) [red] color scheme. In each of the color schemes, the outer (inner) horizons are represented by the solid (dashed) line in the darkest hue, the outer (inner) light ring in the background geometry by the solid (dashed) line in the medium hue, the two innermost light rings in the effective geometry by the dotted lines in the two lightest hues, and the outer light ring in the effective geometry by the solid line in the lightest hue. Differences in the critical horizon and light ring length scales of the three models (see also Table I) are attributable to their different deformation strengths from the Schwarzschild geometry. The inset in the bottom right-hand side corner of (d) serves as a comparison of the outer light rings in the effective geometry of the three models, illustrating their characteristic behavior for varying minimal length ℓ in the interval $0 < \ell \leqslant 3$.

in Sec. IV are illustrated in Fig. 1 for the mass parameter $M = 1$.

For illustrative purposes, we focus on the model by Cadoni *et al.* in what follows since it is the only one out of the three models that exhibits the correct limiting behaviors (see last paragraph of Sec. IV C). The leading terms in the series expansions of the outer and inner light ring in the background geometry of this model about the point $\ell = 0$ are given by

$$r_p^+ = 3M - 4\ell - \frac{2\ell^2}{M} + \mathcal{O}(\ell^3), \tag{5.15}$$

$$r_p^- = \frac{\ell^{4/3}}{(3M)^{1/3}} + \frac{4\ell^{5/3}}{3^{5/3}M^{2/3}} + \frac{2\ell^2}{3M} + \mathcal{O}(\ell^{7/3}), \qquad (5.16)$$

respectively. Based on these expressions, we can ascertain that the outer light ring is situated closer to the black hole than in the Schwarzschild geometry, where it is located at $r = 3M$. As one would expect, the limit of vanishing minimal length $\lim_{\ell\to 0} r_p^+ = 3M$ reduces to this expression. The inner light ring on the other hand vanishes in this limit, $\lim_{\ell\to 0} r_p^- = 0$. The models proposed by Bardeen and Hayward exhibit the same qualitative behavior, which can be verified by examining their exact expressions and/or confirmed graphically as in Fig. 1. Similar to the critical length ℓ_c at which the inner and outer horizon merge, there is a critical length $\ell_c^{(p)}$, $r_p^+(\ell_c^{(p)}) \equiv r_p^-(\ell_c^{(p)})$, at which the inner and outer light rings merge (and then disappear) in the background geometry. This is in line with the analyses of Refs. [51,52] which examine properties of the EMT and quasinormal mode spectra for geometries that smoothly interpolate between RBHs and nonsingular horizonless UCOs based on the value of the regularization parameter ℓ. However, the light ring signature in the effective geometry significantly differs from that of the background geometry. As depicted in Fig. 1, there are generally three distinct light rings in the effective geometry. The outermost light ring [indicated by the solid red line in Figs. 1(a)–1(c)] persists and never disappears (in contrast to the behavior of the outer light ring in the background geometry indicated by the solid blue line), whereas the middle (dashed orange line) and innermost (dashed red line) light rings are present up to some critical length $\bar{\ell}_c^{(p)}$ indicated by the thin vertical dashed orange line in Figs. 1(a)–1(c). These characteristics are consistent across all three UCO models. Interestingly, the radius of the outer light ring in the effective geometry gradually decreases with increasing minimal length ℓ until it reaches a global minimum value at some $\bar{\ell}_{\rm min}^+ > \ell_c^{(p)}$ from which point onward its radius starts to continuously increase with increasing ℓ. We also note that for each model there is a small minimal length scale interval $\ell_c < \ell < \bar{\ell}_c^{(p)}$ [indicated by the region shaded in light orange that is enclosed by the thin vertical solid black line signifying ℓ_c and the thin vertical dashed orange line signifying $\bar{\ell}_c^{(p)}$ in Figs. 1(a)–1(c)] in which the two innermost light rings of the effective geometry are no longer obscured by the horizons (as the UCO is no longer an RBH but a nonsingular horizonless UCO at length scales $\ell > \ell_c$) and become visible to external observers. Similarly, there is a small minimal length interval $\ell_c < \ell < \ell_c^{(p)}$ [indicated by the union of the aforementioned interval $\ell_c < \ell < \bar{\ell}_c^{(p)}$ shaded in light orange and the region shaded in light blue that is enclosed by the thin vertical dashed orange line signifying $\bar{\ell}_c^{(p)}$ and the thin vertical dashed blue line signifying $\ell_c^{(p)}$ in Figs. 1(a)–1(c)], in which the inner light ring of the background geometry becomes visible.

TABLE I. Critical lengths ℓ_c, $\bar{\ell}_c^{(p)}$, and $\ell_c^{(p)}$ at which the horizons, the two innermost light rings in the effective geometry, and the inner and outer light ring in the background geometry merge, respectively. The value $\bar{\ell}_{\rm min}^+$ corresponds to the global minimum of the outer light ring in the effective geometry.

RBH model	ℓ_c	$\bar{\ell}_c^{(p)}$	$\ell_c^{(p)}$	$\bar{\ell}_{\rm min}^+$
Bardeen	$0.7698M$	$0.7811M$	$0.8587M$	$1.0766M$
Hayward	$0.7698M$	$0.7836M$	$0.9509M$	$1.1004M$
Cadoni *et al.*	$0.2963M$	$0.3016M$	$0.3164M$	$0.3991M$

Table I provides an overview of the relevant critical lengths for the three RBH models considered in Sec. IV. A universal result is that the outer light ring in the effective geometry [represented by the solid red line in Figs. 1(a)–1(c)] is located further away from the nonsingular UCO compared to the outer light ring in the background geometry [represented by the solid blue line in Figs. 1(a)–1(c)]. Since this result has observational relevance, we illustrate the difference $\bar{r}_p^+ - r_p^+$ for the three RBH models in Fig. 2.

Another noteworthy feature is that in each geometry (background and effective), there is precisely one observable light ring if the nonsingular UCO is an RBH [$0 < \ell < \ell_c$]. In the interval $\ell_c < \ell < \bar{\ell}_c^{(p)}$ on the other hand, there are three observable light rings in the effective geometry and two in the background geometry as the inner light rings become visible [region shaded in light orange in Figs. 1(a)–1(c).] In the interval $\bar{\ell}_c^{(p)} < \ell < \ell_c^{(p)}$, the innermost light rings in the effective geometry have disappeared and only the outermost light ring remains visible, while in the background geometry both the inner and outer light ring are still visible [region shaded in light blue in Figs. 1(a)–1(c)]. Lastly, in the interval $\ell > \ell_c^{(p)}$ only the outer light ring in the effective geometry remains visible. Table II summarizes the number of observable light rings in different domains of the minimal length scale parameter ℓ in theories with and without birefringence.

According to a well-established theorem nonsingular horizonless UCOs have at least two light rings (with one of them being stable) provided that the metric is a regular stationary solution of the Einstein field equations and the spacetime can be continuously deformed into a flat Minkowski spacetime [46].[8] However, the effective metric [Eq. (2.10)] is singular (see Appendix B for details) and

[8]An alternative approach is considered in Ref. [53], which derives the stability of the inner light ring of nonsingular horizonless UCOs based on the assumption that their outer light ring has the same properties as that of the Kerr geometry, but without invoking assumptions about the status of energy conditions.

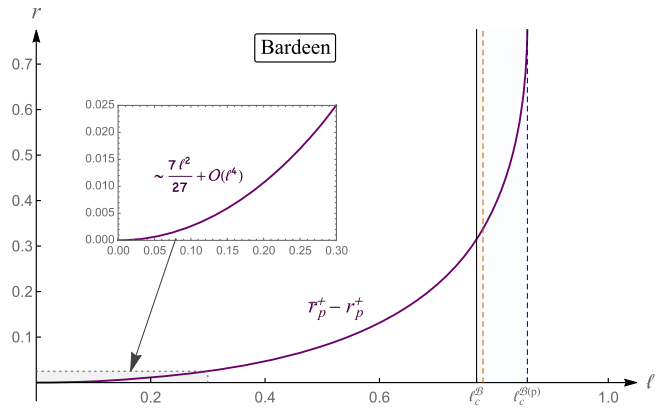

(a) Outer LR difference $\bar{r}_p^+ - r_p^+$ for the Bardeen model [Sec. IV.1, Eq. (4.4)]

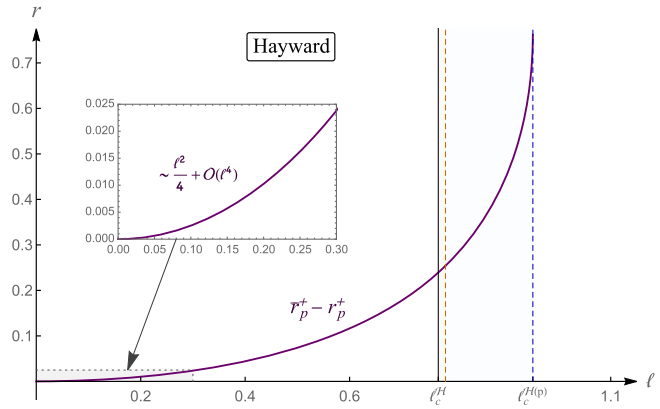

(b) Outer LR difference $\bar{r}_p^+ - r_p^+$ for the Hayward model [Sec. IV.2, Eq. (4.14)]

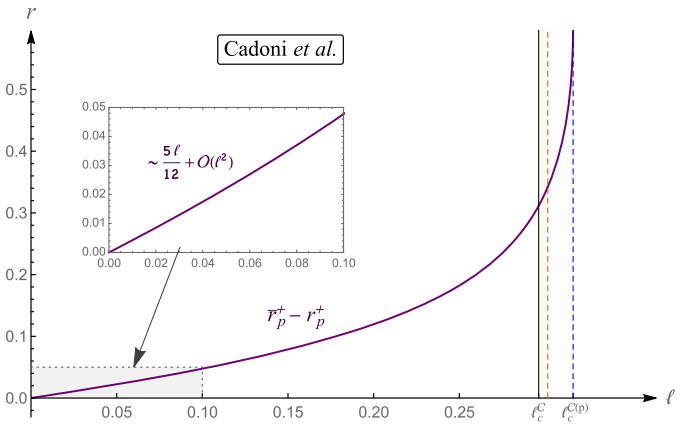

(c) Outer LR difference $\bar{r}_p^+ - r_p^+$ for the Cadoni *et al.* model [Sec. IV.3, Eq. (4.24)]

FIG. 2. Difference $\bar{r}_p^+ - r_p^+$ between the outer light ring (LR) in the effective geometry $\bar{r}_p^+$ [corresponding to the solid red line in Figs. 1(a)–1(c)] and the outer light ring in the background geometry r_p^+ [corresponding to the solid blue line in Figs. 1(a)–1(c)] for the three nonsingular UCO models considered in Sec. IV. For the models proposed by Bardeen and Hayward, the scaling behavior in the regime of small ℓ is quadratic, whereas for the Cadoni *et al.* model it is linear. Consequently, the outer light rings are more easily distinguished in the Cadoni *et al.* model for very small regularization parameter values ℓ. In all three models, the difference between the outer light rings becomes maximal as the critical light ring length $\ell_c^{(p)}$ of the background geometry (indicated by the vertical dashed blue line) is approached.

thus the theorem does not apply.[9] In fact, we find that theories with birefringence predict an odd number of light rings for $\ell > \ell_c$ (i.e., in the parameter domain where the nonsingular UCO is a horizonless UCO rather than an RBH) and a single light ring remains in the effective geometry for $\ell > \bar{\ell}_c^{(p)}$, see Table II. This indicates that the number of light rings on its own may not always serve as a definitive indicator in determining the identity of UCOs without knowledge of the underlying theory as both horizonful and horizonless objects may possess the same number of light rings.

[9]On the other hand, if the polarization mode that is null in the effective geometry is considered in the background geometry, then the corresponding photon trajectories are no longer null geodesics, and again the theorem does not apply.

In the effective geometry, the outermost light ring of the Hayward model is located the furthest away from the UCO for small values of the regularization parameter ℓ, followed

TABLE II. Number of observable light rings (LRs) for different domains of the regularization parameter ℓ (corresponding to different types of nonsingular UCOs) in effective theories with and without birefringence. The parameter domains $\ell_c < \ell < \bar{\ell}_c^{(p)}$ and $\bar{\ell}_c^{(p)} < \ell < \ell_c^{(p)}$ correspond to the regions shaded in light orange and light blue in Figs. 1(a)–1(c) and 2(a)–2(c), respectively.

	$0 < \ell < \ell_c$	$\ell_c < \ell < \bar{\ell}_c^{(p)}$	$\bar{\ell}_c^{(p)} < \ell < \ell_c^{(p)}$	$\ell > \ell_c^{(p)}$
Nonsingular UCO type	RBH	Horizonless	Horizonless	Horizonless
LRs without birefringence	1	2	2	0
LRs with birefringence	2	5	3	1

by those of the Bardeen and Cadoni *et al.* model. However, with increasing ℓ this behavior changes, and the outermost light ring in the Cadoni *et al.* first surpasses that of the Bardeen model and ultimately that of the Hayward model in terms of its distance from the nonsingular UCO, as illustrated by the inset located in the bottom right-hand side corner of Fig. 1(d). The outermost light ring in the effective Hayward geometry is eventually surpassed by that of the Bardeen model as well. These differences in the locations of the outer light ring in the effective geometry for varying ℓ are attributable to the different strengths of deformation from the Schwarzschild geometry exhibited by each model.[10] The different deformation strengths of the three models are also responsible for the different sizes of the intervals $\ell_c < \ell < \overline{\ell}_c^{(p)}$ and $\overline{\ell}_c^{(p)} < \ell < \ell_c^{(p)}$ corresponding to the regions shaded in light orange and light blue in Figs. 1(a)–1(c) and 2(a)–2(c), respectively. More precisely: the stronger the deformation from the Schwarzschild geometry, the smaller the size of the critical length scale intervals, as can be verified from the values provided in Table I. Lastly, we remind the reader that the strength of the deformation is also intimately related to the weak-field limit behavior. Ordering the models we consider in this article in terms of their respective deformation strengths, i.e., $\mathcal{C} > \mathcal{B} > \mathcal{H}$, we observe that the stronger the deformation, the closer the behavior to the Maxwellian weak-field limit, and the smaller the relevant critical length scale intervals.

C. Dynamical stability

The dynamical behavior of light rings is determined by the second-order derivatives of the potential with respect to r. For the three UCO models discussed in Sec. IV, we find

$$V''(r_p^+) < 0, \qquad V''(r_p^-) > 0, \tag{5.17}$$

$$\bar{V}''(\bar{r}_p^+) < 0, \qquad \bar{V}''(\bar{r}_p^0) > 0, \qquad \bar{V}''(\bar{r}_p^-) < 0. \tag{5.18}$$

This implies that in the background metric the inner light ring r_p^- is stable, while the outer light ring r_p^+ is unstable. The outermost light ring $\bar{r}_p^+$ in the effective geometry exhibits the same instability, but here the innermost light ring $\bar{r}_p^-$ is also unstable. This is in stark contrast to the non-NED case. Interestingly, the light ring $\bar{r}_p^{(0)}$ situated between the inner and outer light ring in the effective geometry is stable.

While even in the effective geometry nonsingular UCOs typically possess a stable light ring leading to well-known spacetime instabilities, this stable light ring is absent beyond a certain minimal length scale, namely $\ell > \overline{\ell}_c^{(p)}$. The fact that the outermost light ring $\bar{r}_p^+$ remains (unlike in the background geometry) suggests that—if the effective description of nonsingular horizonless UCOs sourced by NED is valid—they may possess only one unstable light ring, thus presenting a viable alternative to the standard paradigm used to explain observations of astrophysical black hole candidates. Of course, another possibility is that NED theories simply do not provide a viable effective description of nonsingular horizonless UCOs.

Lastly, we note that various models for gravitational collapse resulting in nonsingular UCOs violate the null energy condition (NEC), e.g., Friedmann-Robertson-Walker (FRW) collapse models that incorporate repulsive effects to halt the collapse [56,57] or thin-shell collapse models where the backreaction of Hawking radiation is described as a trace anomaly [58]. The emission of Hawking radiation [59,60] is also known to violate several energy conditions including the NEC, and a violation of the latter is a necessary requirement for the formation of a regular (in the sense of finite curvature scalars) apparent horizon in finite time according to the clock of a distant observer [61–63].

VI. CAUSALITY AND PHASE VELOCITIES

A. Generic expressions

In this section, we focus on the phase velocities of different photon polarizations and the resulting causal structure of their associated light cones. We begin by computing the phase velocity, utilizing the fact that light propagates along null geodesics. Recall that one photon polarization travels on the background metric, while the other travels on the effective metric. For our analysis, which we once again restrict to the equatorial plane without loss of generality (cf. Sec. V A), we proceed with a propagation wave vector k_μ of the form

$$k_\mu = (-\omega, \sqrt{g_{rr}}|\vec{k}|\cos\eta, 0, \sqrt{g_{\phi\phi}}|\vec{k}|\sin\eta), \tag{6.1}$$

where $|\vec{k}| = \sqrt{g^{ij}k_i k_j}$, with indices i, j running from 1 to 3, and $\eta \in [0, \pi]$ representing an angle introduced to conveniently specify the propagation direction in what follows. Radial light rays are described by $\eta = 0$, whereas $\eta = \pi/2$ for circular trajectories. The phase velocity is defined as $\omega/|\vec{k}|$. For the background geometry, the null condition $g^{\mu\nu}k_\mu k_\nu = 0$ [cf. Eq. (5.4)] and Eq. (6.1) lead to

$$v_{\rm ph} = \sqrt{-g_{tt}} \overset{(2.8)}{=} \sqrt{f(r)}\,. \tag{6.2}$$

Since this expression is independent of η, the phase velocity is the same in any direction of the photon propagation. Similarly, using Eqs. (2.10) and (5.6) for the effective metric, we find

[10] A similar feature appears in black hole thermodynamics, where the deviation of the mean-field theory critical ratio also depends on the strength of the deformation from the Schwarzschild geometry [54,55].

$$g^{\mu\nu}k_\mu k_\nu - 4\frac{\mathcal{L}_{\mathcal{FF}}}{\mathcal{L}_{\mathcal{F}}} g_{\rho\sigma}(F^{\mu\rho}k_\mu)(F^{\nu\sigma}k_\nu) = 0, \tag{6.3}$$

and the phase velocity is given by

$$\bar{v}_{\rm ph}(\eta) = \sqrt{f(r)\left(1 + \frac{2\mathcal{F}\mathcal{L}_{\mathcal{FF}}}{\mathcal{L}_{\mathcal{F}}}\sin^2\eta\right)}. \tag{6.4}$$

Unlike the phase velocity in the background geometry given by Eq. (6.2), the phase velocity in the effective geometry Eq. (6.4) depends on the photon's direction of travel. Consequently, due to the fact that one photon polarization mode moves according to the background geometry while the other moves according to the effective geometry, their respective phase velocities will differ, signifying the presence of birefringence. It is worth emphasizing that this phenomenon does not affect radial light rays described by a propagation vector with $\eta = 0$ [cf. Eq. (6.1)]. In this case, $v_{\rm ph} = \bar{v}_{\rm ph}(0)$, and thus radial light rays propagate with the same phase velocity.

As discussed in Secs. IV A and IV B, the effective metric tensor components of the Bardeen and Hayward models do not conform to the proper Schwarzschild limit in the case of vanishing minimal length. This property prevents a direct comparison of the phase velocity in these spacetimes to that of the singular Schwarzschild geometry. In the subsequent analysis, we therefore mainly focus on the model by Cadoni *et al.* (cf. Sec. IV C).

B. Phase velocities in the Cadoni *et al.* model

In this model, the first and second derivative of the Lagrangian density $\mathcal{L}_{\mathcal{C}}(\mathcal{F})$ [Eq. (4.24)] with respect to $\mathcal{F}$ are given as functions of the radial coordinate r by

$$\mathcal{L}'_{\mathcal{C}}(\mathcal{F}) = \frac{12r^5}{(r+\ell)^5}, \qquad \mathcal{L}''_{\mathcal{C}}(\mathcal{F}) = -\frac{15r^9}{M(r+\ell)^6}, \tag{6.5}$$

where we have substituted the corresponding values of the parameters α and Q_m given by Eq. (4.23) after taking the derivatives. Via Eq. (6.2) the phase velocity in the background geometry of the Cadoni *et al.* model is given by

$$v^{(\mathcal{C})}_{\rm ph} = \sqrt{f_{\mathcal{C}}(r)}. \tag{6.6}$$

Using Eqs. (3.3), (4.23), and (6.5) in Eq. (6.4) it follows that the phase velocity in the effective geometry of the Cadoni *et al.* model is given by

$$\bar{v}^{(\mathcal{C})}_{\rm ph}(\eta) = \sqrt{f_{\mathcal{C}}(r)\left(1 - \frac{5\ell}{2(r+\ell)}\sin^2\eta\right)}. \tag{6.7}$$

Figure 3 depicts its dependence on the propagation angle η.

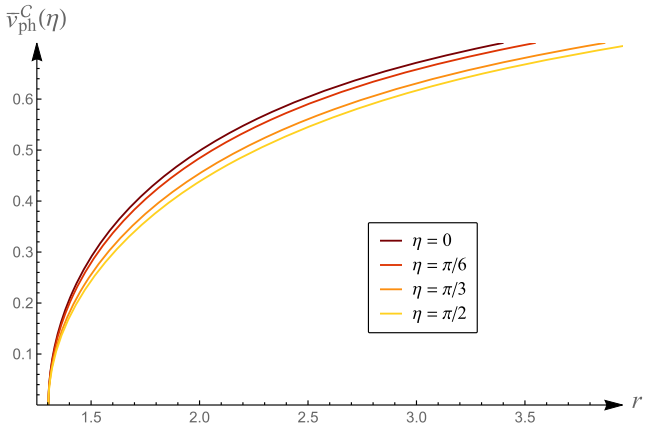

FIG. 3. Illustration of the dependence of the phase velocity $\bar{v}^{\mathcal{C}}_{\rm ph}(\eta)$ in the effective metric of the Cadoni *et al.* model [Eq. (6.7)] on the propagation angle $\eta \in [0, \pi]$ for $M = 1$ and $\ell = 0.2$. From the darkest to the lightest hue, the lines correspond to the values $\eta = \{0, \frac{\pi}{6}, \frac{\pi}{3}, \frac{\pi}{2}\}$.

The following two comments are in order: First, as $r \to \infty$, the influence of the magnetic charge Q_m or, equivalently [via Eq. (4.23)], the minimal length scale ℓ, diminishes, as one would expect intuitively, and the effective phase velocity reduces to that of the background geometry (which coincides with that of the Schwarzschild geometry in this limit), demonstrating the consistency of the calculation. Second, in the limit of vanishing minimal length, the Cadoni *et al.* model reduces to the Schwarzschild limit for every direction of motion, in contrast to the models by Bardeen and Hayward (see Sec. VI C).

For radial trajectories described by $\eta = 0$, the phase velocity of the Cadoni *et al.* model surpasses that in the Schwarzschild geometry, which can be attributed to the presence of a minimal length scale and consequently the absence of a singularity. The velocities coincide only in the asymptotic regime where the presence of a nonvanishing ℓ becomes insignificant.

Nonradial light rays with $\eta \neq 0$ propagating in the effective geometry exhibit an intriguing behavior illustrated in Fig. 4: such rays possess a higher phase velocity compared to those of the Schwarzschild geometry, but only up to a certain critical radius $r_{\rm crit}$ which increases with increasing M and decreasing ℓ. Beyond this critical radius, their phase velocity is smaller compared to the Schwarzschild case.[11] In addition, it is evident from Eqs. (6.6) and (6.7) that

[11]We emphasize that, when we are concerned with circular light trajectories, the phase velocity as a function of r is only meaningful if such trajectories exist. As can be seen in Fig. 1, light rings may be located at distances greater than the location of the Schwarzschild light ring, and therefore it is still meaningful to consider their phase velocity in this regime of r.

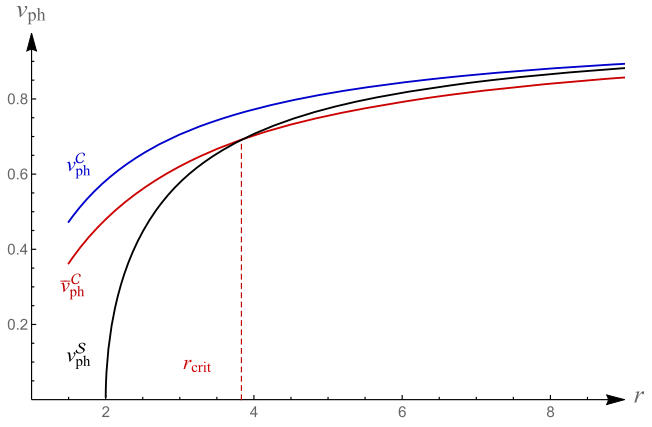

FIG. 4. Comparison of the phase velocities in the background $v^{\mathcal{C}}_{\rm ph}$ (blue) and effective $\bar{v}^{\mathcal{C}}_{\rm ph}$ (red) geometries of the nonsingular Cadoni *et al.* model at its critical length $\ell = \ell^{\mathcal{C}}_c$ to the phase velocity $v^{\mathcal{S}}_{\rm ph}$ in the singular Schwarzschild geometry for $M = 1$ and $\eta = \pi/2$. For these parameter choices, the critical radius which signifies the point beyond which the phase velocity in the Schwarzschild geometry exceeds that in the effective geometry is given by $r_{\rm crit} = 3.8313$.

$$v^{(\mathcal{C})}_{\rm ph} > \bar{v}^{(\mathcal{C})}_{\rm ph}, \tag{6.8}$$

indicating that the wavefronts associated with the background geometry always propagate faster than those of the effective geometry. Moreover, they also always propagate faster than those in the Schwarzschild geometry, cf. Fig. 4.

Nevertheless, the phase velocity never becomes superluminal for any propagation direction, a property that is intimately related to the fact that $\mathcal{L}''_{\mathcal{C}}(\mathcal{F}) < 0$ for the Cadoni *et al.* model. As demonstrated in Sec. VI C, this feature is not shared by the Bardeen and Hayward models. The significance of the signature of $\mathcal{L}''(\mathcal{F})$ becomes clear when examining the light cone structure. It is important to note that the wavevector k_μ is a 1-form (covariant vector), while the photon momentum, i.e., the tangent vector to the photon trajectory, is a contravariant vector [64]. In the linear Maxwell theory, this distinction is unnecessary, but it is necessary in NED theories with both a background and an effective metric. To accurately determine the nature of a null trajectory in the effective geometry with respect to the background geometry, we must start with the covariant form of the effective metric and the contravariant momentum vector:

$$\bar{g}_{\mu\nu} k^\mu k^\nu = 0. \tag{6.9}$$

Using the covariant components of the effective metric given by Eqs. (3.6)–(3.8), we have

$$k^2 = -g_{tt} \frac{2\mathcal{F}\mathcal{L}_{\mathcal{F}\mathcal{F}}}{\mathcal{L}_{\mathcal{F}}} (k^t)^2, \tag{6.10}$$

where $k^2 = g_{\mu\nu} k^\mu k^\nu$. Since both $-g_{tt}$ and $(k^t)^2$ are positive and $\mathcal{L}_{\mathcal{F}} > 0$ for all UCO models considered in this article (see Sec. VI C), the nature of a trajectory that is null in the effective geometry propagating within the background geometry is determined by the sign of $\mathcal{L}_{\mathcal{F}\mathcal{F}}$. Specifically, for $\mathcal{L}_{\mathcal{F}\mathcal{F}} < 0$ the vector k^μ that is null in the effective geometry is timelike in the background geometry, thereby preserving the causal character of the theory.

Alternatively, one can start with the null condition parsed in terms of the contravariant effective metric components,

$$\bar{g}^{\mu\nu} k_\mu k_\nu = 0. \tag{6.11}$$

An explicit calculation then leads to the expression

$$k^2 = -g^{\phi\phi} \frac{2\mathcal{F}\mathcal{L}_{\mathcal{F}\mathcal{F}}}{\mathcal{L}_{\mathcal{F}}} (k_\phi)^2. \tag{6.12}$$

While this appears to contradict the argumentation following Eq. (6.10), in this case the vector k_μ is spacelike in the background metric for $\mathcal{L}_{\mathcal{F}\mathcal{F}} < 0$, and the light cone of the background geometry lies entirely within the light cone of the effective geometry, indicating superluminal propagation velocities. The observation that the nesting of light cones reverses when transitioning from the contravariant metric to the covariant metric is a well-known result [11]. Hence, these two approaches of addressing causality are indeed equivalent, and it is ultimately the signature of $\mathcal{L}_{\mathcal{F}\mathcal{F}}$ that plays a crucial role.

C. Phase velocities in the Bardeen and Hayward models

Following the methodology of Sec. VI A, we calculate the phase velocities in the UCO models by Bardeen [Sec. IV A] and Hayward [Sec. IV B] based on Eqs. (6.2) and (6.4) for the background and effective geometries, respectively.

The derivatives of the NED Bardeen Lagrangian density [Eq. (4.4)] with respect to $\mathcal{F}$ are given by

$$\mathcal{L}'_{\mathcal{B}}(\mathcal{F}) = \frac{15\ell r^6}{(r^2+\ell^2)^{7/2}}, \tag{6.13}$$

$$\mathcal{L}''_{\mathcal{B}}(\mathcal{F}) = \frac{15 r^{10}(r^2-6\ell^2)}{4M(r^2+\ell^2)^{9/2}}, \tag{6.14}$$

where we have substituted the parameters α and Q_m from Eq. (4.3). The corresponding phase velocities in the background and effective geometry are

$$v^{(\mathcal{B})}_{\rm ph} = \sqrt{f_{\mathcal{B}}(r)}, \tag{6.15}$$

$$\bar{v}^{(\mathcal{B})}_{\rm ph} = \sqrt{f_{\mathcal{B}}(r)\left(1 + \frac{(r^2-6\ell^2)}{2(r^2+\ell^2)} \sin^2\eta\right)}, \tag{6.16}$$

respectively. For the NED Hayward Lagrangian density [Eq. (4.14)], the analogous expressions are given by

$$\mathcal{L}'_{\mathcal{H}}(\mathcal{F}) = \frac{18(2M\ell^2)^{2/3}r^7}{(r^3+2M\ell^2)^3}, \tag{6.17}$$

$$\mathcal{L}''_{\mathcal{H}}(\mathcal{F}) = \frac{9\cdot 2^{1/3}\ell^{2/3}(r^3-7M\ell^2)r^{11}}{M^{2/3}(r^3+2M\ell^2)^4}, \tag{6.18}$$

where we have substituted the parameters α and Q_m from Eq. (4.13). The phase velocities in the background and effective geometry are given by

$$v_{\rm ph}^{(\mathcal{H})} = \sqrt{f_{\mathcal{H}}(r)}, \tag{6.19}$$

$$\bar{v}_{\rm ph}^{(\mathcal{H})} = \sqrt{f_{\mathcal{H}}(r)\left(1+\frac{r^3-7M\ell^2}{r^3+2M\ell^2}\sin^2\eta\right)}. \tag{6.20}$$

Based on the relations given in Eqs. (6.16) and (6.20), we can conclude that the Schwarzschild phase velocity is recovered in the limit $\ell \to 0$ only for radial null rays described by $\eta = 0$. This demonstrates once again that for radial null rays the phase velocities in the background and effective geometries coincide, and therefore they do not experience birefringence. Nonradially propagating null rays on the other hand experience birefringence, as illustrated in Figs. 3 and 4 for the Cadoni *et al.* model.

Lastly, it is worth pointing out a distinctive behavior that occurs in the models by Bardeen and Hayward but is absent in the Cadoni *et al.* model. In the latter, $\mathcal{L}''_{\mathcal{C}}(\mathcal{F}) < 0$, ensuring a phase velocity less than one describing a propagation that is causal. However, this is not the case for polarized light moving in the effective geometries of the Bardeen and Hayward models. Specifically, there exists a radial distance $r_\star$ that leads to a signature change in $\mathcal{L}''_{\mathcal{B}}(\mathcal{F})$ and $\mathcal{L}''_{\mathcal{H}}(\mathcal{F})$. From Eqs. (6.14) and (6.18), these critical radii are identified as

$$r_\star^{(\mathcal{B})} = \sqrt{6}\ell, \qquad r_\star^{(\mathcal{H})} = (7M\ell^2)^{1/3}, \tag{6.21}$$

respectively. According to Eq. (6.10), this implies that a null trajectory in the effective metric behaves spacelike in the background metric for $r > r_\star^{(\mathcal{B})}$ and $r > r_\star^{(\mathcal{H})}$, indicating regions of superluminal propagation (provided that physically relevant trajectories exist in these regions, which depends on the value of the minimal length scale ℓ). To verify if superluminal signalling is possible in practice requires an examination of the group velocity of the associated light pulses [65], which may be discussed further in future works.

VII. DISCUSSION AND CONCLUSIONS

NED theories possess many intriguing features and the possibility of regularizing black hole geometries by coupling them to gravity remains an interesting proposal. Their nonlinearity results in the violation of the superposition principle, causing propagating light rays to be affected by electromagnetic background fields [66]. This phenomenon, known as "light-by-light scattering," has been experimentally observed [67]. Vacuum birefringence is another interesting effect, according to which different photon polarizations propagate with different phase velocities. Therefore, if a light ray propagates through a region pervaded by a strong electromagnetic field, it will effectively be separated into two distinct rays. Although this phenomenon has not yet been definitively observed in nature, there is compelling evidence from studies of light rays passing by magnetars—neutron stars with extremely powerful magnetic fields ranging from 10^9 to 10^{11} T [68].

Due to the difficulties in maintaining regularity at the center while simultaneously conforming to the Maxwell weak-field limit [Eq. (2.7)] inherent to solutions with an electric charge (cf. Sec III), our analysis focuses on the geometries of purely magnetic nonsingular UCOs sourced by NED. We examine their observational properties such as light ring signatures and phase velocities. Our analysis illustrates that the phenomenon of birefringence may manifest itself through the presence of additional light rings surrounding the nonsingular UCO (cf. Sec. V, Fig. 1). On the other hand, the number of light rings on its own is insufficient to distinguish RBHs from nonsingular horizonless UCOs as both models may possess either one or two light rings depending on the minimal length scale and the presence or absence of birefringence (cf. Sec. V, Table II).

Interestingly, our analysis reveals that there are narrow intervals in the minimal length scale parameter, namely $\ell_c < \ell < \ell_c^{(p)}$ [corresponding to the union of the regions shaded in light orange and light blue in Figs. 1(a)–1(c) and 2(a)–2(c)] and $\ell_c < \ell < \overline{\ell}_c^{(p)}$ [corresponding to the region shaded in light orange in Figs. 1(a)–1(c) and 2(a)–2(c)], in which the inner light ring in the background geometry and the two innermost light rings in the effective geometry, respectively, become visible to external observers. Another notable result is that the outer light ring in the effective geometry persists beyond the critical light ring length $\ell_c^{(p)}$ of the background geometry, as illustrated in Fig. 1.

While our procedure is generic based on the general form of the NED Lagrangian density proposed by Fan and Wang [Ref. [23], Eq. (26)], we explicitly consider three popular nonsingular UCO models characterized by the strength of their respective deviations from the singular Schwarzschild geometry. Only one of these models, namely that considered by Cadoni *et al.* in Ref. [41], possesses an effective NED metric that exhibits the desired behavior in the limit of

vanishing minimal length and in the asymptotic regime (Sec. IV C). For this particular model, the minimal length parameter is bounded from above by $\ell \lesssim 0.47M$ via observations of the S2 star orbiting Sagittarius A*, the black hole candidate located at the center of the Milky Way Galaxy [41]. However, since the critical light ring lengths of this model sit far below this value (cf. last row in Table I), the current bound is insufficient to

(i) distinguish between an RBH and a nonsingular horizonless UCO; and
(ii) either exclude or confirm the presence of birefringence;

based on the number of light rings surrounding the UCO.

Testing the existence of additional light rings is only possible if the resolution achieved in our astrophysical observations is sufficient to distinguish them. To determine the required resolution for nonsingular UCOs sourced by NED, we compute the light ring locations and compare their differences. A universal result is that the outermost light ring in the effective geometry is always situated at larger radii compared to the outer light ring of the background geometry. As illustrated in Fig. 2, the separation between these two light rings increases with the minimal length scale, reaching its maximum at $\ell_c^{(p)}$, the critical light ring length where the inner and outer light ring of the background geometry merge and disappear. While the minimal length scale need not be Planckian, it is typically assumed to be small. It is therefore useful to examine how the light ring separation behaves in this regime. We find that in the model by Cadoni *et al.*, the separation scales with $\sim\ell$, whereas in the Bardeen and Hayward models it scales with $\sim\ell^2$. This characteristic behavior can be attributed to the stronger deformation of the Cadoni *et al.* model from the Schwarzschild geometry compared to the other two models. As a result, detecting both light rings individually is a more feasible task for the Cadoni *et al.* model at small length scales.

A different interpretation for the light rings in NED geometries is offered in Ref. [69], according to which photons move exclusively in what we refer to as the effective geometry. Complementary analyses related to our interpretation according to which one of the two effective geometries coincides with the background geometry are given in Refs. [70,71] for electrically charged solutions in the class of regularized Maxwell (RegMax) theories and dyonic solutions in ModMax theories, respectively. The light rings, shadows, and gravitational lensing effects of the electrically charged Dymnikova RBH [35] with an NED source are studied in Ref. [72].

In addition to light ring signatures, we analyzed the phase velocities for different photon polarizations and examined the corresponding causal structure for the three nonsingular UCO models considered in this article. Our results indicate that there are no acausal spacetime regions when the NED theory adheres to the Maxwell weak-field limit as in the Cadoni *et al.* model. On the other hand, in models where this is not the case such as those proposed by Bardeen and Hayward, the light cone of the background geometry is fully contained within the light cone of the effective geometry, which indicates the presence of spacetime regions where superluminal motion is possible, provided that the relevant trajectories exist.

The limiting behavior of the Cadoni *et al.* model allows for comparisons to the Schwarzschild geometry. We find that the phase velocity in the background geometry exceeds that of the effective geometry as well as that of the Schwarzschild geometry. Interestingly, the phase velocity in the effective geometry exceeds the Schwarzschild phase velocity only up to some critical radius, beyond which it is smaller, as depicted in Fig. 4. Measuring these phase velocities in experiments could provide an alternative way of establishing bounds on the minimal length scale parameter.

Astrophysical observations of black hole candidates are typically modeled using the Kerr paradigm since realistic UCOs are expected to possess angular momentum and rotate. In particular, the emission of gravitational waves requires at least a mass quadrupole structure and thus cannot be modeled in spherically symmetric settings. On the other hand, a recent study indicates that spherically symmetric solutions in semiclassical gravity can mimic signatures of axially symmetric geometries [73]. Nonetheless, to comprehensively test the validity of NED theories as an effective description of nonsingular UCOs requires an extension to axial symmetry. However, attempts to provide such an extension using the Newman-Janis formalism have not been successful thus far. Fully analytic solutions remain unknown, and only solutions for the case of slowly rotating objects are currently available [74,75].

ACKNOWLEDGMENTS

We would like to thank Pedro Cunha, Carlos Herdeiro, Yasha Neiman, and Daniel Terno for useful discussions and helpful comments. S. M. is supported by the Quantum Gravity Unit of the Okinawa Institute of Science and Technology (OIST). I. S. is supported by an International Macquarie University Research Excellence Scholarship (IMQRES).

APPENDIX A: BIREFRINGENCE

Following the argumentation of Ref. [36], we rederive the phenomenon of birefringence for convenience. As in Sec. II, we restrict our considerations to NED Langrangian densities $\mathcal{L}(\mathcal{F},\mathcal{G}) \equiv \mathcal{L}(\mathcal{F})$. The derivation is based on the assumption that the electromagnetic field $\tilde{F}_{\mu\nu}$ of the UCO is much stronger than that of photons $\Phi_{\mu\nu}$. For simplicity, we work in Minkowski spacetime here, but an analogous derivation can be performed in generic curved spacetimes by considering covariant derivatives instead of partial derivatives in what follows. The total electromagnetic field is given by

$$F_{\mu\nu} = \tilde{F}_{\mu\nu} + \Phi_{\mu\nu}. \tag{A1}$$

Defining

$$h^{\mu\nu} \coloneqq \mathcal{L}_{\mathcal{F}} F^{\mu\nu}, \tag{A2}$$

the leading terms in the series expansion about $\Phi_{\mu\nu}$ are

$$h^{\mu\nu} = h^{\mu\nu}|_{\Phi=0} + \left.\frac{\partial h^{\mu\nu}}{\partial F_{\rho\sigma}}\right|_{F=\tilde{F}} \Phi_{\rho\sigma} + \mathcal{O}(\Phi^2), \tag{A3}$$

where indices have been omitted in the $|_{\bullet}$ subscripts and order $\mathcal{O}(\bullet)$ here and in what follows to avoid clutter. Substituting Eq. (A3) into Eq. (A2) results in the linearized equations

$$\partial_\mu h^{\mu\nu} = \left.\frac{\partial h^{\mu\nu}}{\partial F_{\rho\sigma}}\right|_{F=\tilde{F}} \partial_\mu \Phi_{\rho\sigma} + \mathcal{O}(\Phi) = 0. \tag{A4}$$

We are looking for solutions $\Phi_{\rho\sigma}$ of the form

$$\Phi_{\rho\sigma}(x) = \epsilon_{\rho\sigma}(k) e^{-ikx}, \tag{A5}$$

where

$$\epsilon_{\rho\sigma} \coloneqq k_\rho \epsilon_\sigma(k) - k_\sigma \epsilon_\rho(k) \tag{A6}$$

denotes the antisymmetric polarization tensor, k_ρ the propagation vector, and ϵ_ρ the polarization vector [76]. Substituting the partial derivative

$$\partial_\mu \Phi_{\rho\sigma} = -ik_\mu \epsilon_{\rho\sigma}(k) e^{-ikx} \tag{A7}$$

into Eq. (A4) results in

$$\left.\frac{\partial h^{\mu\nu}}{\partial F_{\rho\sigma}}\right|_{F=\tilde{F}} (-ik_\mu \epsilon_{\rho\sigma}(k) e^{-ikx}) = 0, \tag{A8}$$

and using the definition of the antisymmetric polarization tensor Eq. (A6), we have

$$\left.\frac{\partial h^{\mu\nu}}{\partial F_{\rho\sigma}}\right|_{F=\tilde{F}} k_\mu (k_\rho \epsilon_\sigma - k_\sigma \epsilon_\rho) = 0. \tag{A9}$$

Finally, using the antisymmetry of the electromagnetic field tensor $F_{\rho\sigma}$ [cf. Eq. (2.1)], we arrive at the relation

$$\left.\frac{\partial h^{\mu\nu}}{\partial F_{\rho\sigma}}\right|_{F=\tilde{F}} k_\mu k_\rho \epsilon_\sigma = 0. \tag{A10}$$

The partial derivative is calculated as

$$\frac{\partial h^{\mu\nu}}{\partial F_{\rho\sigma}} \overset{(A2)}{=} \frac{\partial}{\partial F_{\rho\sigma}} (\mathcal{L}_{\mathcal{F}} F^{\mu\nu}) = \mathcal{L}_{\mathcal{F}\mathcal{F}} \frac{\partial \mathcal{F}}{\partial F_{\rho\sigma}} F^{\mu\nu} + \mathcal{L}_{\mathcal{F}} \frac{\partial F^{\mu\nu}}{\partial F_{\rho\sigma}}, \tag{A11}$$

where

$$\frac{\partial F^{\mu\nu}}{\partial F_{\rho\sigma}} = \frac{1}{2}(\eta^{\mu\rho}\eta^{\nu\sigma} - \eta^{\nu\rho}\eta^{\mu\sigma}) \tag{A12}$$

due to the antisymmetry property [cf. Eq. (2.1)]. The derivative of the field strength $\mathcal{F}$ with respect to $F_{\rho\sigma}$ is calculated using this relation and results in

$$\begin{aligned}\frac{\partial \mathcal{F}}{\partial F_{\rho\sigma}} &= \frac{\partial}{\partial F_{\rho\sigma}} (F_{\alpha\beta} F^{\alpha\beta}) \\ &= \frac{\partial}{\partial F_{\rho\sigma}} (\eta_{\alpha\chi}\eta_{\beta\lambda} F^{\alpha\beta} F^{\chi\lambda}) = 2F^{\rho\sigma}.\end{aligned} \tag{A13}$$

Substitution of Eqs. (A12) and (A13) into Eq. (A11) and subsequently into Eq. (A10) results in

$$2\mathcal{L}_{\mathcal{F}\mathcal{F}} (F^{\rho\sigma} k_\rho)(F^{\mu\nu} k_\mu)\epsilon_\sigma + \frac{1}{2}\mathcal{L}_{\mathcal{F}} (\eta^{\nu\sigma} k^2 - k^\nu k^\sigma)\epsilon_\sigma = 0. \tag{A14}$$

It is useful to define the four-vectors

$$a^\mu \coloneqq F^{\mu\nu} k_\nu, \qquad {}^\star a^\mu \coloneqq {}^\star F^{\mu\nu} k_\nu, \qquad b^\mu \coloneqq F^{\mu\nu} a_\nu. \tag{A15}$$

Equation (A14) can then be rewritten as

$$[\mathcal{L}_{\mathcal{F}} (\eta^{\nu\sigma} k^2 - k^\nu k^\sigma) + 4\mathcal{L}_{\mathcal{F}\mathcal{F}} a^\nu a^\sigma]\epsilon_\sigma = 0. \tag{A16}$$

Defining

$$M^{\nu\sigma} \coloneqq \mathcal{L}_{\mathcal{F}} (\eta^{\nu\sigma} k^2 - k^\nu k^\sigma) + 4\mathcal{L}_{\mathcal{F}\mathcal{F}} a^\nu a^\sigma, \tag{A17}$$

Equation (A16) is given by

$$M^{\nu\sigma}\epsilon_\sigma = 0. \tag{A18}$$

To determine the polarization vector ϵ_σ, we express it in terms of four linearly independent vectors a^μ, ${}^\star a^\mu$, k^μ, and b^μ, i.e.,

$$\epsilon_\sigma = c_1 a_\sigma + c_2 {}^\star a_\sigma + c_3 k_\sigma + c_4 b_\sigma. \tag{A19}$$

Equation (A18) is then given by

$$c_1 M^{\nu\sigma} a_\sigma + c_2 M^{\nu\sigma} {}^\star a_\sigma + c_3 M^{\nu\sigma} k_\sigma + c_4 M^{\nu\sigma} b_\sigma = 0. \tag{A20}$$

Using $k^\sigma a_\sigma = k^\sigma F_{\sigma\alpha} k^\alpha = 0$ (due to antisymmetry), the first term is given by

$$M^{\nu\sigma} a_\sigma = (\mathcal{L}_{\mathcal{F}} k^2 + 4\mathcal{L}_{\mathcal{F}\mathcal{F}} a^2) a^\nu, \tag{A21}$$

where $a^2 \coloneqq a_\mu a^\mu$. Similarly, $k^\sigma {}^\star a_\sigma = k^\sigma {}^\star F_{\sigma\nu} k^\nu = 0$ (due to antisymmetry), and the second term is given by

$$M^{\nu\sigma\star}a_\sigma = \mathcal{L}_\mathcal{F} k^{2\star} a^\nu + 4\mathcal{L}_{\mathcal{F}\mathcal{F}}(a^{\sigma\star}a_\sigma)a^\nu. \tag{A22}$$

Analogously, the third and fourth term are given by

$$M^{\nu\sigma}k_\sigma = \mathcal{L}_\mathcal{F}(k^2k^\nu - k^2k^\nu) + 4\mathcal{L}_{\mathcal{F}\mathcal{F}}(a^\sigma k_\sigma)a^\nu = 0, \tag{A23}$$

$$M^{\nu\sigma}b_\sigma = \mathcal{L}_\mathcal{F} k^2 b^\nu - \mathcal{L}_\mathcal{F}(k^\sigma b_\sigma)k^\nu, \tag{A24}$$

respectively, where we have used $a^\sigma k_\sigma = 0$ and $a^\sigma b_\sigma = a^\sigma F_{\sigma\alpha}a^\alpha = 0$ (due to antisymmetry). Substitution of Eqs. (A21)–(A24) into Eq. (A20) yields

$$\begin{aligned}&[c_1(\mathcal{L}_\mathcal{F}k^2 + 4\mathcal{L}_{\mathcal{F}\mathcal{F}}a^2) + c_2 4\mathcal{L}_{\mathcal{F}\mathcal{F}}(a^{\sigma\star}a_\sigma)]a^\nu \\ &\quad + c_2(\mathcal{L}_\mathcal{F}k^2)^\star a^\nu - c_4[\mathcal{L}_\mathcal{F}(k^\sigma b_\sigma)]k^\nu + c_4(\mathcal{L}_\mathcal{F}k^2)b^\nu = 0.\end{aligned} \tag{A25}$$

Since the four-vectors a^μ, ${}^\star a^\mu$, k^μ, and b^μ are linearly independent, the vanishing of $M^{\nu\sigma}\epsilon_\sigma$ implies that the coefficients must vanish. We note that

$$k^\sigma b_\sigma = k^\sigma F_{\sigma\alpha}a^\alpha = -(F_{\alpha\sigma}k^\sigma)a^\alpha = -a_\alpha a^\alpha = -a^2, \tag{A26}$$

and

$$\begin{aligned}a^{\sigma\star}a_\sigma &= F^{\sigma\beta}k_\beta{}^\star F_{\sigma\alpha}k^\alpha = \eta^{\alpha\lambda}(-\mathcal{G}\eta^\beta_\alpha)k_\beta k_\lambda \\ &= -\mathcal{G}\eta^{\beta\lambda}k_\sigma k_\lambda = -\mathcal{G}k^2,\end{aligned} \tag{A27}$$

where we have used the property $F^{\sigma\beta\star}F_{\sigma\alpha} = -\mathcal{G}\eta^\beta_\alpha$ with $\mathcal{G}$ as defined in Eq. (2.2).

Since the last two terms in Eq. (A25) cannot vanish simultaneously unless $c_4 = 0$, we are left with a system of equations for the coefficients c_1 and c_2.[12] For $k^2 = 0$, we have

$$c_1(4\mathcal{L}_{\mathcal{F}\mathcal{F}}a^2) = 0, \tag{A28}$$

and an arbitrary c_2, which necessarily leads to $c_1 = 0$, and thus the polarization vector is

$$\epsilon^\mu = c_2{}^\star a^\mu. \tag{A29}$$

This corresponds to the photon polarization mode that moves on null geodesics in the background geometry. For $k^2 \neq 0$ on the other hand, we find

$$c_1(\mathcal{L}_\mathcal{F}k^2 + 4\mathcal{L}_{\mathcal{F}\mathcal{F}}a^2) = 0. \tag{A30}$$

To find a nontrivial (i.e., $c_1 \neq 0$) solution to the eigenvalue problem $M^{\nu\sigma}\epsilon_\sigma = 0$, we solve

$$\mathcal{L}_\mathcal{F}k^2 + 4\mathcal{L}_{\mathcal{F}\mathcal{F}}a^2 = 0 \Rightarrow k^2 + \frac{4\mathcal{L}_{\mathcal{F}\mathcal{F}}}{\mathcal{L}_\mathcal{F}}a^2 = 0. \tag{A31}$$

Using the definition of the four-vector a^μ, this equation can be rewritten as

$$k^2 + \frac{4\mathcal{L}_{\mathcal{F}\mathcal{F}}}{\mathcal{L}_\mathcal{F}}\eta_{\mu\nu}F^{\mu\alpha}k_\alpha F^{\nu\beta}k_\beta = 0 \tag{A32}$$

$$\Rightarrow \eta^{\alpha\beta}k_\alpha k_\beta + \frac{4\mathcal{L}_{\mathcal{F}\mathcal{F}}}{\mathcal{L}_\mathcal{F}}\eta_{\mu\nu}F^{\mu\alpha}F^{\nu\beta}k_\alpha k_\beta = 0 \tag{A33}$$

$$\Rightarrow \left(\eta^{\alpha\beta} + \frac{4\mathcal{L}_{\mathcal{F}\mathcal{F}}}{\mathcal{L}_\mathcal{F}}\eta_{\mu\nu}F^{\mu\alpha}F^{\nu\beta}\right)k_\alpha k_\beta = 0. \tag{A34}$$

Consequently, the effective metric tensor is given by

$$\bar{g}^{\alpha\beta} = \eta^{\alpha\beta} + \frac{4\mathcal{L}_{\mathcal{F}\mathcal{F}}}{\mathcal{L}_\mathcal{F}}\eta_{\mu\nu}F^{\mu\alpha}F^{\nu\beta}. \tag{A35}$$

Using antisymmetry of the electromagnetic field tensor $F^{\nu\beta} = -F^{\beta\nu}$ and contracting $\eta_{\mu\nu}F^{\beta\nu}$ results in

$$\bar{g}^{\alpha\beta} = \eta^{\alpha\beta} - \frac{4\mathcal{L}_{\mathcal{F}\mathcal{F}}}{\mathcal{L}_\mathcal{F}}F^\alpha{}_\mu F^{\mu\beta}, \tag{A36}$$

which is equivalent to Eq. (2.10). Thus the polarization vector

$$\epsilon^\mu = c_1 a^\mu \tag{A37}$$

corresponds to the photon polarization mode that moves on null geodesics in the effective geometry.

1. Examples

In what follows, we consider circular trajectories. As in Sec. V, we restrict our considerations to the equatorial plane without loss of generality, and thus the wave vector can be written as $k_\mu = (-\omega, 0, 0, k_\phi)$.

a. Magnetic solutions

For purely magnetic solutions [$Q_e = 0 \Rightarrow F_{tr} = 0$], the polarization vector that is null in the background geometry [Eq. (A29)] is given explicitly by

$$\begin{aligned}\epsilon^\mu = c_2{}^\star a^\mu &= \frac{c_2}{2}{}^\star F^{\mu\nu}k_\nu = \frac{c_2}{2}\epsilon^{\mu\nu\rho\sigma}F_{\rho\sigma}k_\nu \\ &= c_2\epsilon^{\mu\nu\theta\phi}F_{\theta\phi}k_\nu = (0, c_2\omega F_{\theta\phi}, 0, 0),\end{aligned} \tag{A38}$$

corresponding to a polarization in the radial direction and a propagation in the ϕ direction.

For the polarization vector that is null in the effective geometry [Eq. (A37)], we have

$$\begin{aligned}\bar{\epsilon}^\mu = c_1 a^\mu &= c_1 F^{\mu\nu}k_\nu = c_1 F^{\theta\phi}k_\phi \\ &= (0, 0, c_1 F^{\theta\phi}k_\phi, 0),\end{aligned} \tag{A39}$$

[12]Note that the coefficient c_3 does not contribute to the polarization as evident from Eq. (A25). This may also be seen from Eqs. (A5) and (A6): if $\epsilon^\mu \propto k^\mu$, then the polarization tensor $\epsilon_{\rho\sigma}$ and its corresponding field vanishes. Physically, this implies that the polarization vector is always perpendicular to the propagation direction. Hence no part of the polarization vector lies in the propagation direction and thus c_3 does not contribute.

corresponding to a polarization in the θ direction and a propagation in the ϕ direction.

b. Electric solutions

For purely electric solutions [$Q_m = 0 \Rightarrow F_{\theta\phi} = 0$], we find

$$\epsilon^\mu = \frac{c_2}{2}\varepsilon^{\mu\nu\rho\sigma}F_{\rho\sigma}k_\nu = c_2\varepsilon^{\mu\nu tr}F_{tr}k_\nu = (0,0,c_2F_{tr}k_\phi,0), \tag{A40}$$

and

$$\bar{\epsilon}^\mu = c_1F^{\mu\nu}k_\nu = (0,c_1\omega F^{tr},0,0), \tag{A41}$$

respectively.

APPENDIX B: SINGULARITY OF THE EFFECTIVE METRIC

The line element described by the covariant effective metric tensor components of Eqs. (3.6)–(3.8) is given by

$$ds^2 = -f_i(r)dt^2 + \frac{dr^2}{f_i(r)} + \frac{r^2}{\bar{h}_i(r)}d\Omega^2, \tag{B1}$$

where the subscript $i \in \{\mathcal{B},\mathcal{H},\mathcal{C}\}$ labels functions associated with the Bardeen [Eq. (4.2)], Hayward [Eq. (4.12)], and Cadoni *et al.* [Eq. (4.22)] model, respectively, and

$$\bar{h}_i(r) \coloneqq 1 + \frac{2\mathcal{F}\mathcal{L}_{\mathcal{F}\mathcal{F}}}{\mathcal{L}_{\mathcal{F}}}, \tag{B2}$$

with $\mathcal{L}(\mathcal{F})$ given by Eqs. (4.4), (4.14), and (4.24), respectively. Explicit evaluation yields [cf. Eqs. (4.9), (4.10), (4.19), (4.20), (4.29), and (4.30)]

$$\bar{h}_{\mathcal{B}}(r) = \frac{3}{2} - \frac{7\ell^2}{2(r^2+\ell^2)}, \tag{B3}$$

$$\bar{h}_{\mathcal{H}}(r) = 2 - \frac{9M\ell^2}{r^3+2M\ell^2}, \tag{B4}$$

$$\bar{h}_{\mathcal{C}}(r) = 1 - \frac{5\ell}{2(r+\ell)}. \tag{B5}$$

Based on these explicit expressions, the equation $\bar{h}_i(r) = 0$ admits real positive solutions for r, indicating a divergence of the effective metric tensor components $\bar{g}_{\theta\theta}$ and $\bar{g}_{\phi\phi}$. The existence of a curvature singularity may also be confirmed via examination of the Ricci (or Kretschmann) scalar corresponding to Eq. (B1), i.e.,

$$\bar{\mathcal{R}}_i(r) = \frac{2\bar{h}_i(2\bar{h}_i^2 + 2r^2f_i'\bar{h}_i' - r\bar{h}_i(4f_i' + rf_i''))}{2r^2\bar{h}_i^2} + \frac{f_i(4r\bar{h}_i(3\bar{h}_i' + r\bar{h}_i'') - 4\bar{h}_i^2 - 7r^2(\bar{h}_i')^2)}{2r^2\bar{h}_i^2}, \tag{B6}$$

where primes denote differentiation with respect to r and explicit dependencies of the functions $f_i(r)$ and $\bar{h}_i(r)$ on r have been omitted for the sake of simplicity. Evaluating Eq. (B6) for each of the three models yields

$$\bar{\mathcal{R}}_{\mathcal{B}}(r) = \frac{\mathcal{A}_{\mathcal{B}}(r)}{(r^2+\ell^2)^{7/2}(3r^3-4r\ell^2)^2}, \tag{B7}$$

$$\bar{\mathcal{R}}_{\mathcal{H}}(r) = \frac{\mathcal{A}_{\mathcal{H}}(r)}{2(r^3+2M\ell^2)^3(2r^4-5Mr\ell^2)^2}, \tag{B8}$$

$$\bar{\mathcal{R}}_{\mathcal{C}}(r) = \frac{\mathcal{A}_{\mathcal{C}}(r)}{2r^2(2r-3\ell)^2(r+\ell)^5}, \tag{B9}$$

which diverge at $r_{\mathcal{B}} = \frac{2\ell}{\sqrt{3}}$, $r_{\mathcal{H}} = (\frac{5}{2})^{1/3}M^{1/3}\ell^{2/3}$, and $r_{\mathcal{C}} = \frac{3\ell}{2}$, respectively, and the numerators are given explicitly by

$$\mathcal{A}_{\mathcal{B}}(r) = (r^2+\ell^2)^{3/2}(9r^8 - 69r^6\ell^2 - 268r^4\ell^4 - 384r^2\ell^6 - 96\ell^8) + 2M(57r^8\ell^2 + 250r^6\ell^4 + 336r^4\ell^6 + 192r^2\ell^8), \tag{B10}$$

$$\mathcal{A}_{\mathcal{H}}(r) = 16r^{15} + 8M(84M-43r)r^{11}\ell^2 + M^2(3726M-2879r)r^8\ell^4 + 2M^3(5040M-4517r)r^5\ell^6 + 80M^4(60M-137r)r^2\ell^8 - 2800M^5\ell^{10}, \tag{B11}$$

$$\mathcal{A}_{\mathcal{C}}(r) = \ell^2\Big(-5(r+\ell)^3(7r^2+30r\ell+18\ell^2) + 2Mr^2(71r^2+12r\ell+216\ell^2)\Big). \tag{B12}$$

[1] M. Born, Modified field equations with a finite radius of the electron, Nature (London) **132**, 282 (1933).
[2] M. Born and L. Infeld, Foundations of the new field theory, Proc. R. Soc. A **144**, 425 (1934).
[3] M. Born and L. Infeld, On the quantization of the new field equations I, Proc. R. Soc. A **147**, 522 (1934).
[4] W. Heisenberg and H. Euler, Folgerungen aus der Diracschen Theorie des Positrons, Z. Phys. **98**, 714 (1936).
[5] A. Peres, Nonlinear electrodynamics in general relativity, Phys. Rev. **122**, 273 (1961).
[6] E. S. Fradkin and A. A. Tseytlin, Non-linear electrodynamics from quantized strings, Phys. Lett. **163B**, 123 (1985).
[7] R. G. Leigh, Dirac-Born-Infeld action from Dirichlet σ-model, Mod. Phys. Lett. A **04**, 2767 (1989).
[8] A. A. Tseytlin, On non-Abelian generalisation of the Born-Infeld action in string theory, Nucl. Phys. **B501**, 41 (1997).
[9] C. G. Callan and J. M. Maldacena, Brane dynamics from the Born-Infeld action, Nucl. Phys. **B513**, 198 (1998).
[10] G. W. Gibbons, Born-Infeld particles and Dirichlet p-branes, Nucl. Phys. **B514**, 603 (1998).
[11] G. W. Gibbons and C. A. R. Herdeiro, Born-Infeld theory and stringy causality, Phys. Rev. D **63**, 064006 (2001).
[12] D. P. Sorokin, Introductory notes on nonlinear electrodynamics and its applications, Fortschr. Phys. **70**, 2200092 (2022).
[13] R. Pellicer and R. J. Torrence, Nonlinear electrodynamics and general relativity, J. Math. Phys. (N.Y.) **10**, 1718 (1969).
[14] K. A. Bronnikov, V. N. Melnikov, G. N. Shikin, and K. P. Staniukovich, Scalar, electromagnetic, and gravitational fields interaction: Particlelike solutions, Ann. Phys. (N.Y.) **118**, 84 (1979).
[15] E. Ayón-Beato and E. García, Regular black hole in general relativity coupled to nonlinear electrodynamics, Phys. Rev. Lett. **80**, 5056 (1998).
[16] E. Ayón-Beato and E. García, Non-singular charged black hole solution for non-linear source, Gen. Relativ. Gravit. **31**, 629 (1999).
[17] E. Ayón-Beato and E. García, New regular black hole solution from nonlinear electrodynamics, Phys. Lett. B **464**, 25 (1999).
[18] K. A. Bronnikov, Comment on "Regular black hole in general relativity coupled to nonlinear electrodynamics", Phys. Rev. Lett. **85**, 4641 (2000).
[19] K. A. Bronnikov, Regular magnetic black holes and monopoles from nonlinear electrodynamics, Phys. Rev. D **63**, 044005 (2001).
[20] A. Burinskii and S. R. Hildebrandt, New type of regular black holes and particlelike solutions from nonlinear electrodynamics, Phys. Rev. D **65**, 104017 (2002).
[21] I. Dymnikova, Regular electrically charged vacuum structures with de Sitter centre in nonlinear electrodynamics coupled to general relativity, Classical Quantum Gravity **21**, 4417 (2004).
[22] L. Balart and E. C. Vagenas, Regular black holes with a nonlinear electrodynamics source, Phys. Rev. D **90**, 124045 (2014).
[23] Z.-Y. Fan and X. Wang, Construction of regular black holes in general relativity, Phys. Rev. D **94**, 124027 (2016).
[24] K. A. Bronnikov, Comment on "Construction of regular black holes in general relativity", Phys. Rev. D **96**, 128501 (2017).
[25] B. Toshmatov, Z. Stuchlík, and B. Ahmedov, Comment on "Construction of regular black holes in general relativity", Phys. Rev. D **98**, 028501 (2018).
[26] K. A. Bronnikov, Regular black holes sourced by nonlinear electrodynamics, in *Regular Black Holes: Towards a New Paradigm of Gravitational Collapse* in edited by C. Bambi (Springer, Singapore, 2023).
[27] V. P. Frolov, Do black holes exist?, arXiv:1411.6981.
[28] V. Cardoso and P. Pani, Testing the nature of dark compact objects: A status report, Living Rev. Relativity **22**, 4 (2019).
[29] R. B. Mann, S. Murk, and D. R. Terno, Black holes and their horizons in semiclassical and modified theories of gravity, Int. J. Mod. Phys. D **31**, 2230015 (2022).
[30] S. Murk, Nomen non est omen: Why it is too soon to identify ultra-compact objects as black holes, Int. J. Mod. Phys. D **32**, 2342012 (2023).
[31] F. Lamy, E. Gourgoulhon, T. Paumard, and F. H. Vincent, Imaging a non-singular rotating black hole at the center of the Galaxy, Classical Quantum Gravity **35**, 115009 (2018).
[32] S. Vagnozzi *et al.*, Horizon-scale tests of gravity theories and fundamental physics from the Event Horizon Telescope image of Sagittarius A*, Classical Quantum Gravity **40**, 165007 (2023).
[33] R. Carballo-Rubio, H. Delaporte, A. Eichhorn, and A. Held, Disentangling photon rings beyond general relativity with future radio-telescope arrays, J. Cosmol. Astropart. Phys. 05 (2024) 103.
[34] I. H. Salazar, A. Garcia, and J. Plebanski, Duality rotations and type D solutions to Einstein equations with nonlinear electromagnetic sources, J. Math. Phys. (N.Y.) **28**, 2171 (1987).
[35] I. Dymnikova, Vacuum nonsingular black hole, Gen. Relativ. Gravit. **24**, 235 (1992).
[36] Z. Bialynicka-Birula and I. Bialynicki-Birula, Nonlinear effects in quantum electrodynamics. Photon propagation and photon splitting in an external field, Phys. Rev. D **2**, 2341 (1970).
[37] M. Novello, V. A. De Lorenci, J. M. Salim, and R. Klippert, Geometrical aspects of light propagation in nonlinear electrodynamics, Phys. Rev. D **61**, 045001 (2000).
[38] V. A. De Lorenci, R. Klippert, M. Novello, and J. M. Salim, Light propagation in non linear electrodynamics, Phys. Lett. B **482**, 134 (2000).
[39] J. M. Bardeen, Non-singular general relativistic gravitational collapse, in *Proceedings of the International Conference GR5* (Tbilisi University Press, Tbilisi, 1968).
[40] S. A. Hayward, Formation and evaporation of nonsingular black holes, Phys. Rev. Lett. **96**, 031103 (2006).
[41] M. Cadoni, M. De Laurentis, I. De Martino, R. Della Monica, M. Oi, and A. P. Sanna, Are nonsingular black holes with super-Planckian hair ruled out by S2 star data?, Phys. Rev. D **107**, 044038 (2023).
[42] S. Nojiri and G. G. L. Nashed, Hayward black hole in scalar-Einstein-Gauss-Bonnet gravity in four dimensions, Phys. Rev. D **108**, 024014 (2023).

[43] A. Ashtekar, J. Olmedo, and P. Singh, Regular black holes from loop quantum gravity, in *Regular Black Holes: Towards a New Paradigm of Gravitational Collapse* edited by C. Bambi (Springer, Singapore, 2023).
[44] P. Bueno, P. A. Cano, and R. A. Hennigar, Regular black holes from pure gravity, arXiv:2403.04827.
[45] E. Noether, Invariante Variationsprobleme, Nachr. König. Gesellsch. Wiss. Göttingen, Math.-Phys. Klasse **1918**, 235 (1918).
[46] P. V. P. Cunha, E. Berti, and C. A. R. Herdeiro, Light-ring stability for ultracompact objects, Phys. Rev. Lett. **119**, 251102 (2017).
[47] P. V. P. Cunha and C. A. R. Herdeiro, Stationary black holes and light rings, Phys. Rev. Lett. **124**, 181101 (2020).
[48] B. Hoffmann and L. Infeld, On the choice of the action function in the new field theory, Phys. Rev. **51**, 765 (1937).
[49] https://github.com/s-murk/2406.07957.
[50] Wolfram Research, Inc., *Mathematica*, Version 12.0, Champaign, IL (2019).
[51] R. Carballo-Rubio, F. Di Filippo, S. Liberati, and M. Visser, A connection between regular black holes and horizonless ultracompact stars, J. High Energy Phys. 08 (2023) 046.
[52] E. Franzin, S. Liberati, and V. Vellucci, From regular black holes to horizonless objects: Quasi-normal modes, instabilities and spectroscopy, J. Cosmol. Astropart. Phys. 01 (2024) 020.
[53] F. Di Filippo, On the nature of inner light-rings, arXiv:2404.07357.
[54] F. Simovic and I. Soranidis, Euclidean and Hamiltonian thermodynamics for regular black holes, Phys. Rev. D **109**, 044029 (2024).
[55] I. Soranidis, Euclidean methods and phase transitions for the strongest deformations compatible with Schwarzschild asymptotics, Phys. Rev. D **109**, 044041 (2024).
[56] C. Bambi, D. Malafarina, and L. Modesto, Non-singular quantum-inspired gravitational collapse, Phys. Rev. D **88**, 044009 (2013).
[57] D. Malafarina and B. Toshmatov, Connection between regular black holes in nonlinear electrodynamics and semi-classical dust collapse, Phys. Rev. D **105**, L121502 (2022).
[58] J. Barenboim, A. V. Frolov, and G. Kunstatter, No drama in 2D black hole evaporation, arXiv:2405.13373.
[59] S. W. Hawking, Black hole explosions?, Nature (London) **248**, 30 (1974).
[60] S. W. Hawking, Particle creation by black holes, Commun. Math. Phys. **43**, 199 (1975); **46**, 206(E) (1976).
[61] P. Binétruy, A. Helou, and F. Lamy, Closed trapping horizons without singularity, Phys. Rev. D **98**, 064058 (2018).
[62] V. Baccetti, R. B. Mann, S. Murk, and D. R. Terno, Energy-momentum tensor and metric near the Schwarzschild sphere, Phys. Rev. D **99**, 124014 (2019).
[63] S. Murk and D. R. Terno, Universal properties of the near-horizon geometry, Phys. Rev. D **103**, 064082 (2021).
[64] G. M. Shore, Faster than light photons in gravitational fields II: Dispersion and vacuum polarisation, Nucl. Phys. **B633**, 271 (2002).
[65] L. Brillouin, *Wave Propagation and Group Velocity*, Pure and Applied Physics: A Series of Monographs Vol. 8. (Academic Press, New York, London, 1960).
[66] V. Perlick, C. Lämmerzahl, and A. Macías, Effects of nonlinear vacuum electrodynamics on the polarization plane of light, Phys. Rev. D **98**, 105014 (2018).
[67] D. L. Burke *et al.*, Positron production in multiphoton light-by-light scattering, Phys. Rev. Lett. **79**, 1626 (1997).
[68] R. P. Mignani, V. Testa, D. González Caniulef, R. Taverna, R. Turolla, S. Zane, and K. Wu, Evidence for vacuum birefringence from the first optical-polarimetry measurement of the isolated neutron star RX J1856.5-3754, Mon. Not. R. Astron. Soc. **465**, 492 (2017).
[69] K. Isomura, R. Suzuki, and S. Tomizawa, Particle motions around regular black holes, Phys. Rev. D **107**, 084003 (2023).
[70] E. Guzman-Herrera and N. Breton, Light propagation in the vicinity of the ModMax black hole, J. Cosmol. Astropart. Phys. 01 (2024) 041.
[71] T. Hale, D. Kubizňák, and J. Menšíková, Optical properties of black holes in regularized Maxwell theory, Phys. Rev. D **109**, 084061 (2024).
[72] M. A. A. de Paula, H. C. D. Lima Junior, P. V. P. Cunha, and L. C. B. Crispino, Electrically charged regular black holes in nonlinear electrodynamics: Light rings, shadows, and gravitational lensing, Phys. Rev. D **108**, 084029 (2023).
[73] F. Simovic and D. R. Terno, Semi-classical imprints on quasinormal mode spectra, arXiv:2405.18631.
[74] T. Hale, D. Kubizňák, O. Svítek, and T. Tahamtan, Solutions and basic properties of regularized Maxwell theory, Phys. Rev. D **107**, 124031 (2023).
[75] D. Kubizňák, T. Tahamtan, and O. Svítek, Slowly rotating black holes in nonlinear electrodynamics, Phys. Rev. D **105**, 104064 (2022).
[76] S. Weinberg, *Gravitation and Cosmology: Principles and Applications of the General Theory of Relativity* (John Wiley and Sons Ltd., New York, 1972).

JOURNAL ARTICLE

Matter and forces near physical black holes

Brief summary

With the last paper, we concluded the first main part of the thesis. In all the previous papers, we did not consider the backreaction of quantum effects, such as Hawking radiation, on the spacetime geometry. This brings us to the second main part of the thesis, where we transition to a fully dynamic framework. We begin with this article because it provides a basic introduction to the self-consistent analysis that will be used in the following two papers (Refs. [5, 6]). Additionally, it introduces the concept of a PBH, which includes RBHs as a special case, and explores its dynamics through near-horizon expansions. We examine the nature of the EMT near the outer apparent horizon and analyze the trajectories of massive particles attempting to escape the trapped region.

Conventions

In this article, r_g is used to denote the outer apparent horizon of the PBH in (t, r) coordinates, while in advanced coordinates (v, r), we maintain the notation from Ref. [3] and use the symbol r_+. Although the inner horizon is not studied in this article, it is defined as $r_{in}(t)$ as a function of the Schwarzschild time t. We also emphasize that r_+ is defined as $2M(v)$ in this article. However, $M(v)$ does not represent the Komar mass of the spacetime, as it did in the first part of the thesis; rather, it is the Misner-Sharp mass evaluated at the outer apparent horizon.

Authorship statement

Contributed to the planning and writing of the article, interpretation of its results, proofreading and revisions. Created figures and performed various calculations for the manuscript. Principal contributor to Section III along with appendices A and B.

Matter and forces near physical black holes

Pravin K. Dahal,[*] Ioannis Soranidis,[†] and Daniel R. Terno[‡]

School of Mathematical and Physical Sciences, Macquarie University, Sydney, New South Wales 2109, Australia

(Received 5 October 2022; accepted 7 December 2022; published 30 December 2022)

We describe general features of formation and disappearance of regular spherically symmetric black holes in semiclassical gravity. The allowed models are critically dependent on the requirement that the resulting objects evolve in finite time according to a distant observer. Violation of the null energy condition is mandatory for this to happen, and we study the properties of the necessary energy-momentum tensor in the vicinity of the apparent horizon. In studies of the kinematics of massive test particles, it is found that the escape from a black hole is possible only on the ingoing trajectories when the particles are overtaken by the contracting outer apparent horizon. Tidal forces experienced by geodesic observers, infalling or escaping, are shown to be finite at the apparent horizon, although this is not true for nongeodesic trajectories.

DOI: 10.1103/PhysRevD.106.124048

I. INTRODUCTION

Black holes are particularly elegant solutions of the Einstein equations. They introduce nontrivial causal structure into spacetime [1–4]. About 100 ultracompact objects are identified as astrophysical black holes [5]. Black holes are domains of strong gravity, arguably the ones that are most accessible to observation. They may exemplify the conceptual tension between quantum mechanics and general relativity. They also may provide some clues about quantum gravity. Given all these different roles, it is still unclear if they are played by the one and the same actor. In fact, the variety of definitions of black holes matches this diversity of the roles [6].

It is useful to adapt the terminology of Ref. [7] that distinguished between the mathematical and physical black holes. A mathematical black hole is a solution of the Einstein equations of classical general relativity. It is the source of our ideas about what are the typical black hole features. The most well known of them is the event horizon, which for the Schwarzschild black hole is located at the gravitational radius $r_g = 2GM/c^2$. It separates an interior spacetime containing a singularity from the outside observers.

All current observational data can be explained within this paradigm. However, an event horizon is a global teleological construct and is not accessible to local observers [8,9]. On the other hand, a trapped spacetime region from which currently nothing, not even light, can escape—a crucial black hole property—constitutes what one would reasonably regard as a physical black hole (PBH). A trapped region is a domain where both ingoing and outgoing future-directed null geodesics emanating from a spacelike two-dimensional surface with spherical topology have negative expansion [1,10]. The apparent horizon is the outer boundary of the trapped region (here and elsewhere, we use the same name for both the 2D entity on a particular time slice and its 3D development; Ref. [11] collects various relevant definitions).

It turns out that a careful analysis of the consequences of this definition, together with two natural assumptions (that we describe below in Sec. II), provide a strong constraint on the near-horizon behavior of the possible models [11]. In this work, we extend the previous results to identify several black hole properties that are important both for resolving conceptual issues and for modeling ultracompact objects.

We assume the validity of semiclassical gravity. That means we use classical notions such as horizons and consider test particles with well-defined trajectories. The semiclassical Einstein equations

$$G_{\mu\nu} := R_{\mu\nu} - \frac{1}{2} g_{\mu\nu} R = \langle \hat{T}_{\mu\nu} \rangle_\omega =: T_{\mu\nu} \tag{1}$$

describe the dynamics. Here the standard left-hand side is equated to the expectation value of the renormalized energy-momentum tensor (EMT). The latter represents both the collapsing matter and the created excitations of the quantum fields.

Apart from assuming the validity of the semiclassical gravity, we make two further assumptions [11]. First, we assume the weakest form of the cosmic censorship conjecture. Usually, it is a statement that event horizons obscure spacetime singularities. Here we assume only that

[*]pravin-kumar.dahal@hdr.mq.edu.au
[†]ioannis.soranidis@hdr.mq.edu.au
[‡]daniel.terno@mq.edu.au

all curvature scalars that are built from polynomials of components of the Riemann tensor are finite in some neighborhood of the apparent horizon [12].

Second, we assume that the trapped region forms at a finite time of a distant observer (which we refer to as Bob) [12]. This is the only possible interpretation of regular black holes—transient trapped regions without the event horizon and singularity. Formulation of the information loss problems requires both the Hawking radiation and the transient event horizon. Existence of the latter implies that the apparent horizon forms in finite time of Bob as well [13].

The resulting analysis is based on self-consistency [11,12]. We study the semiclassical properties of the near-horizon geometry that follow from its existence that is subject to the two above assumptions. In particular, no global aspects of the spacetime structure, nature of the state ω or presence of the Hawking radiation are assumed. We restrict the discussion to spherical symmetry. Because of its simplifying assumptions, the self-consistent approach results in a nearly complete description of the near-horizon geometry and physics.

The rest of this paper is organized as follows. First, we review the properties of PBHs in Sec. II. We also present the necessary conditions that any model of a regular black hole should satisfy. We discuss the classification of the EMT in Sec. III. In Sec. IV we present some peculiar aspects of escaping massive test particles from a black hole. We consider the tidal forces experienced by an observer (Alice) in the vicinity of the apparent horizon in Sec. V.

We use the $(-+++)$ signature of the metric and work in units where $\hbar = c = G = 1$. Derivatives of a function of a single variable are marked with a prime: $r_g'(t) \equiv dr_g/dt$, $r_+'(v) \equiv dr_+/dv$, etc. Derivatives with respect to the proper time τ or the affine parameter λ are denoted by the dot: $\dot{r} = dr/d\tau$. We refer to a distant stationary observer as Bob and a traveling observer in the vicinity of the apparent horizon as Alice.

II. PHYSICAL BLACK HOLES

The self-consistent approach is best illustrated by the example of regular black holes (RBHs). Figure 1(a) is a sketch of a generic regular black hole, and Fig. 1(b)

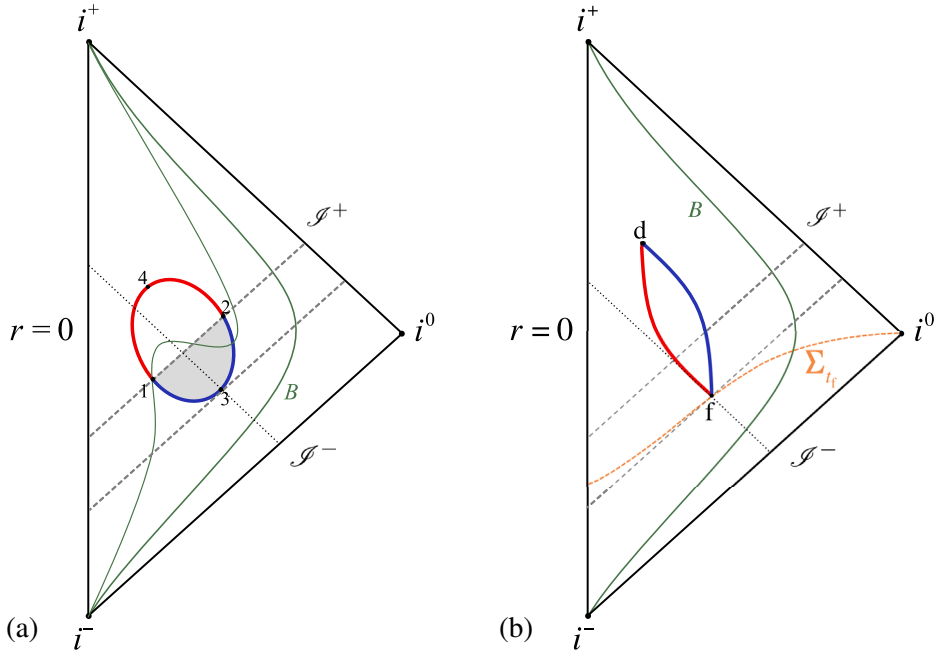

FIG. 1. Schematic Carter-Penrose diagram for depicting formation and evaporation of a conventional RBH (a) and a RBH that is treated as a PBH (b). The trajectory of a distant observer, Bob, is indicated in green and marked by the initial B. The dashed gray lines correspond to outgoing radial null geodesics that reach the future null infinity $\mathcal{I}^+$, and the dotted lines represent the ingoing radial null geodesics. The asymptotic structure of a simple RBH spacetime coincides with that of Minkowski spacetime. An immediate neighborhood of $r = 0$ never belongs to the trapped region. (a) The outer (132, dark blue) and inner (142, dark red) apparent horizons are indicated according to the invariant definition of Eq. (18). These also correspond to the largest and the smallest roots of $f(v, r) = 0$. This RBH has smoothly joined inner and outer horizons [14,15]. The quantum ergosphere is indicated by the light gray shading. One of the hypersurfaces $r = \text{const}$ is shown as a curved line that connects i^- and i^+ and goes through the trapped region. The null energy condition (NEC) is satisfied along the segment (413). The segments (14) and (23) are timelike. (b) RBH treated as PBH with the outer (dark blue) and inner (dark red) apparent horizons. The points f and d represent the events of formation and disappearance of the trapped region. The equal time hypersurface Σ_{t_f} is shown as a dashed orange line connecting $r = 0$ and i^0. The outer and the inner horizons are timelike (membranes).

illustrates the features that necessarily arise when this putative object is treated as a physical black hole.

A general spherically symmetric metric in Schwarzschild coordinates is given by [1,10]

$$ds^2 = -e^{2h(t,r)}f(t,r)dt^2 + f(t,r)^{-1}dr^2 + r^2 d\Omega_2, \quad (2)$$

where r is the circumferential radius and $d\Omega_2$ is the area element on a unit two-sphere. These coordinates provide geometrically preferred foliations with respect to Kodama time [10]. Some of the derivations become more transparent when they are expressed in radiative coordinates. Using the advanced null coordinate v, the metric is written as

$$ds^2 = -e^{2h_+}f(v,r)dv^2 + 2e^{h_+}dvdr + r^2 d\Omega_2. \quad (3)$$

The Misner-Sharp (MS) mass $C(t,r)/2 \equiv M(t,r)$ is invariantly defined [10,16] via

$$\partial_\mu r \partial^\mu r := f(t,r) =: 1 - C/r, \quad (4)$$

and thus $C(t,r) \equiv C_+(v(t,r),r)$. The functions $h(t,r)$ and $h_+(v,r)$ play the role of integrating factors in coordinate transformations [11], such as

$$dt = e^{-h}(e^{h_+}dv - f^{-1}dr). \quad (5)$$

For the Schwarzschild metric $C = 2M = \text{const}$ and $h \equiv 0$, while the coordinate v becomes the ingoing Eddington-Finkelstein coordinate.

The trapped region corresponds to the spacetime domain $f \leq 0$. The Schwarzschild radius $r_g(t)$ is the largest root of $f(t,r) = 0$. Because of the invariance of C, it is invariant in the sense that $r_g(t) \equiv r_+(v(t,r_g))$. Hence the outer apparent horizon is located at the Schwarzschild radius r_g [10,16], justifying the definition of the black hole mass as $2M(v) = r_+(v)$. Despite the fact that the apparent horizon is observer dependent in general, in spherically symmetric spacetimes, it is invariantly defined in all foliations that respect this symmetry [16].

It is convenient to introduce the effective EMT components

$$\tau_t := e^{-2h}T_{tt}, \qquad \tau^r := T^{rr}, \qquad \tau_t^r := e^{-h}T_t^r. \quad (6)$$

In spherical symmetry, the three Einstein equations (for the components G_{tt}, G_t^r, and G^{rr}) are

$$\partial_r C = 8\pi r^2 \tau_t / f, \quad (7)$$

$$\partial_t C = 8\pi r^2 e^h \tau_t^r, \quad (8)$$

$$\partial_r h = 4\pi r(\tau_t + \tau^r)/f^2. \quad (9)$$

Relationships between the EMT components in the (t,r) and the (v,r) coordinates and the corresponding forms of the Einstein equations are given in Appendix A 1. We use the singular nature of the Schwarzschild coordinates at the apparent horizon to extract information about the EMT. To ensure the finite values of the curvature scalars, it is sufficient to work with

$$\mathrm{T} := (\tau^r - \tau_t)/f, \qquad \mathfrak{T} := ((\tau^r)^2 + (\tau_t)^2 - 2(\tau_t^r)^2)/f^2, \quad (10)$$

where the contribution of $T_\theta^\theta \equiv T_\phi^\phi$ is disregarded, and then to verify that the resulting metric functions do not introduce further divergences [11].

Thus, the three effective EMT components either diverge, converge to finite limits, or converge to zero in such a way that the above combinations are finite. One option is the scaling

$$\tau_t \sim f^{k_E}, \qquad \tau^r \sim f^{k_P}, \qquad \tau_t^r \sim f^{k_\Phi}, \quad (11)$$

for some powers $k_a > 1$, $a = E, P, \Phi$. Another involves convergence or divergence with the same $k \leq 1$. For PBHs, only solutions with $k = 0$, 1 are relevant.

The $k = 0$ solution leads to the leading terms of the metric functions

$$C = r_g - 4\sqrt{\pi} r_g^{3/2} \Upsilon \sqrt{x} + \mathcal{O}(x), \quad (12)$$

$$h = -\frac{1}{2}\ln\frac{x}{\xi} + \mathcal{O}(\sqrt{x}), \quad (13)$$

where $\xi(t)$ is determined by choice of the time variable, and the higher-order terms are matched with the higher-order terms in the EMT expansion [11,17]. The consistency condition that is given by the Einstein equation (8) results in the relationship

$$r_g'/\sqrt{\xi} = 4\epsilon_\pm \sqrt{\pi r_g}\Upsilon, \quad (14)$$

where $\epsilon_\pm = \pm 1$ corresponds to the expansion and contraction of the Schwarzschild sphere, respectively. The contracting Schwarzschild sphere that allows for a regular description in the (v,r) coordinates corresponds to a black hole of diminishing mass. The case $r_g' > 0$ allows for a regular description in the (u,r) coordinates, where u is the retarded null coordinate and corresponds to an expanding white hole. In the (v,r) coordinates, the black hole metric is described by

$$C_+(v,r) = r_+(v) + w_1(v)y + \mathcal{O}(y^2), \quad (15)$$

$$h_+(v,r) = \chi_1(v)y + \mathcal{O}(y^2), \tag{16}$$

where we used the freedom of redefining the v coordinate to set $h_+(v,r_+) \equiv 0$ and $w_1 \leq 1$ and $\chi_1(v)$ are some functions. The condition $w_1 \leq 1$ is due to the definition of the Schwarzschild radius, and as we see below, this inequality is strict for the bulk of the black hole evolution. Some relationships with the quantities in the (t,r) coordinates are summarized in Appendix A 2, and more details are given in Ref. [11].

Two features of this solution are to be noted: the Schwarzschild radius is a timelike hypersurface in both cases, while the NEC is violated in its vicinity. We discuss the latter issue more in Sec. III. Analysis of the EMT and the metric around the smaller root $r_{\rm in}(t)$ of $f(t,r) = 0$ leads to similar expressions. The inner horizon is also a timelike hypersurface, but the NEC is satisfied in its vicinity.

The $k = 1$ solutions play a role in describing the formation of a physical black hole. The detailed properties of these solutions can be found in [11,18]. Here we stress the features that are needed for the understanding of Fig. 1(b).

Let the first marginally trapped surface be denoted by $r_g(t_{\rm f})$. In (v,r) coordinates, it appears at some $v_{\rm f}$ at the circumferential radius $r_+(v_{\rm f})$ that corresponds to Bob's $(t_{\rm f}, r_g(t_{\rm f}) = r_+)$. For $v \leq v_{\rm f}$, the MS mass can be expanded as

$$C(v,r) = \Delta(v) + r_*(v) + \sum_{i\geq 1} w_i(v)(r - r_*)^i, \tag{17}$$

where $r_*(v)$ corresponds to the maximum of $\mathbb{D}_v(r) \coloneqq C(v,r) - r$, and the deficit function $\Delta(v) \coloneqq \mathbb{D}_v(r_*)$. At the advanced time $v_{\rm f}$ the location of the maximum corresponds to the first marginally trapped surface $r_*(v_{\rm f}) = r_+(v_{\rm f})$ and $\Delta(v_{\rm f}) = 0$. For $v \geq v_{\rm f}$, the MS mass $\Delta(v) \equiv 0$.

For $v \leq v_{\rm f}$, we have $w_1(v) - 1 \equiv 0$ since the (local) maximum of $\mathbb{D}_v$ is determined by $d\mathbb{D}_v/dr = 0$. For $v > v_{\rm f}$ evaporation means $r'_+(v_{\rm f}) \leq 0$. Since the trapped region is of finite size for $v > v_{\rm f}$, the maximum of $C(v,r)$ does not coincide with $r_+(v)$. As a result, $w_1(v) < 1$ for $v > v_{\rm f}$. The NEC is violated in some vicinity of the apparent horizon, but not at $r = r_g(t_{\rm f})$ itself, allowing a consistent matching of the NEC-violating and the NEC-satisfying regions.

The self-consistent approach on its own cannot predict the final state of the collapsing matter. If the ultracompact object in question is a regular black hole, then there is also the final event, named the disappearance of the trapped region $(v_{\rm d}, r_{\rm d})$ for which $w_1(v_{\rm d}) = 1$. As both the inner and outer horizon components are timelike, their intersection (or intersections) cannot join smoothly in any coordinate system, providing the coordinate-independent characterization of these events.

We can now present several important features of PBHs, particularly their application to modeling regular black holes. Recall that, in spherical symmetry, the apparent horizon (and thus the notion of a trapped region) are coordinate independent in all foliations that respect this symmetry. A general coordinate-independent notion of the (future) outer and inner horizons is introduced via the condition on Lie derivatives of the expansion of the outgoing null geodesics [19]. If $\vartheta_{(l)}$ and $\vartheta_{(n)}$ are the expansions of the future-directed outgoing and ingoing null geodesic congruences, respectively, then $\theta_{(l)} = 0$ defines the apparent horizon. Its components are the outer (trapping) horizon that satisfies

$$\mathcal{L}_n \vartheta_{(l)} = n^\mu \partial_\mu \vartheta_{(l)} < 0, \tag{18}$$

and the inner (trapping) horizon that satisfies

$$\mathcal{L}_n \vartheta_{(l)} > 0. \tag{19}$$

A generic representation of a RBH in Fig. 1(a) is distinct from the PBH-based models in several important respects. The outer horizon as defined invariantly via Eq. (18) coincides with the larger root of $f(v,r) = 0$. However, the NEC is violated only along section (32) and section (24) of the inner horizon. The roots of $f(u,r) = 0$ do not agree with the invariant definition. The inner and the outer horizon segments join smoothly, and this is effected by having spacelike segments of both. This smooth joining prevents the identification of invariant events of formation and collapse (or evaporation) of the trapped region. This makes such models unsuitable for representing RBHs that, among other things, have a finite lifetime according to a distant observer.

Hypersurfaces of constant r are timelike outside the trapped region and spacelike inside, while the opposite is true for hypersurfaces of constant t. We illustrate these transitions on the hypersurfaces Σ_t. A hypersurface can be defined by restricting the coordinates via $\Psi(\Sigma_{t_0}) =: t - t_0 \equiv 0$. Then $\mathfrak{l}_\mu \coloneqq \Psi_{,\mu}$ is the normal vector field [4], which is timelike for a spacelike segment of the hypersurface and spacelike for a timelike segment. Using $\Psi_{,\mu}$, one can define a normalized vector field that points in the direction of increasing Ψ.

Using either (t,r) or (v,r) coordinates, we find that [20]

$$\mathfrak{l}_\mu \mathfrak{l}^\mu = -e^{-2h} f^{-1}. \tag{20}$$

As $r \to r_g$ (and similarly at the inner apparent horizon), $\mathfrak{l}^2 \to 0$. Thus, along Σ_{t_0} that passes through a PBH, the normal field changes continuously. Moreover [20], at $(t, r_g(t))$, the vector $\mathfrak{l}^\mu$ is proportional to l^μ of Eq. (A7). Figure 1(b) shows the hypersurface $\Sigma_{t_{\rm f}}$ that corresponds to the formation time of the trapped region, according to Bob. It is spacelike everywhere apart from $(t_{\rm f}, r_g(t_{\rm f}))$ where it is null.

An ostensibly innocent requirement of finite formation time, according to Bob, has far-reaching consequences. In this case, both $r_g(t)$ and $r_{\rm in}(t)$ are timelike; they correspond to the invariant definitions of the outer and inner horizons, as we now show.

A direct calculation shows that the inner and outer horizons [defined as the roots of $f(v,r)=0$, $r_{<+}(v)$ and $r_+(v)$, respectively], correspond to the invariant definition of Eq. (18). The lines of constant u intersect each of these two segments only once. If we parametrize a future-directed outgoing radial null geodesic as $(v(\lambda), r(\lambda), 0, 0)$, then

$$\frac{dr}{dv}=\frac{1}{2}e^{h_+(v,r)}f(v,r). \tag{21}$$

Let us assume that this geodesic intersects $r_+(v)$ twice, corresponding to the values of the affine parameter $\lambda_1<\lambda_2$. Then,

$$v_1=v(\lambda_1), \qquad r_+(v_1)=r(\lambda_1)=:r_1, \tag{22}$$

$$v_2=v(\lambda_2), \qquad r_+(v_2)=r(\lambda_2)=:r_2, \tag{23}$$

and $v_1<v_2$, while $r_1>r_2$ [as $r'_+(v)<0$]. Hence, Eq. (21) requires the outgoing null geodesic to pass through the trapped region $f<0$ for the values of the affine parameter $\lambda_1<\lambda<\lambda_2$. However, at the apparent horizon $dr/dv|_{r_+}=0$, making it impossible for the geodesic to enter the contracting trapped region, at least for some $\lambda>\lambda_1$.

As both the inner and the outer components of the apparent horizon are nonspacelike, they do not join smoothly, and the invariance of this taxonomy allows one to introduce well-defined events of formation and disappearance of the trapped region.

III. EMT NEAR THE APPARENT HORIZON

In spherical symmetry $T^\theta_\theta\equiv T^\varphi_\varphi$, and the most general form of the EMT [1,11] in an orthonormal basis attached to a fiducial static observer is given by

$$T_{\hat\mu\hat\nu}=\begin{pmatrix}\rho & \psi & 0 & 0\\ \psi & p & 0 & 0\\ 0 & 0 & \mathfrak{p} & 0\\ 0 & 0 & 0 & \mathfrak{p}\end{pmatrix}, \tag{24}$$

where ρ, p, ψ, and $\mathfrak{p}$ are functions of t and r. For $k=0$ solutions, components in the (tr) block are sums of the divergent

$$q=-\frac{\Upsilon}{4\sqrt{\pi r_g x}} \tag{25}$$

and additional finite terms μ_i that depend on the higher-order coefficients,

$$\rho=q+\mu_1, \qquad p=q+\mu_3, \qquad \psi=q+\mu_2. \tag{26}$$

Classification of the EMT according to the Segre-Hawking-Ellis scheme [1,21] is based on the properties of the Lorentz-invariant eigenvalues of $T_{\hat\mu\hat\nu}$. Among the classes I–IV, the known classical matter distributions correspond to classes I and II. Type IV is considered to be the most exotic, as two of its Lorentz-invariant eigenvalues are complex conjugates. Calculations with fields that propagate on a given background are of type IV for [22–24] $r\le 1.39r_g$. However, once backreaction is included, in many interesting scenarios, the more exotic forms of the EMT (types III and IV) are excluded [25].

The two nontrivial Lorentz-invariant eigenvalues of the EMT of Eq. (24) are given by

$$\mathfrak{t}_{1,2}=\frac{1}{2}(\mu_3-\mu_1\pm\sqrt{(\mu_1-2\mu_2+\mu_3)(\mu_1+2\mu_2+\mu_3+q)}). \tag{27}$$

The direct calculation (see Appendix A 2 for details), shows that the classification at $r=r_g=r_+$ depends on the sign of

$$(\mu_1-2\mu_2+\mu_3)q\propto-\theta^+_r, \tag{28}$$

i.e., it is determined by the sign of $\Theta_{rr}(v,r_+)=e^{h_+}\Theta^v_r$ there.

The EMT is type II at r_+ only if the metric is sufficiently close to Vaidya, i.e., $\mu_1-2\mu_2+\mu_3=0$.

IV. EXITING THE BLACK HOLE

The timelike nature of the retreating outer apparent horizon of a physical black hole allows for the escape of test particles from it. Outgoing null geodesics of Fig. 1 reach the future null infinity by crossing the outer apparent horizon. An analysis of Sec. II shows that the entire regular black hole is indeed the quantum ergosphere. Null geodesics on the Vaidya background can be reduced to a system of the first-order equations, and for a linear case $C(v)=r_0-\alpha v$, it allows an analytic solution [26,27]. Appendix B 2 uses the methods of Ref. [27] to describe trajectories that start inside the trapped region.

We should note that inside the trapped region $f<0$ distinction between the two families of the future-directed radial null geodesics as "ingoing" and "outgoing" is not determined by their local properties and, depending on the global spacetime structure, may be purely conventional. For a mathematical black hole, the curves $v=$ const, as well as the outgoing null geodesics that originate inside it, reach the singularity. For a RBH of Fig. 1(b), they cross the

inner apparent horizon and reach $r = 0$, while the outgoing geodesics cross the outer apparent horizon and reach the null infinity.

The motion of timelike test particles is more intricate. To simplify the exposition, we describe the near-horizon geometry by the Vaidya metric with $r'_+(v) < 0$. The ingoing and outgoing families inside the trapped region satisfy the timelike condition

$$-f\dot{v}^2 + 2\dot{v}\,\dot{r} = -1, \tag{29}$$

implying that the components of the four-velocity are related by

$$\dot{v} = \frac{\dot{r} \pm \sqrt{\dot{r}^2 + f}}{f}, \tag{30}$$

respectively, and are identified by their null limits for $|\dot{r}| \to \infty$. It is known [28] that the contracting outer apparent horizon can overtake the test particle, releasing it (temporarily or permanently) from the black hole. Using the Vaidya metric as an example, we highlight another property: in contrast with the null case, the outgoing timelike geodesics cannot reach the apparent horizon. Beyond some value of the proper time τ_*, $r(\tau_*) < r_+(v(\tau_*))$ [that is implicitly characterized by $\dot{v} = 1/\sqrt{-f(v,r)}$] the integral curves of the geodesic equation can be continued only by the ingoing geodesics.

The geodesic equations for the radial timelike geodesics take the form,

$$\ddot{r} = -\frac{r_+}{2r^2} - \frac{r'_+}{2r}\dot{v}^2, \tag{31}$$

$$\ddot{v} = -\frac{r_+}{2r^2}\dot{v}^2, \tag{32}$$

and the first term on the right-hand side of Eq. (31) is absent for null geodesics. (Equations of motion for a general metric are given in Appendix B 1.)

We now consider a simple model to illustrate some of the properties of the outgoing trajectories. The model we are going to use is that of the linearly evaporating Vaidya black hole. We study a massive particle starting its motion from the black hole's interior and following an outgoing geodesic. As we can see from Fig. 2(a), the particle can exit the PBH, but the gravitational attraction is enough to force it back inside. This behavior is heavily dependent on the initial conditions of its motion. Some initial conditions allow particles to escape forever and reach future null infinity, others force a reentry, as shown in Fig. 2(a), while other particles will never escape and head toward the center. In all of these motions, it is important to take into account Eq. (30), which implies that inside the PBH $\dot{r} \leq -\sqrt{-f(v,r)}$. As illustrated in Fig. 2(b), the outgoing geodesic approaches this value until $\dot{r}^2 = -f$ and then becomes the ingoing geodesic. So a particle can only exit the PBH following an ingoing geodesic and not an outgoing one. This behavior can be revealed by the following simple steps.

We first note that according to Eq. (32) $\dot{v}$ is a decreasing function of τ and thus $\dot{v}(\tau_1) > \dot{v}(\tau_2)$ for $\tau_2 > \tau_1$. On the other hand, as both $\dot{r}$ and f are negative inside the trapped region, for the outgoing geodesics, the inequality

$$\dot{v} = \frac{\dot{r}\beta}{f} \geq \frac{1}{\sqrt{-f}}, \qquad 1 \leq \beta < 2, \tag{33}$$

must hold. The minimum value of $\beta = 1$ corresponds to the point where $\dot{r} = -\sqrt{-f}$.

Thus, the outgoing geodesics [that starts at some $r(0) < r_+(0)$ with some finite value of $\dot{v}(0)$], cannot exit through r_+, as in this case $f(v, r = r_+) = 0$ implies the divergence

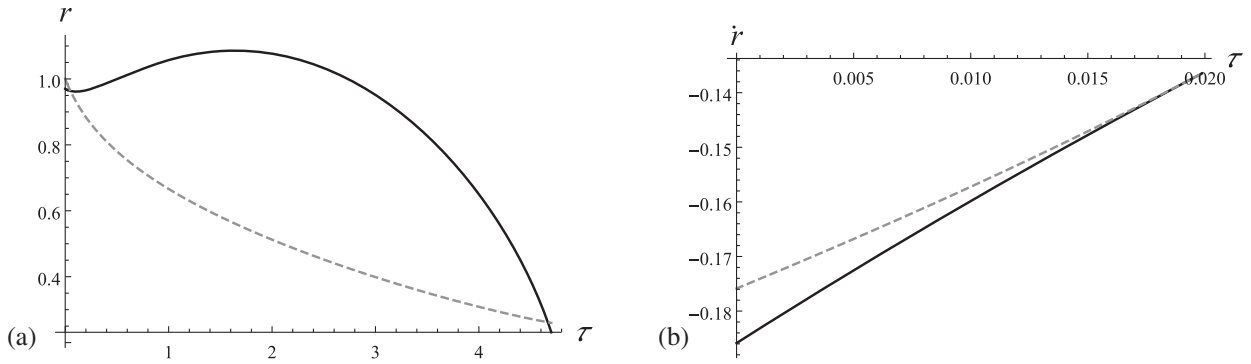

FIG. 2. Exit of a massive test particle from the Vaidya black hole (with the subsequent reentry). Both figures are based on the linear evaporation law $r_+(v) = r_+(0) - \alpha v$ with $r_+(0) = 1$ and $\alpha = 0.1$ The initial conditions are $v(0) = 0$, $r(0) = 0.9$, and $\dot{r}(0) = -\sqrt{-f(0, r(0))} - 0.01 = -0.18586$. (a) Trajectory from the initial moment until the reentry. The areal radius $r(\tau)$ (black line) and the (outer) apparent horizon $r_+(v(\tau))$ (gray dashed line) are shown as functions of the proper time τ. (b) The first segment of the trajectory until the "reversal" (the geodesic switches from being outgoing to ingoing). The areal radius derivative $\dot{r}$ is shown as a solid line and the limiting value $-\sqrt{-f(v(\tau), r(\tau))}$ as a dashed gray line.

of $\dot{v}$ via Eq. (33). However, as it is a decreasing function according to Eq. (32), such occurrence is impossible, and there should be a value τ_* where the geodesic changes from being outgoing to being ingoing. It occurs continuously at the point where

$$\dot{r}(\tau_*) = -\sqrt{-f(v(\tau_*), r(\tau_*))}, \tag{34}$$

and $\dot{v} = 1/\sqrt{-f}$.

V. TIDAL FORCES

Curvature scalars are finite by construction at the apparent horizon of a PBH. However, the absence of these singularities (so-called parallel propagated singularities) does not rule out a weaker form of singular behavior. In fact, the apparent horizon is a weakly singular surface [11,20]. For example, it is possible to find a null tetrad where one of the Ricci spinors Φ_{00} or Φ_{22} diverge. The energy density is finite from the point of view of an infalling observer, geodesic or not, so long as $\dot{r} < 0$. On the other hand, the energy density diverges in the proper frame of an outgoing test particle on a nongeodesic trajectory that approaches the outer apparent horizon.

Consider a trajectory $x^\mu_{\rm A}(\tau)$ that is implicitly given for its entire duration inside the black hole by Eq. (34). Curiously enough, the geodesic equation (31) is satisfied, even if Eq. (32) is not. In this case, close to the apparent horizon, the energy density is

$$\rho_{\rm A} = T_{\mu\nu}\dot{x}^\mu_{\rm A}\dot{x}^\nu_{\rm A} \approx \frac{r'_+}{8\pi r_+|y|}, \tag{35}$$

where $y = r - r_+$. It diverges, but the integrated energy density remains finite. The divergence has an intuitive explanation if one notes that the square of the four-acceleration diverges as $r \to r_+$.

Divergent tidal forces are one of the hallmarks of spacetime singularities. It is a standard textbook result [2] that the tidal forces on an infalling Alice at the horizon of a Schwarzschild black hole are large but finite. Falling through the apparent horizon of the Vaidya black hole is qualitatively similar. Indeed, using the geodesic deviation equation to determine the three components of acceleration in the proper frame of Alice with $\dot{r} = 1$ at the apparent horizon (see Appendix C for the detailed description of the frame),

$$\frac{D^2\zeta^{(j)}}{d\tau} = -R_{(\tau)(j)(\tau)(k)}\zeta^{(k)}, \tag{36}$$

where $j, k = \rho, \theta, \phi$, the three nonzero curvature terms are

$$R_{(\tau)(\rho)(\tau)(\rho)} = -\frac{r_+(v)}{r^3} = -\frac{1}{r_+^2} + \mathcal{O}(y), \tag{37}$$

$$R_{(\tau)(\theta)(\tau)(\theta)} = \frac{1}{2r_+^2}\left(1 + \frac{r'_+}{4}\right) + \mathcal{O}(y), \tag{38}$$

where $y = r - r_+$ and $R_{(\tau)(\phi)(\tau)(\phi)} = R_{(\tau)(\theta)(\tau)(\theta)}$. Thus, evaporation produces just corrections that are proportional to the evaporation rate to the tidal force experienced by the infalling Alice.

The result is the same if the retreating apparent horizon overtakes the infalling particle inside the RBH. The situation is different for a nongeodesic outgoing particle. Consider again the trajectory that is implicitly given for its entire duration inside the black hole by Eq. (34). Then the two nonradial tidal force components diverge as

$$R_{(\tau)(\theta)(\tau)(\theta)} = -\frac{r'_+}{2r_+ y} + \mathcal{O}(y^0). \tag{39}$$

VI. DISCUSSION

We studied the properties a spherically symmetric PBH must have in the context of semiclassical gravity. An ostensibly innocent requirement of finite formation time, according to Bob, has far-reaching consequences. The NEC must be violated in the vicinity of the outer apparent horizon, but it is satisfied in the vicinity of the inner horizon. We have well defined events of formation and disappearance of the trapped region because both horizons are timelike (Fig. 1). The EMT classification, according to the Segre-Hawking-Ellis scheme on the apparent horizon, is of type I, under certain assumptions, consistent with what is believed to happen when backreaction is included.

In contrast with the Schwarzschild solution, both massless and massive particles inside the quantum ergosphere of a PBH are able to escape the trapped region. For massless particles, this is evident from the timelike character of the outer apparent horizon. A careful analysis of massive particles' trajectories, using the Vaidya limit as an example, shows that they can only escape when following ingoing geodesic trajectories. We calculated the tidal forces experienced by observers, in general, for objects of finite size. For infalling geodesic observers, the tidal forces are finite. This is also the case for observers inside the quantum ergosphere, since they can only cross the outer apparent horizon when following an ingoing geodesic and letting the receding horizon overtake them. This is not the case for nongeodesic observers who experience infinite tidal forces when they try to force themselves out of the trapped region. Furthermore, nongeodesic observers experience infinite negative energy density in the form of a firewall [20] when they try to escape the trapped region, something that does not happen for geodesic observers. Despite the fact that the apparent horizon is assumed to be regular in the sense of finite curvature scalars, all these properties indicate

that it possesses a mildly singular nature, manifesting itself as infinite tidal forces and firewalls for specific observers.

Astrophysical black holes are rotating, and study of general axially symmetric PBHs is subject of our future research. However, a special case of the Kerr-Vaidya metric illustrates that the violation of the NEC and a mild firewall are not artifacts of spherical symmetry [29]. In the Kerr-Vaidya geometry, which is of Petrov-II, the NEC is always violated due to the type III EMT (based on the Segre-Hawking-Ellis classification [1,21]) on the apparent horizon. Moreover, in the equatorial plane of the Kerr-Vaidya metric there are radial geodesics whose equations of motion are the same as those of their counterparts in the Vaidya metric. Thus, while we expect that the axial symmetry introduces more complicated scenarios of motion of test particles, they also include the results that were described above.

ACKNOWLEDGMENTS

Useful discussions with Eleni Kontou, Sebastian Murk, Joe Schindler, and Justin Tzou are gratefully acknowledged. P. K. D. and I. S. are supported by an International Macquarie University Research Excellence Scholarship. The work of D. R. T. is supported by the ARC Discovery project Grant No. DP210101279.

APPENDIX A: SUMMARY OF USEFUL RELATIONS

1. Einstein equations and basic definitions

A useful relationship between the EMT components in (t, r) and (v, r) coordinates is given by

$$\theta_v \coloneqq e^{-2h_+}\Theta_{vv} = \tau_t, \tag{A1}$$

$$\theta_{vr} \coloneqq e^{-h_+}\Theta_{vr} = (\tau_t^r - \tau_t)/f, \tag{A2}$$

$$\theta_r \coloneqq \Theta_{rr} = (\tau^r + \tau_t - 2\tau_t^r)/f^2, \tag{A3}$$

where $\Theta_{\mu\nu}$ denotes the EMT components in (v, r) coordinates. We denote the limit of θ_v as $r \to r_+$ as θ_v^+, etc. The Einstein equations are then given by

$$\partial_v C_+ = 8\pi r^2 e^{h_+}(\theta_v + f\theta_{vr}) \equiv 8\pi r^2 \Theta_v^r, \tag{A4}$$

$$\partial_r C_+ = -8\pi r^2 \theta_{vr} \equiv 8\pi r^2 \Theta_v^v, \tag{A5}$$

$$\partial_r h_+ = 4\pi r \theta_r \equiv 4\pi r e^{h_+}\Theta_r^v. \tag{A6}$$

Tangents to the congruences of ingoing and outgoing radial null geodesics (note that these designations make literal sense only in a space with simple topology) are given in (v, r) coordinates by

$$n^\mu = (0, -e^{-h_+}, 0, 0), \qquad l^\mu = \left(1, \frac{1}{2}e^{h_+}f, 0, 0\right), \tag{A7}$$

respectively. The vectors are normalized to satisfy $n \cdot l = -1$. Their expansions [1,4,30] are

$$\vartheta_{(n)} = -\frac{2e^{-h_+}}{r}, \qquad \vartheta_{(l)} = \frac{e^{h_+}f}{r}, \tag{A8}$$

respectively. Hence the (outer) apparent horizon is located at the Schwarzschild radius r_g [10,16,27], justifying the definition of the black hole mass as [31] $2M(v) = r_+(v)$.

2. Velocity components, EMT, and metric functions

In (v, r) coordinates outside of the apparent horizon the relationship between four-velocity components of the timelike trajectory is

$$\dot{v} = \frac{\dot{r} + \sqrt{\dot{r}^2 + f}}{e^{h_+}f}, \tag{A9}$$

for both ingoing ($\dot{r} < 0$) and outgoing ($\dot{r} > 0$) test particles, where $f = f(v(\tau), r(\tau))$, and $h_+ = h_+(v(\tau), r(\tau))$. On the other hand, inside the trapped region $f < 0$ and thus to maintain the timelike character of the trajectory,

$$\dot{r} \le -\sqrt{-f} \tag{A10}$$

must hold. The null velocity component of ingoing particles still satisfies Eq. (A9), with the ingoing null geodesics $\dot{v} = 0$ being their ultrarelativistic limit. The future-directed outgoing trajectories satisfy

$$\dot{v} = \frac{\dot{r} - \sqrt{\dot{r}^2 + f}}{e^{h_+}f} > 0. \tag{A11}$$

The limiting values of the EMT components in (v, r) coordinates, $\theta_{\mu\nu}^+ \coloneqq \lim_{r\to r_+}\Theta_{\mu\nu}$, are

$$\theta_v^+ = (1 - w_1)\frac{r_+'}{8\pi r_+^2}, \tag{A12}$$

$$\theta_{vr}^+ = -\frac{w_1}{8\pi r_+^2}, \tag{A13}$$

$$\theta_r^+ = \frac{\chi_1}{4\pi r_+}. \tag{A14}$$

The effective EMT components in the (t, r) coordinates for $x \coloneqq r - r_g(t) > 0$ are

$$\tau_t = -\Upsilon^2 + e_{12}\sqrt{x} + e_1 x + \mathcal{O}(x^{3/2}), \tag{A15}$$

$$\tau_t^r = \pm\Upsilon^2 + \phi_{12}\sqrt{x} + \phi_1 x + \mathcal{O}(x^{3/2}), \tag{A16}$$

$$\tau^r = -\Upsilon^2 + p_{12}\sqrt{x} + p_1 x + \mathcal{O}(x^{3/2}). \quad \text{(A17)}$$

Since $f \propto \sqrt{x}$ and the rhs of Eq. (9) results in a finite limit, we have

$$\phi_{12} = \frac{1}{2}(e_{12} + p_{12}). \quad \text{(A18)}$$

The metric functions are then given by

$$C = r_g - 4\sqrt{\pi r_g^3}\Upsilon\sqrt{x} + \left(\frac{1}{3} + \frac{4\sqrt{\pi}e_{12}r_g^{3/2}}{3\Upsilon}\right)x + \mathcal{O}(x^{3/2}), \quad \text{(A19)}$$

$$h = -\frac{1}{2}\ln\frac{x}{\xi} + \left(\frac{1}{3\sqrt{\pi}r_g^{3/2}\Upsilon} - \frac{e_{12} - 3p_{12}}{6\Upsilon^2}\right)\sqrt{x} + \mathcal{O}(x). \quad \text{(A20)}$$

By substitution into Eq. (A2), we find that the limiting values of the effective EMT components in (v, r) coordinates are given by

$$\theta_v^+ = -\Upsilon^2, \quad \text{(A21)}$$

$$\theta_{vr}^+ = \frac{p_{12} - e_{12}}{8\sqrt{\pi}r_g\Upsilon}, \quad \text{(A22)}$$

$$\theta_r^+ = \frac{e_1 - 2\phi_1 + p_1}{16\pi r_g\Upsilon^2}. \quad \text{(A23)}$$

The leading terms of the EMT components of Eq. (24) are expressed with

$$\mu_1 = \frac{4\sqrt{\pi}e_{12}r_g^{3/2} + \Upsilon}{24\pi r_g^2\Upsilon} + \mathcal{O}(\sqrt{x}), \quad \text{(A24)}$$

$$\mu_3 = \frac{\sqrt{\pi}r_g^{3/2}(e_{12} + 3p_{12}) + \Upsilon}{24\pi r_g^2\Upsilon} + \mathcal{O}(\sqrt{x}), \quad \text{(A25)}$$

$$\mu_2 = \frac{1}{2}(\mu_1 + \mu_3) + \mathcal{O}(\sqrt{x}). \quad \text{(A26)}$$

The quantity

$$\mu_1 - 2\mu_2 + \mu_3 = \frac{(e_1 - 2\phi_1 + p_1)\sqrt{x}}{4\sqrt{\pi r_g}\Upsilon} + \mathcal{O}(x) \quad \text{(A27)}$$

is important for the EMT classification. Using Eqs. (A23) and (25) we find

$$(\mu_1 - 2\mu_2 + \mu_3)q = -\frac{(e_1 - 2\phi_1 + p_1)}{16\pi r_g} \propto -\theta_r^+, \quad \text{(A28)}$$

and due to Eq. (A6) $\Theta_{rr} \propto \Theta_r^v$.

From Eqs. (A4) and (A21) it follows that $\Theta_v^r < 0$ at the apparent horizon. If at the outer apparent horizon $\Theta_r^v \sim \Theta_v^r$, then the EMT has only real Lorentz-invariant eigenvalues and belongs to type I.

APPENDIX B: EXITING RBH

1. Equations of motion on the background of a general spherically symmetric metric

For the general spherically symmetric metric in the (v, r) coordinates

$$ds^2 = -e^{2h_+}f(v, r)dv^2 + 2e^{h_+}dvdr + r^2d\Omega_2, \quad \text{(B1)}$$

we have the following equations of motion for radially moving massive particles:

$$\ddot{v} + \left((\partial_v h_+) + e^{h_+}(\partial_r h_+) + \frac{1}{2}e^{h_+}(\partial_r f)\right)\dot{v}^2 = 0, \quad \text{(B2)}$$

$$\ddot{r} + (\partial_r h_+)\dot{r}^2 + \left(-\frac{1}{2}e^{h_+}(\partial_v f)\right)\dot{v}^2, + \left((\partial_r h_+)f + \frac{1}{2}(\partial_r f)\right) = 0, \quad \text{(B3)}$$

with the timelike normalization condition

$$-e^{2h_+}f\dot{v}^2 + 2e^{h_+}\dot{v}\,\dot{r} = -1. \quad \text{(B4)}$$

The above relations for $h_+ = 0$ and $f(v, r) = 1 - r_+(v)/r$ reduce to the geodesic equations (31) and (32) for the Vaidya metric.

2. Outgoing null geodesics in the ingoing Vaidya metric

Here we consider the future-directed null geodesics that are outgoing from the Vaidya black hole with $r'_+(v) < 0$. They satisfy the geodesic equation

$$\dot{v} = 0, \qquad \dot{v} = \frac{2\dot{r}}{f}, \quad \text{(B5)}$$

for the ingoing and outgoing geodesics.

Adapting the results of Refs. [26,27], the equations are simplified by introducing $\dot{r}_+ = r'_+\dot{v}$ and noting

$$\ddot{r} + \frac{r'_+}{2r}\dot{v}^2 = \ddot{r} + \frac{\dot{r}\dot{r}_+}{r - r_+} = \ddot{r} - \dot{r}\frac{d}{d\lambda}\ln(r - r_+) + \frac{\dot{r}^2}{r - r_+}. \quad \text{(B6)}$$

For a nonzero $\dot{r}$ (that is definitely true up to the apparent horizon), it can be rearranged as

$$\frac{d}{d\lambda}\ln\frac{\dot{r}}{r-r_+}=-\frac{\dot{r}}{r-r_+}, \tag{B7}$$

whose integration results in

$$\frac{\dot{r}}{r-r_+}=\frac{1}{\lambda+c}, \tag{B8}$$

where c is set by the initial conditions. Hence Eq. (31) is equivalent to

$$\dot{r}(\lambda)=\frac{r(\lambda)-r_+(v(\lambda))}{\lambda+c}. \tag{B9}$$

Then Eq. (B5) results in

$$\dot{v}(\lambda)=\frac{2r(\lambda)}{\lambda+c}. \tag{B10}$$

The initial condition [we can choose $\lambda=0,\ v(0)=0$] identifies the constant as

$$c=\frac{r(0)-r_0}{\dot{r}(0)}>0. \tag{B11}$$

If the black hole evaporation rate is constant, $r_+=r_0-\alpha v$, for some $\alpha>0$, then the substitution

$$\lambda+c=ce^{\ell} \tag{B12}$$

results in a first-order linear system

$$\frac{dr}{d\ell}=r(\ell)-r_0+\alpha v(\ell), \tag{B13}$$

$$\frac{dv}{d\ell}=2r(\ell), \tag{B14}$$

which can be rewritten in the form of matrices as

$$\frac{d}{d\ell}\begin{pmatrix}r\\v\end{pmatrix}=\begin{pmatrix}1&\alpha\\2&0\end{pmatrix}\begin{pmatrix}r\\v\end{pmatrix}+\begin{pmatrix}-r_0\\0\end{pmatrix}, \tag{B15}$$

with the matrix

$$A=\begin{pmatrix}1&\alpha\\2&0\end{pmatrix} \tag{B16}$$

having eigenvalues

$$\omega_1=\frac{1}{2}(1+\sqrt{1+8\alpha})>0, \tag{B17}$$

$$\omega_2=\frac{1}{2}(1-\sqrt{1+8\alpha})<0, \tag{B18}$$

so one can find that the solution to the linear system is

$$r(\ell)=\frac{1}{\omega_1-\omega_2}((-r_0+\omega_1 r(0))e^{\omega_1\ell}+(r_0-\omega_2 r(0))e^{\omega_2\ell}), \tag{B19}$$

$$v(\ell)=-\frac{2r_0}{\omega_1\omega_2}+\frac{1}{\omega_1-\omega_2}\left(\left(r(0)-\frac{r_0}{\omega_1}\right)e^{\omega_1\ell}+\left(-r(0)+\frac{r_0}{\omega_2}\right)e^{\omega_2\ell}\right). \tag{B20}$$

The event horizon (Fig. 3) is found by identifying the rays that do not reach the future null infinity $\mathcal{I}^+$. As $\omega_2<0$, the second term on Eq. (B19) vanishes in the limit $\ell\to+\infty$. Hence the arrival of a null particle $\mathcal{I}^+$ depends on the sign of the coefficient of the first term of the equation of trajectory,

$$\delta:=\omega_1 r(0)-r_0. \tag{B21}$$

The null particles that at $\lambda=0$ start from the areal radius $r<r_{\rm eh}(0)$,

$$r_{\rm eh}(0)=\frac{r_0}{\omega_1}=\frac{2r_+(0)}{1+\sqrt{1+8\alpha}}, \tag{B22}$$

do not reach $\mathcal{I}^+$. By varying the initial affine parameter, one obtains the following time-dependent expression for this hypersurface:

$$r_{\rm eh}(\ell)=\frac{2r_+(v(\ell))}{1+\sqrt{1+8\alpha}}. \tag{B23}$$

It is indeed a null hypersurface, as can be easily verified by calculating the norm of the normal vector. Describing the hypersurface as

$$\Psi=r-r_{\rm eh}=0, \tag{B24}$$

we find that the normal vector $\mathfrak{l}_\mu=-\partial_\mu\Psi$ is given by

$$\mathfrak{l}_\mu=\left(-\frac{2\alpha}{1+\sqrt{1+8\alpha}},-1,0,0\right) \tag{B25}$$

and satisfies $\mathfrak{l}^\mu\mathfrak{l}_\mu=0$. It is also worth noting that, for very small evaporation rate $\alpha\ll1$, one can show that the hypersurface is approximately the separatrix [14],

$$r_{\rm eh}\approx r_+(1-2\alpha)=r_++2r'_+r_+. \tag{B26}$$

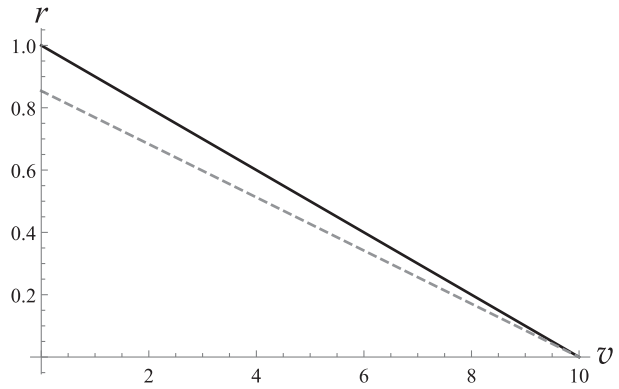

FIG. 3. The black line represents the evolution of the apparent horizon $r_+(v) = r_0 - av$, following a linear evaporation law, and the gray dashed line represents the evolution of the null hypersurface $r_S(v)$. For this diagram, the constants α and r_0 are chosen to be $r_0 = 1$ and $\alpha = 0.1$.

3. Turning point for the outgoing timelike geodesics

As $h_+ = 0$ at the apparent horizon, Eq. (A11) implies that $\dot{v} \to +\infty$ as a test particle on the outgoing timelike trajectory approaches the apparent horizon form inside. On the other hand, $\ddot{v}$ is always finite, and at the apparent horizon

$$\ddot{v}_{|_{r_+}} = -\left(\chi_1 + \frac{1 - w_1}{r_+}\right), \tag{B27}$$

where we substituted the expansion of Eqs. (15) and (16) into the geodesic equation (B2). If $\chi_1 > 0$ (i.e., the EMT belongs to the type I), then $\ddot{v} < 0$ in some vicinity of the apparent horizon. In this case, the arguments of Sec. IV that establish the existence of the turning point apply without any change.

Even when it cannot be asserted that $\dot{v}$ is a decreasing function of the proper time, $\ddot{v}$ remains finite. As a result, $\dot{v}$ diverges only if the outgoing timelike geodesic reaches r_+ as $\tau \to \infty$. However, it implies that $v \to \infty$, contradicting the assumption of finite evaporation time.

APPENDIX C: TIDAL FORCE CALCULATIONS

For a radially moving observer with the four-velocity $u_A = (\dot{v}, \dot{r}, 0, 0)$, the comoving orthogonal tetrad is formed by

$$e^\mu_{(\lambda)} = u^\mu_A, \tag{C1}$$

$$e^\mu_{(\rho)} = \frac{1}{\sqrt{e^{2h_+} f - 2e^{h_+}\dot{r}/\dot{v}}}(1, e^{h_+} f - \dot{r}/\dot{v}, 0, 0), \tag{C2}$$

$$e^\mu_{(\theta)} = (0, 0, 1/r, 0), \tag{C3}$$

$$e^\mu_{(\phi)} = (0, 0, 0, 1/(r \sin\theta)). \tag{C4}$$

For a massive test particle falling through the apparent horizon, a useful approximate expression for the four-velocity u_A can be readily obtained. We set

$$\dot{r}^2 =: -f(v, r) + E^2 + r'_+(v) g(v, r), \tag{C5}$$

where the function $g(v, r)$ is to be determined.

For a Schwarzschild black hole, the constant E represents the conserved energy per unit mass, and $g \equiv 0$. If the test particle starts from infinity with zero velocity, then $E = 1$.

Expanding in powers of $y := r - r_+$, we have

$$f = y/r_+ + \mathcal{O}(y^2), \tag{C6}$$

and assuming

$$g = \gamma(v) y + \mathcal{O}(y^2), \tag{C7}$$

for some function $\gamma(v)$, we have

$$\dot{r} = -E + \left(\frac{1}{r_+} - \gamma r'_+\right)\frac{y}{2E} + \mathcal{O}(y^2). \tag{C8}$$

Outside the apparent horizon,

$$\dot{v} = \frac{\dot{r} + \sqrt{f + \dot{r}^2}}{f}, \tag{C9}$$

for both ingoing and outgoing geodesics. Thus,

$$\dot{v} = \dot{v}_0 + \dot{v}_1 + \mathcal{O}(y^2), \tag{C10}$$

where

$$\dot{v}_0 = \frac{1}{2E}, \qquad \dot{v}_1 = \frac{y}{8E^3}\left(\frac{1}{r_+} - 2\gamma r'_+\right), \tag{C11}$$

and here and in the following, we keep only the leading-order terms in both y and r'_+.

Taking the derivative over the proper time τ and substitution into the equation of motion (32) results in the identity

$$\frac{(1 - 4E^2\gamma r_+) r'_+}{16E^4 r_+} + \mathcal{O}(y) = 0, \tag{C12}$$

from which the leading correction coefficient

$$\gamma = \partial_r g(v, r_+(v)) = \frac{1}{4E^2 r_+} \tag{C13}$$

is extracted. As a result, the radial velocity in the vicinity of the apparent horizon is approximated as

$$\dot{r}^2 = E^2 + \frac{y}{r_+}\left(1 + \frac{r'_+}{4E^2}\right) + \mathcal{O}(y^2). \tag{C14}$$

To compare the results of Sec. V with the standard estimates of the experiences of a freely falling observer at the black hole horizon [2], we set $E = 1$ in the calculations of Sec. V.

[1] S. W. Hawking and G. F. R. Ellis, *The Large Scale Structure of Space-Time* (Cambridge University Press, Cambridge, England, 1973).
[2] C. Misner, K. Thorne, and J. A. Wheeler, *Gravitation* (Princeton University Press, Princeton, NJ, 1973).
[3] V. P. Frolov and I. D. Novikov, *Black Hole Physics: Basic Concepts and New Developments* (Kluwer, Dordrecht, 1998).
[4] E. Poisson, *A Relativist's Toolkit: The Mathematics of Black-Hole Mechanics* (Cambridge University Press, Cambridge, England, 2004).
[5] LIGO Scientific Collaboration, KAGRA Collaboration, and Virgo Collaboration, Astrophys. J. Lett. **915**, L5 (2021).
[6] E. Curiel, Nat. Astron. **3**, 27 (2019).
[7] V. P. Frolov, arXiv:/1411.6981.
[8] S. A. Hayward, arXiv:gr-qc/0008071.
[9] M. Visser, Phys. Rev. D **90**, 127502 (2014).
[10] V. Faraoni, *Cosmological and Black Hole Apparent Horizons* (Springer, Heidelberg, 2015).
[11] R. B. Mann, S. Murk, and D. R. Terno, Int. J. Mod. Phys. D **31**, 2230015 (2022).
[12] V. Baccetti, R. B. Mann, S. Murk, and D. R. Terno, Phys. Rev. D **99**, 124014 (2019).
[13] R. B. Mann, S. Murk, and D. R. Terno, Phys. Rev. D **105**, 124032 (2022).
[14] P. Binétruy, A. Helou, and F. Lamy, Phys. Rev. D **98**, 064058 (2018).
[15] R. Carballo-Rubio, F. Di Filippo, S. Liberati, and M. Visser, Phys. Rev. D **101**, 084047 (2020).
[16] V. Faraoni, G. F. R. Ellis, J. T. Firouzjaee, A. Helou, and I. Musco, Phys. Rev. D **95**, 024008 (2017).
[17] V. Baccetti, S. Murk, and D. R. Terno, Phys. Rev. D **100**, 064054 (2019).
[18] S. Murk and D. R. Terno, Phys. Rev. D **104**, 064048 (2021).
[19] S. A. Hayward, Phys. Rev. D **49**, 6467 (1994).
[20] P. K. Dahal, S. Murk, and D. R. Terno, AVS Quantum Sci. **4**, 015606 (2022).
[21] P. Martín-Moruno and M. Visser, Classical and semi-classical energy conditions, in *Wormholes, Warp Drives and Energy Conditions*, edited by F. N. S. Lobo (Springer, New York, 2017), p. 193.
[22] A. Levi and A. Ori, Phys. Rev. Lett. **117**, 231101 (2016).
[23] A. Levi, Phys. Rev. D **95**, 025007 (2017).
[24] S. Abdolrahimi, D. N. Page, and C. Tzounis, Phys. Rev. D **100**, 124038 (2019).
[25] P. Martín-Moruno and M. Visser, Phys. Rev. D **103**, 124003 (2021).
[26] R. Waugh and K. Lake, Phys. Lett. **116B**, 154 (1986).
[27] M. Blau, Lecture Notes on General Relativity (2016), http://www.blau.itp.unibe.ch/newlecturesGR.pdf.
[28] J. Piesnack and K. Kassner, Am. J. Phys. **90**, 37 (2022).
[29] P. K. Dahal and D. R. Terno, Phys. Rev. D **102**, 124032 (2020).
[30] Y. Choquet-Bruhat, *General Relativity and the Einstein Equations* (Oxford University Press, Oxford, England, 2009).
[31] J. M. Bardeen, Phys. Rev. Lett. **46**, 382 (1981).

JOURNAL ARTICLE

Kinematic and energy properties of dynamical regular black holes

Brief summary

In the previous article, we demonstrated that massive particles can escape the trapped region by crossing the outer apparent horizon on an ingoing radial geodesic, experiencing finite tidal forces and energy densities. This analysis was based on the self-consistent approach that naturally leads to evaporating trapping apparent horizons. We now apply this framework to the special case of RBHs. Our study focuses on the type of the EMT according to the Hawking–Ellis classification, the energy conditions — particularly the NEC — throughout the dynamic evolution of the RBH until the trapped region disappears. Additionally, we examine the trajectories of massive particles as they cross both the inner and outer apparent horizons.

Errata and conventions

In this article, we use r_+ and r_- to denote the outer and inner apparent horizons, respectively. The expansions of ingoing and outgoing radial null geodesics are represented by θ_- and θ_+, respectively. This contrasts with the previous article (Ref. [4]), where θ_n and θ_l were used for ingoing and outgoing geodesics, respectively.

In the final paragraph of Section III.A on page 5 of this article, the following statement appears: "Since the NEC is the weakest of all energy conditions, its violation implies that all other energy conditions (strong, weak, dominant) are violated as well.". Although the first part of the statement is accurate — the NEC is indeed the weakest of the energy conditions — there are instances where the NEC can be satisfied while the strong energy condition (SEC) is violated. An example of this is demonstrated using a scalar field in Ref. [33].

Authorship statement

Conceptualization of the research project and calculations for its development. Also contributed to the planning and writing of the article, creating of figures, interpretation of its results, proofreading, and revisions. Principal contributor to Sections III and IV along with Appendix A.

Kinematic and energy properties of dynamical regular black holes

Sebastian Murk[1,*] and Ioannis Soranidis[2,†]

[1]*Okinawa Institute of Science and Technology, 1919-1 Tancha, Onna-son, Okinawa 904-0495, Japan*

[2]*School of Mathematical and Physical Sciences, Macquarie University, Sydney, New South Wales 2109, Australia*

(Received 21 September 2023; accepted 8 November 2023; published 4 December 2023)

Nonsingular black holes have received much attention in recent years as they provide an opportunity to avoid the singularities inherent to the mathematical black holes predicted by general relativity. Based on the assumption that semiclassical physics remains valid in the vicinity of their horizons, we derive kinematic properties of dynamically evolving spherically symmetric regular black holes. We review the Hawking-Ellis classification of their associated energy-momentum tensors and examine the status of the null energy condition in the vicinity of their horizons as well as their interior. In addition, we analyze the trajectory of a moving observer, find that the horizons can be crossed on an ingoing geodesic, and thus entering and exiting the supposedly trapped spacetime region is possible. We outline the ramifications of this result for the information loss problem and black hole thermodynamics. Throughout the article, we illustrate relevant features based on the dynamical generalization of the regular black hole model proposed in Carballo-Rubio *et al.* [J. High Energy Phys. 09 (2022) 118] and elucidate connections to the only self-consistent dynamical physical black hole solutions in spherical symmetry.

DOI: 10.1103/PhysRevD.108.124007

I. INTRODUCTION

While the existence of dark massive compact objects has been established beyond any reasonable doubt, their precise physical nature remains enigmatic, with a range of possibilities under consideration [1–6]. The prevalent astrophysical description is the Schwarzschild/Kerr black hole paradigm, which is based on the mathematical black hole (MBH) solutions of general relativity (GR). Their hallmark features are the presence of an event horizon and central singularity. Despite the successes of the paradigm, both features that distinguish MBHs are accompanied by empirical and conceptual pathologies which are absent by design in many alternative models describing dark ultracompact objects (UCOs) that are also compatible with observational data.

By its very definition, the event horizon is a global geometric property and thus physically unobservable [7]. While current data is consistent with having the Schwarzschild/Kerr solutions as asymptotic final states of gravitational collapse, such objects are *de facto* horizonless for distant observers (as their horizons exist only for $t \to \infty$). In contrast, physical black holes (PBHs) [8] bounded by a dynamically evolving quasilocal horizon formed in finite time according to the clock of a distant observer are (at least in principle) physically observable, i.e. there is a measurement that can be performed in a finite time interval and within a finite-size region of spacetime to determine the presence or absence of a quasilocal horizon. The presence of a physical singularity (i.e. one that is not an artifact of a particular choice of coordinates) inevitably introduces nontrivial causal structures into the spacetime at large [9] and is typically interpreted as a harbinger that the underlying theory breaks down.[1] An immediate consequence that is frequently discussed in the literature is the so-called information loss paradox [11]: in this scenario, the apparent lack of unitarity in the black hole evaporation process is typically ascribed to the propagation of quantum correlations into the singularity located at the black hole's interior [12]. To maintain unitarity and avoid information loss, it has been conjectured that the time dependence of the Hawking radiation's entanglement entropy follows the Page curve [13,14], i.e. it first increases until it reaches its peak at the Page time (where it coincides with the Bekenstein–Hawking entropy [15–20] of the black hole) and subsequently decreases until it reaches zero at the end

*sebastian.murk@oist.jp

†ioannis.soranidis@hdr.mq.edu.au

[1]"The crushing of matter to infinite density by infinite tidal gravitational forces is a phenomenon with which one cannot live comfortably. […] it is difficult to believe that physical singularities are a fundamental and unavoidable feature of our universe. […] one is inclined to discard or modify that theory rather than accept the suggestion that the singularity actually occurs in nature" [10].

of the evaporation process (corresponding to a final pure state).[2]

Several alternatives to MBHs have been proposed to describe the observed astrophysical black hole candidates and avoid the presence of singularities, including horizonless UCOs [5], gravastars [22,23], wormholes [24–26], and fuzzballs [27,28]. Our analysis in this article focuses on dynamical models of "horizonful" but singularity-free regular black holes (RBHs) [29–32] that are bounded by a quasilocal inner and outer horizon. In such models, the spacetime is typically regularized through the introduction of a minimal length scale that arises from a theory of quantum gravity and acts as a Planckian cutoff. In spherical symmetry, the central singularity is replaced by a de Sitter core and the introduction of a minimal length scale leads to the emergence of an inner horizon [33]. The minimal length scale is bounded from above by observational data, such as the trajectory of the S2 star orbiting Sagittarius A* [34], i.e. the astrophysical black hole candidate at the center of the Milky Way galaxy. The close contact with astrophysical observations of dark UCOs highlights the importance of studying realistic candidate models such as dynamically evolving RBHs more thoroughly.

It is worth noting that significant challenges arise from the presence of an inner horizon due to the fact that they are typically unstable under small perturbations. These instabilities are characterized by an exponential growth of the gravitational energy in the neighborhood of the inner horizon (which can be checked by tracking the relevant curvature scalars), a problem known as mass inflation instability [35–40]. We use the dynamical generalization of the so-called inner-extremal RBH model proposed in Ref. [41] to illustrate the key aspects of our analysis. In this model, the mass inflation problem is resolved at the expense of a degenerate inner horizon with vanishing surface gravity, although a recent study argues that even in this case the mass inflation instability cannot be avoided once semiclassical effects are taken into account [42]. Nevertheless, we stress that the properties we derive in this article are generic and apply to any and all dynamical RBH models described by a metric function of the form given in Eq. (7).

The absence of the central singularity is the principal characteristic of nonsingular black holes and offers a potential resolution to the information loss problem. In such models, the infalling matter never disappears from the manifold, and may possibly escape. By considering dynamical RBH models rather than their static counterparts, we explore this phenomenon based on the assumption that semiclassical gravity remains valid in the vicinity of their horizons.

The remainder of this article is organized as follows: in Sec. II, we review the construction of spherically symmetric dynamical RBHs in semiclassical gravity from a model-agnostic point of view, and introduce the inner-extremal RBH model we use to illustrate relevant physical features in Figs. 2–6. We then focus on the classification of energy-momentum tensors (EMTs) describing dynamical RBH metrics, discuss implications for the associated matter content, and in particular for the status of the null energy condition (NEC) in the vicinity and interior of RBHs (Sec. III). In Sec. IV, we consider the perspective of a moving observer attempting to escape the trapped spacetime region. Based on an expression for the linear coefficient of the Misner-Sharp (MS) mass, we highlight the relevance of our results for black hole thermodynamics and the transition between self-consistent dynamical PBH solutions (Sec. V). Lastly, we summarize the physical implications of our results and comment on possible avenues for future research related to nonsingular black hole spacetimes (Sec. VI). Throughout this article, we use the metric signature $(-,+,+,+)$ and work in dimensionless units such that $c = G = \hbar = k_B = 1$.

II. DYNAMICAL REGULAR BLACK HOLES IN SEMICLASSICAL GRAVITY

The geometry of a general spherically symmetric spacetime is described by the line element

$$ds^2 = -e^{2h_+(v,r)}f(v,r)dv^2 + 2e^{h_+(v,r)}dvdr + r^2d\Omega^2, \quad (1)$$

where $d\Omega^2$ denotes the normalized spherically symmetric Riemannian metric on the 2-sphere S^2. The metric function $f(v,r)$ is related to the MS mass [43] $M(v,r) = C(v,r)/2$ via

$$f(v,r) \coloneqq \partial_\mu r \partial^\mu r = 1 - \frac{C(v,r)}{r}, \quad (2)$$

where r denotes the areal radius, the MS mass[3] is described by the series expansion

$$C(v,r) = r_+(v) + \sum_{i=1}^{\infty} w_i(v)(r - r_+(v))^i, \quad (3)$$

with coefficients

[2]The results of a recent study [21] indicate that the evaporation of two-dimensional nonsingular dilatonic black holes, which can be used to model some of the thermodynamic properties of four-dimensional nonsingular black holes, conforms to the unitary evolution predicted by the Page curve.

[3]While the MS mass is technically $C(v,r)/2$, we take the liberty to refer to $C(v,r)$ itself as the MS mass as well when there is no need (in terms of its physical relevance) to account for the factor of one half.

$$w_i(v) = \frac{1}{i!}\frac{\partial^i C(v,r)}{\partial r^i}\bigg|_{r_+(v)}, \tag{4}$$

and the functions $h(t,r)$ and $h_+(v,r)$ play the role of integrating factors that turn the expression

$$dt = e^{-h(t,r)}\left(e^{h_+(v,r)}dv - \frac{dr}{f(v,r)}\right) \tag{5}$$

into an exact differential (provided that the coordinate transformation exists). Since $h_+(v,r) = 0$ in all spherically symmetric RBH spacetimes that we are aware of, we limit our considerations to this case in what follows.[4] The general spherically symmetric metric specified in Eq. (1) then simplifies to

$$ds^2 = -f(v,r)dv^2 + 2dvdr + r^2 d\Omega^2, \tag{6}$$

and a dynamically evolving RBH is described by a metric function of the form

$$f(v,r) = g(v,r)(r - r_-(v))^a (r - r_+(v))^b, \tag{7}$$

where $r_-(v)$ and $r_+(v)$ denote the inner and outer horizon, respectively, and $a, b \in \mathbb{N}_{>0} = \{1, 2, \ldots\}$ are positive integers labeling their degeneracy. The role of the *a priori* undetermined function $g(v,r)$ is to ensure regularity at the center as well as the proper asymptotic behavior of the metric at infinity [44]. It must be positive for the entire existence of the trapped region, that is $g(v,r) > 0$ for every $v_f \le v \le v_d$, where v_f and v_d denote the formation and disappearance of the trapped region, respectively, as indicated in Fig. 1.

The expansions of ingoing and outgoing radial null geodesics are given by

$$\theta_- = -\frac{2}{r}, \qquad \theta_+ = \frac{f(v,r)}{r}, \tag{8}$$

respectively. The existence of a trapped spacetime region is determined by the signature of their product $\theta_-\theta_+ \overset{?}{\lesseqgtr} 0$. Following the argumentation in Ref. [45], a trapped region is present if and only if $\theta_-\theta_+ > 0$. In consequence, the disappearance of the trapped region at $v = v_d$ implies $\theta_-\theta_+|_{v_d} \le 0$. At this point, the inner and outer horizon merge, i.e. $r_-(v_d) \equiv r_+(v_d)$. From Eqs. (7) and (8), it then follows that

$$\theta_-\theta_+|_{v_d} = -\frac{2}{r^2}g(v_d, r)(r - r_+(v_d))^{a+b} \le 0. \tag{9}$$

[4]Note also that $h_+(v,r) = 0$ at the outer horizon $r = r_+(v)$. For $h_+(v,r) = 0$ and $C(v,r) \equiv C(v)$, the metric of Eq. (1) reduces to the Vaidya metric.

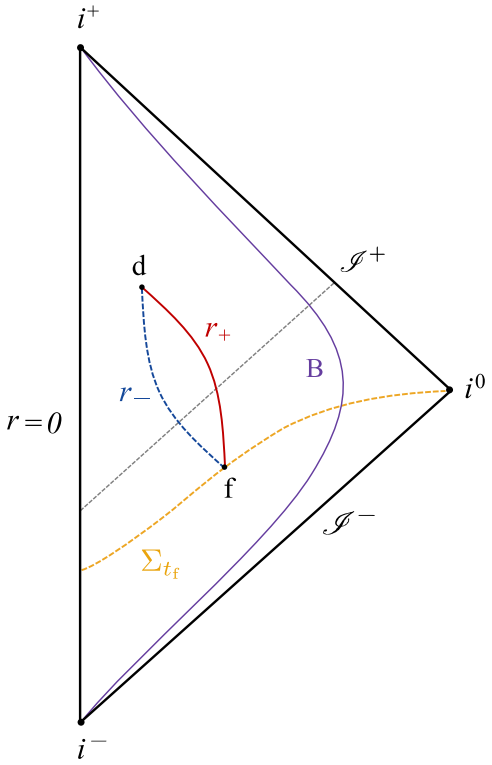

FIG. 1. Schematic Carter-Penrose diagram depicting the formation and evaporation of a RBH with an apparent horizon r_g that has a shrinking inner r_- (dashed blue line) and shrinking outer r_+ (solid red line) component. The trajectory of a distant observer Bob is indicated in purple and marked by the initial B. The dashed gray line corresponds to an outgoing radial null geodesic that reaches future null infinity $\mathscr{I}^+$. The asymptotic structure of a simple RBH spacetime coincides with that of Minkowski spacetime. An immediate neighborhood of $r = 0$ never belongs to the trapped region. The points f and d represent the events of formation and disappearance of the trapped region. The equal time hypersurface Σ_{t_f} is shown as a dashed orange line connecting the center $r = 0$ and spacelike infinity i^0. Both the outer and inner horizon are timelike membranes over the course of the lifespan of the RBH, i.e. $\forall\ v \in (v_f, v_d)$.

For this to hold true $\forall\ r \ge 0$, we must have $g(v,r) > 0$, and the sum of the powers $a + b$ must be even (otherwise the trapped region cannot disappear, which would imply that an RBH cannot evaporate completely). In addition, the sign of the outgoing radial null geodesic θ_+ can only change (which is a prerequisite to enable the formation of a trapped region) if both a and b are odd numbers due to the fact that the immediate neighborhood of the RBH center must be an untrapped region [44].

A model that—once generalized to the dynamical case [i.e. $r'_- \neq 0$ and $r'_+ \neq 0$]—satisfies all of the requirements outlined above is the inner-extremal RBH model introduced in Ref. [41] (whose associated mathematical expressions are indicated by the subscript "ie" in what follows). In the dynamical case, it is described by the metric function

$$f_{\rm ie}(v,r) = g_{\rm ie}(v,r)(r-r_-)^3(r-r_+), \tag{10}$$

$$g_{\rm ie}(v,r) = \frac{1}{r_-^3 r_+ - (3r_-^2 r_+ + r_-^3)r + c_2 r^2 - 3r_- r^3 + r^4}, \tag{11}$$

where

$$c_2 = \tilde{c}_2 + \frac{15}{4}r_-^2 + \frac{9}{4}r_- r_+ + \frac{1}{4}\frac{r_-^3}{r_+}, \qquad \tilde{c}_2 \geq 0, \tag{12}$$

and we have omitted dependencies on v [$r_\pm \equiv r_\pm(v)$, $c_2 \equiv c_2(v)$, $\tilde{c}_2 \equiv \tilde{c}_2(v)$] for the sake of readability. The explicit form of the coefficient $\tilde{c}_2$ is constrained by the positivity requirement of the MS mass. An explicit derivation of Eqs. (10)–(12) including our choice for $\tilde{c}_2$ [cf. Eq. (A16)] is provided in Appendix A.

Since this is a dynamical model, we must consider appropriate generalizations of surface gravity to quasilocal non-Killing horizons [46,47]. The two principal generalizations to dynamical black hole spacetimes are related to either the affine peeling surface gravity [48] or the so-called Kodama surface gravity [49–51]. Here, we restrict our considerations to the latter since the peeling surface gravity is ill-defined for transient objects that form in finite time of a distant observer [52–54] (which includes dynamical RBHs), and there are strong arguments that Kodama surface gravity is the critical quantity with respect to the emission of Hawking radiation [51,54].

It is worth noting that any dynamical generalization of surface gravity vanishes at a degenerate horizon [45]. Thus, the inner [$a = 3$] and outer [$b = 1$] horizon degenaracies of the inner-extremal RBH model [cf. Eqs. (7) and (10)] imply a nonzero Kodama surface gravity at the outer horizon and a vanishing Kodama surface gravity at the inner horizon. The latter is what ultimately cures the mass inflation instability problem that typically plagues RBHs [41] (at least in classical GR).

The assumption that a regular (in the sense that scalar curvature invariants remain finite) apparent horizon r_g forms in finite time of a distant observer implies a violation of the NEC [8]. This leaves only evaporating black holes [$r_g' < 0$] and accreting white holes [$r_g' > 0$] as viable (i.e. real-valued) horizonful solutions to the spherically symmetric semiclassical Einstein equations (see Ref. [8], Table 2). As our interest lies in describing singularity-free objects resulting from gravitational collapse, we limit our considerations to evaporating RBH solutions [i.e. $r_-' < 0$ and $r_+' < 0$] in what follows. In this case, the inner and outer components of the apparent horizon are timelike membranes for the entire evolution $v \in (v_{\rm f}, v_{\rm d})$ of the black hole, i.e. from immediately after the instant of horizon formation at $v = v_{\rm f}$ until just before the disappearance of the trapped region at $v = v_{\rm d}$ [55]. This can be seen as follows: a hypersurface Σ can be defined by restricting the coordinates via $\Phi(\Sigma_{r_\xi}) =: r - r_\xi \equiv 0$. The inner and outer horizon correspond to the constraint

$$\Phi(\Sigma_{r_\pm}) = r - r_\pm \equiv 0, \tag{13}$$

which leads to a normal vector n_μ defined by

$$n_\mu =: \eta \partial_\mu \Phi(\Sigma_{r_\pm}) = \eta(-r_\pm', 1, 0, 0), \tag{14}$$

where η is a normalization factor. Using the simplified metric of Eq. (6), the inner product of this normal vector at the inner/outer horizon is given by

$$n_\mu n^\mu|_{r_\pm} = -2\eta^2 r_\pm'. \tag{15}$$

For evaporating RBHs [$r_\pm' < 0$] this inner product is spacelike, $n_\mu n^\mu > 0$. Consequently, the causal character of the inner and outer horizon is timelike.

III. ENERGY MOMENTUM TENSOR AND ENERGY CONDITIONS FOR AN EVAPORATING REGULAR BLACK HOLE

A. Hawking-Ellis classification

The Hawking-Ellis classification of the EMT [56] provides a convenient model-independent framework to study the matter content of a spacetime geometry as well as its connection to various energy conditions [57,58]. The different EMT types I-IV are distinguished through their eigenvectors, and more specifically through their causal structure (timelike vs. null vs. spacelike) and degeneracy (single, double, triple). We work in an orthonormal frame (abbreviated ONF; indicated by a hat "$\hat{}$" on the tensor indices in what follows) in which the eigenvalues λ of the EMT are the solutions of the equation

$$\det\left(T_{\hat{\mu}\hat{\nu}} - \lambda \eta_{\hat{\mu}\hat{\nu}}\right) = 0. \tag{16}$$

In spherical symmetry, the generic form of the EMT in the ONF is given by

$$T_{\hat{\mu}\hat{\nu}} = \begin{pmatrix} T_{\hat{0}\hat{0}} & T_{\hat{0}\hat{1}} & 0 & 0 \\ T_{\hat{1}\hat{0}} & T_{\hat{1}\hat{1}} & 0 & 0 \\ 0 & 0 & T_{\hat{2}\hat{2}} & 0 \\ 0 & 0 & 0 & T_{\hat{3}\hat{3}} \end{pmatrix}, \tag{17}$$

where explicit expressions for the EMT components are provided in Appendix B, and $T_{\hat{2}\hat{2}} = T_{\hat{3}\hat{3}}$ due to the symmetries of the spacetime. Both of these components are also eigenvalues of the EMT. Their corresponding eigenvectors are $v_{\hat{2}} = (0,0,1,0)$ and $v_{\hat{3}} = (0,0,0,1)$, respectively. The remaining eigenvalues are determined by the (reduced) characteristic polynomial

$$\lambda^2 + (T_{\hat{0}\hat{0}} - T_{\hat{1}\hat{1}})\lambda + (T_{\hat{0}\hat{1}}^2 - T_{\hat{1}\hat{1}}T_{\hat{0}\hat{0}}) = 0, \quad (18)$$

and their degeneracy is specified by its discriminant

$$\Delta = (T_{\hat{0}\hat{0}} + T_{\hat{1}\hat{1}})^2 - 4T_{\hat{0}\hat{1}}^2. \quad (19)$$

For the general spherically symmetric metric specified in Eq. (1), the discriminant is given by

$$\Delta(v, r) = \frac{\partial_r h_+}{16\pi^2 r^2}[(\partial_r h_+)f^2 - 2e^{-h_+}\partial_v f]. \quad (20)$$

For $h_+ = 0$ we have $\Delta = 0$, meaning that—depending on the value of the EMT component $T_{\hat{0}\hat{1}}$—the EMT will be either of type II or degenerate type I [58]. Dynamical RBHs necessarily have $T_{\hat{0}\hat{1}} \neq 0$. In this case, there exists only one additional eigenvector, and the corresponding EMT is of type II (null dust/massless radiation). For static RBH models, on the other hand, $T_{\hat{0}\hat{1}} = 0$, $T_{\hat{1}\hat{1}} = -T_{\hat{0}\hat{0}}$, and the EMT admits four eigenvectors corresponding to type I, which is degenerate in this case because two different eigenvectors are associated with the same eigenvalue. These results are consistent with the theorem derived in Ref. [59]. The same type of EMT arises for the cosmological constant fluid [58]. However, in contrast to the perfect fluid associated with the cosmological constant, RBH models (both static and dynamical) correspond to an imperfect (anisotropic) fluid since $T_{\hat{1}\hat{1}} \neq T_{\hat{2}\hat{2}}$ [60,61].

The type of EMT that is associated with a particular solution of the Einstein equations has implications for the status of various energy conditions [56]. Here, we focus on the null energy condition (NEC), which posits that $T_{\mu\nu}\ell^\mu\ell^\nu \geq 0$, i.e. the contraction of the EMT with any future-directed null vector ℓ^μ is non-negative. Since the NEC is the weakest of all energy conditions, its violation implies that all other energy conditions (strong, weak, dominant) are violated as well. In spherical symmetry, an EMT of type IV is generally considered to be the most exotic as it always violates the NEC. The expectation value of the renormalized EMT near the apparent horizon of a spherically symmetric black hole has been shown to be of this type [62,63]. Conversely, as we have outlined above, dynamical RBHs are described by an EMT of type II. This raises the question of how the NEC behaves in the vicinity of the inner and outer horizon, as well as inside of the RBH's trapped region.

B. Null energy condition

An apparent horizon can be observed from future null infinity $\mathscr{I}^+$ only if the NEC is violated in its vicinity [56,64,65]. For PBHs (which include RBHs as the singularity-free subset) with $h_+ = 0$, the NEC is marginally satisfied for ingoing null vectors [8]. For the metric specified in Eq. (6), an outgoing null vector is described by $\ell^\mu = (1, f/2, 0, 0)$. Since the NEC is a classical energy condition, it is reasonable to expect violations in the presence of quantum effects that ultimately lead to the evaporation of RBHs [66]. In fact, it has been demonstrated that the emission of Hawking radiation [18,19] violates several energy conditions [12,67–69]. It should also be noted that—contrary to popular belief—an event horizon is not required to enable the emission of Hawking radiation: a slowly evolving future apparent horizon is sufficient [70].

Using the components of the Einstein tensor $G_{\mu\nu} = 8\pi T_{\mu\nu}$, the NEC can be expressed as

$$T_{\mu\nu}\ell^\mu\ell^\nu = \frac{1}{8\pi}\left(G_{00} + G_{01}f + G_{11}\frac{f^2}{4}\right) \geq 0, \quad (21)$$

evaluated at the horizon. For the metric of Eq. (6), we find

$$T_{\mu\nu}\ell^\mu\ell^\nu = -\frac{\partial_v f}{8\pi r}. \quad (22)$$

As argued in Sec. II, we consider only evaporating RBH solutions [$r'_- < 0$ and $r'_+ < 0$]. Evaluating Eq. (22) at the horizons, we find that the NEC is violated in the vicinity of the outer horizon while being satisfied in the vicinity of the inner horizon. Assuming that semiclassical gravity is valid, this is a universal property for spherically symmetric dynamical RBHs. As we will see below, the change in the signature of the NEC expression implies the presence of a hypersurface $r_0(v)$ that acts as a boundary between the NEC-violating and the NEC-nonviolating region within the trapped spacetime domain.

For the generic metric function Eq. (7) describing dynamical RBHs, performing a series expansion of Eq. (22) at the outer apparent horizon yields

$$T_{\mu\nu}\ell^\mu\ell^\nu|_{r_+} = \frac{-bg(v, r_+)(-r'_+)(r_+ - r_-)^a}{8\pi r_+}(r - r_+)^{b-1} + \mathcal{O}(r - r_+)^b. \quad (23)$$

Therefore, the NEC is always violated in the vicinity of the outer horizon (both inside and outside of the trapped region) irrespective of its degeneracy, as our argumentation in Sec. II revealed that b is odd. For a degenerate outer horizon [$b > 1$], the NEC is marginally satisfied at the outer horizon $r = r_+$ itself. However, note that having a nonzero surface gravity at the outer horizon is only possible if it is nondegenerate [45], i.e. if $b = 1$ [cf. Eq. (12) in Ref. [44]]. Once again, we stress that the violation of the NEC is not only consistent with, but rather, it is a prerequisite for the observability of the outer apparent horizon from future null infinity.

TABLE I. Overview of NEC-nonviolating (✓) and NEC-violating (✗) regions of an evaporating RBH with a nondegenarate outer horizon [$b = 1$]. If the outer horizon is degenerate [$b > 1$], the NEC-violating region is given by $r_0 < r < r_+$, i.e. it no longer includes the outer horizon $r = r_+$ itself.

	$0 \le r \le r_-$	$r_- < r \le r_0$	$r_0 < r \le r_+$
$T_{\mu\nu}\ell^\mu\ell^\nu \overset{?}{\ge} 0$	✓	✓	✗

At the inner horizon, we find

$$T_{\mu\nu}\ell^\mu\ell^\nu|_{r_-} = (-1)^{b+1}\frac{ag(v,r_-)(-r'_-)}{8\pi r_-}(r_+ - r_-)^b \cdot (r - r_-)^{a-1} + \mathcal{O}(r - r_-)^a. \tag{24}$$

Consequently, the NEC is satisfied in the vicinity of the inner horizon, and marginally satisfied at $r = r_-$ if it is degenerate [$a > 1$]. Since the NEC is always violated in the vicinity of the outer apparent horizon, consistency requires the existence of a hypersurface $r_0 \in (r_-, r_+)$ located between the inner and outer horizon, thus effectively separating the trapped region into two distinct spacetime domains as detailed in Table I.

To illustrate this behavior in more detail, we consider the dynamical generalization of the inner-extremal RBH model [41] described by Eqs. (10)–(12). Evaluating Eq. (22) at the outer horizon for the metric function of Eq. (10), we find

$$T_{\mu\nu}\ell^\mu\ell^\nu|_{r_+} = \frac{(r_+ - r_-)^3 r'_+}{8\pi r_+^3(r_+^2 + r_-^2)}, \tag{25}$$

which is either negative or zero due to $r'_+ < 0$; equality occurs only at the extremal cases, i.e. at the formation $v = v_\mathrm{f}$ and disappearance $v = v_\mathrm{d}$ of the trapped region. At the inner horizon, the corresponding expression is always zero due to its degenerate nature [$a = 3$ in the inner-extremal RBH model, cf. Eq. (10)], and thus the NEC is always satisfied. At the formation $v = v_\mathrm{f}$ and disappearance $v = v_\mathrm{d}$ of the trapped region, the two expressions for the NEC coincide as the inner and outer apparent horizon (e)merge.

Figure 2 illustrates the extent of the NEC violation for an evaporating inner-extremal RBH. We note that the minimum (i.e. a maximally violated NEC) occurs close to the disappearance of the trapped region, indicating that the quantum effects responsible for the NEC violation are more pronounced toward the final stages of the evaporation process. This is in qualitative agreement with the results obtained for evaporating two-dimensional regular dilatonic black holes [21].

The existence of an NEC boundary has been pointed out previously for RBHs with horizons that are not exclusively timelike [64]. However, in our analysis, both the inner and outer horizon are timelike for the entire evolution of the

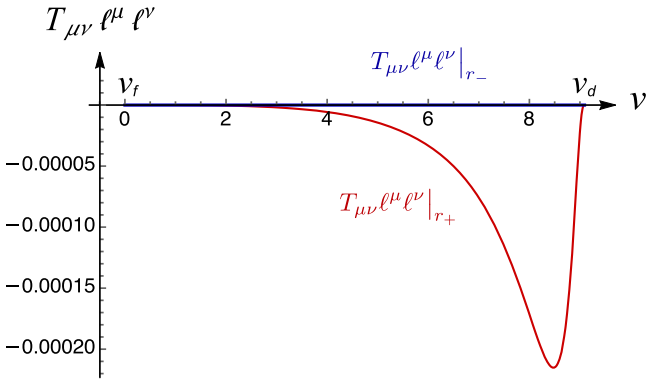

FIG. 2. Evaluation of the NEC for the entire evolution period $v \in [v_\mathrm{f}, v_\mathrm{d}]$ of an evaporating inner-extremal RBH. The red (blue) line represents the NEC evaluated at the outer (inner) apparent horizon $r_+(v)$ [$r_-(v)$]. The points $v = v_\mathrm{f}$ and $v = v_\mathrm{d}$ denote the advanced null coordinate at the formation and disappearance of the trapped region, respectively. For the purpose of modeling the NEC violation, the outer and inner horizon are chosen as $r_+(v) = r_+(0) - a_+ v - b_+ v^2$ and $r_-(v) = r_-(0) - a_- v - b_- v^2$ with parameter values $a_+ = 0.1$, $b_+ = 0.1$, $a_- = 1$, $b_- = 0.001$, and initial radii $r_+(0) = r_-(0) = 10$. With this particular choice, the equation $r_+(v) = r_-(v)$ has exactly two roots, which represent the formation and the disappearance point.

evaporating RBH as motivated by our argumentation in Sec. II. Determining the location of the hypersurface separating the NEC-violating from the NEC-nonviolating region requires solving the schematic equation

$$T_{\mu\nu}\ell^\mu\ell^\nu \overset{!}{=} 0. \tag{26}$$

For the inner-extremal RBH model [that is, using Eq. (22) with the metric functions Eqs. (10)–(12)], we obtain five roots, namely $r = 0$, $r = r_-$ (double root), r_0, and two complex conjugate roots which are excluded since r is real. The expression obtained for the root r_0 is too convoluted to determine its exact location. However, in the vicinity of the inner apparent horizon $r \sim r_-$, we find

$$T_{\mu\nu}\ell^\mu\ell^\nu|_{r\sim r_-} = \frac{-3r'_-(r_+ - r_-)}{8\pi r_-^4(r_+ + r_-)}(r - r_-)^2 + \mathcal{O}(r - r_-)^3, \tag{27}$$

indicating that the NEC is satisfied as $r'_- < 0$.

Our analysis in this section is valid for $v_\mathrm{f} \le v \le v_\mathrm{d}$, i.e. for as long as the trapped spacetime region persists, including the instants of its formation and disappearance. Figure 3 illustrates the trapped spacetime region and the status of the NEC over the course of the RBH's lifetime. In the next section, we consider the energy density observed by a moving observer, and find that a similar feature of the trapped region emerges.

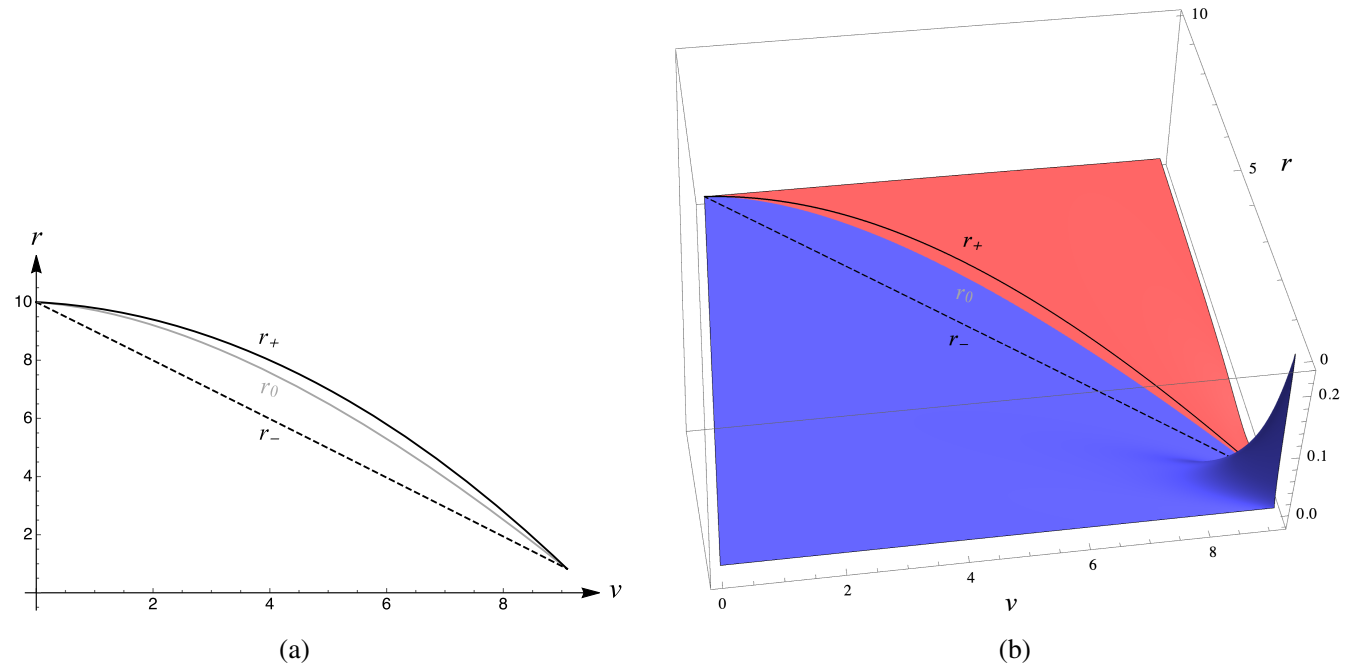

FIG. 3. The solid and dashed black lines represent the evolution of the outer r_+ and inner r_- apparent horizon, respectively, until the disappearance of the trapped region. The solid gray line indicates the location of the hypersurface r_0 which separates the NEC-violating region between r_0 and r_+ from the NEC-nonviolating region between r_0 and r_-. (a) Illustration of the trapped spacetime region in the v-r-plane. (b) Status of the NEC within the trapped region and its vicinity. The spacetime domain where the NEC is violated (satisfied) is shaded in red (blue). The hypersurface r_0 located between the two horizons corresponds to the boundary of the two domains.

IV. TRAJECTORIES OF MOVING OBSERVERS

In this section, we study the trajectory of a moving observer Alice. We start by examining the energy density she observes while following a particular geodesic that allows her to enter and exit the trapped region.

A. Ingoing and outgoing trajectories: Entering and exiting the trapped region

Assume that Alice begins her expedition from the untrapped region near the RBH center and initially follows an outgoing geodesic. After making a few generic statements about her trajectory, we once again illustrate our results based on the dynamical inner-extremal model described by Eqs. (10)–(12) and comment on important features that arise over the course of her journey.

For radially moving timelike observers and particles, the Lagrangian associated with the metric of Eq. (6) is given by

$$\mathcal{L} = \frac{1}{2} f \dot{v}^2 - \dot{v}\,\dot{r}, \tag{28}$$

where the overdot denotes derivatives with respect to Alice's proper time.[5] The corresponding Euler-Lagrange equations are

$$\ddot{v} = -\frac{1}{2}(\partial_r f)\dot{v}^2, \tag{29}$$

$$\ddot{r} = \frac{1}{2}(\partial_v f)\dot{v}^2 - \frac{1}{2}(\partial_r f). \tag{30}$$

Alice's four-velocity is normalized by $u^\mu u_\mu = -1$, which results in

$$-f\dot{v}^2 + 2\dot{v}\,\dot{r} = -1. \tag{31}$$

From the normalization conditions, we obtain two possible solutions for $\dot{v}$, which in turn restrict the admissible values of the radial velocity $\dot{r}$. Specifically, we find that

$$\dot{v} = \frac{\dot{r} \pm \sqrt{\dot{r}^2 + f}}{f}. \tag{32}$$

To ensure that Eq. (32) maintains real-valued solutions inside of the trapped region, the relation

$$\dot{r} \leq -\sqrt{-f} \tag{33}$$

must hold $\forall\ v \in (v_\mathrm{f}, v_\mathrm{d})$. Outside of the trapped region there are no restrictions since $f(v,r)$ is always positive there. It is important to note that, during Alice's motion, $\dot{v}$ must be positive. This condition necessitates different choices for the sign in the numerator of Eq. (32) to

[5]Since the action and its corresponding Lagrangian are invariant under reparametrization of the trajectory and our argumentation in this section requires only the equations of motion, we have the freedom to choose the time parameter in the Lagrangian.

accommodate different types of motion associated with the spacetime regions Alice is traversing. For untrapped regions, i.e. for $0 \leq r < r_-$ and $r > r_+$, it is straightforward to verify that the correct choice of signature is "+" for both ingoing and outgoing trajectories. On the other hand, this is not the case when trajectories inside the trapped region are considered. The deviation occurs because $\dot{r} < 0$ for both ingoing and outgoing trajectories, which is a well-known feature associated with the presence of a trapped region due to the fact that $f(v, r)$ is negative there [55,71,72]. In this case, to guarantee the positivity of $\dot{v}$ and ensure that it takes on only real values, ingoing and outgoing trajectories must satisfy the respective relations

$$\dot{v} = \frac{\dot{r} + \sqrt{\dot{r}^2 + f}}{f}, \qquad r_- < r < r_+ \quad \text{(ingoing)}, \tag{34}$$

$$\dot{v} = \frac{\dot{r} - \sqrt{\dot{r}^2 + f}}{f}, \qquad r_- < r < r_+ \quad \text{(outgoing)}. \tag{35}$$

With this in mind, an interesting exercise is to investigate what happens to the radial acceleration of Alice's motion in the general case described by Eq. (7). As Alice begins her journey from an untrapped region, her trajectory (both ingoing and outgoing) is described by the signature given in Eq. (34). On her outgoing trajectory, she first encounters the inner horizon. Performing a series expansion on the right-hand side of Eq. (30) reveals that, when approaching the inner horizon on an outgoing geodesic that satisfies Eq. (34), her radial acceleration is given by

$$\ddot{r} = \frac{(-1)^{a+b} 2a\dot{r}^2}{g(v, r_-)(r_+ - r_-)^b} \frac{r'_-(v)}{|r - r_-|^{a+1}} + \mathcal{O}\left(\frac{1}{(r - r_-)^a}\right). \tag{36}$$

From our argumentation in Sec. II, we know that

(A) the disappearance of a trapped region in finite time according to the clock of a distant observer is only possible if the sum of the horizon degeneracies $a + b$ is an even number;

(B) the only viable dynamically evolving semiclassical black hole solutions in spherical symmetry are evaporating black holes; for dynamical RBHs, this implies that both the inner and outer component of the apparent horizon must shrink.

Therefore, while traveling on an outgoing trajectory, Alice's acceleration is negative and divergent, thus forcing her to stop and reverse her trajectory so as to follow an ingoing geodesic. We note that the value $\dot{r} = 0$ for the radial velocity is allowed since Alice is still in the untrapped region $r < r_-$. Assuming that semiclassical gravity remains valid in this regime, this is another universal result that holds for every dynamical RBH described by Eq. (7).

Close to the evaporating inner horizon, specific trajectories undergo a transition from outgoing to ingoing. As a result, the inner horizon can overtake Alice, and she may find herself inside of the trapped region. In fact, this is the only way to enter the trapped region from areal radii $r < r_-$. Once inside, Alice's motion is characterized by $\dot{r} < 0$ and $\ddot{r} < 0$. This implies that her radial velocity $\dot{r}$ will continue to become increasingly more negative until it reaches the minimum value $-\sqrt{-f}$. At this point, a continuous transition from Eq. (34) to Eq. (35) occurs, and Alice will once again find herself on an outgoing geodesic. As she approaches the outer apparent horizon, her acceleration is given by

$$\ddot{r} = \frac{2b\dot{r}^2}{g(v, r_+)(r_+ - r_-)^a} \frac{-r'_+(v)}{|r - r_+|^{b+1}} + \mathcal{O}\left(\frac{1}{|r - r_+|^b}\right), \tag{37}$$

which is positive. Therefore, as she approaches the horizon, her velocity becomes less and less negative until she reaches the maximum allowed value. Once again, a transition occurs, this time from Eq. (35) to Eq. (34), meaning that Alice now finds herself on an ingoing trajectory, and she can only exit the trapped region if the outer apparent horizon overtakes her. Consequently, no matter which horizon Alice approaches on an outgoing geodesic, there is a unique way to cross it, namely on an ingoing geodesic. This analysis provides relevant insights on how information (e.g. in the form of particles) can exit the trapped region, thus offering a natural resolution to the information loss problem [11] as information that is supposedly trapped can once again become visible to an observer who is performing measurements in the exterior of the trapped region. However, as illustrated in Fig. 4(a), information will become visible for distant observers only after the two horizons have merged and the trapped region has disappeared.

B. Energy density at the horizon crossing

In this subsection, we calculate the energy density experienced by Alice upon her exit from the trapped region. Recall that Alice's motion is described by the four-velocity

$$u_A^\mu = (\dot{v}, \dot{r}, 0, 0), \tag{38}$$

and the energy density she observes is given by the contraction

$$\rho_A = T_{\mu\nu} u_A^\mu u_A^\nu, \tag{39}$$

or, equivalently,

$$\rho_A = \frac{1}{8\pi}(G_{00}\dot{v}^2 + 2G_{01}\dot{v}\,\dot{r} + G_{11}\dot{r}^2). \tag{40}$$

Instants where Alice crosses the horizons are of particular interest. Horizon crossings always occur while she is on an ingoing geodesic trajectory, meaning that $\dot{v}$ is given by

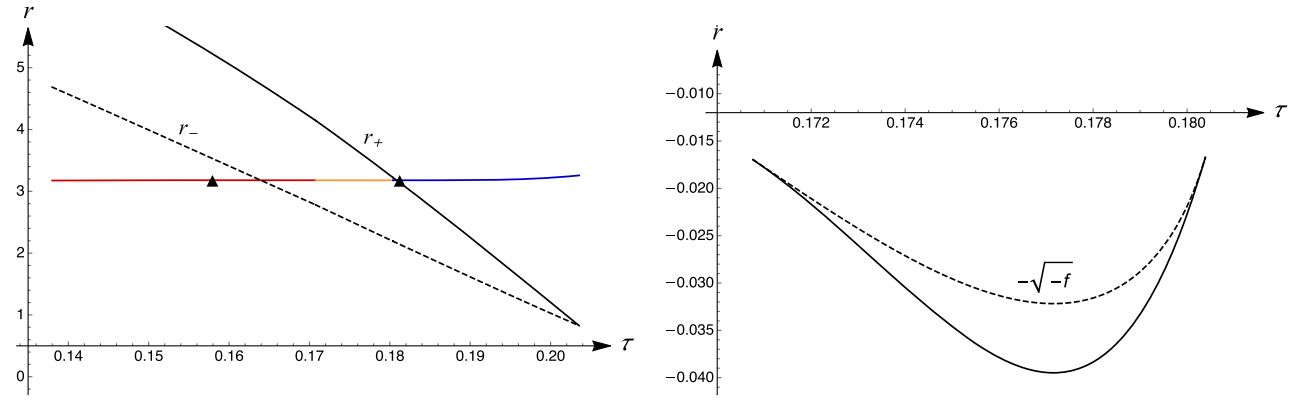

(a) (b)

FIG. 4. Properties of outgoing trajectories illustrated using the generalized dynamical inner-extremal RBH model described by Eqs. (10)–(12). (a) An observer Alice starts her journey at areal radius $r < r_-$ and follows an outgoing trajectory. The red line represents the outgoing motion up to the first black triangle, which signifies the point where $\dot{r} = 0$. The second segment of the red line corresponds to an ingoing trajectory. The orange line represents Alice's outgoing trajectory inside of the trapped region. The first segment of the blue line corresponds to an ingoing geodesic up to the black triangle, and the second segment describes an outgoing geodesic. (b) The solid black line illustrates the evolution of Alice's radial velocity $\dot{r}$ as a function of her proper time, and the dashed line the evolution of $-\sqrt{-f}$ during the outgoing motion of Alice inside of the trapped region [indicated by the orange segment in (a)]. We note that the beginning and end of Alice's outgoing trajectory correspond to the points where her radial velocity equals the maximum possible value $\dot{r} = -\sqrt{-f}$.

Eq. (34), and $\dot{r}$ is negative at each crossing. Close to both horizons $f(v, r) \simeq 0$, and thus we can expand her ingoing trajectory [Eq. (34)] and measured energy density [Eq. (40)] as follows:

$$\dot{v}|_{r_\pm} = -\frac{1}{2\dot{r}} + \frac{f}{8\dot{r}^3} + \mathcal{O}(f^2), \tag{41}$$

$$\rho_A|_{r_\pm} = \left[\frac{1}{8\pi r^2}\left(1 - r\partial_r f - \frac{r}{4\dot{r}^2}\partial_v f\right)\right]\Bigg|_{r_\pm} + \mathcal{O}(f). \tag{42}$$

Using Eqs. (41) and (42), we can confirm that Alice observes a finite energy density when crossing the horizons, although the specific values will depend on their degeneracy, see Eqs. (43)–(46). Therefore, unlike nongeodesic observers, Alice does not experience any firewalls (in the sense of a diverging energy density) on her ingoing geodesic. When she is traveling in the vicinity of a nondegenerate inner horizon [$a = 1$], we find that

$$\rho_A|_{r_-}^{\text{nondeg}} = \frac{4\dot{r}^2 - g(v, r_-)r_-(r_- - r_+)^b(4\dot{r}^2 - r'_-)}{32\pi\dot{r}^2 r_-^2} + \mathcal{O}(r - r_-), \tag{43}$$

whereas for a degenerate inner horizon [$a > 1$]

$$\rho_A|_{r_-}^{\text{deg}} = \frac{1}{8\pi r_-^2} - \frac{r - r_-}{8\pi r_-^3} + \mathcal{O}(r - r_-)^2, \tag{44}$$

which is independent of the outer horizon degeneracy b. Similarly, we can calculate the relevant expressions when Alice travels near the vicinity of the outer horizon. For the nondegenerate case [$b = 1$], we obtain

$$\rho_A|_{r_+}^{\text{nondeg}} = \frac{4\dot{r}^2 - g(v, r_+)r_+(r_+ - r_-)^a(4\dot{r}^2 - r'_+)}{32\pi\dot{r}^2 r_+^2} + \mathcal{O}(r - r_+), \tag{45}$$

while in the degenerate case [$b > 1$]

$$\rho_A|_{r_+}^{\text{deg}} = \frac{1}{8\pi r_+^2} - \frac{r - r_+}{8\pi r_+^3} + \mathcal{O}(r - r_+)^2. \tag{46}$$

Again, we demonstrate the physical implications of these results based on the dynamical inner-extremal model described by Eqs. (10)–(12). From Eq. (42), or, equivalently, from Eqs. (44) and (45) [recall that $a = 3$ and $b = 1$ in this model], we find that the energy density Alice observes at the degenerate inner horizon is given by

$$\rho_A|_{r_-}^{a=3} = \frac{1}{8\pi r_-^2}, \tag{47}$$

which is positive, while at the nondegenerate outer horizon we obtain the more intricate expression

$$\rho_A|_{r_+}^{b=1} = \frac{4\dot{r}^2 r_-(r_-^2 - 2r_-r_+ + 3r_+^2) + (r_+ - r_-)^3 r'_+}{32\pi\dot{r}^2 r_+^3(r_+^2 + r_-^2)}. \tag{48}$$

Figure 5 represents the energy density Alice records throughout her journey. A negative energy density is observed close to the outer apparent horizon in agreement

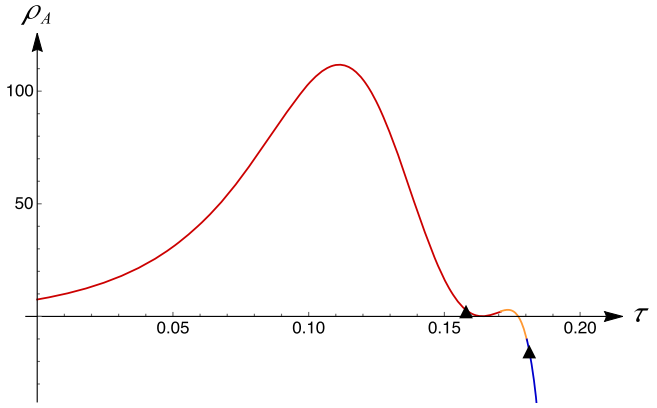

FIG. 5. Energy density measured by a moving observer Alice throughout her trajectory as a function of her proper time. The red, orange, and blue lines as well as the two points indicated by black triangles have the same physical meaning as in Fig. 4(a).

with the presence of an NEC-violating region, cf. Table I. In consonance with the results obtained in Sec. III B, we conclude that—in the evolution of evaporating RBHs—quantum effects are more pronounced near the outer apparent horizon and toward the final stages of the evaporation process. The absence of firewalls, i.e. the fact that the energy density observed by Alice upon crossing the horizons on her geodesic trajectory is always finite and never divergent, is a universal result due to the uniqueness of the horizon crossing scenario (there is no other way of crossing the horizon). Lastly, we note that at the disappearance point $v = v_{\rm d}$ of the trapped region $[r_-(v_{\rm d}) \equiv r_+(v_{\rm d})]$, the expressions derived in Eqs. (47) and (48) coincide. While this is of course expected from self-consistency requirements, it can also be understood as an observable consequence of the transition from $k = 0$ to $k = 1$ PBH solutions, with the energy density taking on its appropriate value for the extremal case [8]. This will be explained further in the next section.

V. TRANSITION FROM $k = 0$ TO $k = 1$

With the assumptions of regularity and finite-time horizon formation (as described at the end of Sec. II), the semiclassical Einstein equations admit only two distinct classes of dynamical spherically symmetric black hole solutions, which are distinguished by the scaling behavior $\sim f^k$ [cf. Eq. (2)] of their effective EMT components close to the horizon. The only self-consistent values are $k \in \{0, 1\}$ [52,73]. Hence, the two classes are typically referred to as $k = 0$ and $k = 1$ solutions. In addition to evaporating black holes $[r_g' < 0]$, each class also includes accreting white hole solutions $[r_g' > 0]$. A detailed exposition of the two classes of solutions is provided in Chapter 2 of Ref. [8], and a brief overview is given in Table I of Ref. [74]. Explicit relations for $k = 0$ solutions in different coordinate systems can be found in Ref. [75].

A straightforward way to determine which class of solutions a particular metric belongs to is the value of the linear coefficient $w_1(v)$ of its corresponding MS mass [cf. Eq. (3)]: metrics with $w_1(v) < 1$ belong to the $k = 0$ class, whereas metrics in the $k = 1$ class have $w_1(v) = 1$.

Rearranging Eq. (2), we can write

$$C(v, r) = r(1 - f(v, r)). \tag{49}$$

By comparison with the series expansion of Eq. (3), we note that $w_1(v) = \partial_r C|_{r_+}$. Using Eq. (49) in combination with the metric function Eq. (7) describing generic dynamical RBHs, it is easy to confirm that $w_1(v) = 1 \ \forall \ v \in [v_{\rm f}, v_{\rm d}]$ when the outer horizon is degenerate $[b > 1]$. On the other hand, if the outer horizon is nondegenerate $[b = 1]$, the linear coefficient of the MS mass is given by

$$w_1(v)|_{r_+} = 1 - g(v, r_+) r_+ (r_+ - r_-)^a < 1, \tag{50}$$

which is strictly smaller than one $\forall \ v \in (v_{\rm f}, v_{\rm d})$ since $r_+ > r_- > 0$ by construction and $g(v, r)$ is positive (see Sec. II). Recall that at the instants of formation $v = v_{\rm f}$ and disappearance $v = v_{\rm d}$ of the trapped region, the inner and outer horizon (e)merge, i.e. $r_-(v_{\rm f|d}) \equiv r_+(v_{\rm f|d})$. From Eq. (50), we see that in this case $w_1(v_{\rm f|d}) = 1$. In this sense, the value of the linear coefficient of the MS mass $w_1(v)$ indicates the transition from a $k = 1$ to a $k = 0$ solution at the formation of the trapped region $[w_1(v_{\rm f}) = 1 \to w_1(v > v_{\rm f}) < 1]$, and similarly the transition from a $k = 0$ to a $k = 1$ solution at the disappearance of the trapped region $[w_1(v < v_{\rm d}) < 1 \to w_1(v_{\rm d}) = 1]$.

Figure 6 illustrates the evolution of $w_1(v)$ for the dynamical inner-extremal RBH model described by Eqs. (10)–(12). During the evaporation of the RBH, the value of $w_1(v)$ initially starts to decrease from its initial value $w_1(v_{\rm f}) = 1$ at the instant of formation. At some point in the evaporation process, it reaches a minimum value

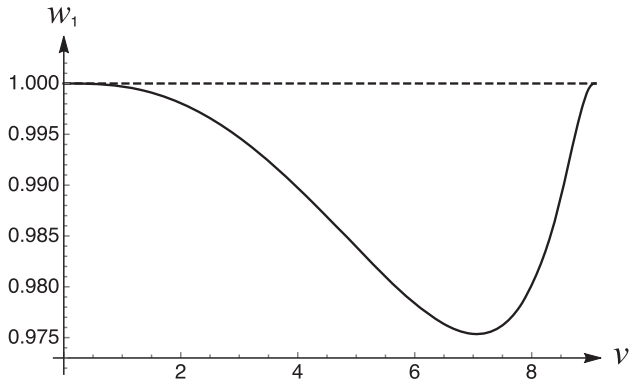

FIG. 6. Evolution of the linear coefficient of the MS mass $w_1(v)$ from the instant of formation of the trapped region at $v_{\rm f} = 0$ until its complete evaporation at $v_{\rm d} \approx 8.8$.

$w_1(v_m) \approx 0.975$ at $v_m \approx 7.15$. It then increases until the complete evaporation of the RBH at $w_1(v_\mathrm{d}) = 1$.

Apart from its role in modeling the transition between the two classes of dynamical PBH solutions in spherical symmetry, the linear coefficient of the MS mass $w_1(v)$ is of immediate relevance in the thermodynamic description of RBHs. In fact, it fully specifies the relevant work terms in the generalized dynamical first law of black hole mechanics [see Eq. (22) in Ref. [44]]. A more comprehensive discussion of its role in black hole thermodynamics and specifically the first law of black hole mechanics is provided in Ref. [44].

To illustrate the connection with our results from Sec. IV, we note that the Kodama surface gravity at the horizon is given by

$$\kappa_K|_{r_\pm} = \frac{1}{2}\partial_r f\Big|_{r_\pm}, \tag{51}$$

which depends on the linear coefficient $w_1(v)$ of the MS mass due to the relations prescribed by Eqs. (2) and (3). In conjunction with Eq. (22), this allows us to rewrite the energy density measured by a moving observer [cf. Eq. (42)] as

$$\rho_A|_{r_\pm} = \left(\frac{1}{8\pi r^2} - \frac{\kappa_K}{4\pi r} + \frac{T_{\mu\nu}\ell^\mu\ell^\nu}{4i^2}\right)\Big|_{r_\pm} + \mathcal{O}(f). \tag{52}$$

At the outer horizon, the Kodama surface gravity is given by

$$\kappa_K|_{r_+} = \frac{1 - w_1(v)}{2r_+(v)}. \tag{53}$$

Due to the transition to a $k = 1$ solution at the disappearance point $v = v_\mathrm{d}$ with $w_1(v_\mathrm{d}) = 1$, the Kodama surface gravity is zero when the evaporation process terminates. If we interpret the Kodama surface gravity as an effective temperature parameter, as is standard practice in black hole thermodynamics [76], this implies that the remnant is a cold remnant with zero temperature. Our analysis therefore confirms the previously obtained result that RBHs end their life as cold remnants [77] and demonstrates directly observable (at least in principle) physical consequences.

VI. CONCLUSIONS

Starting from the general metric function that describes generic spherically symmetric dynamical RBHs in semiclassical gravity [Sec. II, Eq. (7); see also Fig. 1] we derive their kinematic properties and analyze the behavior of the NEC in the vicinity of their horizons. Specifically, we find that the NEC is violated in the vicinity of the outer horizon and satisfied in the vicinity of the inner horizon, which implies that the trapped spacetime region (as determined from the behavior of null geodesic congruences) is effectively separated into an NEC-violating and an NEC-nonviolating domain by a hypersurface situated between the two horizons [Sec. III B, Table I and Fig. 3].

In addition, we demonstrate that there is a unique way for massive observers and particles to escape the trapped region on a geodesic trajectory, whereby crossing the horizon is only possible on an ingoing trajectory. This result has two rather pleasant side effects, namely (i) the absence of firewalls (energy densities measured by the geodesic observer do not diverge); and (ii) by virtue of particles (and thus any information content associated with their existence on the manifold) being able to escape the trapped spacetime region, a natural resolution to the information loss paradox [Sec. IV, Figs. 4 and 5].

The presence of spacetime regions where the NEC is violated and the energy density is negative is inherently linked to the quantum effects underlying the evaporation of black holes. Our results suggest that, at least for dynamical RBHs, these effects are more dominant near the outer horizon and become more pronounced toward the final stages of the evaporation process [Sec. III, Fig. 2].

The formation and disappearance of the trapped spacetime region are associated with a transition between the only two self-consistent classes of dynamical semiclassical black hole solutions in spherical symmetry. We show that the value of the linear coefficient of the MS mass can be used to distinguish the two classes of solutions and model the transition, and comment on implications for the thermodynamic description of RBHs [Sec. V, Fig. 6].

While keeping our analysis as generic as possible, we highlight the importance of the degeneracy of the inner horizon (e.g. in curing mass inflation instabilities) and nondegeneracy of the outer horizon (e.g. in ensuring a nonzero Kodama surface gravity) where it is physically relevant. Throughout the article, we illustrate relevant features based on the dynamical generalization of the inner-extremal RBH model [Sec. II, Eqs. (10)–(12); see also Ref. [41]]. Although our considerations here focus on spherically symmetric dynamical RBHs, realistic dark UCOs possess angular momentum, and modeling the emission of gravitational waves requires at least a (mass) quadrupole moment that cannot be captured in spherically symmetric settings. On this account, it will be interesting to extend the present analysis to nonsingular axially symmetric black hole spacetimes to confirm whether or not they exhibit similar physical features, and investigate what (if anything) can be learned about nonsingular black holes from the observed emission spectra of gravitational waves (e.g. the extraction of upper bounds on the minimal length scale l).

ACKNOWLEDGMENTS

We would like to thank Valentin Boyanov, Daniel Grumiller, Yasha Neiman, and Daniel Terno for helpful comments. S. M. is supported by the Quantum Gravity Unit of the Okinawa Institute of Science and Technology

(OIST). I. S. is supported by an International Macquarie University Research Excellence Scholarship (IMQRES).

APPENDIX A: DERIVATION OF THE COEFFICIENTS IN THE METRIC FUNCTION OF THE INNER-EXTREMAL REGULAR BLACK HOLE MODEL [EQS. (10)–(12)]

Here, we explicitly (re)derive the metric functions Eqs. (10)–(12) of the dynamical generalization of the inner-extremal RBH model [41] and elaborate on the physical intuition for the underlying assumptions. Our starting point is Eq. (2.9) of Ref. [41], which specifies the inner [$a = 3$] and outer horizon [$b = 1$] degeneracies, i.e. [cf. Eq. (7)]

$$f(v,r) = g(v,r)(r-r_-)^3(r-r_+), \tag{A1}$$

as well as the polynomial decomposition of $g(v,r)$ as a function of the radial coordinate r, namely

$$g(v,r) = \frac{1}{c_0 + c_1 r + c_2 r^2 + c_3 r^3 + c_4 r^4}, \tag{A2}$$

where explicit dependencies on the advanced null coordinate v have been omitted here and in what follows unless they add mathematically relevant context. The more explicit form given in Eq. (11) is obtained by demanding that g satisfy several requirements: first, we note that it is usually assumed that f and $1/g$ are polynomials of the same degree in r [33]. Otherwise it would be impossible to recover the Vaidya form of the metric $f = 1 - r_+/r$ in the asymptotic limit $r \to \infty$. With respect to Eq. (A2), the choice $a = 3$ and $b = 1$ then implies that higher-order powers $r > 4$ in the denominator of g are not permissible. Substituting Eq. (A2) into Eq. (A1) and dividing by r^4, we obtain

$$f(v,r) = \frac{(1-\frac{r_-}{r})^3(1-\frac{r_+}{r})}{\frac{c_0}{r^4} + \frac{c_1}{r^3} + \frac{c_2}{r^2} + \frac{c_3}{r} + c_4}. \tag{A3}$$

Performing a Taylor expansion about the point $z := \frac{1}{r} = 0$ to represent the limit $r \to \infty$ leads to the expression

$$f(v,r)|_{z=0} = \frac{1}{c_4} - \left(\frac{c_3 + 3c_4 r_- + c_4 r_+}{c_4^2}\right)\frac{1}{r} + \mathcal{O}\left(\frac{1}{r^2}\right). \tag{A4}$$

Therefore, to recover the Vaidya form of the metric in the asymptotic limit, we must have

$$c_4 = 1, \tag{A5}$$

$$r_+ = \frac{c_3 + 3c_4 r_- + c_4 r_+}{c_4^2} \Rightarrow c_3 = -3r_-, \tag{A6}$$

where Eq. (A5) was used to obtain the rightmost equality in Eq. (A6). Another requirement for nonsingular black holes is that their center be devoid of singularities (as implied by their name). Mathematically, this regularity manifests itself through the nondivergence of spacetime curvature at $r = 0$, which can be tracked by evaluating the relevant curvature scalars. Performing a series expansion of the Ricci scalar $R := g^{\mu\nu}R_{\mu\nu}$ about this point results in

$$R = (1 - g(v,0)r_-^3 r_+)\frac{2}{r^2} + \Big[g(v,0)(r_- + 3r_+) - r_- r_+ (\partial_r g)|_{r=0}\Big]\frac{6r_-^2}{r} + \mathcal{O}(r^0). \tag{A7}$$

To avoid divergences at the center, the coefficients of the first two terms of this expansion must vanish. Consequently, the regularity requirement prescribes the following expressions for the two lowest-order coefficients[6] of the polynomial $1/g(v,r)$:

$$g(v,0) = \frac{1}{r_-^3 r_+} \Rightarrow c_0 = r_-^3 r_+, \tag{A8}$$

$$(\partial_r g)|_{r=0} = \frac{r_- + 3r_+}{r_-^4 r_+^2} \Rightarrow c_1 = -r_-^2(r_- + 3r_+). \tag{A9}$$

Additionally, to avoid divergences in $f(v,r)$, the equation $D(v,r) := 1/g(v,r) = 0$ must not have real solutions [cf. Eq. (A1)]. This allows us to determine the remaining coefficient c_2. Substituting Eqs. (A5), (A6), (A8), and (A9) into Eq. (A2) yields

$$D(v,r) = r_-^3 r_+ - r_-^2(r_- + 3r_+)r + c_2 r^2 - 3r_- r^3 + r^4. \tag{A10}$$

This expression can be rewritten as

$$D(v,r) = r^2\left(r - \frac{3r_-}{2}\right)^2 + \left(c_2 - \frac{15}{4}r_-^2 - \frac{9}{4}r_- r_+ - \frac{r_-^3}{4r_+}\right) + r_-^3 r_+\left[1 - \frac{1}{2}r\left(\frac{3}{r_-} + \frac{1}{r_+}\right)\right]^2. \tag{A11}$$

Since the first and the third term are non-negative and they cannot be zero simultaneously, it suffices to require that the second term be non-negative, i.e.

$$c_2 - \frac{15}{4}r_-^2 - \frac{9}{4}r_- r_+ - \frac{r_-^3}{4r_+} \geq 0, \tag{A12}$$

to ensure that the denominator $D(v,r)$ has no real roots. This non-strict inequality guarantees the positivity of the function $g(v,r)$. We can rewrite Eq. (A12) as

[6]Note that the same result can be obtained by evaluating other scalar curvature invariants, e.g. the Kretschmann scalar $K := R_{\mu\nu\rho\sigma}R^{\mu\nu\rho\sigma}$.

$$c_2 = \tilde{c}_2 + \frac{15}{4} r_-^2 + \frac{9}{4} r_- r_+ + \frac{r_-^3}{4 r_+} \tag{A13}$$

for some $\tilde{c}_2 \geq 0$, which corresponds to the expression in Eq. (12). A more explicit form can be obtained from the requirement that the MS mass $C(v,r)/2$ be positive near the black hole center. From the expansion of $C(v,r)$ about $r = 0$,

$$C(v,r) = \frac{c_2 - 3r_-^2 - 3r_- r_+}{r_-^3 r_+} r^3 + \mathcal{O}(r^4), \tag{A14}$$

it then follows that $c_2 > 3r_-^2 + 3r_- r_+$, which implies that the coefficient c_2 can be written as

$$c_2 = 3r_-^2 + 3r_- r_+ + \gamma_2, \ \gamma_2 > 0. \tag{A15}$$

The smallest possible length scale is given by r_-, which is a plausible choice, although not unique. We use this particular choice in our numerical calculations throughout the paper. In combination with Eq. (A13), it leads to the expression

$$\tilde{c}_2 = \frac{r_-}{4 r_+} (3r_+^2 + r_- r_+ - r_-^2). \tag{A16}$$

APPENDIX B: ENERGY-MOMENTUM TENSOR COMPONENTS IN THE ORTHONORMAL FRAME

The EMT components $T_{\mu\nu}$ associated with the general spherically symmetric metric of Eq. (1) are specified through the following relations:

$$T_{00} = \frac{e^{h_+}}{8\pi r^2} (-e^{h_+} f(-1 + f + r\partial_r f) - r\partial_v f), \tag{B1}$$

$$T_{01} = \frac{e^{h_+}}{8\pi r^2} (-1 + f + r\partial_r f), \tag{B2}$$

$$T_{11} = \frac{1}{4\pi r} \partial_r h_+. \tag{B3}$$

To obtain the relevant expressions needed for our calculation in Sec. III A, we first write the orthonormal tetrad vectors

$$e^\mu_{\hat{0}} = (e^{-h_+} f^{-1/2}, 0, 0, 0), \tag{B4}$$

$$e^\mu_{\hat{1}} = (e^{-h_+} f^{-1/2}, f^{1/2}, 0, 0), \tag{B5}$$

$$e^\mu_{\hat{2}} = \left(0, 0, \frac{1}{r}, 0\right), \qquad e^\mu_{\hat{3}} = \left(0, 0, \frac{1}{r \sin\theta}, 0\right). \tag{B6}$$

To obtain explicit expressions for the orthonormal EMT components from those given in Eqs. (B1)–(B3), we use the transformation

$$T_{\hat{a}\hat{b}} = e^\mu_{\hat{a}} e^\nu_{\hat{b}} T_{\mu\nu}. \tag{B7}$$

The resulting orthonormal EMT components are

$$T_{\hat{0}\hat{0}} = -\frac{f(-1 + f + r\partial_r f) + e^{-h_+} r\partial_v f}{8\pi r^2 f}, \tag{B8}$$

$$T_{\hat{0}\hat{1}} = -\frac{e^{-h_+} \partial_v f}{8\pi r f}, \tag{B9}$$

$$T_{\hat{1}\hat{1}} = -\frac{-f[-1 + r\partial_r f + f(1 + 2r(\partial_r h_+))] + e^{-h_+} r\partial_v f}{8\pi r^2 f}, \tag{B10}$$

$$T_{\hat{2}\hat{2}} = T_{\hat{3}\hat{3}} = \frac{1}{16\pi r} \Big[\partial_r f (2 + 3r\partial_r h_+) + 2f[\partial_r h_+ + r(\partial_r h_+)^2 + r(\partial_r^2 h_+)] + r(\partial_r^2 f + 2e^{-h_+} \partial_r \partial_v h_+) \Big]. \tag{B11}$$

[1] M. Visser, Proc. Sci. BHs GRandStrings 2008 (**2008**) 001.
[2] S. W. Hawking, arXiv:1401.5761.
[3] V. P. Frolov, arXiv:1411.6981.
[4] V. Baccetti, R. B. Mann, and D. R. Terno, Int. J. Mod. Phys. D **26**, 1743008 (2017).
[5] V. Cardoso and P. Pani, Living Rev. Relativity **22**, 4 (2019).
[6] S. Murk, Int. J. Mod. Phys. D **32**, 2342012 (2023).
[7] M. Visser, Phys. Rev. D **90**, 127502 (2014).
[8] R. B. Mann, S. Murk, and D. R. Terno, Int. J. Mod. Phys. D **31**, 2230015 (2022).
[9] R. Penrose, Phys. Rev. Lett. **14**, 57 (1965).
[10] K. S. Thorne, The general-relativistic theory of stellar structure and dynamics, in *Proceedings of the International School of Physics "Enrico Fermi", Course XXXV, at Varenna, Italy, 1965*, edited by L. Gratton (Academic Press, New York, 1966), p. 273.
[11] D. Harlow, Rev. Mod. Phys. **88**, 015002 (2016).
[12] R. M. Wald, Living Rev. Relativity **4**, 6 (2001).
[13] D. N. Page, Phys. Rev. Lett. **71**, 3743 (1993).
[14] D. N. Page, J. Cosmol. Astropart. Phys. 09 (2013) 028.

[15] J. Bekenstein, Lett. Nuovo Cimento **4**, 737 (1972).
[16] J. Bekenstein, Phys. Rev. D **7**, 2333 (1973).
[17] J. Bekenstein, Phys. Rev. D **9**, 3292 (1974).
[18] S. W. Hawking, Nature (London) **248**, 30 (1974).
[19] S. W. Hawking, Commun. Math. Phys. **43**, 199 (1975).
[20] S. W. Hawking, Phys. Rev. D **13**, 191 (1976).
[21] M. Cadoni, M. Oi, and A. P. Sanna, J. High Energy Phys. 06 (2023) 211.
[22] P. O. Mazur and E. Mottola, Proc. Natl. Acad. Sci. U.S.A. **101**, 9545 (2004).
[23] P. O. Mazur and E. Mottola, Universe **9**, 88 (2023).
[24] H. G. Ellis, J. Math. Phys. (N.Y.) **14**, 104 (1973).
[25] M. S. Morris and K. S. Thorne, Am. J. Phys. **56**, 395 (1988).
[26] A. Simpson and M. Visser, J. Cosmol. Astropart. Phys. 02 (2019) 042.
[27] O. Lunin and S. D. Mathur, Nucl. Phys. **B623**, 342 (2002).
[28] S. D. Mathur, Fortschr. Phys. **53**, 793 (2005).
[29] J. M. Bardeen in *Proceedings of the International Conference GR5* (Tbilisi University Press, Tbilisi, 1968).
[30] I. Dymnikova, Gen. Relativ. Gravit. **24**, 235 (1992).
[31] S. A. Hayward, Phys. Rev. Lett. **96**, 031103 (2006).
[32] *Regular Black Holes: Towards a New Paradigm of Gravitational Collapse*, edited by C. Bambi (Springer, Singapore, 2023).
[33] V. P. Frolov, Phys. Rev. D **94**, 104056 (2016).
[34] M. Cadoni, M. De Laurentis, I. De Martino, R. Della Monica, M. Oi, and A. P. Sanna, Phys. Rev. D **107**, 044038 (2023).
[35] E. Poisson and W. Israel, Phys. Rev. Lett. **63**, 1663 (1989).
[36] E. Poisson and W. Israel, Phys. Rev. D **41**, 1796 (1990).
[37] A. Ori, Phys. Rev. Lett. **67**, 789 (1991).
[38] A. J. S. Hamilton and P. P. Avelino, Phys. Rep. **495**, 1 (2010).
[39] R. Carballo-Rubio, F. Di Filippo, S. Liberati, C. Pacilio, and M. Visser, J. High Energy Phys. 05 (2021) 132.
[40] P. K. Dahal, S. Murk, and D. R. Terno, AVS Quantum Sci. **4**, 015606 (2022).
[41] R. Carballo-Rubio, F. Di Filippo, S. Liberati, C. Pacilio, and M. Visser, J. High Energy Phys. 09 (2022) 118.
[42] T. McMaken, Phys. Rev. D **107**, 125023 (2023).
[43] C. W. Misner and D. H. Sharp, Phys. Rev. **136**, B571 (1964).
[44] S. Murk and I. Soranidis, Phys. Rev. D **108**, 044002 (2023).
[45] S. A. Hayward, Phys. Rev. D **49**, 6467 (1994).
[46] A. B. Nielsen and J. H. Yoon, Classical Quantum Gravity **25**, 085010 (2008).
[47] B. Cropp, S. Liberati, and M. Visser, Classical Quantum Gravity **30**, 125001 (2013).
[48] C. Barceló, S. Liberati, S. Sonego, and M. Visser, Phys. Rev. D **83**, 041501(R) (2011).
[49] H. Kodama, Prog. Theor. Phys. **63**, 1217 (1980).
[50] G. Abreu and M. Visser, Phys. Rev. D **82**, 044027 (2010).
[51] F. Kurpicz, N. Pinamonti, and R. Verch, Lett. Math. Phys. **111**, 110 (2021).
[52] S. Murk and D. R. Terno, Phys. Rev. D **103**, 064082 (2021).
[53] S. Murk and D. R. Terno, *The Sixteenth Marcel Grossmann Meeting* (World Scientific, Singapore, 2023), pp. 1196–1211, 10.1142/9789811269776_0095.
[54] R. B. Mann, S. Murk, and D. R. Terno, Phys. Rev. D **105**, 124032 (2022).
[55] P. K. Dahal, I. Soranidis, and D. R. Terno, Phys. Rev. D **106**, 124048 (2022).
[56] S. W. Hawking and G. F. R. Ellis, *The Large Scale Structure of Space-Time* (Cambridge University Press, Cambridge, England, 1973), Chap. 4.3, Chap. 9.2.
[57] P. Martín-Moruno and M. Visser, Classical Quantum Gravity **35**, 125003 (2018).
[58] P. Martín-Moruno and M. Visser, Phys. Rev. D **103**, 124003 (2021).
[59] H. Maeda, Gen. Relativ. Gravit. **53**, 90 (2021).
[60] L. Rezzolla and O. Zanotti, *Relativistic Hydrodynamics* (Oxford University Press, New York, 2013).
[61] N. Andersson and G. L. Comer, Living Rev. Relativity **24**, 3 (2021).
[62] T. A. Roman, Phys. Rev. D **33**, 3526 (1986).
[63] P. Martín-Moruno and M. Visser, J. High Energy Phys. 09 (2013) 050.
[64] P. Binétruy, A. Helou, and F. Lamy, Phys. Rev. D **98**, 064058 (2018).
[65] V. Baccetti, R. B. Mann, S. Murk, and D. R. Terno, Phys. Rev. D **99**, 124014 (2019).
[66] E. A. Kontou and K. Sanders, Classical Quantum Gravity **37**, 193001 (2020).
[67] M. Visser, Phys. Rev. D **56**, 936 (1997).
[68] V. P. Frolov and I. D. Novikov, *Black Holes: Basic Concepts and New Developments* (Kluwer, Dordrecht, 1998).
[69] A. Levi and A. Ori, Phys. Rev. Lett. **117**, 231101 (2016).
[70] M. Visser, Int. J. Mod. Phys. D **12**, 649 (2003).
[71] C. Misner, K. Thorne, and J. A. Wheeler, *Gravitation* (Princeton University Press, Princeton, NJ, 1973).
[72] M. Blau, Lecture Notes on General Relativity (2023), http://www.blau.itp.unibe.ch/newlecturesGR.pdf.
[73] D. R. Terno, Phys. Rev. D **101**, 124053 (2020).
[74] S. Murk, Phys. Rev. D **105**, 044051 (2022).
[75] P. K. Dahal, F. Simovic, I. Soranidis, and D. R. Terno, Phys. Rev. D **108**, 104014 (2023).
[76] S. A. Hayward, Classical Quantum Gravity **15**, 3147 (1998).
[77] M. Cadoni, M. Oi, and A. P. Sanna, Phys. Rev. D **106**, 024030 (2022).

JOURNAL ARTICLE

Regular black holes and the first law of black hole mechanics

Brief summary

After analyzing the kinematic and energetic properties of RBHs in a dynamic setting, we move on to the final paper in this thesis, which focuses on the study of thermodynamics in such a dynamic context. We establish the presence of a first law of black hole thermodynamics based on near-horizon quantities and demonstrate that the internal energy is represented by the Misner-Sharp mass evaluated at the outer apparent horizon. Additionally, we show the existence of pressure terms arising from the presence of the minimal length scale, or equivalently, from the regularization of spacetime.

Conventions

In this article, r_g represents the Schwarzschild radius, or more accurately, a dynamical generalization of it, defined as $r_g = 2M(v)$.

Authorship statement

Conceptualization of the research project and calculations for its development. Also contributed to the planning and writing of the article, interpretation of its results, proofreading, and revisions. Principal contributor to Sections III and IV.

Regular black holes and the first law of black hole mechanics

Sebastian Murk[1,*] and Ioannis Soranidis[2,†]

[1]*Okinawa Institute of Science and Technology, 1919-1 Tancha, Onna-son, Okinawa 904-0495, Japan*
[2]*School of Mathematical and Physical Sciences, Macquarie University, Sydney, New South Wales 2109, Australia*

(Received 13 April 2023; accepted 6 July 2023; published 1 August 2023)

Singularity-free regular black holes are a popular alternative to the singular mathematical black holes predicted by general relativity. Here, we derive a generic condition that spherically symmetric dynamical regular black holes must satisfy to be compatible with the first law of black hole mechanics based on an expression for the surface gravity at the outer horizon. We examine the dynamical generalizations of models typically considered in the literature and demonstrate that none of them satisfies the condition required for compatibility with the first law, suggesting that modifications are required to maintain its physical meaning. We show that the need for corrections is inherently linked to the introduction of a minimal length scale and can therefore be seen as a direct consequence of the spacetime regularization. We explicitly identify the additional work terms in the extended first law, comment on their thermodynamic interpretation, and show that the linear coefficient of the Misner-Sharp mass suffices to determine the relevant thermodynamic properties.

DOI: 10.1103/PhysRevD.108.044002

I. INTRODUCTION

In their 1973 milestone paper [1], Bardeen, Carter, and Hawking introduced four laws of black hole mechanics and elucidated close analogies with the four laws of thermodynamics. This important link connecting the two fields has since proven to be a powerful tool in advancing our understanding of black holes. In particular, the physical insights revealed in the rigorous mathematical derivation of the first law in the integral and differential formalism of Ref. [1] have provided strong motivation for further investigating their thermodynamic properties [2–7].

While the existence of dark massive ultracompact objects has been established beyond any reasonable doubt, the question of whether these objects are black holes is still open [8–13]. In the absence of a clear answer, singularity-free models of so-called regular black holes (RBHs) [14–16] have received much attention in recent years, as they provide a way to avoid the nontrivial causal structures inherent to the black holes predicted by general relativity (GR). Unlike the singular mathematical black holes of GR, which are bounded by globally defined and physically unobservable event horizons [17], RBH models are characterized by a separate inner (Cauchy) and outer (in the case of an evolving RBH spacetime quasilocal, e.g., apparent or trapping) horizon. Both the inner and outer horizon generally have a nonzero surface gravity. However, inner horizons with nonzero surface gravity are typically unstable under small perturbations, which gives rise to so-called mass inflation instabilities, i.e., exponential instabilities characterized by an exponential growth of the gravitational energy in a neighborhood of the inner horizon (as measured, for instance, by evaluating the Weyl scalar) [18–23]. Recently, a novel "inner-extremal" RBH model that cures the exponential instability by making the inner horizon surface gravity vanish, while maintaining the separation between the inner and outer horizon, and a nonzero surface gravity at the outer horizon, has been proposed [24].

It is important to note that the original 1973 paper considered stationary black holes [1]. While the mass loss of an evaporating black hole is usually ascribed to the emission of Hawking radiation [5,6], the backreaction of spacetime geometry is not accounted for in its derivation, which assumes that the underlying geometry is (at least asymptotically) stationary. This is a physically significant omission: if the backreaction from the Hawking flux is not ignored, variations between nearby equilibrium states are no longer accurately described by the first law.

To resolve this limitation and go beyond physically unrealistic stationary scenarios, the concept of a dynamical (and thus quasilocal) horizon has been developed [25–27]. It allows us to describe the geometry of an evolving black hole spacetime and has become an indispensable mathematical tool to accurately model dynamical processes such as the formation and possible evaporation of black holes, as well as to enable generalizations of the laws of black hole mechanics and their thermodynamic interpretation [25,28], including that of surface gravity as a temperature parameter.

*sebastian.murk@oist.jp
†ioannis.soranidis@hdr.mq.edu.au

In this article, we investigate the physical consequences of the first law of black hole mechanics for dynamical models of RBHs embedded in asymptotically flat spacetimes. We restrict our considerations to the case where the entropy scales with the area of the outer horizon.[1] Compared to the evolution of the Universe, the evaporation of black holes is considered to be a thermodynamically slow process [31]. Therefore, if the first law is true, then the behavior of dynamically evolving black holes should match that prescribed by the first law in the quasistatic limit. Based on this assertion, we derive a generic condition that RBHs must satisfy to be compatible with the first law by considering the surface gravity at the outer horizon. We explicitly test the dynamical generalizations of popular models such as those proposed by Bardeen [32] (Sec. IV C), Dymnikova [33] (Sec. IV D), Hayward [34] (Sec. IV B), the model considered in Ref. [35] (Sec. IV E) which produces the strongest possible corrections to the Schwarzschild geometry while still being compatible with its asymptotic behavior, and the aforementioned inner-extremal RBH model [24] (Sec. V). Our analysis shows that none of these models is compatible with the conventional form of the first law of black hole mechanics.

The remainder of this article is organized as follows: In Sec. II, we introduce mathematical concepts used in the construction of RBHs (Sec. II A) and review the first law of black hole mechanics and its relation to surface gravity (Sec. II B). In Sec. III, we derive a generic condition that dynamical black holes must satisfy to be compatible with the first law of black hole mechanics. Based on this compatibility condition, we test the dynamical generalizations of commonly considered RBH models and find that none of them satisfies the required relation (Sec. IV and Sec. V), suggesting that either these models do not conform to the first law or modifications of the first law are required to maintain its essence. In Sec. VI, we briefly outline the consequences of this result in the context of the so-called Page evaporation law. Lastly, we discuss the implications of our findings more generally and comment on possible directions for future research related to nonsingular black hole spacetimes (Sec. VII). Throughout this article, we use the metric signature $(-,+,+,+)$ and work in dimensionless units such that $c = G = \hbar = k_B = 1$.

II. MATHEMATICAL PREREQUISITES

A. Trapped regions and regular black holes

A general spherically symmetric metric in advanced null coordinates (v, r) is described by the line element

$$ds^2 = -e^{2h(v,r)}f(v,r)dv^2 + 2e^{h(v,r)}dvdr + r^2 d\Omega^2, \tag{1}$$

where $d\Omega^2 = d\theta^2 + \sin^2\theta d\phi^2$ denotes the line element of the 2-sphere. Since our argumentation in Sec. II B and Sec. III is based on the analysis of surface gravity at the outer horizon [i.e., at $r = r_+(v)$] and it is always possible to write the function $h(v, r)$ as a series with respect to the coordinate distance $r - r_+(v)$ from the outer horizon (see Ref. [36] for details),

$$h(v,r) = \sum_{i=1}^{\infty} \chi_i(v)(r - r_+(v))^i, \tag{2}$$

we can assume $h(v, r) = 0$ without loss of generality in what follows.[2] Generic dynamical models of RBHs are then described by the metric function

$$f(v,r) \coloneqq g(v,r)(r - r_-(v))^a (r - r_+(v))^b, \tag{3}$$

where $r_-(v)$ and $r_+(v)$ denote the inner and outer horizon, respectively, and $a, b \in \mathbb{N}_{>0} = \{1, 2, ...\}$ are positive integers labeling their degeneracy. In spherical symmetry, nonsingular black hole metrics possess an inner horizon due to the fact that the outer horizon (which is located close to the classical gravitational radius) cannot cross the center $r = 0$ without creating a curvature singularity [37]. The inner horizon is generated by the additional hair, i.e., the minimal length scale l that is introduced to regularize the spacetime [cf. Eqs. (32), (40), (45), and (50)] and possibly other parameters such as charge [cf. Eqs. (58) and (62)]. Constraints for the *a priori* undetermined function $g(v, r)$ are discussed in what follows.

The expansions of ingoing and outgoing radial null geodesic congruences are given by

$$\theta_- = -\frac{2}{r}, \qquad \theta_+ = \frac{f(v,r)}{r}, \tag{4}$$

respectively. The existence of a trapped spacetime region is contingent on the signature of their product $\theta_-\theta_+ \lesseqgtr 0$. We follow the widely used convention proposed in Ref. [38], according to which the presence of a trapped region bounded by the outer horizon r_+ is signified by $\theta_-\theta_+ > 0$ (i.e., the future-directed expansions of both ingoing and outgoing null geodesics are negative), and no trapped region is present for $\theta_-\theta_+ < 0$. Since θ_- is always negative, this implies that $f < 0$ inside of the trapped region $r \in (r_-, r_+)$, and $f > 0$ outside of the trapped region $r > r_+$, and thus $g > 0$ and b odd (otherwise g would have to be negative inside, but positive outside of the trapped region). The inner and outer horizon are identified as the roots of the equation $f = 0$ [39,40]. At the "disappearance point" of the trapped region $v = v_d$,

[1] Alternatives have been considered, for instance, in Refs. [29] and [30].

[2] Note also that $h = 0$ for all RBH models typically considered in the literature, including all of those examined explicitly in Secs. IV and V.

they coalesce, i.e., $r_-(v_d) \equiv r_+(v_d)$. From Eqs. (3) and (4), it then follows that

$$\theta_-\theta_+|_{v=v_d} = -\frac{2}{r^2} g(v_d, r)(r - r_+(v_d))^{a+b} \leq 0 \quad \forall\, r, \tag{5}$$

which implies that the sum $a + b$ must be even and thus a odd.

We note that the formation of a trapped spacetime region in finite time according to the clock of a distant observer inevitably requires a violation of the null energy condition (NEC) near the outer horizon [40–43], which posits that $T_{\mu\nu}\ell^\mu\ell^\nu \geq 0$, i.e., the contraction of the energy-momentum tensor with any future-directed null vector ℓ^μ is nonnegative. Similarly, violating the NEC is a prerequisite for the emission of Hawking radiation. While quantum effects are necessary, it is worth noting that Hawking radiation is a purely kinematical phenomenon [44], and neither the Einstein equations nor the Bekenstein entropy relation [2–4] are required for its derivation.

B. Surface gravity and the first law of black hole mechanics

The first law of black hole mechanics derived in Ref. [1] has been proven to hold in any theory of gravity arising from a diffeomorphism-invariant Lagrangian [45,46]. Assuming $\delta J = \delta Q = 0$, it can be stated mathematically as

$$\delta M = \frac{\kappa}{8\pi}\delta A, \tag{6}$$

where M, κ, and A denote the black hole's gravitational energy, surface gravity, and horizon area, respectively. The notion of gravitational energy within a sphere of radius r is captured by the so-called Misner-Sharp (MS) mass [47] $M \coloneqq C/2$ [see Eqs. (16) and (17)].[3] In spherically symmetric solutions of the Einstein equations, such as the static Schwarzschild[4] or the nonstatic Vaidya metric, $C(v, r_+) = 2M(v) = r_+(v)$. Using $A = 4\pi r_+^2$ for the horizon area, this leads to the famous expression for the surface gravity at the outer horizon:

$$\frac{\delta M}{\delta r_+} = \frac{\kappa}{8\pi}\frac{\delta A}{\delta r_+} \Rightarrow \kappa = \frac{1}{2r_+}. \tag{7}$$

It is important to note that the surface gravity κ is unambiguously defined only in stationary spacetimes, where it is related to the black hole's Hawking temperature T_H via $\kappa = 2\pi T_H$. Nonetheless, even in generic dynamical black hole spacetimes the first law and its associated expression for the surface gravity are expected to approach Eqs. (6) and (7) in the quasistatic limit due to the timescale of the evaporation process. We show here that this is not the case for the RBH models typically considered in the literature.

Generalizations of surface gravity to dynamical spacetimes [48,49] are generally related to either the affine peeling surface gravity [50] or the so-called Kodama surface gravity [28,51,52]. Since the peeling surface gravity is ill-defined for a transient object that forms in finite time of a distant observer [53–55], and there are strong arguments that Kodama surface gravity is the critical quantity with respect to Hawking radiation [28,55], we focus on this generalization of surface gravity in what follows.

The main difficulty in the generalization of surface gravity to evolving black hole spacetimes is that, unlike their stationary counterparts, they are not guaranteed to admit a timelike Killing vector field that generates the null hypersurface (known as Killing horizon) needed to define surface gravity. However, a dynamical notion of surface gravity can be defined at the (quasilocal) outer horizon using the Kodama vector field [51,52], which is well-defined even in nonstationary spherically symmetric spacetimes, and thus in some sense supersedes the concept of a Killing vector field.

At the outer horizon, the Kodama surface gravity κ_K is defined via

$$\kappa_K K_\nu =: \frac{1}{2} K^\mu(\nabla_\mu K_\nu - \nabla_\nu K_\mu), \tag{8}$$

where K^μ denotes the contravariant Kodama vector [51,52]. The Kodama vector field is conserved,

$$\nabla_\mu K^\mu = 0, \tag{9}$$

and generates a conserved current,

$$\nabla_\mu J^\mu = 0, \qquad J^\mu \coloneqq G^{\mu\nu}K_\nu, \tag{10}$$

for any symmetric rank-2 tensor $G_{\mu\nu} = G_{\nu\mu}$ that is invariant under the spherical symmetries of the spacetime. If $G_{\mu\nu}$ is the Einstein tensor, then the current's Noether charge is the MS mass.

III. DERIVATION OF THE COMPATIBILITY CONDITION

For the metric specified in Eq. (1) (recall that, as established in Sec. II A, we can use $h = 0$ without loss of generality), $K^\mu = (1, 0, 0, 0)$, and its only nonzero covariant component at the outer horizon is $K_r = 1$.

[3]While the MS mass is technically $C/2$ by virtue of its definition in Eq. (16), we often take the liberty to refer to C itself simply as the MS mass.

[4]Note that in the Schwarzschild solution, $M = \text{const}$ corresponds to the Arnowitt-Deser-Misner (ADM) mass, and the object's Schwarzschild radius r_g corresponds to the outer horizon, $r_g \equiv r_+ = 2M$.

Hence the Kodama surface gravity [cf. Eq. (8)] at the outer horizon is given by

$$\kappa_K|_{r=r_+} = \frac{1}{2}\partial_r f(v,r)\Big|_{r=r_+} \tag{11}$$

$$\overset{(3)}{=} \lim_{r\to r_+} \frac{(r-r_+)^{-1+b} b g(v,r)(r-r_-)^a}{2}, \tag{12}$$

which implies that a nonzero Kodama surface gravity at the outer horizon can be achieved only if the outer horizon is nondegenerate, i.e., $b = 1$. We thus focus on this scenario in what follows.

Assuming that $f(v,r)$ is decomposable as a rational function of the radial coordinate r, i.e.,

$$f(v,r) = \frac{\mathcal{P}_n(r)}{\tilde{\mathcal{P}}_n(r)}, \tag{13}$$

where $\mathcal{P}_n$ and $\tilde{\mathcal{P}}_n$ are polynomials (whose coefficients depend on v in generic dynamical spacetimes) of the same degree $n \geq 3$ in r as motivated in Ref. [37], we can write

$$g(v,r) = \frac{\sum_{z=0}^{m} \lambda_z r^z}{\sum_{i=0}^{n} c_i r^i}, \tag{14}$$

where the coefficients $\lambda_z \equiv \lambda_z(r_-, r_+)$ and $c_i \equiv c_i(r_-, r_+)$ depend explicitly only on $r_-(v)$ and $r_+(v)$ (and thus implicitly on v) as they are the only relevant length scales, and $n - m = a + 1$ and $\lambda_m/c_n = 1$ are required to recover the Vaidya form of the metric in the asymptotic limit $r \to \infty$. These considerations will prove useful in our analysis of the inner-extremal RBH model in Sec. V. We also note that—complemented by the assumptions of regularity of the spacetime at the origin $r = 0$ and a proper Schwarzschild/Vaidya form of the metric in the asymptotic limit—the polynomial decomposition of the metric function according to Eq. (13) immediately leads to a class of metric families of the form (see Ref. [37] for a detailed derivation)

$$f(v,r) = 1 - \frac{r_g(v) r^2}{r_g(v) l(v)^2 + c_1(v) r + c_2(v) r^2 + r^3}, \tag{15}$$

for the case $n = 3$, where $l(v)$ denotes the minimal length scale, $r_g(v) = 2M(v)$, and the case $c_1(v) = c_2(v) = 0$ corresponds to the dynamical Hayward metric of Eq. (34) considered in Sec. IV B.

The metric function f [cf. Eq. (3)] is usually defined in terms of the MS mass via

$$f(v,r) \coloneqq \partial_\mu r \partial^\mu r = 1 - \frac{C(v,r)}{r}, \tag{16}$$

with the MS mass given by

$$C(v,r) = r_+(v) + \sum_{i=1}^{\infty} w_i(v)(r - r_+(v))^i. \tag{17}$$

By means of Eq. (16), the Kodama surface gravity of Eq. (11) can then be expressed directly in terms of the MS mass as

$$\kappa_K|_{r=r_+} = \frac{1}{2r^2}[C(v,r) - r\partial_r C(v,r)]\Big|_{r=r_+} \overset{(17)}{=} \frac{1-w_1}{2r_+}, \tag{18}$$

where the rightmost expression is obtained by explicitly substituting the MS mass expansion of Eq. (17). Evaluation at the outer horizon yields

$$\delta M|_{r=r_+} = \frac{\delta C}{2}\Big|_{r=r_+} = \frac{1}{2}(1-w_1)\delta r_+. \tag{19}$$

Substituting the expression for the surface gravity on the rhs of Eq. (18) into the rhs of Eq. (6), we obtain

$$\delta M = \frac{1-w_1}{16\pi r_+}\delta A. \tag{20}$$

Subsequent substitution of Eq. (19) into Eq. (20) leads to

$$\delta\left(\frac{r_+}{2}\right) = \frac{1-w_1}{16\pi r_+}\delta A + \frac{w_1}{2}\delta r_+. \tag{21}$$

Using the relation $\delta A = 8\pi r_+ \delta r_+ = \frac{2}{r_+}\delta V$ between area $A = 4\pi r_+^2$ and volume $V = \frac{4}{3}\pi r_+^3$, we obtain

$$\delta\left(\frac{r_+}{2}\right) = \frac{1-w_1}{16\pi r_+}\delta A + \frac{w_1}{8\pi r_+^2}\delta V, \tag{22}$$

which is an extension of the standard form of the first law of black hole mechanics that includes an additional work term. The notion of internal/thermal energy is captured by the expression $r_+/2$, which corresponds to the MS mass $C/2$ evaluated at the outer horizon. However, this internal energy is not necessarily the same as the ADM mass when matter fields are present [56], as is the case for dynamically evolving black holes. Comparison with the traditional form of the first law of mechanics $\delta M = \frac{\kappa}{8\pi}\delta A - p\delta V$ [57] identifies the pressure p in terms of w_1, i.e.,

$$p = -\frac{w_1}{8\pi r_+^2}. \tag{23}$$

A few brief comments are in order: first, it is important to note that higher-order terms $i > 1$ in the MS mass expansion have not been neglected in this derivation, but rather, they simply do not enter the expression for the Kodama surface gravity of Eq. (18). Second, the conventional form of the first law of black hole mechanics [Eq. (6)] and its associated expression for the surface gravity $\kappa = 1/(2r_+)$ [cf. Eq. (7)] are attainable only if $w_1 = 0$, as can be seen from Eqs. (18) and (22). Therefore,

$$\boxed{w_1|_{r=r_+} = 0} \tag{24}$$

is a necessary condition to be compatible with the first law, i.e., the linear coefficient in the MS mass expansion w_1 [cf. Eq. (17)] must vanish at the outer horizon. Physically, this implies that the metric approximates the Vaidya solution near the outer horizon. Third, the expressions derived in Eqs. (18)–(24) apply generically to black holes described by a metric function of the form of Eq. (16). For RBHs described by a metric function of the form of Eq. (3), performing a series expansion of Eq. (17) about the outer horizon yields

$$w_1|_{r=r_+} = 1 - g(v, r_+) r_+ (r_+ - r_-)^a. \tag{25}$$

If the inner horizon is nondegenerate ($a = 1$), as is typically the case for the RBHs most commonly considered in the literature (e.g., those of Refs. [32–35] examined in Sec. IV), the compatibility condition prescribed by Eq. (24) can be evaluated straighforwardly from the expression derived in Eq. (25) by considering the series expansion of the MS mass about the outer horizon using Eq. (16) since the metric function f (and thus by extension g) is known explicitly. The case of a degenerate inner horizon ($a > 1$) is treated in Sec. V on the basis of the inner-extremal RBH model proposed in Ref. [24], where $\sum_z \lambda_z r^z = 1$ [cf. Eq. (14)]. In this case, the equation $f = 0$ has two positive real-valued solutions, and the smaller one which corresponds to the inner horizon is degenerate. If the outer horizon $r = r_+$ is a single root, then the inner horizon root $r = r_-$ has to be at least cubic in order for the inner horizon surface gravity to vanish, which plays a crucial role in preventing mass inflation instabilities and ensuring that the backreaction of perturbations vanishes asymptotically.

In the next two sections, we investigate whether the consistency condition Eq. (24) that is required to be compatible with the first law of black hole mechanics is satisfied by the RBH models typically considered in the literature. Since, as argued in Sec. I, dynamical models are necessary to accurately model the evolution of evaporating black holes, our analysis in Secs. II and III was designed to accommodate generic dynamical RBH models, and we consider the dynamical generalizations of popular models rather than their static counterparts in what follows. To be more precise, static RBH metrics belongs to a different class of black hole solutions whose effective energy-momentum-tensor component scaling behavior $\tau_{\mu\nu} \sim f^k$ close to the outer horizon is characterized by $k = 1$ as opposed to $k = 0$ (see chapter 2 in Ref. [36] for a detailed exposition of the two classes of admissible solutions in spherical symmetry, or Table 1 in Ref. [58] for a succinct overview). While the unique $k = 1$ solution describes black holes at the instant of their formation, they are described by a $k = 0$ solution for the remainder of their entire evolution or until their disappearance (e.g., through complete evaporation) [53]. The relation between the Kodama surface gravity at the outer horizon and the linear coefficient w_1 of the MS mass that we derived in Eq. (18) is valid for $k = 0$ solutions, which includes all dynamical models. However, it no longer applies (at least not in general) to static metrics such as the Reissner-Nordström solution briefly considered in Sec. IV F [cf. Eq. (54)].

While we strive to be as generic as possible in our analysis, recall that a nondegenerate outer horizon ($b = 1$) is necessary to allow for a nonzero Kodama surface gravity at the outer horizon [cf. Eq. (12)]. However, in Sec. V we do allow for the possibility that the inner horizon is degenerate ($a > 1$), as such models have been shown to exhibit interesting physical properties making it possible to evade the mass inflation problem that typically plagues RBHs (as detailed in Ref. [24]).

IV. TESTING REGULAR BLACK HOLES PART 1: MODELS WITH A NONDEGENERATE INNER HORIZON

In this section, we proceed by examining RBH models with a nondegenerate inner horizon ($a = 1$), including the proposals of Bardeen [32] (Sec. IV C), Dymnikova [33] (Sec. IV D), and Hayward [34] (Sec. IV B). We write explicit dependencies on v only once when specifying the metric function $f(v, r)$ for the generalized dynamical model and omit them thereafter for the sake of readability. However, we later reinstate the explicit dependencies in Sec. IV F for clarity.

A. A simple nonsingular "dynamical" spacetime

Arguably the simplest nonsingular dynamical spacetime one can construct based on Eq. (3) is given by the choice $a = b = 1$ and $\sum_z \lambda_z r^z = 1$ [cf. Eq. (14)], such that Eq. (3) can be written as

$$f(v, r) = g(v, r)(r - r_-(v))(r - r_+(v)), \tag{26}$$

and, by virtue of Eq. (13),

$$g(v, r) = \frac{1}{c_0 + c_1 r + c_2 r^2}, \tag{27}$$

where $c_2 = 1$ is necessary to recover the Vaidya form of the metric in the asymptotic limit. Regularity at the center $r = 0$ requires that

$$c_0 = r_- r_+, \qquad c_1 = -r_- - r_+, \tag{28}$$

as can be verified by evaluating the Ricci ($g_{\mu\nu} R^{\mu\nu}$) or the Kretschmann ($R_{\mu\nu\rho\sigma} R^{\mu\nu\rho\sigma}$) scalar. However, substitution of Eqs. (27) and (28) into Eq. (26) reveals that these coefficients lead to a trivial metric function,

$$f(v, r) = \frac{(r - r_-)(r - r_+)}{r_- r_+ - (r_- + r_+) r + r^2} = 1. \tag{29}$$

In other words, we have rediscovered flat Minkowski spacetime.

B. Hayward model

A nontrivial minimal RBH model that reduces to a de Sitter spacetime in the limit $r \to 0$ and a Schwarzschild/Vaidya spacetime in the limit $r \to \infty$ was proposed by Hayward in Ref. [34]. In this model, the metric is specified by the function

$$f(r) = 1 - \frac{r_g r^2}{r^3 + r_g l^2}, \tag{30}$$

where $l \geq 0$ represents a minimal length scale (which can be interpreted as an additional hair of the black hole) akin to a Planckian cutoff, $l = 0$ corresponds to the Schwarzschild solution, and $r_g = 2M$ denotes the black hole's Schwarzschild radius. The horizons are identified through the equation $f(r) = 0$ [39,40], which can be solved using Cardano's formula [59] and admits three real solutions, namely,

$$r_0 = -l + \frac{l^2}{2r_g} + \mathcal{O}(l^3) < 0, \tag{31}$$

$$r_- = l + \frac{l^2}{2r_g} + \mathcal{O}(l^3), \tag{32}$$

$$r_+ = r_g - \frac{l^2}{r_g} + \mathcal{O}(l^4). \tag{33}$$

Note that this is a necessary requirement in order for the metric function of Eq. (30) to describe a RBH, as one real and two complex solutions would imply that no inner horizon is present [40].

We can generalize this model to describe a dynamical RBH spacetime by allowing for an explicit dependence of r_g and l on v, i.e.,

$$f(v, r) = 1 - \frac{r_g(v) r^2}{r^3 + r_g(v) l(v)^2}. \tag{34}$$

Using the roots of $f(v, r) = 0$, this can be rewritten as

$$f(v, r) = \frac{r - r_0}{r^3 + r_g l^2}(r - r_-)(r - r_+). \tag{35}$$

By comparison with Eq. (3), we identify

$$g(v, r) = \frac{r - r_0}{r^3 + r_g l^2} > 0, \tag{36}$$

which is positive due to $r_0 < 0$. The MS mass $C(v, r)$ [cf. Eq. (17)] for the generalized dynamical Hayward model is specified by Eq. (34) through the relation given in Eq. (16). By considering its expansion about the outer horizon in the regime $l \ll 1$, we obtain the linear coefficient

$$w_1|_{r=r_+} \overset{(33)}{=} \frac{3l^2}{r_g^2} + \mathcal{O}(l^4) \geq 0. \tag{37}$$

This expression is zero only if $l = 0$, but then $r_- = 0$ [cf. Eq. (32)], indicating that there is no inner horizon. Consequently, the dynamical Hayward model specified by Eq. (34) cannot satisfy the compatibility condition Eq. (24) while $l \neq 0$.

C. Bardeen model

The first nonsingular black hole spacetime was proposed by Bardeen in 1968 [32]. It is defined by the metric function

$$f(r) = 1 - \frac{r_g r^2}{(r^2 + l^2)^{3/2}}, \tag{38}$$

where r_g and l have the same physical meaning as in Sec. IV B. Once again, we consider its dynamical generalization,

$$f(v, r) = 1 - \frac{r_g(v) r^2}{(r^2 + l(v)^2)^{3/2}}. \tag{39}$$

Writing the inner and outer horizon in terms of r_g and l, we find

$$r_- = \frac{l^{3/2}}{\sqrt{r_g}} + \mathcal{O}(l^{5/2}), \tag{40}$$

$$r_+ = r_g - \frac{3l^2}{2r_g} + \mathcal{O}(l^4). \tag{41}$$

Following the same steps as in Sec. IV B, we obtain

$$w_1|_{r=r_+} \overset{(41)}{=} \frac{3l^2}{r_g^2} + \mathcal{O}(l^4) \geq 0, \tag{42}$$

which coincides with the linear MS mass coefficient of the dynamical Hayward model [cf. Eq. (37)] at leading order, although higher-order contributions will differ once sufficiently high orders $\mathcal{O}(l^x)$ in Eqs. (33) and (41) are taken into account. Similar to the dynamical Hayward model discussed in the previous subsection, this expression is only zero if $l = 0$ and thus $r_- = 0$ [cf. Eq. (40)].

D. Dymnikova model

Another well-known RBH model was proposed by Dymnikova [33]. It is specified by the metric function

$$f(r) = 1 - \frac{r_g(1 - e^{-r^3/r_\star^3})}{r}, \tag{43}$$

where $r_\star^3 := l^2 r_g$, r_g denotes the Schwarzschild radius and l a minimal length parameter. A generalized dynamical version is given by

$$f(v,r) = 1 - \frac{r_g(v)(1 - e^{-r^3/r_\star(v)^3})}{r}, \tag{44}$$

and the inner and outer horizon can be expressed in terms of the parameters l and r_g as

$$r_- = l(1 + \mathcal{O}(e^{-r_g^2/l^2})), \tag{45}$$

$$r_+ = r_g(1 + \mathcal{O}(e^{-r_g^2/l^2})). \tag{46}$$

From the expansion of the MS mass about the outer horizon, we obtain its linear coefficient

$$w_1|_{r=r_+} \overset{(46)}{=} \frac{3r_g^2}{l^2} e^{-\frac{r_g^2}{l^2}} + \mathcal{O}(e^{-r_g^2/l^2}) \geq 0, \tag{47}$$

which is strictly greater than zero provided that $l \neq 0$, which would once again imply that the inner horizon is absent, i.e., $r_- = 0$ [cf. Eq. (45)].

E. RBH model with the strongest Schwarzschild corrections

The RBH considered in Ref. [35] exhibits the strongest possible corrections to the Schwarzschild geometry while still being compatible with its asymptotics. It is described by the metric function

$$f(r) = 1 - \frac{r_g r^2}{(r+l)^3} \tag{48}$$

and is of particular interest as observational data of the S2 star orbiting Sgr A* can be used to test its geometry and derive upper bounds for the new length scale l. We once again generalize this metric by allowing for an explicit time dependence, i.e.,

$$f(v,r) = 1 - \frac{r_g(v) r^2}{(r + l(v))^3}. \tag{49}$$

Using the same procedure as in the previous subsections, we find that the inner and outer horizon are given by

$$r_- = \frac{l^{3/2}}{\sqrt{r_g}} + \frac{3l^2}{2r_g} + \mathcal{O}(l^{5/2}), \tag{50}$$

$$r_+ = r_g - 3l - \frac{3l^2}{r_g} + \mathcal{O}(l^3). \tag{51}$$

For the linear coefficient of the MS mass at the outer horizon, we find

$$w_1|_{r=r_+} \overset{(51)}{=} \frac{3l}{r_g} + \frac{6l^2}{r_g^2} + \mathcal{O}(l^3) \geq 0. \tag{52}$$

As in the previously considered models, this expression cannot be zero unless $l = 0$ and thus $r_- = 0$ [cf. Eq. (50)].

F. Charged Hayward-Frolov model

In Ref. [37], Frolov proposed a generalization of the Hayward model to include an electric charge q. In the generalized dynamical case, the metric function for this type of RBH is given by

$$f(v,r) = 1 - \frac{(r_g(v) r - q(v)^2) r^2}{r^4 + (r_g(v) r + q(v)^2) l(v)^2}, \tag{53}$$

where, as in Sec. IV B, r_g and l denote the Schwarzschild radius and minimal length scale, and the case $q = 0$ reduces to the metric function of the uncharged dynamical Hayward model [Eq. (34)]. The static case with $l = 0$ reproduces the Reissner-Nordström metric. For both $q = l = 0$, Eq. (53) corresponds to the Vaidya (or, in the static case, Schwarzschild) metric.

As alluded to at the end of Sec. III, the Reissner-Nordström metric belongs to the $k = 1$ class of black hole solutions, and thus we must not use Eq. (18) *a priori*. The surface gravity of a Reissner-Nordström black hole is given by

$$\kappa_{\mathrm{RN}} = \frac{r_+ - r_-}{2r_+^2}, \tag{54}$$

where

$$r_- = m - \sqrt{m^2 - q^2}, \tag{55}$$

$$r_+ = m + \sqrt{m^2 - q^2}. \tag{56}$$

The dynamical generalization of the Reissner-Nordström metric is described by the metric function

$$f(v,r) = \frac{1}{r^2}(r - r_-(v))(r - r_+(v)), \tag{57}$$

with the evolving inner and outer horizon specified by

$$r_-(v) = m(v) - \sqrt{m(v)^2 - q(v)^2}, \tag{58}$$

$$r_+(v) = m(v) + \sqrt{m(v)^2 - q(v)^2}. \tag{59}$$

Since this is a $k = 0$ solution, we can make use of Eq. (11) to determine the Kodama surface gravity at the outer horizon of an evolving Reissner-Nordström black hole and find

$$\kappa_{K_{\mathrm{RN}}} = \frac{1}{2}\partial_r f(v,r) = \frac{r_+(v) - r_-(v)}{2r_+(v)^2}. \tag{60}$$

On the other hand, from the charged Hayward-Frolov metric [Eq. (53)], we obtain

$$\kappa_{K_{\mathrm{HF}}} = \frac{1 - w_1(v,l)}{2r_+(v,l)}, \tag{61}$$

and the inner and outer horizon are given by

$$r_-(v,l) = r_-(v) + \beta_-(v)l^2 + \mathcal{O}(l^3), \tag{62}$$

$$r_+(v,l) = r_+(v) + \beta_+(v)l^2 + \mathcal{O}(l^4). \tag{63}$$

Following the methodology of Sec. III, considering the MS mass expansion allows us to identify the linear coefficient,

$$w_1(v,l) = \frac{q(v)^2}{r_+(v)^2} + \beta(v)l^2 + \mathcal{O}(l^4), \tag{64}$$

where $\beta(v)$ denotes a lengthy coefficient that simplifies to $\beta(v) \to 3/r_g(v)^2$ in the uncharged case $q(v) \to 0$, in agreement with the expression derived for the uncharged dynamical Hayward model [cf. Eq. (37)]. Substituting this result into Eq. (61) and using Eqs. (62)–(63), we find

$$\kappa_{K_{\mathrm{HF}}} = \frac{r_+(v) - r_-(v)}{2r_+(v)^2} + \mathcal{O}(l^2). \tag{65}$$

As can be seen by comparison with Eq. (60), this expression matches that of the evolving Reissner-Nordström black hole only if $l = 0$, in which case the horizons of the charged dynamical Hayward-Frolov RBH specified by Eqs. (62)–(63) reduce to those of Eqs. (58)–(59). However, unlike the previously considered examples, the inner horizon $r_- \neq 0$ even if $l = 0$ due to the presence of a charge term that is independent of l, cf. Eqs. (58) and (62).

As evident from Eqs. (64) and (65), the condition for the compatibility of a dynamically evolving charged RBH with the first law of black hole mechanics is no longer encoded by the relation $w_1 = 0$. However, in the special circumstance where $l \to 0$, the new compatibility condition can be stated as

$$w_1(v,0) = \frac{q(v)^2}{r_+(v)^2}. \tag{66}$$

V. TESTING REGULAR BLACK HOLES PART 2: INNER-EXTREMAL MODEL WITH A DEGENERATE INNER HORIZON

The inner-extremal RBH model proposed in Ref. [24] solves the mass inflation instability problem at the expense of a degenerate inner horizon with vanishing surface gravity. As argued above, we consider its dynamical generalization. The metric function is given by choosing $a = 3$, $b = 1$ in Eq. (3) such that in the generalized dynamical case

$$f(v,r) = g(v,r)(r - r_-(v))^3(r - r_+(v)) \tag{67}$$

and by virtue of Eq. (13) the choice $\sum_z \lambda_z r^z = 1 \Rightarrow m = 0$ determines the degree $n - 0 = 4 = a + 1$ of the polynomial in the denominator of Eq. (14), i.e.,

$$g(v,r) = \frac{1}{c_0 + c_1 r + c_2 r^2 + c_3 r^3 + c_4 r^4}, \tag{68}$$

where we have once again omitted the dependencies of the coefficients $c_i \equiv c_i(r_-(v), r_+(v))$ for the sake of readability and will omit dependencies on v in what follows as well. While $a = 3$ for the model considered in Ref. [24], our derivation in what follows is valid for arbitrary RBH models with $m = 0$ and $b = 1$ [as otherwise the Kodama surface gravity would vanish at the outer horizon, cf. Eq. (12)], i.e., those where Eq. (14) admits the form

$$g(v,r) = \frac{1}{c_0 + c_1 r + \cdots + c_{a+1} r^{a+1}}, \tag{69}$$

where $c_{a+1}(r_-, r_+) = 1$ is required to recover the Vaidya form of the metric in the asymptotic limit $r \to \infty$. Based on dimensional grounds, the generic form of the coefficients $c_i(r_-, r_+)$ is prescribed by

$$c_i(r_-, r_+) = \sum_{j=1}^{\infty} d_{ij} r_-^j r_+^{-j-i+(a+1)} \quad \forall\, i \neq a+1, \tag{70}$$

where the coefficients d_{ij} are dimensionless.[5] If the inner horizon is absent ($r_- \to 0$), then we should also recover the Vaidya form $f = 1 - r_+/r$ as the black hole center is then no longer regular. In this case, Eq. (3) is given by

$$f(v,r)|_{r_- \to 0} = \frac{r^{a+1}(1 - \frac{r_+}{r})}{c_0(0,r_+) + c_1(0,r_+)r + \cdots + r^{a+1}}. \tag{71}$$

[5]Note that the coefficients of our simple nonsingular spacetime [Sec. IV A, Eq. (28)] are consistent with the required coefficient form specified in Eq. (70) only if $r_- = 0$ and $r_+ = 0$, i.e., if the spacetime has no horizons, in agreement with the trivial form of the metric function in Eq. (29).

Therefore, to recover the Vaidya form of the metric, we must have

$$c_i(0,r_+)=0 \quad \forall\, i\neq a+1 \Rightarrow g(v,r)|_{r_-\to 0}=\frac{1}{r^{a+1}}. \tag{72}$$

Using Eqs. (25) and (69), the compatibility condition Eq. (24) can be rewritten as

$$g(v,r_+)r_+(r_+-r_-)^a=1, \tag{73}$$

$$\Leftrightarrow (r_+-r_-)^a r_+=\frac{1}{g(v,r_+)}\overset{(69)}{=}\sum_{i=0}^{a+1}c_i(r_-,r_+)r_+^i. \tag{74}$$

Using the binomial theorem to expand the lhs, and Eq. (70) for the coefficients on the rhs, Eq. (74) can be rewritten as

$$\sum_{k=0}^{a}\binom{a}{k}(-1)^{a-k}r_-^{a-k}r_+^{k+1}=\sum_{i=0}^{a}\sum_{j=1}^{\infty}d_{ij}r_-^j r_+^{-j+(a+1)}+r_+^{a+1}. \tag{75}$$

Separating the $k=a$ term (whose contribution is r_+^{a+1}) from the summation on the lhs, this simplifies further to

$$\sum_{k=0}^{a-1}\binom{a}{k}(-r_-)^{a-k}r_+^{k+1}=\sum_{i=0}^{a}\sum_{j=1}^{\infty}d_{ij}r_-^j r_+^{-j+(a+1)}. \tag{76}$$

Note that the maximum possible exponent of r_- on the lhs is a (for $k=0$). Consequently, if Eq. (76) is treated as a polynomial with respect to r_-, then the only way to have a solution is to truncate the summation over j on the rhs at $j=a$. Furthermore, since $0\le k\le a-1$ and $1\le j\le a$, we can redefine the summation with respect to k on the lhs and use the transformation $j\mapsto a-k$ to rewrite Eq. (76) as

$$\sum_{j=1}^{a}\binom{a}{a-j}(-r_-)^j r_+^{-j+(a+1)}=\sum_{i=0}^{a}\sum_{j=1}^{a}d_{ij}r_-^j r_+^{-j+(a+1)}. \tag{77}$$

As a result, the compatibility condition Eq. (24) is satisfied if and only if

$$\sum_{j=1}^{a}r_-^j\left[\binom{a}{a-j}(-1)^j r_+^{-j+(a+1)}-\sum_{i=0}^{a}d_{ij}r_+^{-j+(a+1)}\right]=0. \tag{78}$$

We note that, in consonance with our analysis of nondegenerate RBH models in Sec. IV, this relation is trivially satisfied if there is no inner horizon ($r_-\to 0$). On the other hand, if an inner horizon is present ($r_-\neq 0$), then satisfying Eq. (78) requires

$$\boxed{\sum_{i=0}^{a}d_{ij}=\binom{a}{a-j}(-1)^j.} \tag{79}$$

This alternative form of the compatibility condition derived in Sec. III allows us to test RBH models for which evaluating the expression given in Eq. (25) is not straightforward due to the fact that $a>1$ and the coefficients in the polynomial decomposition of g [Eq. (14)] are *a priori* undetermined. With the commonly used assumptions of a positive MS mass $C>0$ [cf. Eq. (17)] and regularity (expressed mathematically through the finiteness of relevant curvature scalars, such as the Ricci and Kretschmann scalar), it is possible to determine the lowest-order coefficients of Eq. (69). However, this alone does not suffice to determine whether or not relation Eq. (79) is satisfied in general, as this would require the ability to determine every individual coefficient $c_i(r_-,r_+)$. Nonetheless, it is often possible to evaluate Eq. (79) in physically motivated scenarios where the degeneracy of the inner horizon a in Eq. (3) is known explicitly.

We now examine the dynamical generalization [Eqs. (67)–(68)] of the inner-extremal RBH model with $a=3$ proposed in Ref. [24] and demonstrate that it cannot satisfy the condition Eq. (79) required to be compatible with the first law. In this model, $c_4=1$ and $c_3=-3r_-$ [cf. Eq. (68)] are necessary to recover the Vaidya form of the metric asymptotically. The latter can be seen by expanding Eq. (67) about the point $z:=1/r=0$ to represent the limit $r\to\infty$, which results in

$$f(v,r)|_{\frac{1}{r}=0}=\frac{1}{c_4}-\frac{c_3+c_4(3r_-+r_+)}{c_4^2}\frac{1}{r}+\mathcal{O}\left(\frac{1}{r^2}\right). \tag{80}$$

Substitution of $c_4=1$ in Eq. (80) and subsequent comparison with the Vaidya form $f=1-r_+/r$ yields $c_3=-3r_-$. From the requirement of regularity, we obtain

$$c_0=r_-^3 r_+, \qquad c_1=-r_-^2(r_-+3r_+), \tag{81}$$

as can be verified, for instance, by evaluating the Ricci or the Kretschmann scalar.

The remaining coefficient c_2 can be determined from the requirement that f be nondivergent, which in turn requires that its denominator,

$$D(v,r):=1/g(v,r)\overset{(68)}{=}r_-^3 r_+-r_-^2(r_-+3r_+)r+c_2r^2-3r_-r^3+r^4, \tag{82}$$

be nonzero. We rewrite Eq. (82) as

$$\tilde{D}(v,r) = \tilde{c}_2 r^2 + \left(r - \frac{3r_-}{2}\right)^2 + r_-^3 r_+ \left[1 - \frac{r}{2}\left(\frac{3}{r_-} + \frac{1}{r_+}\right)\right]^2, \tag{83}$$

where

$$c_2 = \tilde{c}_2 + \frac{15}{4} r_-^2 + \frac{9}{4} r_- r_+ + \frac{r_-^3}{4r_+}, \qquad \tilde{c}_2 \geq 0. \tag{84}$$

Using Eq. (16) to express the MS mass C in terms of f and expanding about the center $r = 0$, we find

$$C(v,r) = \frac{r_-^3 + 4\tilde{c}_2 r_+ + 3r_-^2 r_+ - 3r_- r_+^2}{4r_-^3 r_+^2} r^3 + \mathcal{O}(r^4). \tag{85}$$

The positivity requirement for the MS mass then constrains the coefficient $\tilde{c}_2$ via

$$\begin{aligned} &r_-^3 + 4\tilde{c}_2 r_+ + 3r_-^2 r_+ - 3r_- r_+^2 > 0 \\ &\Rightarrow \tilde{c}_2 = \frac{\zeta - r_-^3 - 3r_-^2 r_+ + 3r_- r_+^2}{4r_+}, \qquad \zeta > 0. \end{aligned} \tag{86}$$

Substituting Eq. (86) into Eq. (84) yields

$$c_2 = \frac{\zeta}{4r_+} + 3r_-^2 + 3r_- r_+. \tag{87}$$

This is all we need to explicitly identify the dimensionless coefficients d_{ij} introduced in Eq. (70). We find

$$\begin{aligned} c_0 = r_-^3 r_+ &= d_{01} r_- r_+^3 + d_{02} r_-^2 r_+^2 + d_{03} r_-^3 r_+ \\ &\Rightarrow d_{01} = 0, \qquad d_{02} = 0, \qquad d_{03} = 1, \end{aligned} \tag{88}$$

$$\begin{aligned} c_1 = -r_-^3 - 3r_-^2 r_+ &= d_{11} r_- r_+^2 + d_{12} r_-^2 r_+ + d_{13} r_-^3 \\ &\Rightarrow d_{11} = 0, \qquad d_{12} = -3, \qquad d_{13} = -1, \end{aligned} \tag{89}$$

$$\begin{aligned} c_3 = -3r_- &= d_{31} r_- + d_{32} r_-^2 r_+^{-1} + d_{33} r_-^3 r_+^{-2} \\ &\Rightarrow d_{31} = -3, \qquad d_{32} = 0, \qquad d_{33} = 0. \end{aligned} \tag{90}$$

To proceed with the identification of the coefficients d_{2j}, we note that the dimensions of ζ are $[\zeta] = L^3$ (i.e., ζ is cubic in length), as can be seen from Eq. (87). Therefore, we can write the first term in Eq. (87) as

$$\frac{\zeta}{4r_+} = \zeta_1 r_- r_+ + \zeta_2 r_-^2 + \zeta_3 r_-^3 r_+^{-1} > 0, \tag{91}$$

where the coefficients ζ_i are dimensionless. Hence,

$$\begin{aligned} c_2 &= d_{21} r_- r_+ + d_{22} r_-^2 + d_{23} r_-^3 r_+^{-1} \\ &= (\zeta_1 + 3) r_- r_+ + (\zeta_2 + 3) r_-^2 + \zeta_3 r_-^3 r_+^{-1} \\ &\Rightarrow d_{21} = \zeta_1 + 3, \quad d_{22} = \zeta_2 + 3, \quad d_{23} = \zeta_3. \end{aligned} \tag{92}$$

Next, we use Eq. (79) to determine the coefficients ζ_i. We find

$$\begin{aligned} \sum_{i=0}^{3} d_{i1} &= \binom{3}{2}(-1)^1 = -3 \\ &= d_{01} + d_{11} + d_{21} + d_{31} \Rightarrow \zeta_1 = -3, \end{aligned} \tag{93}$$

$$\begin{aligned} \sum_{i=0}^{3} d_{i2} &= \binom{3}{1}(-1)^2 = 3 \\ &= d_{02} + d_{12} + d_{22} + d_{32} \Rightarrow \zeta_2 = 3, \end{aligned} \tag{94}$$

$$\begin{aligned} \sum_{i=0}^{3} d_{i3} &= \binom{3}{0}(-1)^3 = -1 \\ &= d_{03} + d_{13} + d_{23} + d_{33} \Rightarrow \zeta_3 = -1. \end{aligned} \tag{95}$$

Substituting these values into Eq. (91), we obtain

$$\begin{aligned} &-3r_- r_+ + 3r_-^2 - r_-^3 r_+^{-1} > 0 \\ &\Leftrightarrow 3r_+^2 - 3r_- r_+ + r_-^2 < 0. \end{aligned} \tag{96}$$

Considering Eq. (96) as a polynomial in r_+, its discriminant is given by $-3r_-^2 < 0$, which implies that the polynomial has two distinct complex conjugate roots and is thus always positive. However, this is in direct contradiction with the inequality in the second line of Eq. (96), indicating that it is impossible for the inner-extremal RBH model to satisfy the necessary relation Eq. (79) that is required to be compatible with the first law of black hole mechanics.

VI. PAGE EVAPORATION LAW

Building on Hawking's result [6], Page demonstrated that the mass loss due to the emission of Hawking radiation is described by the formula

$$\frac{dM}{dt} = -\sum_{j,\ell,m,p} \frac{1}{2\pi} \int_0^\infty \frac{\omega \Gamma_{j\omega\ell mp}}{e^{2\pi\omega/\kappa} - 1} d\omega, \tag{97}$$

where j labels the emitted particle species, and $\Gamma_{j\omega\ell mp}$ denotes the absorption probability[6] for an incoming wave

[6]In practice, these are determined using analytical and numerical techniques in a formalism originally developed by Teukolsky and Press [60,61].

mode labeled by the frequency ω, spheroidal harmonic ℓ, axial quantum number m, and polarization p. Although this formula accounts for both angular momentum and charge, an isolated black hole is expected to be well approximated by an uncharged spherically symmetric metric due to the fact that in the Hawking process angular momentum is shed much faster than mass [7], and charged black holes rapidly discharge in a Schwinger-like pair production process [62,63].

Since the ingoing Vaidya metric with decreasing mass ($C'(v) < 0$) is the appropriate choice to model the effects of Hawking radiation (see Table 2 in Ref. [36]), Eq. (97) is often expressed in advanced null coordinates (v, r) using several physically motivated simplifying assumptions (most notably the restriction to $\ell = m = 0$ modes and the approximate relation $\Gamma \simeq \omega^2 r_g^2$; see Refs. [31,64,65] for a more detailed account) as

$$\frac{dM}{dv} \simeq -\frac{a}{M^2} \Leftrightarrow \frac{dr_+}{dv} \simeq -\frac{\alpha}{r_+^2}, \tag{98}$$

which implies that a black hole of initial mass M_0 will evaporate in a time $t_e \sim M_0^3$, and the explicit form of the coefficients and their expansion about $w_1 = 0$ are given by

$$\alpha = 8a = -\frac{4}{\pi}\frac{1}{e^{\frac{4\pi}{1-w_1}} - 1}, \tag{99}$$

$$\alpha = -\frac{4}{\pi}\frac{1}{e^{4\pi} - 1} + \mathcal{O}(w_1), \tag{100}$$

respectively. Consequently, the standard Page evaporation law is modified if the condition $w_1 = 0$ derived in Sec. III is not satisfied.

VII. CONCLUSIONS

Based on the assertion that the surface gravity of an evolving black hole horizon should approach the expression prescribed by the first law of black hole mechanics [Eq. (7)] in the quasistatic limit, we have derived a compatibility condition for generic spherically symmetric dynamical black holes [Sec. III, Eq. (24)]. In our analysis of the dynamical generalizations of RBH models typically considered in the literature, we have evaluated the compatibility condition explicitly for the respective metric functions that describe them and demonstrated that none of them satisfies the necessary condition required to be compatible with the conventional form of the first law of black hole mechanics (Sec. IV and Sec. V). As outlined in Sec. VI, this also implies that—if the decrease in mass $\delta M < 0$ due to the emission of Hawking radiation is indeed proportional to the surface gravity as stipulated by the first law—then the dynamical evolution of such RBHs cannot be accurately described by the standard Page evaporation law. One may argue that this is a somewhat counterintuitive result, considering that the derivation of Eq. (97) is based on Hawking fluxes perceived in the asymptotic limit, and thus one would naively expect that the minimal length scale introduced for the purpose of regularization should not affect the outcome.

Our analysis suggests that the incompatibility of dynamical RBHs with the first law of black hole mechanics is directly linked to the minimal length scale l (which can be interpreted as an additional hair) introduced for the regularization and the presence of an inner horizon, which are the main characteristics (together with their regular center) that distinguish RBH models from alternative descriptions of trapped spacetime domains. Since both are necessary ingredients in the regularization procedure to avoid singularities, one may conjecture that there is a more fundamental physical or topological principle at play that prevents nonsingular black hole spacetimes from satisfying the first law.

In their most conservative form, the conclusions of our analysis may be stated as follows: nonsingular black holes are incompatible with the widely accepted semiclassical description of evaporating black holes that is based on the results of Refs. [1] and [5–7]. Unless one is willing to give up either the idea of regularity and an interior that is physically well behaved all the way down to the center or the first law of black hole mechanics (and its associated thermodynamic interpretation of surface gravity as an effective temperature), our results demonstrate that modifications of the first law are required even at the level of semiclassical gravity.

We note that our analysis is consistent with the interpretation of the deviation from the standard form of the first law [Eq. (6)] as a thermodynamic pressure term as has been proposed, for instance, in Refs. [25] and [57], which can be seen from Eqs. (22)–(23). In this sense, the linear coefficient of the MS mass w_1 encodes rather specific information about the thermodynamic properties of black holes. In fact, as evident from Eq. (22), knowledge of w_1 suffices to fully specify the generalized first law of black hole mechanics.

ACKNOWLEDGMENTS

We would like to thank Yasha Neiman, Fil Simovic, and Daniel Terno for useful discussions and helpful comments. S. M. is supported by the Quantum Gravity Unit of the Okinawa Institute of Science and Technology (OIST). I. S. is supported by an International Macquarie University Research Excellence Scholarship (IMQRES).

[1] J. M. Bardeen, B. Carter, and S. W. Hawking, Commun. Math. Phys. **31**, 161 (1973).
[2] J. Bekenstein, Lett. Nuovo Cimento **4**, 737 (1972).
[3] J. Bekenstein, Phys. Rev. D **7**, 2333 (1973).
[4] J. Bekenstein, Phys. Rev. D **9**, 3292 (1974).
[5] S. W. Hawking, Nature (London) **248**, 30 (1974).
[6] S. W. Hawking, Commun. Math. Phys. **43**, 199 (1975); **46**, 206(E) (1976).
[7] D. N. Page, Phys. Rev. D **13**, 198 (1976).
[8] M. Visser, Proc. Sci., GRandStrings2008 (**2008**) 001.
[9] C. Bambi, Mod. Phys. Lett. A **26**, 2453 (2011).
[10] S. W. Hawking, arXiv:1401.5761.
[11] V. P. Frolov, arXiv:1411.6981.
[12] V. Cardoso and P. Pani, Living Rev. Relativity **22**, 4 (2019).
[13] S. Murk, Int. J. Mod. Phys. D; arXiv:2210.03750.
[14] S. Ansoldi, arXiv:0802.0330.
[15] L. Sebastiani and S. Zerbini, Astronomy **1**, 99 (2022).
[16] C. Lan, H. Yang, Y. Guo, and Y.-G. Miao, arXiv:2303.11696.
[17] M. Visser, Phys. Rev. D **90**, 127502 (2014).
[18] E. Poisson and W. Israel, Phys. Rev. Lett. **63**, 1663 (1989).
[19] E. Poisson and W. Israel, Phys. Rev. D **41**, 1796 (1990).
[20] A. Ori, Phys. Rev. Lett. **67**, 789 (1991).
[21] A. J. S. Hamilton and P. P. Avelino, Phys. Rep. **495**, 1 (2010).
[22] R. Carballo-Rubio, F. Di Filippo, S. Liberati, C. Pacilio, and M. Visser, J. High Energy Phys. 05 (2021) 132.
[23] P. K. Dahal, S. Murk, and D. R. Terno, AVS Quantum Sci. **4**, 015606 (2022).
[24] R. Carballo-Rubio, F. Di Filippo, S. Liberati, C. Pacilio, and M. Visser, J. High Energy Phys. 09 (2022) 118.
[25] S. A. Hayward, Classical Quantum Gravity **15**, 3147 (1998).
[26] A. Ashtekar and B. Krishnan, Living Rev. Relativity **7**, 10 (2004).
[27] J. M. M. Senovilla, Int. J. Mod. Phys. D **20**, 2139 (2011).
[28] F. Kurpicz, N. Pinamonti, and R. Verch, Lett. Math. Phys. **111**, 110 (2021).
[29] D. Kastor, S. Ray, and J. Traschen, Classical Quantum Gravity **27**, 235014 (2010).
[30] C. Pacilio and S. Liberati, Phys. Rev. D **96**, 104060 (2017).
[31] D. Harlow, Rev. Mod. Phys. **88**, 015002 (2016).
[32] J. M. Bardeen, in *Proceedings of the International Conference GR5* (Tbilisi University Press, Tbilisi, 1968).
[33] I. Dymnikova, Gen. Relativ. Gravit. **24**, 235 (1992).
[34] S. A. Hayward, Phys. Rev. Lett. **96**, 031103 (2006).
[35] M. Cadoni, M. De Laurentis, I. De Martino, R. Della Monica, M. Oi, and A. P. Sanna, Phys. Rev. D **107**, 044038 (2023).
[36] R. B. Mann, S. Murk, and D. R. Terno, Int. J. Mod. Phys. D **31**, 2230015 (2022).
[37] V. P. Frolov, Phys. Rev. D **94**, 104056 (2016).
[38] S. A. Hayward, Phys. Rev. D **49**, 6467 (1994).
[39] V. Faraoni, G. F. R. Ellis, J. T. Firouzjaee, A. Helou, and I. Musco, Phys. Rev. D **95**, 024008 (2017).
[40] P. Binétruy, A. Helou, and F. Lamy, Phys. Rev. D **98**, 064058 (2018).
[41] S. W. Hawking and G. F. R. Ellis, *The Large Scale Structure of Space-Time* (Cambridge University Press, Cambridge, England, 1973), Chap. 9.2.
[42] V. P. Frolov and I. D. Novikov, *Black Hole Physics: Basic Concepts and New Developments* (Springer, Dordrecht, 1998).
[43] V. Baccetti, R. B. Mann, S. Murk, and D. R. Terno, Phys. Rev. D **99**, 124014 (2019).
[44] M. Visser, Int. J. Mod. Phys. D **12**, 649 (2003).
[45] R. M. Wald, Phys. Rev. D **48**, R3427(R) (1993).
[46] V. Iyer and R. M. Wald, Phys. Rev. D **50**, 846 (1994).
[47] C. W. Misner and D. H. Sharp, Phys. Rev. **136**, B571 (1964).
[48] A. B. Nielsen and J. H. Yoon, Classical Quantum Gravity **25**, 085010 (2008).
[49] B. Cropp, S. Liberati, and M. Visser, Classical Quantum Gravity **30**, 125001 (2013).
[50] C. Barceló, S. Liberati, S. Sonego, and M. Visser, Phys. Rev. D **83**, 041501(R) (2011).
[51] H. Kodama, Prog. Theor. Phys. **63**, 1217 (1980).
[52] G. Abreu and M. Visser, Phys. Rev. D **82**, 044027 (2010).
[53] S. Murk and D. R. Terno, Phys. Rev. D **103**, 064082 (2021).
[54] S. Murk and D. R. Terno, The Sixteenth Marcel Grossmann Meeting (2023), pp. 1196–1211, arXiv:2110.12761.
[55] R. B. Mann, S. Murk, and D. R. Terno, Phys. Rev. D **105**, 124032 (2022).
[56] M.-S. Ma and R. Zhao, Classical Quantum Gravity **31**, 245014 (2014).
[57] C. Lan and Y.-G. Miao, Eur. Phys. J. C **82**, 1152 (2022).
[58] S. Murk, Phys. Rev. D **105**, 044051 (2022).
[59] B. L. van der Waerden, *Moderne Algebra 1*, 2nd ed. (Springer, Berlin Heidelberg, 1937), p. 188.
[60] S. A. Teukolsky, Astrophys. J. **185**, 635 (1973).
[61] S. A. Teukolsky and W. H. Press, Astrophys. J. **193**, 443 (1974).
[62] J. Schwinger, Phys. Rev. **82**, 664 (1951).
[63] G. W. Gibbons, Commun. Math. Phys. **44**, 245 (1975).
[64] R. M. Wald (ed.), *Quantum Field Theory in Curved Spacetime and Black Hole Thermodynamics* (The University of Chicago Press, Chicago, 1994), Chap. 7.
[65] L. Parker and D. Toms, *Quantum Field Theory in Curved Spacetime* (Cambridge University Press, Cambridge, England, 2009), Chap. 4.

Conclusion

The study of RBH solutions within GR is a crucial step toward unraveling the fundamental aspects of quantum gravity. Investigating various RBH models is vital for understanding how the regularization of singularities — common in conventional black holes — affects the classical sector. If a quantum gravity theory can achieve such regularization while maintaining the defining characteristic of the event horizon, RBHs, or potentially their horizonless alternatives, become the most viable candidates for describing UCOs.

In the first main part of this thesis, we demonstrated within the framework of GR that using NED theories as an effective source for regular, horizonful geometries supports the existence of a first law of black hole thermodynamics across AdS, Minkowski, and dS spacetimes. We also established the presence of a linear Smarr relation and reconciled discrepancies in the literature by ensuring consistency between Hamiltonian and Euclidean thermodynamics in the appropriate limits. Building on this foundation, we employed these thermodynamic quantities to explore the phase structure of RBHs.

Our analysis revealed a key finding: the Hawking–Page transition, typically observed in the singular Schwarzschild metric, is absent in 4D RBHs when studied in the canonical ensemble and sourced by NED theories. This absence can be attributed to quantum gravity corrections, which effectively smooth out singularities and generally prevent the transition from occurring. Instead of the Hawking–Page transition we find a first-order small-to-large phase transition which terminates at a critical point, where it becomes second-order. The behavior of various thermodynamic parameters near this point is governed by critical exponents, which classify physical systems into universality classes where the scaling behavior of these parameters is identical, even if the systems' microscopic structures differ significantly.

In many asymptotic AdS examples, the critical exponents are the same as those of the Van der Waals fluids, which is surprising given that their equations of state are not identical. RBHs are no exception, sharing these critical exponents. However, the critical ratio $P_c v_c/T_c$, where P_c, T_c, and v_c are the pressure, temperature, and reduced volume (volume over the number of particles) at the critical point, respectively, deviates from the mean-field theory value $3/8$. This suggests a potential departure from the mean-field theory critical behavior. Specifically, different models of NED theories, each with distinct weak-field limits, exhibit differing degrees of deformation from the Schwarzschild geometry. This dependence on the deformation strength manifests in the critical ratio. In this thesis, we demonstrated that the greater the deformation from Schwarzschild geometry, the larger the deviation from this ratio. This illustrates how the choice of singularity regularization method influences the extent of departure from the striking similarity between fluid phases and black hole phases.

Lastly, observational signatures are essential for confirming or refuting the nature and characteristics of UCOs. Our research concentrated on analyzing the behavior of light rings around

these objects, revealing that merely counting the number of light rings, without knowing the underlying theory, may not be sufficient for accurate identification. We found that nonsingular horizonless UCOs, sourced by NED, exhibit an odd number of light rings and discussed the viability of this effective description of their properties. Furthermore, we compared the phase velocities of polarized light rays in these nonsingular geometries with those in Schwarzschild spacetime. Our findings indicate that regularizing singularities with a theory that does not adhere to the Maxwell weak-field limit can result in the formation of acausal regions.

With these findings, we concluded the first part of the thesis. Our study of black hole thermodynamics relied on the existence of Hawking radiation, to provide the necessary thermodynamic equilibrium, and the assumption of a stationary metric with event horizons. However, realistic scenarios that account for the backreaction of Hawking radiation on the metric are inherently dynamic. In such cases, an accurate description that captures all relevant physical aspects requires the use of quasi-local apparent horizons.

The collapse of a star to an RBH in finite time as seen by a distant observer is the moment of formation of the trapped region. At this point, the apparent horizon splits into inner and outer components. We demonstrated that, assuming the validity of semiclassical gravity near these horizons, both horizons can only evaporate, making them timelike throughout their entire existence. The evaporation process ceases when the two horizons merge, resulting in the disappearance of the trapped region and leaving an extremal black hole as the final state. This extremal black hole has zero temperature, violating the third law of black hole mechanics.

Assuming that the dynamical evolution of RBHs is driven solely by quantum effects, we can quantify these effects by evaluating the NEC, which is the weakest among the energy conditions. Our results show that the NEC is satisfied near the inner horizon but violated at the outer horizon. We identified a boundary that effectively divides the trapped region into areas where the NEC is either violated or not. The evaluation of the NEC at the outer apparent horizon indicates that the maximal violation occurs near the point of complete evaporation, highlighting the prominence of quantum effects at this stage. Moreover, the dynamic nature of this geometry provides insights into the black hole information paradox. Since the horizons are timelike, light can escape and become visible to distant observers on timescales comparable to the evaporation time. Similarly, massive particles can also escape, but only in a specific manner that involves crossing the apparent horizons on an ingoing geodesic trajectory, i.e., allowing the horizons to overtake them.

Finally, a dynamic first law of black hole mechanics can be formulated by introducing the Kodama vector. Recent studies have provided evidence supporting this formulation and the emergence of a dynamical entropy [103]. Our research has shown that deriving this law through near-horizon expansions reveals that the inclusion of work terms is inherently connected to the introduction of a minimal length scale, which can be interpreted as a direct consequence of spacetime regularization. However, while the regularization of spacetime is desirable, it also reveals peculiar properties and raises unresolved questions that may only be addressed through a complete theory of quantum gravity. Even when quantum effects are taken into account, the challenges are merely shifted to other areas, underscoring the complexities that require further exploration.

From a broader perspective, we hope to have conveyed that the study of RBH spacetimes is not only worthwhile and intriguing but also a crucial step toward a deeper understanding of the fundamental nature of reality. Throughout this work, we have addressed many unresolved

questions, both conceptual and technical, yet several avenues for further research naturally emerge. First, a key open question is determining which classes of black hole solutions — and the corresponding theories — permit a consistent thermodynamic formulation from both the Hamiltonian and Euclidean frameworks when matter fields are present. While it is established that perfect fluids can be incorporated into the covariant formalism, this result has not been generalized beyond symmetry-inheriting matter fields. Additionally, the linearity of the Smarr relation for NED theories has only been proven for those that adhere to a Maxwell weak-field limit. Second, another important area for further investigation involves astrophysical observations of black hole candidates, which are typically modeled using the Kerr paradigm since realistic UCOs are expected to possess angular momentum and rotate. Notably, the emission of gravitational waves requires at least a mass quadrupole structure, which cannot be accurately modeled in spherically symmetric settings. To fully test the validity of NED theories as an effective description of nonsingular UCOs, it is necessary to extend these models to include axial symmetry. However, attempts to achieve this using the Newman–Janis formalism have so far been unsuccessful. Fully analytic solutions remain elusive, and only solutions for slowly rotating objects are currently known [104, 105].

References

[1] F. Simovic and I. Soranidis, Phys. Rev. D **109**, 044029 (2024).

[2] I. Soranidis, Phys. Rev. D **109**, 044041 (2024).

[3] S. Murk and I. Soranidis, Phys. Rev. D **110**, 044064 (2024).

[4] P. K. Dahal, I. Soranidis, and D. R. Terno, Phys. Rev. D **106**, 124048 (2022).

[5] S. Murk and I. Soranidis, Phys. Rev. D **108**, 124007 (2023).

[6] S. Murk and I. Soranidis, Phys. Rev. D **108**, 044002 (2023).

[7] P. K. Dahal, F. Simovic, I. Soranidis, and D. R. Terno, Phys. Rev. D **108**, 104014 (2023).

[8] P. K. Dahal, S. Maharana, F. Simovic, I. Soranidis, and D. R. Terno, Phys. Rev. D **110**, 044032 (2024).

[9] S. Maharana, F. Simovic, I. Soranidis, and D. R. Terno, Phys. Rev. D **111**, 104063 (2025).

[10] I. Soranidis, arXiv:2408.07290 (2024).

[11] I. Soranidis and D. R. Terno, arXiv:2505.09189 (2025).

[12] R. A. Hennigar, D. Kubizňák, S. Murk, and I. Soranidis, arXiv:2505.11623 (2025).

[13] R. Penrose, Phys. Rev. Lett. **14**, 57 (1965).

[14] E. Witten, Rev. Mod. Phys. **92**, 45004 (2020).

[15] S. M. Scott and B. E. Whale, Classical Quantum Gravity **38**, 065012 (2021).

[16] S. M. Scott and B. E. Whale, Int. J. Mod. Phys. D **30**, 2142007 (2021).

[17] S. W. Hawking, Phys. Rev. D **14**, 2460 (1976).

[18] R. P. Kerr, arXiv:2312.00841 (2023).

[19] V. Cardoso and P. Pani, Living Rev. Relativity **22**, 4 (2019).

[20] P. V. P. Cunha, E. Berti, and C. A. R. Herdeiro, Phys. Rev. Lett. **119**, 251102 (2014).

[21] F. Di Filippo, arXiv:2404.07357 (2024).

[22] C. Bambi (ed.), *Regular Black Holes: Towards a New Paradigm of Gravitational Collapse* (Springer Singapore, 2023).

[23] E. Poisson and W. Israel, Phys. Rev. Lett. **63**, 1663 (1989).

[24] E. Poisson and W. Israel, Phys. Rev. D **41**, 1796 (1990).

[25] A. Ori, Phys. Rev. Lett. **67**, 789 (1991).

[26] A. J. S. Hamilton and P. P. Avelino, Phys. Rep. **495**, 1 (2010).

[27] R. Carballo-Rubio, F. Di Filippo, S. Liberati, C. Pacilio, and M. Visser, J. High Energy Phys. **05**, 132 (2021).

[28] P. K. Dahal, S. Murk, and D. R. Terno, AVS Quantum Sci. **4**, 015606 (2022).

[29] S. Murk, Int. J. Mod. Phys. D **32**, 2342012 (2023).

[30] M. Visser, Phys. Rev. D **90**, 127502 (2014).

[31] J. M. M. Senovilla, Gen. Relativ. Gravit. **30**, 701 (1998).

[32] J. M. M. Senovilla and D. Garfinkle, Classical Quantum Gravity **32**, 124008 (2015).

[33] E.-A. Kontou and K. Sanders, Classical Quantum Gravity **37**,193001 (2020).

[34] J. R. Oppenheimer and H. Snyder, Phys. Rev. **56**, 455 (1939).

[35] D. Malafarina and B. Toshmatov, Phys. Rev. D **105**, L121502 (2022).

[36] C. Bambi, D. Malafarina, and L. Modesto, Phys. Rev. D **88**, 044009 (2013).

[37] R. B. Mann, S. Murk, and D. R. Terno, Int. J. Mod. Phys. D **31**, 2230015 (2022).

[38] S. W. Hawking, Commun. Math. Phys. **43**, 199 (1975)

[39] J. M. Bardeen, B. Carter, and S. W. Hawking, Commun. Math. Phys. **31**, 161 (1973).

[40] D. Harlow, Rev. Mod. Phys. **88**, 015002 (2016).

[41] A. Strominger, arXiv:1703.05448 (2018).

[42] V. Iyer and R. M. Wald, Phys. Rev. D **50**, 846 (1994).

[43] G. W. Gibbons and S. W. Hawking, Phys. Rev. D **15**, 2738 (1977).

[44] S. W. Hawking and D. N. Page, Commun. Math. Phys. **87**, 577 (1983).

[45] A. M. Frassino, D. Kubizňák, R. B. Mann, and F. Simovic, J. High Energy Phys. **09** (2014) 080.

[46] G. W. Gibbons, M. J. Perry, and C. N. Pope, Classical Quantum Gravity **22**, 1503 (2005).

[47] J. M. Maldacena, Int. J. Theor. Phys. **38**, 1113 (1999).

[48] D. Kubizňák, R. B. Mann and M. Teo, Classical Quantum Gravity **34**, 063001 (2017).

[49] M. B. Ahmed, W. Cong, D. Kubizňák, R. B. Mann, and M. R. Visser, arXiv:2305.03161 (2023).

[50] M. Born and L. Infeld, Proc. R. Soc. A **144**, 425 (1934).

[51] E. S. Fradkin and A. A. Tseytlin, Phys. Lett. B **163**, 123 (1985).

[52] W. Heisenberg and H. Euler, Z. Physik **98**, 714 (1936).

[53] ATLAS Collaboration, Nature Phys. **13**, 852 (2017).

[54] ATLAS Collaboration, Phys. Rev. Lett. **123**, 052001 (2019).

[55] J. S. Heyl, N. J. Shavin, and D. Lloyd, Mon. Not. R. Astron. Soc. **342**, 134 (2003).

[56] R. Taverna, R. Turolla, D. González Caniulef, S. Zane, F. Muleri, and P. Soffitta, Mon. Not. R. Astron. Soc. **454**, 3254 (2015).

[57] R. P. Mignani, V. Testa, D. González Caniulef, R. Taverna, R. Turolla, S. Zane, and K. Wu, Mon. Not. R. Astron. Soc. **465**, 1492 (2016).

[58] Planck Collaboration, Astronomy & Astrophysics **596**, A109 (2016).

[59] Y. Minami and E. Komatsu, Phys. Rev. Lett. **125**, 221301 (2020).

[60] A. Hoseinpour, M. Zarei, G. Orlando, N. Bartolo, and S. Matarrese, Phys. Rev. D **102**, 063501 (2020).

[61] S. Balestra *et al.*, Eur. Phys. J. C **55**, 57 (2008).

[62] M. Ambrosio *et al.* (The MACRO Collaborations), Eur. Phys. J. C **25**, 511 (2002).

[63] B. Acharya, J. Alexandre, P. Benes *et al.*, Nature (London) **602**, 63 (2022).

[64] G. 't Hooft, Nuclear Physics B **79**, 276–284 (1974).

[65] T. W. B. Kibble, Physics Reports 67, 183–199 (1980).

[66] A. M. Polyakov, JETP Letters **20**, 430 (1974).

[67] J. Preskill, Ann. Rev. Nucl. Part. Sci. 34, 461–530 (1984).

[68] B.-L. Hu and E. Verdaguer, *Semiclassical and Stochastic Gravity: Quantum Field Effects on Curved Spacetime* (Cambridge University Press, Cambridge, England, 2020).

[69] S. W. Hawking and G. F. R. Ellis, *The Large Scale Structure of Space-Time* (Cambridge University Press, Cambridge, England, 1973).

[70] J. M. M. Senovilla, Int. J. Mod. Phys. D **20**, 2139 (2011).

[71] V. Faraoni, *Cosmological and Black Hole Apparent Horizons* (Springer, Heidelberg, 2015).

[72] V. P. Frolov and I. D. Novikov, *Black Hole Physics: Basic Concepts and New Developments* (Kluwer, Dordrecht, 1998).

[73] R. Penrose, *Singularities and time-asymmetry*, in S. W. Hawking and W. Israel (eds.), *General Relativity: An Einstein Centenary Survey* (Cambridge University Press, Cambridge, 1979), pp. 581–638.

[74] H. Stephani, D. Kramer, M. MacCallum, C. Hoenselaers, and E. Herlt, *Exact Solutions of Einstein's Field Equations*, 2nd ed. (Cambridge University Press, Cambridge, England, 2003).

[75] M. Visser, Phys. Rev. D **56**, 936 (1997).

[76] R. M. Wald, Living Rev. Relativ. **4**, 6 (2001).

[77] A. Levi and A. Ori, Phys. Rev. Lett. **117**, 231101 (2016).

[78] N. Graham and K. D. Olum, Phys. Rev. D **76**, 064001 (2007).

[79] R. Bousso, Z. Fisher, J. Koeller, S. Leichenauer, and A. C. Wall, Phys. Rev. D **93**, 024017 (2016).

[80] M. Blau, *Lecture Notes on General Relativity* (2023).

[81] A. B. Nielsen and J. H. Yoon, Class. Quantum Gravity **25**, 085010 (2008).

[82] B. Cropp, S. Liberati, and M. Visser, Class. Quantum Gravity **30**, 125001 (2013).

[83] C. Barceló, S. Liberati, S. Sonego, and M. Visser, Phys. Rev. D **83**, 041501(R) (2011).

[84] F. Kurpicz, N. Pinamonti, and R. Verch, Lett. Math. Phys. **111**, 110 (2021).

[85] G. Abreu and M. Visser, Phys. Rev. D **82**, 044027 (2010).

[86] H. Kodama, Prog. Theor. Phys. **63**, 1217 (1980).

[87] S. Murk and D. R. Terno, Phys. Rev. D **103**, 064082 (2021).

[88] S. Murk and D. R. Terno, The Sixteenth Marcel Grossmann Meeting, pp. 1196-1211 (2023); arXiv:2110.12761.

[89] R. B. Mann, S. Murk, and D. R. Terno, Phys. Rev. D **105**, 124032 (2022).

[90] D. R. Terno, Phys. Rev. D **100**, 124025 (2019).

[91] V. Baccetti, S. Murk, and D. R. Terno, Phys. Rev. D **100**, 064054 (2019).

[92] C. W. Misner and D. H. Sharp, Phys. Rev. **136**, B571 (1964).

[93] S. A. Hayward, Phys. Rev. Lett. **96**, 031103 (2006).

[94] J. M. Bardeen in *Proceedings of the International Conference GR5* (Tbilisi University Press, Tbilisi, 1968).

[95] M. Cadoni, M. De Laurentis, I. De Martino, R. D. Monica, M. Oi and A. P. Sanna, Phys. Rev. D **107**, 044038 (2023).

[96] S. N. Solodukhin, Phys. Rev. D **51**, 618 (1994).

[97] S. N. Solodukhin, Living Rev. Relativ. **14**, 8 (2011).

[98] L. D. Landau and E. M. Lifshitz, *Statistical Physics* (Pergamon Press, Oxford, 1969).

[99] S. Hergott, V. Husain, and S. Rastgoo, Phys. Rev. D **106**, 046012 (2022).

[100] H. M. Haggard and C. Rovelli, Phys. Rev. D **92**, 104020 (2015).

[101] S. A. Hayward, Class. Quantum Gravity **15**, 3147 (1998).

[102] S. A. Hayward, Phys. Rev. D **49**, 6467 (1994).

[103] S. Hollands, R. M. Wald, V. G. Zhang, arXiv:2402.00818 (2024).

[104] T. Hale, D. Kubizňák, O. Svítek, and T. Tahamtan, Phys. Rev. D **107**, 124031 (2023).

[105] D. Kubizňák, T. Tahamtan, and O. Svítek, Phys. Rev. D **105**, 104064 (2022).